UNIVERSITY OF ALBERTA

EFFECTIVE STRESS MODELING OF CREEP BEHAVIOUR OF CLAY

BY

MOHAMMED MONIER MORSY

A thesis submitted to the Faculty of Graduate Studies and Research in partial fulfillment of the requirements for the degree of Doctor of Philosophy.

DEPARTMENT OF CIVIL ENGINEERING

Edmonton, Alberta

Fall 1994

UNIVERSITY OF ALBERTA

RELEASE FORM

NAME OF AUTHOR: MOHAMMED MONIER MORSY.

TITLE OF THESIS: EFFECTIVE STRESS MODELING OF CREEP BEHAVIOUR OF CLAY.

DEGREE: DOCTOR OF PHILOSOPHY

YEAR THIS DEGREE GRANTED: 1994

41 St. El-SHAID FARID SEMIKA
HELIOPLICE, CAIRO
EGYPT

Date:

DEDICATION

TO MY MOTHER NADRA

TO MY FATHER MONIER AND MY SISTER CHERINE

TO MY WIFE HEBA

FOR BEING THERE.....

ABSTRACT

The creep mechanism has been extensively studied and well understood as a reheological model or in the laboratory over the past three decades. The ability to study and model the creep behaviour of cohesive soil in field has been considered as a secondary problem for geotechnical engineer.

The main thrust of this thesis is to propose an effective stress numerical scheme to study the problem of creep in the field. A double-yield surface model for the stress-strain-time behaviour of wet clay is described. The yield surfaces employed are the modified Cam-Clay ellipsoid and the Von Mises cylinder inscribed in the ellipsoid. In the model both the secondary compression relationship and the Singh-Mitchell relationship are used to evaluate the creep strain tensor. The proposed numerical scheme incorporates the pore pressure into a finite element analysis based on field observations. An interpolation technique is used to determine the pore pressure at every element. The scheme not only avoids the complexity of making predictions of pore pressure, but also allows the analysis to be carried out in term of effective stresses based on the actual observed pore pressure. Two stress integration algorithms based on implicit calculation of plastic strain are implemented and tested for the double-yield surface model. The proposed numerical scheme is used to analyze the time dependent deformation of the clay foundation of Tar Island Dyke, Fort McMurray, Alberta. A brief overview of the construction and operation of the dyke since 1967 is presented. The lateral deformations were recorded by several inclinometers. Based on the nature of the lateral deformations and piezometers readings in the clay foundation, it is postulated that the movements are a result of creep mechanism that depend on effective stresses. The results of the numerical analysis are presented and

compared with the field measurements. The calculated results show an excellent agreement with the field measurements.

The results of the sensitivity analyses provide an insight to the accuracy of laboratory determined creep properties used to model field behaviour.

To provide better understanding of the creep mechanism in field, the creep effect on the time dependent deformaation in the dyke foundation is isolated from other factors causing the time dependent such as the dissipation of pore pressure in the dyke foundation. An effective stress time independent analysis is carried out for the dyke. The results illustrates the importance of the inclusion of the creep effect in the analysis and design of such type of projects. The effect of the creep mechanism on the stress distribution within the dyke foundation is discussed.

ACKNOWLEDGMENTS

Before all, I do indeed thank Allah Almighty who guided and aided me to bring-forth to light this thesis.

The author wishes to express his gratitude to his supervisor Dr. N.R. Morgenstern for his continuous interest and intense enthusiasm in the subject, and his guidance and support for this research. His ideas, time and invaluable discussions throughout the course of this research in making it a success will be forever appreciated.

I am deeply grateful to Dr. D.H. Chan for his support and orientation since the beginning of this work. His critical comments and our long discussions on numerical modeling aspects of this research were invaluable for the accomplishment of this research.

Geotechnical research at the University of Alberta takes place in an exceptional environment. Technical and social interactions with fellow students and staff have been a major part of my life for many years and no individual details will ever justly record the value of these relationships.

The support offered by Suncor and HBT AGRA Ltd. allowing access to the records relative to the construction of Tar Island Dyke is gratefully acknowledged.

I am very grateful to all my new friends in Edmonton for their constant support, encouragement and brotherhood throughout my stay here, in particular Ashraf Ghanem, Khaled Obbaya, Mashhour Ghoneim, Yehia El-Ezabi, Amr El-Sheik, Wala Khogali,

Ahmed Hassan, Amr Kamel and Ahmed Moawad and their families. We have shared many unforgettable moments together over the last four years. I can only say that they made my life here enjoyable and memorable.

The love and support of my parents Nadra and Monier, and my sister Cherine have always been an essential source of strength at all my life. Despite the difficulties of the intercontinental communications they always managed to track me down and provided constant encouragement every time I needed. To them I was and I am and I will always be grateful.

Finally, I would like to acknowledge the love and support of my wife Heba during the final stage of my "thesis years".

TABLE OF CONTENTS

Chapter **Page**

Chapter **Page**

Chapter **Page**

Chapter **Page**

LIST OF TABLES

LIST OF FIGURES

Figure **Page**

Figure **Page**

Figure **Page**

Figure **Page**

Figure **Page**

LIST OF TABLES

CHAPTER 1

INTRODUCTION

1.1 STATEMENT OF PURPOSE:

In soil mechanics, we encounter problems where accurate forecasting of time-dependent effects may be essential for the analysis of various geotechnical problems, including the stability and deformation of embankments and excavations, the stand-up time of tunnels in squeezing ground, and the settlement of foundations.

A major goal of the research on time-dependent stress-strain behaviour of soil is to develop constitutive models for use in the solution of such geotechnical projects which require the determination of change in deformation, stress, and shear strength of soil with time. Various approaches have been used including empirical curve fitting, extension of rate process theory, rheological models and advanced theories of viscoelasticity and plasticity.

Owing to the complexity of the stress states in a real problem, many factors influence the creep properties of soil, and the difficulty of accounting for concurrent volumetric and deviatoric deformations in systems which may undergoing consolidation as well as creep, it is not surprising that a sufficiently general model that can be readily implemented in engineering practices is not yet available.

In order to achieve the goal of developing such a numerical model, a number of factors must be considered :

1) The numerical model should be developed in terms of effective stresses in order to consider the variation in pore pressure encountered in practice and to simulate the intrinsic behaviour of soil in the field.

2) The numerical model should be simple in terms of required material parameters. This simplicity means that the physical meaning of such parameters should be well understood by geotechnical engineers. These parameters must also be readily obtainable from traditional laboratory tests.

3) The capability of the model should be tested by predicting the time-dependent behaviour of real geotechnical structures in order to show how the model can be used as a practical numerical tool in the design of similar structures.

There are two main objectives in this study. The first one, is to develop and implement an improved numerical model for the analysis of time-dependent behaviour of cohesive soils. The model has to take into account both the variation of pore pressure and the creep effects, which are important for the analysis of field cases. The second objective, is to test the capability of the model by means of history-matching and the prediction of the time-dependent behaviour of a field case over a long period of time.

1.2 THE PHENOMENA OF CREEP:

Soil and many other materials exhibit viscous creep behaviour in which deformation and movement proceed under a state of constant load and stress. For creep stresses that are large enough to lead ultimately to failure, the creep deformation occurs in sequential primary, secondary, and tertiary satges, as shown in Figure (1.1), during which the deformation rate decreases, remains constant, and increases with time respectively. Over the last five decades, some progress has been made in establishing rheological and phenomenological relationships to describe creep of soils (Taylor 1942; Murayama and Shibata 1958; Christensen and Wu 1964; and Singh and Mitchell 1968). These relationships can be applied in simple analyses, and are useful to define major factors affecting creep in the well defined boundary conditions of laboratory creep tests. In the case of field creep cases, there is a need for a three dimensional model to analyze creep behaviour under complicated boundary conditions. This would also provide a better understanding of the influence of creep on the time-dependent stress and strain state of soil in the field.

1.3 THE NUMERICAL MODEL DEVELOPMENT:

The time-dependent deformation of cohesive soils is due to both hydrodynamic lag (consolidation) and the viscous behaviour of the soil skeleton (creep). Recent advances in the formulation of a creep constitutive model (Kavazanjian 1978; Borja 1984; and Hsieh et al. 1990) have led to the development of a double-yield surface plasticity model for the description of time-dependent behaviour of cohesive soils under general load conditions. This model has been developed based upon a philosophy of unifying a comprehensive set of existing phenomenological relationships that are well established in geotechnical engineering.

Adopting the consolidation concept of Bjerrum (1967), it is assumed that the deformation of soils can be separated into a time-independent component and a time-dependent component. The modified Cam-Clay theory is used to represent the time-independent behaviour of soil in the model. An additional horizontal deviatoric yield surface is introduced beneath the modified Cam-Clay volumetric yield surface to better account for the shear deformation developed during loading beneath the modified Cam-Clay yield surface. The location of this horizontal yield surface is scaled according to Kondner's (1963) empirical hyperbolic stress-strain model. An important numerical implication of this horizontal yield surface is that it results in a non-associated plastic flow rule.

Time-dependent deformations in this model consist of contributions from both volumetric and deviatoric creep. The total creep strain rate is evaluated by employing the non-associative flow rule on both deviatoric and volumetric yield surfaces and forcing the creep strain rate to satisfy empirical volumetric and deviatoric creep functions simultaneously.

To perform a time-dependent analysis in term of effective stresses within the framework of the finite element analysis, it requires explicit consideration of the pore pressures. In many field cases pore pressures are measured in the field. This is true especially in large projects, in which the monitoring of pore pressure has become a routine practice. The numerical model used in this study adopted a numerical scheme proposed by De Alencar (1988) to incorporate the pore pressure as input data into the finite element analysis based on field measurements.

The numerical model is implemented in the finite element code PISA^{TM} (Program for Incremental Stress Analysis) developed at the University of Alberta (Chan and Morgenstern 1992).

1.4 TAR ISLAND DYKE:

The case history to be analyzed in this study, using the proposed numerical model in Chapter 3, is Tar Island Dyke. Tar Island Dyke is located on the west bank of the Athabasca River near Fort McMurray, Alberta. The purpose of the dyke is to provide containment for the tailings produced by the oil sand industry in the area. The construction of the dyke started in 1966 and it reached a height of 92 meters in 1984. For over twenty eight years of construction and operation, the time-dependent behaviour of the clay foundation of the dyke has been monitored extensively. The monitoring consisted of pore pressure measurements (piezometer and stand pipe), horizontal deformations (inclinometer), and vertical deformations (borehole). According to the proposed numerical model, the field measurements are divided into two groups. The first group is the pore pressure measurements, which are used as input data in the time-dependent analysis of the dyke foundation. The second group is the horizontal and vertical deformation measurements, which are compared to the results of the analysis to explore the capability of the model in simulating the time-dependent (creep) behaviour of the dyke foundation.

1.5 THESIS OUTLINE:

This thesis is written in a paper format. The scope of each chapter is:

i)- Chapter 2: This chapter presents a review of the established phenomenological relationships for the deformation behaviour of cohesive soils that are relevant to the development of the proposed constitutive model. The review also shows different approaches which have been used to analyze the creep behaviour of cohesive soil. A review of the Cam-Clay theory and the concept of the horizontal yield surface is presented.

ii)- Chapter 3: The numerical scheme adopted in this study to analyse the problem of creep is presented. The double-yield surface model for the stress-strain-time behaviour

of wet clay is described. The finite element formulation of the scheme is illustrated showing the incorporation of the pore pressure into the finite element analysis.

iii)-Chapter 4: This chapter deals with the numerical verification of the model. The capability of the model is tested in numerically simulating a series of incremental drained creep triaxial tests. These tests were performed on samples from the foundation of the Tar Island Dyke.

iv)-Chapter 5: The numerical analysis of the time-dependent behaviour of the foundation of Tar Island Dyke is described. A brief review of the construction and the operation of the dyke is presented. A comparison between the calculated and measured time-dependent deformation is shown to evaluate the capability of the proposed numerical scheme.

v)-Chapter 6: This chapter focuses on the creep behaviour of the dyke clay foundation. The effect of the model creep parameters on the calculated time-dependent deformation is discussed. The effect of the creep mechanism on the stress and the strain state in the foundation of the dyke is presented.

vi)-Chapter 7: This chapter summarizes the work done and presents conclusions and recommendations for further work.

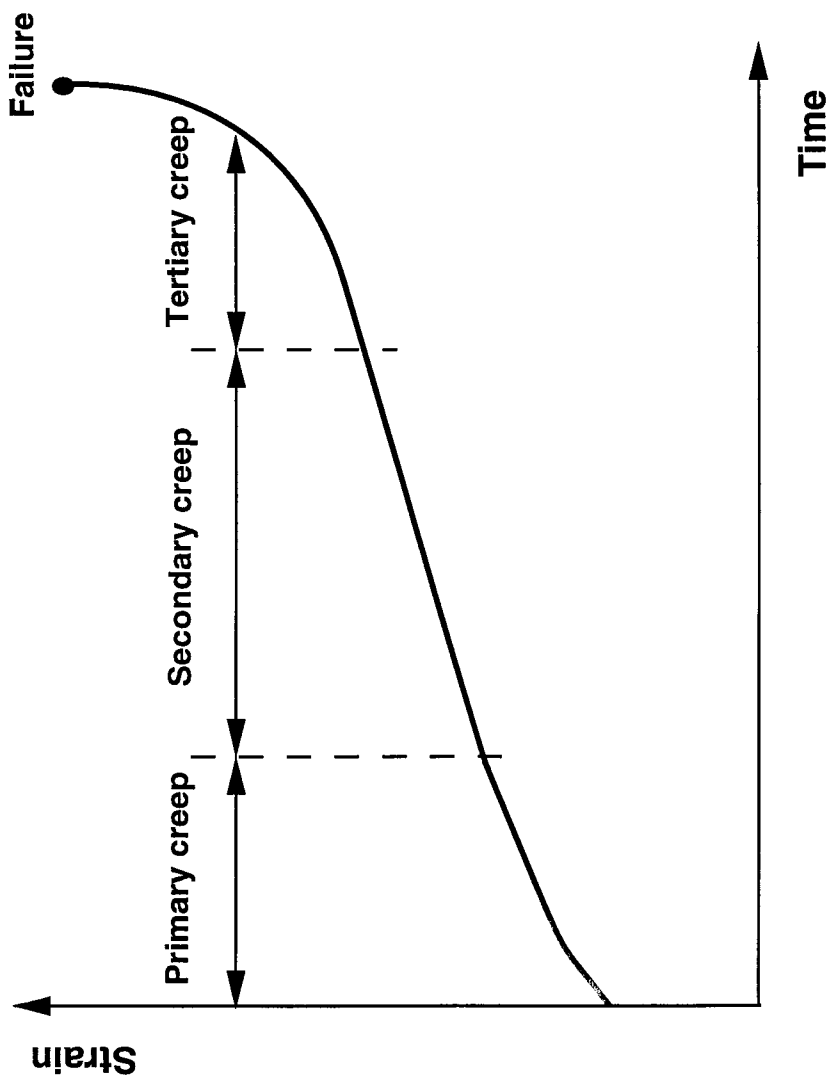

Figure (1.1) Creep in soils.

References:

Bjerrum, L. 1967. Engineering geology of Norwegian normally consolidated marine clays as related to settlements of buildings. Geotechnique, **17**: .83-117.

Borja, R.I. 1984. Finite element analysis of the time-dependent behaviour of soft clays. Ph.D. thesis, Stanford University, California.

Chan, D.H. and Morgenstern, N.R. 1992. User manual of program PISA. University of Alberta, Edmonton, Alberta, Canada.

Christensen, R.W., and Wu, T.H. 1964. Analysis of clay deformation as a rate process. ASCE Journal of Soil Mechanics and Foundation Engineering Division, **90**(SM6): 125-157.

De Alencar, J.A. 1988. Deformation of dams on sheared foundations. Ph.D. thesis, University of Alberta, Edmonton, Alberta, Canada.

Hsieh, H.S., Kavazanjian, E. Jr., and Borja, R.I. 1990. Double-yield surface model.I:Theory. ASCE Journal of the Geotechnical Engineering Division, **116**(GT9): 1381-1401.

Kavazanjian, E. Jr. 1978. A general stress-strain-time formulation for soils. Ph.D. thesis, University of California, Berkeley.

Kondner, R.L. 1963 . Hyperbolic stress-strain response: Cohesive soils. ASCE Journal of Soil Mechanics and Foundation Engineering Division, **89** (SM1): 115-144.

Murayama, S., and Shibata, T. 1958. On the rheological characters of clay, part 1. Disaster Preventation Research Institute, Koyoto University. Bulletin **26**.

Singh, A., and Mitchell, J.K. 1968. Generalized stress-strain-time function for soil. ASCE Journal of Soil Mechanics and Foundation Engineering Division, **94**(SM1): 21-46.

Taylor, D.W. 1942. Research on consolidation of clays. Report Serial No. 82, Department of Civil Engineering, MIT, Cambridge, Massachusetts.

CHAPTER 2

LITERATURE REVIEW

2.1 INTRODUCTION:

The objective of this research is to develop a general effective stress model to study the creep behaviour of cohesive soil for use in the design and analysis of geotechnical problems. Creep deformation of soils is an important consideration in a wide variety of geotechnical problems. These problems range from the time-dependent settlements of foundations after all excess pore pressure has been dissipated, to the time-dependent deformation of soft embankment foundation which may eventually fail in creep rupture before all excess pore pressure has been dissipated. The philosophy underlying the development of this model is based upon established phenomenological models for soil behaviour under restricted boundary conditions. The general model uses parameters from established models that are familiar to engineers and can be correlated to soil index properties

In this chapter, the established phenomenological models for soft clay behaviour that pertain to model development are reviewed. The background review also focuses on the main object of this research, creep behaviour of soft clay, showing different approaches that have been used over the past thirty-five years to provide a better understanding of the problem of creep and to define the major factors affecting the creep behaviour.

A unified stress-strain-time model developed by Kavazanjian (1978) is presented in detail. This model was developed based on the one-dimensional phenomenological models previously developed for the stress-strain-time behaviour of cohesive clay.

Finally, the elasto-plastic constitutive equations from Cam-Clay theory and the critical state concept (Roscoe and Burland 1968) are also addressed here. Besides that the concept

of the inclusion of horizontal yield surface in the modified Cam-Clay model is also illustrated.

2.2 REVIEW OF PHENOMENOLOGICAL SOIL MODELS:

In continuum mechanics, deformation can be separated into volumetric and deviatoric contributions. While these two components are considered separately for convenience and conceptual purposes, they are not independent. In the following sections the phenomenological models for both volumetric and deviatoric facets of soil behaviour are discussed.

2.2.1 Volumetric facet:

In the seventh Rankine lecture, Bjerrum (1967) proposed the concept that the one-dimensional deformation of clays can be separated into an immediate (time-independent) part and a delayed (time-dependent) part. Bjerrum's hypothesis of immediate and delayed compression is illustrated schematically in Figure (2.1). The plot of void ratio and effective vertical stress versus time show an immediate component occurring at the same instant the external load is applied and a delayed component that persists indefinitely with time. This decomposition scheme does not consider the influence of hydrodynamic lag.

In Figure (2.1), the solid curve illustrates Taylor's (1948) description of consolidation, which is divided into two phases, a primary consolidation phase for $t \leq t_p$ in which excess pore pressure dissipates and a secondary compression phase for $t \geq t_p$. The time t_p corresponds to the end of pore pressure dissipation.

Bjerrum's general concept for one-dimensional consolidation of cohesive soil is shown in Figure (2.2) as a system of parallel lines on the void ratio-log pressure diagram. Each line represents a unique relationship between void ratio and effective overburden pressure at a specific time of substantial loading. These lines are equally spaced at equal intervals of log time, which implies that the coefficient of secondary compression C_α is independent of time.

In Figure (2.2), the heavy solid lines illustrate the concept of quasipreconsolidation (see Leonard and Ramiah 1959). If an element of soil undergoes volumetric creep at a constant effective overburden pressure P_o for 3000 years, the volume of the soil element

decreases until it reaches an equilibrium void ratio e_o on the 3000-year isochrone. This process is represented by a vertical line as shown in Figure (2.2). The soil element will develop more strength with increase in stiffness against further compression during this period of delayed consolidation. For further loading of the soil element, it behaves as an overconsolidated soil provided that the vertical stress does not exceed the developed quasi-preconsolidation pressure P_c during the period of delayed consolidation. If the load increment is greater than P_c deformation will take place along the instant compression line for that part of loading exceeding P_c.

Bjerrum also postulated a unique relationship between undrained shear strength and void ratio, represented by a line parallel to the instant compression line, as shown in Figure (2.2). As the void ratio decreased during delayed compression, undrained shear strength increased.

2.2.2 Deviatoric facet:

Kondner (1963) analyzed the results of consolidation triaxial compression tests conducted at various overconsolidation ratios under various strain rates and concluded that the stress-strain relationship can be approximated by a hyperbola of the form:

[2.1] $$\sigma_1 - \sigma_3 = \frac{\varepsilon_a}{a + b\varepsilon_a},$$

where σ_1 and σ_3 are the major and the minor principal stresses respectively; ε_a is the axial strain; a is the reciprocal of the initial tangent modulus E_i; and b is the reciprocal of the asymptotic value of stress difference at infinite strain. Mathematically

[2.2] $$E_i = \left.\frac{d(\sigma_1 - \sigma_3)}{d\varepsilon_a}\right|_{\varepsilon_a = 0} = \frac{1}{a},$$

[2.3] $$(\sigma_1 - \sigma_3)_{ult} = \lim_{\varepsilon_a \to \infty} \frac{\varepsilon_a}{a + b\varepsilon_a} = \frac{1}{b}.$$

Equation (2.1) can be rewritten as:

[2.4] $$\frac{\varepsilon_a}{\sigma_1 - \sigma_3} = a + b\varepsilon_a,$$

which illustrates a linear relationship between $\frac{\varepsilon_a}{\sigma_1 - \sigma_3}$ and ε_a; where a is the intercept of the straight line with the y-axis and b is the slope of the line (see Figure (2.3)).

The asymptotic value of $(\sigma_1 - \sigma_3)$ is usually larger than the compressive strength of the soil by a finite amount. In order to overcome this discrepancy, a factor R_f is introduced to force the hyperbolic curve to pass through the observed failure point such that,

[2.5] $$R_f = \frac{(\sigma_1 - \sigma_3)_f}{(\sigma_1 - \sigma_3)_{ult}},$$

where $(\sigma_1 - \sigma_3)_f$ is the deviatoric stress at failure, while $(\sigma_1 - \sigma_3)_{ult}$ denotes the asymptotic value of the best fit hyperbola. For numerical analysis, the hyperbola is truncated at $(\sigma_1 - \sigma_3)_f$.

In 1970, Duncan and Chang introduced a comprehensive hyperbolic stress-strain relationship for use in numerical analysis. Their formulation accounted for the influence of confining pressure on both the initial tangent modulus (E_i) and shear strength $(\sigma_1 - \sigma_3)_f$. Janbu's (1963) power law was used to show the influence of the confining pressure on initial tangent modulus. The relationship between the initial modulus and the confining pressure was expressed as :

[2.6] $$E_i = KP_a\left(\frac{\sigma_3}{P_a}\right)^n,$$

where K and n are material parameters and P_a is the atmospheric pressure, a normalizing constant as shown in Figure (2.4), expressed in the same unit as E_i and σ_3. The Mohr -Coulomb failure criterion was used to introduce the influence of the confining pressure on the shear strength. If it is assumed that failure occurs with no change in the σ_3, the relationship between compressive strength and confining stress may be expressed as :

[2.7] $$(\sigma_1 - \sigma_3)_f = \frac{2C\cos\phi + 2\sigma_3 \sin\phi}{1 - \sin\phi},$$

where C and ϕ are the Mohr-Coulomb strength parameters.

The hyperbolic model was further refined by Duncan and co-workers (1980). However the current model cannot account for volume increase due to a change in shear stress. Therefore, its application to dilatant soils is limited.

In 1974, Ladd and Foott observed in the laboratory that the triaxial and simple shear test results on clay samples with the same overconsolidation ratio but different consolidation pressures exhibited very similar strength and stress-strain characteristics, when normalized with respect to the effective consolidation pressure. Such stress-strain curves fall in a narrow band. An idealized plot for the normalized soil properties principle is shown in Figure (2.5).

Combining the hyperbolic model and the normalized soil properties concept, the following equation is used to describe the immediate deformation of soft clays when subjected to a deviatoric stress,

[2.8] $$(\sigma_1 - \sigma_3) = \frac{\varepsilon_a \sigma_c R_f}{a + b\varepsilon_a},$$

where σ_c is the effective consolidation pressure.

A slight divergence from a unique normalized curve is generally observed in laboratory test data. This divergence may be attributed to the effect of heterogeneity in the soil deposit, different consolidation stresses and shortcoming in the normalized soil properties concept. The divergence is found to be within 10% of the mean value in terms of deviatoric stresses (Ladd and Foott 1974) for typical soft clays of low to intermediate sensitivity, which is acceptable for practical purpose. However, the normalized soil properties concept is not applicable to cemented clay and quick clays whose structures are susceptible to significant alteration at high consolidation stresses.

In 1978, Kavazanjian proposed that the immediate deviatoric behaviour of lightly overconsolidated clay can be accounted for by the normalized stress-strain curve using the equivalent consolidation pressure concept. Kavazanjian postulated that the deviatoric stress versus axial strain behaviour of lightly overconsolidated clay is the same as for the clay normally consolidated at the same void ratio. As shown in Figure (2.6), the consolidation pressure corresponding to the normally consolidated clay at the same void ratio is defined

as the equivalent consolidation pressure P_e (Hvorslev 1960). A simple relationship exists between P_c, the in-situ volumetric pressure of the lightly overconsolidated clay, and P_e :

$$P_e = P_c(OCR)^{1-\frac{C_r}{C_c}}, \qquad [2.9]$$

where OCR is the overconsolidation ratio; C_r is the recompression index; and C_c is the virgin compression index.

Incorporating the equivalent consolidation concept with the normalized soil properties concept, Kavazanjian (1978) revised equation (2.8) as:

$$(\sigma_1 - \sigma_3) = \frac{\varepsilon_a P_e R_f}{a + b\varepsilon_a}. \qquad [2.10]$$

The above concept is assumed valid regardless of whether the soil has been over-consolidated by unloading or through a quasi-preconsolidation process. Kavazanjian, Mitchell and Bonaparte (1980) found that the measured undrained shear strength and the predicted values using the equivalent consolidation pressure concept (S_u/P_e) agreed well up to an OCR of 4 for the Atchafalaya and Boston Blue clay, as shown in Figure (2.7). As a consequence, the applicability of equations (2.9) and (2.10) appears to be limited to soil with OCR less than 4.

2.3 REVIEW OF CREEP BEHAVIOUR OF SOIL:

The estimation and importance of creep deformation in design has been the subject of considerable research over the last thirty-five years. Most of the research has been directed towards understanding creep behaviour in the laboratory. Regrettably, there are few case histories of field behaviour which link a rational design approach to actual field behaviour (Foss 1969; Soydemir and Schmid 1970; de Ambrosis 1974; Poulus et al. 1976; Wu et al. 1978; and Borja et al. 1990).

Creep is defined here as the time-dependent deformation under sustained stresses, exclusive of hydrodynamic effects. Creep in soil depends upon a host of factors which include time, temperature, soil type, soil structure, stress history, stress state and drainage

conditions. Figure (2.8) illustrates the wide variation of creep response among different soil types.

For the investigation of creep behaviour of soils, there are three main approaches. The first approach is the fundamental approach, in which creep behaviour is related to events occurring at the particle level. The second approach is the rheological modeling approach, which involves combining spring, dashpot, and slider elements in a mathematical analogy that fits the observed soil behaviour. The third approach is the phenomenological approach, in which the creep behaviour is related to macroscopic findings of laboratory tests. A brief outline of the first two approaches is presented in this section. This outline has been included because it adds to the understanding of soil behaviour, but kept brief because these methods have not generally been successful in providing a constitutive relationship that can be used in practice.

The phenomenological approach is presented in more detail as constitutive relationships, albeit empirical, have evolved from this approach which are used in this study in the development of the proposed effective stress model for the creep behaviour of soils.

2.3.1 Fundamental approach:

There have been a number of researchers who have developed theories to explain and predict the creep behaviour of soils on a particle level. Most of these theories can be grouped into three categories. A brief review of the main elements of each of these theories are given.

2.3.1.1 Consideration based on viscosity of adsorbed water:

Clay particles are surrounded by a layer of adsorbed water that has a bonding and structure which is different than the pore water (see Mitchell 1993). The presence of these adsorbed water layers was known in the early 1940's and attempts were made to explain secondary consolidation in term of their viscosity. Terzaghi (1941) postulated that, after primary consolidation, the load carried by the soil was somehow distributed at grain to grain contacts. He also held that the viscosity of the adsorbed water bonds increased as the particles moved together and, therefore, the load transfer occurred at an even decreasing rate.

Taylor (1942) hypothesized that the viscosity of the adsorbed water layers were of a substantially higher magnitude than that of the pore water and, that the adsorbed water was responsible for the viscous component in the effective stress-strain-time behaviour.

Barden (1965) summarized the work of Terzaghi and Taylor and contended that they are in agreement on the following points :

1) Primary and secondary consolidation are part of a single process.
2) The seat of secondary or creep effects is gradual readjustment or remoulding of the soil structure initiated during primary consolidation.
3) The rate at which secondary compression proceeds is strongly influenced by the viscous effects of the adsorbed water layer.

One method of validating the influence of the viscosity of the adsorbed water bonds on secondary consolidation is to replace the adsorbed water and pore water in a soil by an inert liquid such as carbon tetrachloride or benzene. Both Leonards and Girault (1961) and Mesri (1973) conducted such experiments and found that the nature of the pore fluid has some influence on the rate of secondary consolidation. However, both authors agree that the presence of adsorbed water is not necessary in order for secondary consolidation to occur.

2.3.1.2 Rate process theory:

Rate process theory is based upon the proposition that atoms, molecules or particles (termed flow units) participating in a time-dependent deformation process are constrained from movement relative to each other by virtue of energy barriers which separate adjacent energy positions. In order for a flow unit, a soil particle in this case, to move to a new equilibrium position it must require sufficient energy to surmount the imposed energy barrier. This energy is called the activation energy and it has some frequency of occurrence (see Figure (2.9)). A shear stress distorts the energy barriers allowing flow units to move preferentially in the direction of distortion, as shown in Figure (2.10).

Rate process theory was first proposed by Eyring (1963) and became popular in the soil mechanics literature in the 1960's. Detailed development of the theory, which is based on statistical mechanics, may be found in Eyring (1963), Glasston et al. (1941), and elsewhere in the physical chemistry literature.

Mitchell (1993) provides a compact overview of the Rate Process theory significance to different aspects of soil mechanics such as soil deformation, soil strength and shear resistance.

Mitchell et al. (1968) proposed the following equation derived from rate process theory to determine the creep strain rate:

[2.11] $$\dot{\varepsilon} = 2X\frac{KT}{h}\exp(\frac{-\Delta F}{RT})\sinh(\frac{f\lambda}{2KT}),$$

where

X is a function of the number of flow units in the direction of deformation and the average component of displacement due to a single unit mounting energy barrier.

K is Boltzmann's constant, 1.38×10^{-16}erg/^{o}K.

h is Planck's constant, 6.624×10^{-27} erg/ sec.

T is the temperature in ^{o}K.

ΔF is the free energy of activation calories/mole.

R is the universal gas constant, 1.98 cal/^{o}K-mole.

f is the average shear force on each flow unit, dynes.

λ is the separation distance between successive equilibrium positions.

Adaptations of the theory to study the soil behaviour are given by Murayama and Shibata (1964); Mitchell (1964); Wu et al. (1966); Keedwell (1984); Feda (1989); and Kuhn and Mitchell (1992). Because of its complexity, rate process theory has not been widely used in practice and remains primarily a research tool.

2.3.1.3 A model based on cavity channel network:

In 1968, De Jong introduced a concept of primary and secondary consolidation that models the soil pores as cavities of different compressibility linked together by channels with different permeability. During primary consolidation pore water pressure drains from the accessible cavities and the ambient excess pore water pressure eventually goes to zero. However in a certain number of cavities linked to the network by channels of low permeability, the excess pore pressure remains greater than zero.

The slow drainage of water from these cavities gives rise to secondary consolidation. Due to the complexity of the model, it has only been employed by a few other researchers (see Holzer et al. 1973).

2.3.2 Rheological models:

Different rheological models have been proposed for the mathematical description of the stress-strain-time behaviour of soils. Figure (2.11) shows some rheological models which have been proposed for characterization of stress-strain-time behaviour of soils (Murayama and Shibata 1958; Schiffman 1959; Christensen and Wu 1964; and Abdel-Hady and Herrin 1966).

The criticism often directed to the rheological models approach for soils (Singh 1966; Singh and Mitchell 1968) is that they are generally limited to a particular soil, for a particular range of variables and do not permit easy extrapolation. Mathematical expressions from rheological models are complicated and none has yet been proposed which is as simple as the three parameters relationship presented later in equation (2.13). Due to their complexity rheological models are not used extensively in creep modeling of soil.

2.3.3 Phenomenological approach:

The phenomenological approach is the endeavor to produce empirical relationships that predict creep behaviour based solely on observed creep behaviour in the laboratory. Singh and Mitchell (1968) contend that an empirical creep relationship must satisfy the following general requirements :

1) It must be applicable to a reasonable range of creep stresses.
2) It must describe the behaviour of a range of a soil types.
3) It must account for both linear and curved relationships between strain and the logarithm of time.
4) It must contain parameters that are easily determined.

Kavazanjian and Mitchell (1977) postulated that the creep strain tensor can be divided into distinct but interdependent, volumetric and deviatoric components.

2.3.3.1 Volumetric component:

The volumetric component of creep is traditionally referred to in the literature as secondary compression. Taylor (1942) made a significant modification of Terzaghi's consolidation theory by the inclusion of the secondary compression. According to Taylor's definition, secondary compression is the continuous deformation of the soil skeleton under constant load after the excess pore pressure has been fully dissipated. Figure (2.12) illustrates the separation of a typical one-dimensional consolidation curve into primary and secondary compression.

It is often assumed that there is a linear relationship between secondary compression and log time. This assumption results in a constant value for the coefficient of secondary compression, C_α, defined as:

[2.12] $$C_\alpha = \frac{\Delta e}{\Delta \log t},$$

where Δe is the change in void ratio over the time interval Δt.

Summarizing the effects of stress history and the type of stress system on the rate of secondary compression of remoulded Boston Blue Clay and Vicksburg Buckshot Clay, Ladd and Preston (1965) proposed the following engineering hypotheses:

1) C_α is independent of time.
2) C_α is independent of sample thickness.
3) C_α is independent of load increment ratio for normally consolidated clays with a constant compression index.
4) C_α is a function of the overconsolidation ratio (stress history) and deviatoric stress level.

In current practice, it is generally agreed that time, sample thickness and load increment ratio have no effect on the magnitude of C_α for normally consolidated clays. Therefore, only item (4) of the above hypothesis will be discussed.

Laboratory oedometer and triaxial consolidation tests performed by Ladd and Preston (1965) on Boston Blue Clay indicated that the rate of secondary compression under isotropic stresses is virtually equal to that under K_o stress, where K_o is the at rest earth

pressure coefficient. For deviatoric stress level, $\overline{D}$, beyond K_o conditions, they suggested that since the soil skeleton is more susceptible to creep under a high deviatoric stress level, C_α will undoubtedly increase for stress between K_o and $\overline{D}=\overline{D}_f$, where $\overline{D}_f$ is the deviatoric stress level at failure.

In addition to Ladd and Preston's study (1965), other researchers including Murayama and Shibata (1961); Bishop and Lovenbury (1969); and Walker (1969) also presented laboratory test results concerning the drained creep behaviour of clay under stress conditions other than isotropic and one-dimensional stress state. Figure (2.13) summarizes the test results of the above mentioned researchers. It was concluded by Fuleihan and Ladd that the apparent C_α value, denoted by C^*_α, increases linearly with the deviatoric stress level to a 'yield value', after which C^*_α increases at a faster rate. These investigators also concluded that the possibility of 'drained creep rupture' at high deviatoric stress levels, as observed by Murayama and Shibata (1961), is remote since the excellent test results of Bishop and Lovenbury (1969) indicate that "strain softening' is unlikely to develop during a drained creep test.

Another important factor influencing the rate of secondary compression is stress history. The effect of stress history on the rate of secondary compression is shown in Figure (2.14). The apparent coefficient of secondary compression C^*_α is plotted against the ratio $\overline{\sigma}_{vc} / \overline{\sigma}_{vm}$, in which $\overline{\sigma}_{vc}$ is the vertical consolidation pressure when C^*_α is measured and $\overline{\sigma}_{vm}$ denotes the maximum past vertical consolidation pressure. Figure (2.14) shows that C^*_α is only 5 to 10% of the value for normally consolidated samples when the ratio $\overline{\sigma}_{vc} / \overline{\sigma}_{vm}$ is less than 0.5. A rapid increase in C^*_α is observed with increasing $\overline{\sigma}_{vc} / \overline{\sigma}_{vm}$ ratio. C^*_α reaches a maximum when $\overline{\sigma}_{vc}$ is about two times the preconsolidation pressure.

Mesri and Goldewski (1977) postulated, based on consolidation data on samples of three natural clay deposits as well as laboratory and field data, that for normal soils a unique relationship exists between C_α and C_c. They further postulate that for fine-grained soils at any effective stress and void ratio during secondary compression, the ratio C_α/C_c is constant with values that lie within a range of 0.025-0.10. This constant relationship between C_α and C_c implies C_α is a constant for a normally consolidated cohesive soil with a constant C_c.

2.3.3.2 Deviatoric component:

The deviatoric component of the creep strain tensor has not received much attention in the literature. Again, this is a consequence of the majority of researchers using the oedometer for the investigation of creep behaviour. Kavazanjian and Mitchell (1980) stated that the deviatoric component of the creep strain tensor can be described by the Singh-Mitchell relationship.

In 1968, Singh and Mitchell investigated the time-dependent response of soils and suggested a simple three-parameter phenomenological equation to describe the relationship between axial strain rate and time of soil samples subjected to a constant deviatoric stress for a wide variety of soils. The Singh- Mitchell creep equation takes the form:

$$[2.13] \qquad \dot{\varepsilon}_a = A\exp(\alpha D)(\frac{t_i}{t})^m,$$

where $\dot{\varepsilon}_a$ is the axial strain rate in a triaxial creep test; t_i is an initial reference time after loading when creep is assumed to commence. A, α and m are the Singh-Mitchell equation material parameters and D is the deviatoric stress. In the case of soil samples subjected to rapid loading, according to the initial reference time (t_i) concept, the rapid loading will result in different initial reference times corresponding to different loading steps. In this case the Singh-Mitchell equation cannot describe the creep behaviour of the soil using the superposition method since the equation does not account for the effect of the previous loading on the present creep strain rate in the soil. By integrating equation (2.13), the axial strain ε_a may be obtained as follows:

$$[2.14] \qquad \varepsilon_a = \frac{A}{(1-m)}\exp(\alpha D)t_i^{\,m}t^{(1-m)} + constant; \quad for \quad m \neq 1,$$
$$= At_i\exp(\alpha D)\ln(t) + constant; \quad for \quad m = 1.$$

A schematic representation of the Singh-Mitchell creep function is shown in Figure (2.15a). Note that under a sustained deviatoric stress loading, the logarithm of creep strain rate decreases linearly with respect to the logarithm of time. Equation (2.13) also forms contours of parallel lines with slope m for different deviatoric stress levels $\overline{D}$, where $\overline{D} = \frac{(\sigma_1 - \sigma_3)}{(\sigma_1 - \sigma_3)_f}$.

At low stress level, the axial creep strain rate is relatively small. In the midrange of $\overline{D}$, a nearly linear relationship exists between logarithm of strain rate and $\overline{D}$. At high stress level, the strain rate becomes excessively large and signals the onset of failure.

The Singh-Mitchell equation is only valid over a range of $\overline{D}$ from about 30% to 90%. It is generally accepted that equation (2.13) seriously overpredicts the creep strain rate at low stress levels while it underpredicts the creep strain rate at near-failure stress levels. By evaluating the available data, Singh and Mitchell concluded that equation (2.13) is applicable irrespective of whether the clay is undisturbed or remolded, wet or dry, normally consolidated or overconsolidated, or tested drained or undrained.

Tavenas et al. (1978) investigated the drained and undrained creep behaviour of overconsolidated Saint-Alban clay and suggested that the Singh-Mitchell creep function can be generalized into the following form:

[2.15] $$\dot{\varepsilon} = A \; g(\sigma') \; (\frac{t_i}{t})^m,$$

where the creep parameter m can be assumed constant and falls in the range of 0.7-0.8, while $g(\sigma')$ is the stress function. For normally consolidated clay, the stress function can be expressed in terms of deviatoric stress level using the same exponential term as used in the Singh-Mitchell relationship. For an overconsolidated clay, the stress function can be defined according to the limit state surface which, according to Tavenas et al. (1978), is a surface of equal shear strain rate in the area of stress space outside the Mohr-Coulomb criterion of the normally consolidated clay, as shown in Figure (2.16). Figure (2.16) indicates the lines of equal shear strain rates representing both the drained and undrained creep test results of overconsolidated Saint-Alban clay. The equations of these lines represent the stress function $g(\sigma')$.

Mesri et al. (1981) examined the Singh-Mitchell equation in terms of undrained triaxial compression tests, with pore water measurements, using reconstituted specimens of Kaolinite and Cucaracha shale. They found that the exponential model adequately describes the observed stress-strain data of soils at shear stress levels in the range of 20-80%. However, it predicts unrealistic stress-strain behaviour at the remaining shear stress levels, especially at shear stress levels less than 20%. Mesri et al. introduced an alternative stress-strain equation, which is the hyperbolic stress-strain model, which they

combined with the exponential equation to provide a stress-strain-time relationship which can adequately describe the strain behaviour from zero strain to failure. The proposed relationship is:

$$[2.16] \qquad \varepsilon = \frac{2}{(E_u / S_u)_i} \frac{D_i}{(1-(R_f)_i D_i} (\frac{t}{t_i})^{\lambda},$$

where $(E_u)_i$ is the initial undrained tangent modulus for hyperbolic fitting of data at time t_i; t_i is the reference time; $(S_u)_i$ undrained shear strength at time t_i ; D_i is the stress level at time t_i ; R_f is the failure ratio $= (\sigma_1 - \sigma_3)_f / (\sigma_1 - \sigma_{3)_{ult}}$ at time t_i; and λ is the power parameter.

The value of $\frac{2}{(E_u / S_u)_i}$ and $(R_f)_i$ can be obtained from a plot of ε / D_i against ε at time t_i . For λ, based on the observed data on the Kaolinite and Cucaracha soil, they suggested an empirical relationship (see Figure (2.17)) :

$$[2.17] \qquad \lambda = \frac{1}{6000} \frac{E_u}{S_u}.$$

In Figure (2.18) , both the hyperbolic model and the exponential model are compared with the observed data from a constant load test on a Kaolinite sample.

2.4 PHENOMENOLOGICAL STRESS-STRAIN-TIME MODEL:

For each of the theoretical or phenomenological constitutive equation mentioned above to describe soil behaviour, the range of applicability is somehow limited. For example, Taylor's secondary consolidation theory is only used to describe the volumetric creep behaviour of soil when loaded under one-dimensional conditions while Kondner's hyperbolic model is useful only when soil is subjected to deviatoric loading.

In the case of geotechnical problems, the state of stress and the boundary conditions are sufficiently complex that a theory or constitutive equation restricted to specified boundary conditions is simply not adequate to provide a satisfactory solution.

Over the past 16 years, a unified constitutive model which covers a wide spectrum of soil behaviour to be used in numerical analysis has been developed by Kavazanjian (1978). He formulated a multi-axial, time-dependent constitutive model by unifying existing

phenomenological relationships of soft clay within the critical state framework. He postulated that deformation is described by separate but interdependent volumetric and deviatoric contributions. It is further assumed that both of these contributions consist of immediate and delayed components analogous to immediate and delayed compression discussed in section (2.2.1.1). The general equations can be written in the following form:

[2.18] $$\varepsilon_v = \varepsilon_{vi} + \varepsilon_{vd};$$

[2.19] $$\varepsilon_D = \varepsilon_{Di} + \varepsilon_{Dd},$$

where ε_v and ε_D are the volumetric and deviatoric strain tensor respectively, while the subscript i denotes the immediate component of the deformation and subscript d indicates the delayed component. Models for each component were developed by generalizing existing theories which are compatible with the critical state framework and also provide a good fit with real soil behaviour.

2.4.1 Volumetric model:

By assuming that the delayed volumetric behaviour is independent of deviatoric stress level and using the normalized soil properties concept, Bjerrum's (1967) one-dimensional compression model was generalized to represent the volumetric behaviour of soft clays. The schematic representation of volumetric model is shown in Figure (2.19). It consists of parallel planes of constant stress level in void ratio-log time-log mean stress (e-logt-logP) space. The planes are assumed to represent a unique relationship among void ratio, effective stress and time of an element of cohesive soil. The spacing of the planes is governed by the values of virgin compression index C_c and coefficient of secondary compression C_α both of which are assumed constant.

Upon an instantaneous increase in volumetric effective stress, the state of a normally consolidated soil sample moves along a straight line with slope C_c on the void ratio-log stress plot. The response of an overconsolidated soil sample is governed by the quasi-preconsolidation concept. Unloading and reloading are assumed to cause the soil state to move along a straight line in the e-logt-logP space with slope C_r. The rate of volumetric change during consolidation can be evaluated on the basis of soil permeability and boundary pore water pressure.

Deviatoric model:

Ladd and Foott's (1974) normalized soil properties concept in conjunction with Kondner's (1963) hyperbolic stress-strain curve are used to determine the immediate deviatoric deformations of cohesive soil. The delayed deformation is described by the Singh-Mitchell creep equation. The immediate stress-strain curve is assumed to take the shape of a hyperbola with parameters a, b and R_f.

[2.20] $$\sigma_1 - \sigma_3 = \frac{\varepsilon_a R_f}{a + b\varepsilon_a}.$$

The normalized soil properties concept is incorporated to account for the stress-dependence of shear modulus. The hyperbola can be normalized by dividing the deviatoric stress by the effective isotropic consolidation pressure σ_c . Furthermore, if the soil sample is lightly overconsolidated, σ_c is replaced by the equivalent consolidation pressure P_e. The immediate deviatoric stress-strain relationship is given by equation (2.10).

Figure (2.20) shows Kavazanjian's general deviatoric model. When a soil element is initially loaded, its stress-strain behaviour will follow a hyperbola with an initial stiffness E_i. Under sustained deviatoric loading, the soil element creeps according to the Singh-Mitchell equation. Upon further loading, or upon unloading beneath the immediate curve, the soil element behaves like an elastic material with an initial modulus E_i. Hysteresis effects during the unloading-reloading cycle are neglected.

2.5 CAM-CLAY THEORY:

The study of yielding of soils can be traced back to the work of Rendulic (1936). Rendulic observed that constant void ratio contours on the triaxial plane, plotting σ_1 (major principal stress) versus $\sqrt{2}\sigma_2 = \sqrt{2}\sigma_3$ (intermediate and minor principal stress respectively), were the same under drained and undrained conditions. Figure (2.21) shows Henkel's (1960) triaxial test results on remoulded clay that illustrates Rendulic's observations. Rendulic concluded that for a given clay sample in equilibrium under given effective stress at given initial specific volume, the specific volume under any principal stress increments was uniquely determined by those increments. Based upon Rendulic's works, Roscoe, Schofield and Thurairajah (1963) developed the Cam-Clay model to describe the yielding behaviour of soft cohesive soils.

2.5.1 Critical state concept:

In a direct or triaxial shear test, if a soil sample is allowed to change volume during a shearing test, it will either dilate or contract depending on its initial state of density. The volumetric yielding process will continue until the soil sample reaches a critical void ratio, after which the void ratio will remain constant during further deformations. This constant volume state is referred to as the critical state. A soil deforming with a void ratio lower than the critical value tends to increase in volume, whereas at a void ratio higher than the critical value a decrease in volume will be observed during drained deformation.

When the effective stress paths of the triaxial tests are plotted on the (P,q) plane, the constant volume points on the stress paths are found to form a straight line with a slope M, which is called the critical state line, where P and q are defined as:

[2.21] $$P = \frac{1}{3}(\sigma_1 + 2\sigma_3);$$

[2.22] $$q = (\sigma_1 - \sigma_3).$$

The plot of the void ratio at the critical state versus the natural logarithm of hydrostatic effective stress P (see Figure (22)) is approximately a straight line with slope C_c or λ on a natural logarithm plot. Reloading and swelling of soil are assumed to follow straight lines with identical slope C_r or κ on a natural logarithm plot. Therefore, two equations are used to characterize the critical state are:

[2.23] $$q = MP;$$

[2.24] $$e = \Gamma - \lambda \ln P;$$

where Γ is the critical void ratio at P=1.

The projection of the conventional isotropic consolidation line onto the e-lnP plane is also a straight line with slope λ,

[2.25] $$e = e_a - \lambda \ln P,$$

where e_a is the void ratio at P=1.

A clay sample is called wet when its state corresponds to a point which lies between the isotropic virgin consolidation and critical state line, and is called dry when its state point lies nearer the P and q axes than the critical state line (see Figure (2.22)).

The loci of all the possible states on P-q-e space is bounded by the state boundary surface (see Figure (2.23)). Plastic state can only occur on the state boundary surface. Unloading or reloading beneath the state boundary surface results in elastic deformation only.

2.5.2 Original cam-clay theory:

The original Cam-Clay theory was developed by Roscoe, Schofield and Thurairajah (1963) to describe the behaviour of wet clay. They assumed that there is no recoverable component of shear distortion and that energy δW dissipates according to:

[2.26] $$\delta W = MP\delta\varepsilon_d,$$

where the deviatoric strain $\delta\varepsilon_d$ is defined as:

[2.27] $$\delta\varepsilon_d = \frac{2}{3}(\delta\varepsilon_1 - \delta\varepsilon_3).$$

Based upon these assumptions, Roscoe et al (1963) derived the following expression for the yield surface (see Figure (2.24)) of the form:

[2.28] $$\frac{q}{P} + M \ln P = M \ln P_c,$$

where P_c is the preconsolidation stress.

Schofield and Worth (1968) also derived the following expression as the equation of the state boundary surface on (P,e,q) space,

[2.29] $$q = \frac{MP}{\lambda - \kappa}(e_a - e - \lambda \ \ln P).$$

The total volumetric strain $\delta\varepsilon_v$ is found to be:

[2.30] $$\delta\varepsilon_v = \frac{1}{1+e}(\frac{\lambda - \kappa}{M}\delta\eta + \lambda\frac{\delta P}{P}),$$

where η = stress ratio q/P. The deviator strain increment can be obtained using the normality principle:

[2.31] $$\delta\varepsilon_d = \frac{\lambda - \kappa}{1+e}(\frac{P\delta\eta + M\delta P}{MP(M-\eta)}).$$

The foregoing development requires only 4 material constants, namely, κ, λ, M, and e_a. However, there were a number of shortcomings with the original Cam-Clay model. It was found to overpredict the strain increments for changes of stress ratio (η) at small values of η. This model also tends to overpredict the at-rest lateral pressure coefficient K_o. Furthermore, the original Cam-Clay bullet shaped yield surface has a corner along the isotropic effective stress axis. Consequently, there exists two alternative limiting plastic strain increments, depending on the direction from which the P-axis is approached. Any plastic strain increment vector lying between these two limiting vectors is theoretically permissible.

2.5.3 Modified cam-clay theory:

To overcome the shortcomings of the original Cam-Clay model, Burland (1965) proposed a modified Cam-Clay theory by using a new work-dissipation equation for wet clay of the form:

[2.32] $$\delta W = P\sqrt{(\delta\varepsilon_v^P)^2 + (M\delta\varepsilon_d^P)^2},$$

where the superscript P indicates the plastic component of both the volumetric and the deviatoric strain respectively.

Working along the ideas proposed by Roscoe and Schofield (1963), an equation for the new yield surface was obtained as follows:

[2.33] $$P(P-P_c)+\frac{q^2}{M^2}=0.$$

Equation (2.33) represents an ellipse in P,q space with its center at $P_c/2$. Figure (2.25) illustrates the shape of the Modified Cam-Clay yield surface. The modified Cam-Clay state boundary yield surface has the alternative form:

[2.34] $$e-e_a=\lambda \ \ln P \ (\frac{M^2}{M^2+\eta^2})^{(1-\frac{\kappa}{\lambda})}.$$

Similarly, the following equations for the volumetric and deviatoric strain increment were derived (Roscoe and Burland, 1968) :

[2.35] $$\delta\varepsilon_v=\frac{1}{1+e}[(\lambda-\kappa)\frac{2\eta\delta\eta}{M^2-\eta^2}+\lambda\frac{\delta P}{P}],$$

[2.36] $$\delta\varepsilon_d=\frac{\lambda-\kappa}{1+e}(\frac{2\eta}{M^2-\eta^2})(\frac{2\eta\delta\eta}{M^2+\eta^2}+\frac{\delta P}{P}).$$

Using the modified theory, Roscoe and Burland (1968) were able to make an excellent prediction of the triaxial compression behaviour of normally consolidated Kaolin. Although a tendency for underprediction of shear strain was observed, there was a distinct improvement from the original Cam-Clay theory. The underprediction of shear strain is more evident in an undrained triaxial test than in a drained triaxial test, as shown in Figure (2.26).

2.5.4 Plastic shear distortion beneath the state boundary surface:

It is assumed in the modified Cam-Clay theory that no shear distortion can be associated with a stress path beneath the state boundary surface. Wroth and Loudon (1967) show based on experimental results that considerable plastic shear distortions take place for stress paths inside the yield surface. Loudon (1967) performed a series of consolidated undrained triaxial tests on Kaolin over a wide range of overconsolidation ratios to investigate the pattern of shear strain and the effect of stress history upon it.

Loudon (1967) and Wroth and Loudon (1967) obtained the series of eight stress paths and strain contours on the P-q plane, normalized with respect to the preconsolidation pressure P_c as shown in Figure (2.27). Four of these stress paths were on the wet side and the other four on the dry side of the critical state line. The points marked on each stress paths are those corresponding to values of total shear strain of 0.0005, 0.001, 0.002, 0.005, 0.01, 0.02, 0.05, and 0.1 (contours 1-8, respectively). On the wet side these contours are almost parallel with the P/P_c axis, while on the dry side these contours form a fan of straight lines which appear to converge on the point defined by $(P/P_c,q/P_c) = (-0.13,0.0)$. The spacing of the contours is dependent on the stress level as can be seen in Figure (2.27). Contours become closer together as the critical state is approached. Loudon also found a linear relationship between q/P_c and $\ln\varepsilon$ for wet Kaolin (see Figure (2.28)). As for dry Kaolin, a similar relationship exists between $q/(P+1.3P_c)$ and $\ln\varepsilon$.

Based upon the available experimental evidence, Roscoe and Burland (1968) and Hsieh (1987) proposed the concept of horizontal yield surface to include the plastic shear distortion for stress state beneath the state boundary surface. Figure (2.29) shows the elliptical yield surface AB which is part of the modified Cam-Clay surface, while XY is the horizontal yield surface which is associated with the component of the plastic shear deformation which takes place beneath the modified Cam-Clay yield surface with no simultaneous plastic volume change.

Borja (1984) demonstrated the concept of a horizontal deviatoric yield surface within the modified Cam-Clay yield surface. Consider point X is the initial stress state of an overconsolidated soil specimen as shown in Figure (2.30a). Applying a stress increment (dP,dq) on the soil sample such that the final stress state remains inside the modified Cam-Clay yield surface, the plastic shear distortion will increase according to the following equation :

[2.37] $$(\delta\varepsilon^p)_{vp} = \left(\frac{\partial\varepsilon}{\partial\eta}\right)_{vp}\delta\eta,$$

where the suffix vp implies that there is no plastic volumetric strain involved for such a process, the plastic strain-increment vector is therefore normal to the horizontal yield surface (Figure 2.30b). As a result of the plastic shear distortion the horizontal yield

surface XY will expand to a new location X_1Y_1 while the modified Cam-Clay yield surface remains at its initial location. It is hypothesized that only stress probes causing η to increase will induce a plastic shear distortion.

A stress probe that lies within the region between the upward tangent to the elliptical and horizontal yield surface, such as the vector XY, shown in Figure (2.30c), will cause both yield surfaces to expand. This dual expansion results in a net plastic distortion given as:

[2.38] $$(\delta\varepsilon^p)_{vp} = (\frac{\partial\varepsilon}{\partial\eta})_{vp}\delta\eta + (\frac{\partial\varepsilon^p}{\partial v^p})_{\eta}\delta v^p,$$

where the second term in above equation is the contribution from modified Cam-Clay yield surface. Plastic volumetric strain also occurs since the modified Cam-Clay yield surface is engaged for such a stress probe.

Equation (2.38) is derived by applying the associative flow rule to both yield surfaces. The net strain increment vector lies between XN_1 and XN_2, the normals to the two yield surfaces at point X. The net strain increment vector is no longer perpendicular to either one of the two yield surfaces (Figure (2.30d)) and the total flow is no longer associative.

For a stress increment on a sample in state X which lies in the region between the horizontal yield surface and the downward tangent to the modified Cam-Clay yield surface, the first term in equation (2.38) would vanish. The resulting strain increment is then normal to the modified Cam-Clay yield surface (Figure (2.30f). In this case, the modified Cam-Clay yield surface expands but the size parameter η of the horizontal yield surface remains unchanged (Figure (2.30e). Though η remains unchanged, note that the horizontal yield surface expands with the volumetric yield surface.

If the stress increment vector is pointing in the directions other than those discussed above, only elastic strain can take place (Figures (2.30g) and (2.30h)).

2.6 SUMMARY:

In this chapter, the literature review covered the contributions of the researchers in the geotechnical field since Terzaghi (1941) and Taylor (1942) untill now to develop a unified phenomenological model to describe the stress-strain-time behaviour of cohesive soil under different boundary conditions.

The first part of the review demonstrates the one-dimensional phenomenological models developed to determine the volumetric component (Taylor 1942; Bjerrum 1967; Mesri and Goldewski 1977) and the deviatoric component (Kondner 1963; Duncan et al. 1980; Ladd and Foott 1974; Singh and Mitchell 1968; Tavenas et al. 1978; Mesri et al. 1981) of the soil deformation.

As the creep behaviour of cohesive soil is the main object of this study, the second part of this chapter is devoted to discuss different approaches used by the researchers to improve and provide better understanding of the creep mechanism in cohesive soil. One of these approaches is the phenomenological approach which led to the developing of valuable one-dimensional constitutive equations to simulate the creep behaviour of cohesive soil (Taylor (1942); Singh and Mitchell (1968)). These one-dimensional constitutive equations were later generalized into three dimensions (i.e. as in the proposed effective stress model in this study) in order to provide a numerical model for the analysis of the time-dependent behaviour of cohesive soil under the effect of different boundary conditions in a three-dimensional stress space.

Based on the one-dimensional phenomenological model, a constitutive model was developed by Kavazanjian (1978) for the time-dependent deformation behaviour of cohesive soil more general than the available models. The model unified the existing phenomenological models for the stress-strain-time behaviour of cohesive soils under specific boundary conditions. Separate, but not independent, deviatoric and volumetric model components have been defined. Each model component is assumed to consist of immediate and delayed contribution as suggested by Bjerrum (1967). The volumetric model was developed by generalizing Bjerrum's one-dimensional compression model to encompass the entire range of principal stress ratios. The deviatoric model uses Ladd and Foott's (1974) normalized soil properties concept in conjunction with Kondner's (1963) hyperbolic formulation to describe immediate deformation. Delayed deviatoric deformations are described by the Singh-Mitchell (1968) creep equation.

Finally, the concept of critical state theory is demonstrated in term of the modified Cam-Clay theory. The modified Cam-Clay model is used in the proposed effective stress time-dependent model in this study to calculate the time-independent deformation component of cohesive soil. The idea of including a horizontal yield surface in the modified Cam-Clay theory is adopted, which is used to predict the plastic shear distortion that occurs without volume change below the state boundary surface (Roscoe and Burland 1968; Wroth and Loudon 1967; Borja 1984).

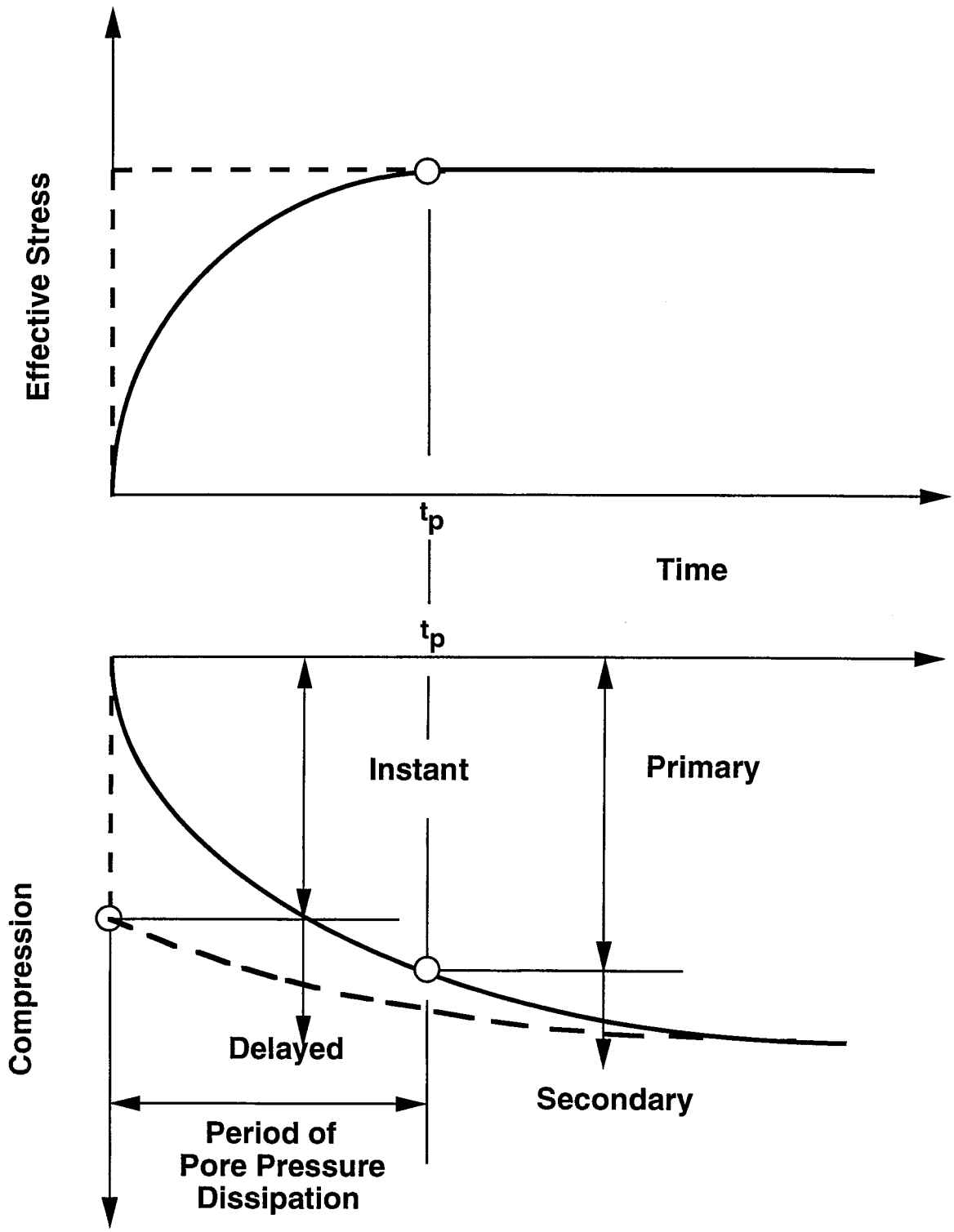

Figure (2.1) Instant and delayed deformation (modified after Bjerrum (1967)).

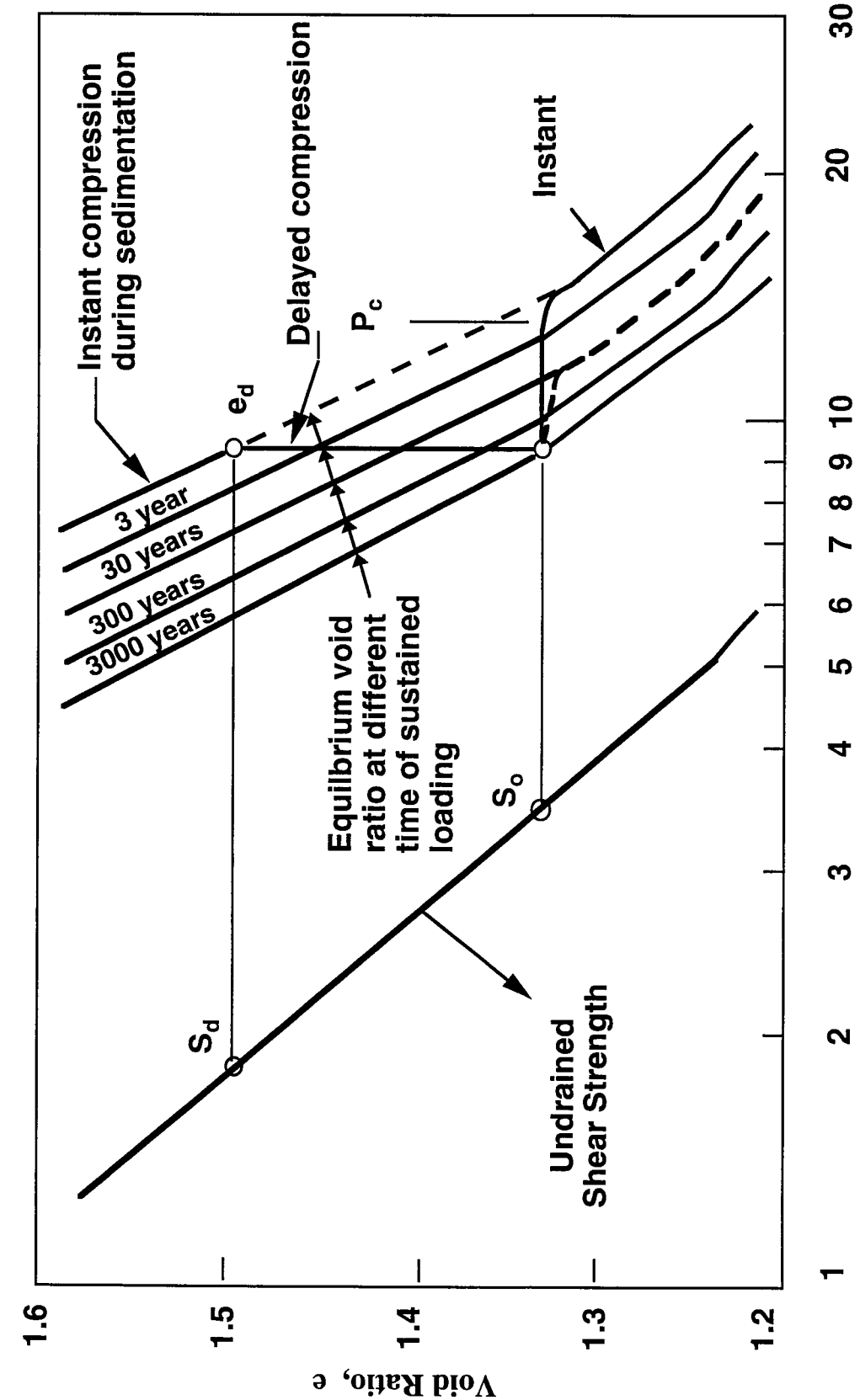

Figure (2.2) Bjerrum's model for one-dimensional compression (modified after Bjerrum (1967)).

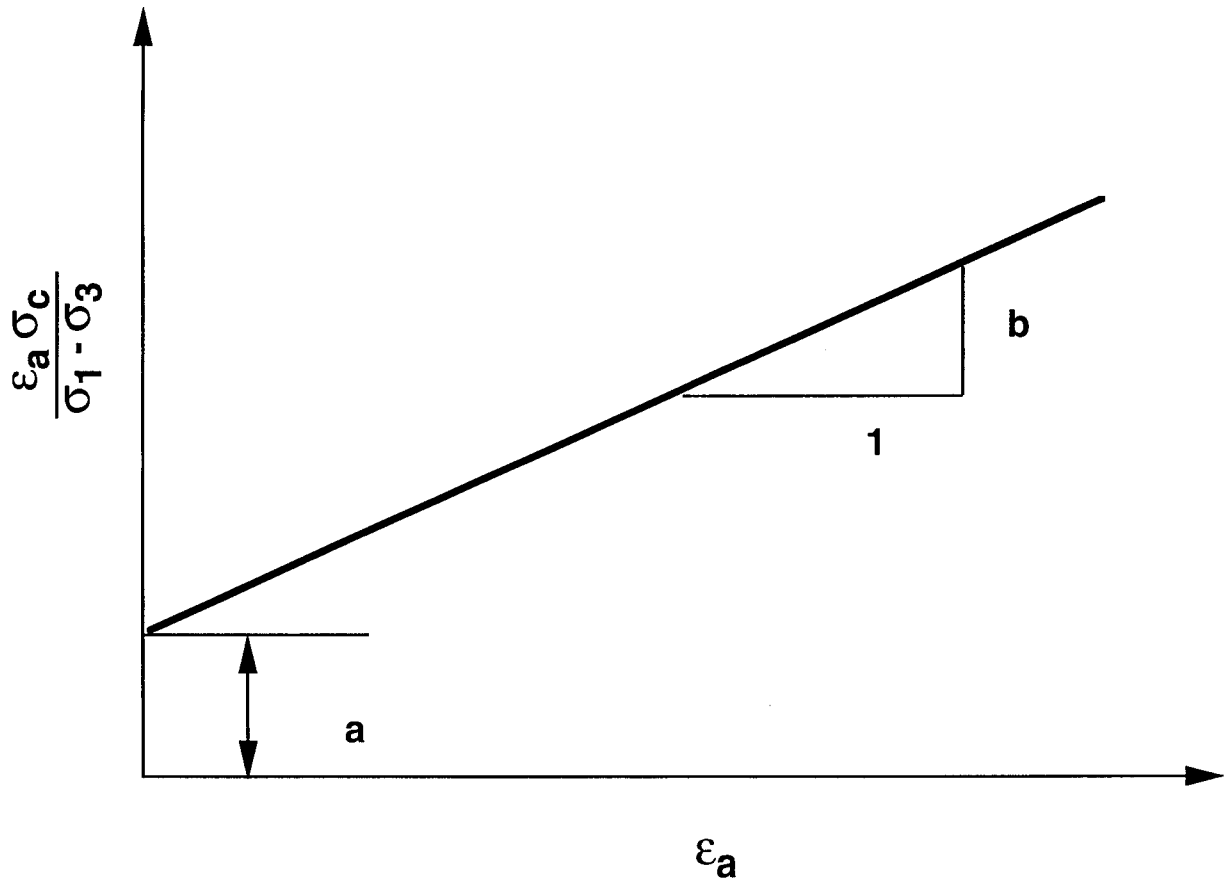

Figure (2.3) Transformed hyperbolic curve.

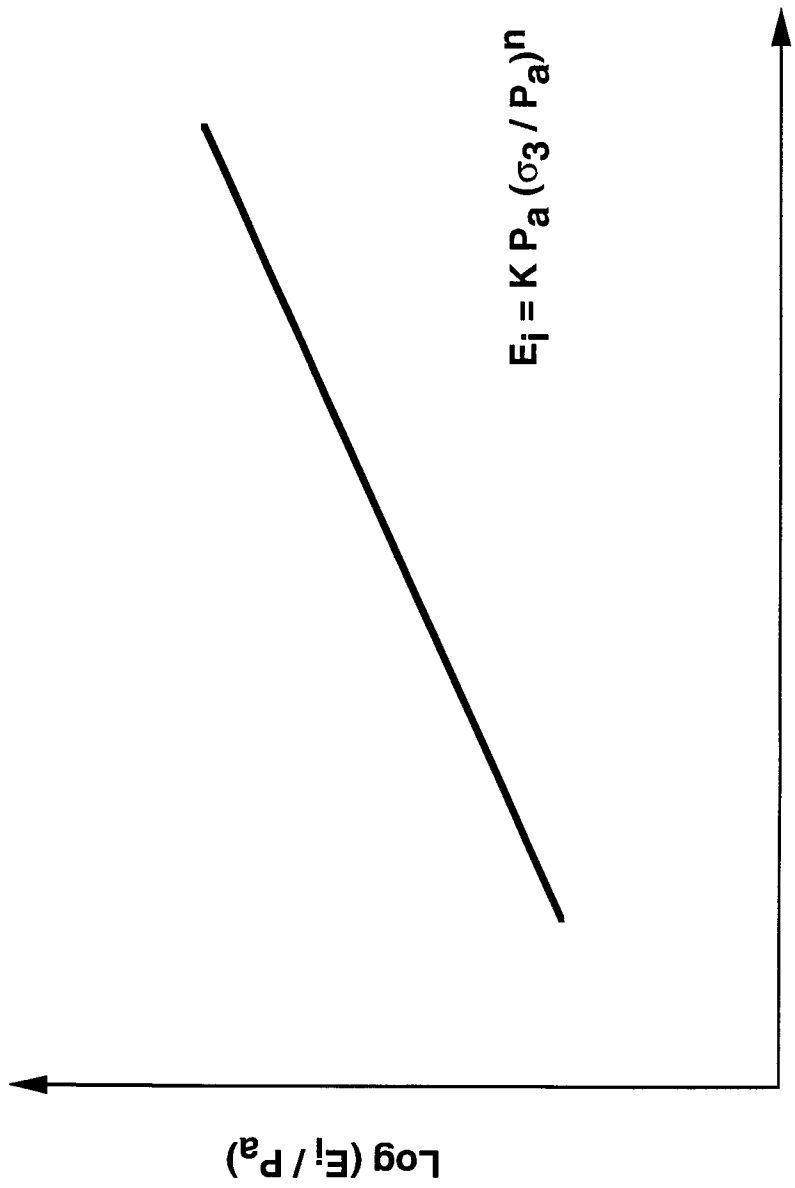

Figure (2.4) Variation of initial tangent modulus with confining pressure.

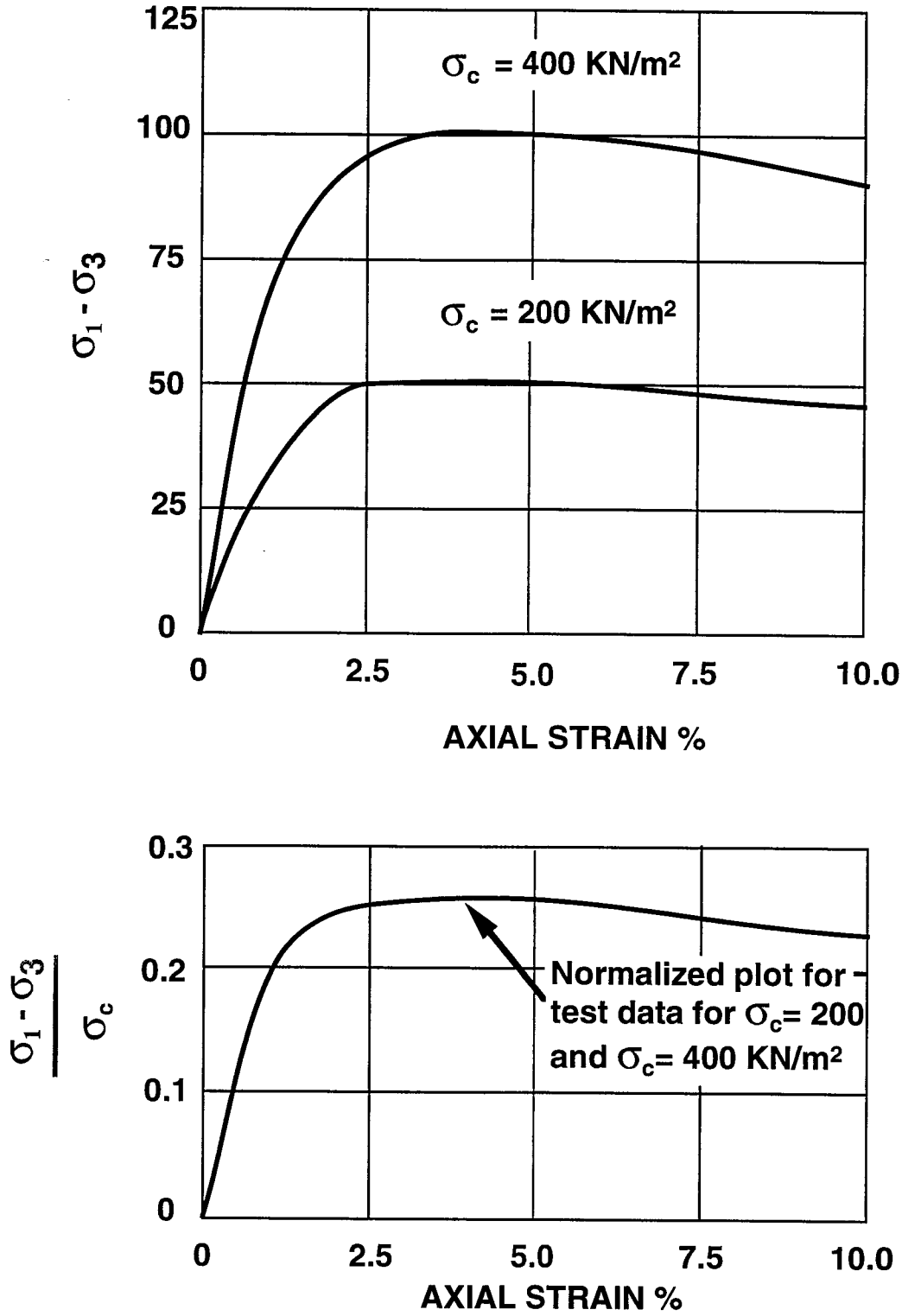

Figure (2.5) Normalized soil properties (modified after Ladd and Foott(1974)).

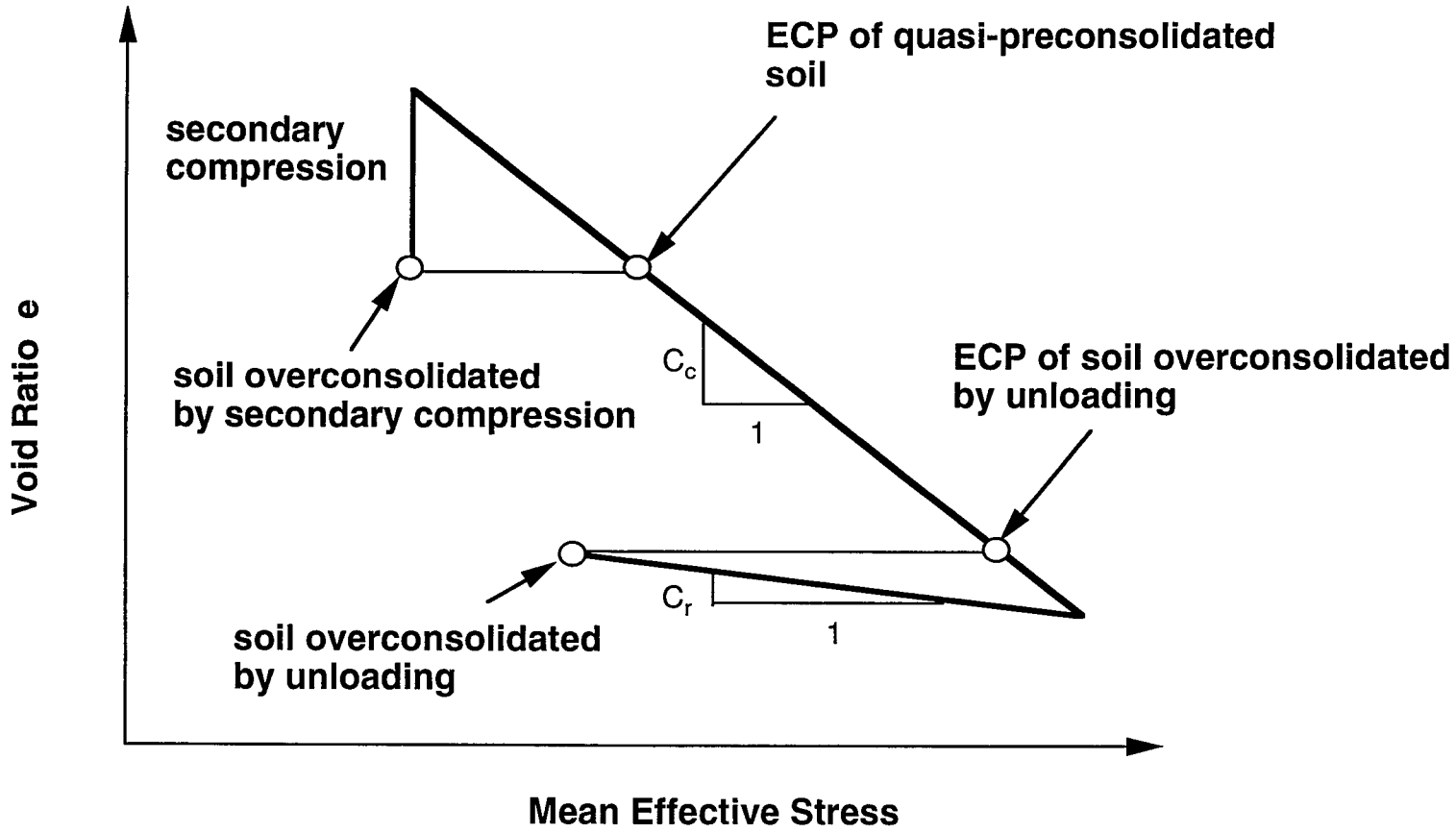

Figure (2.6) Equivalent consolidation pressure (ECP) concept (modified after Hsieh (1987)).

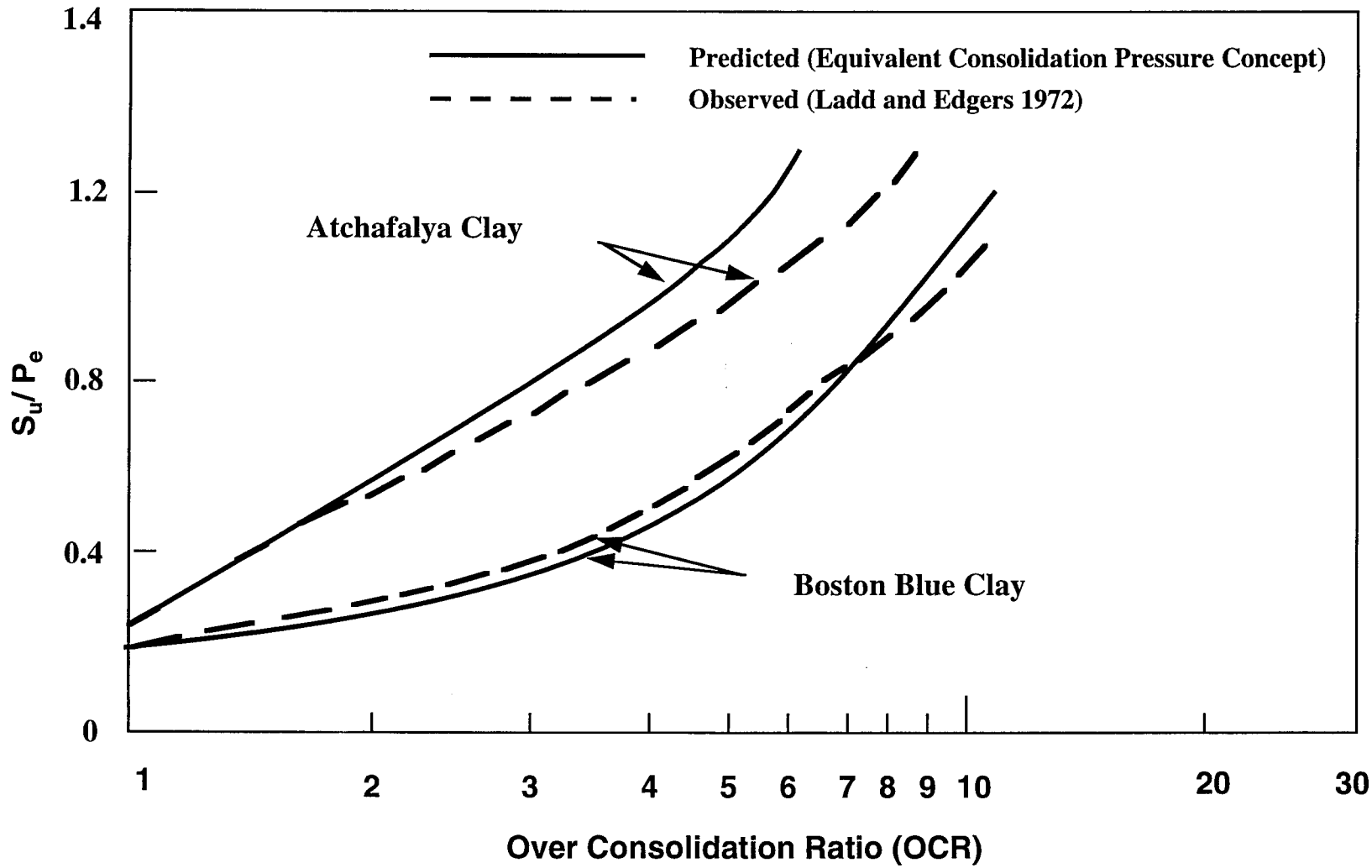

Figure (2.7) The variation of undrained shear strength with OCR (modified after Kavazanjian, Mitchell and Bonaparte (1980)).

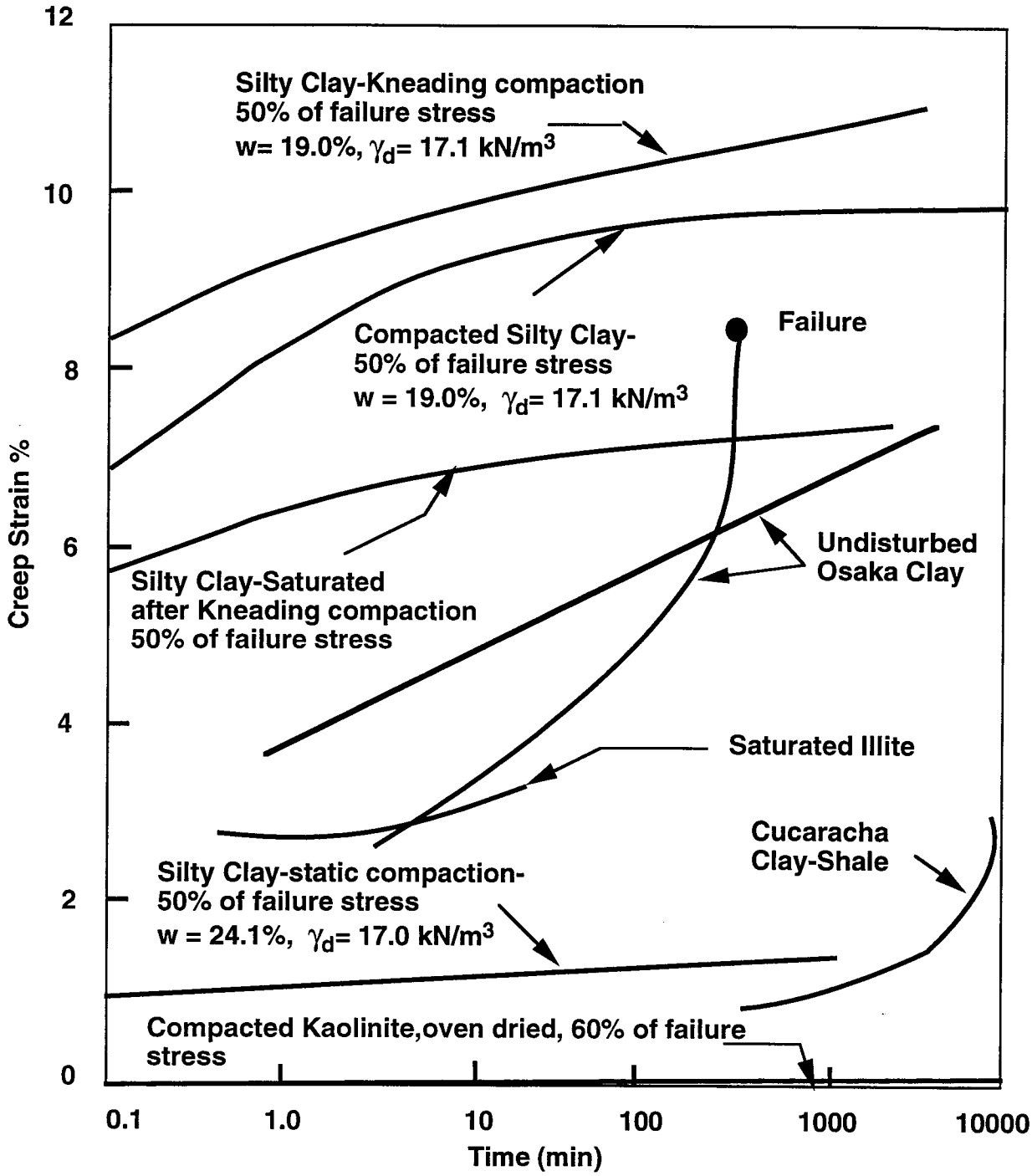

Figure (2.8) Variation of creep behaviour in soils (modified after Mitchell and Campanella (1963)).

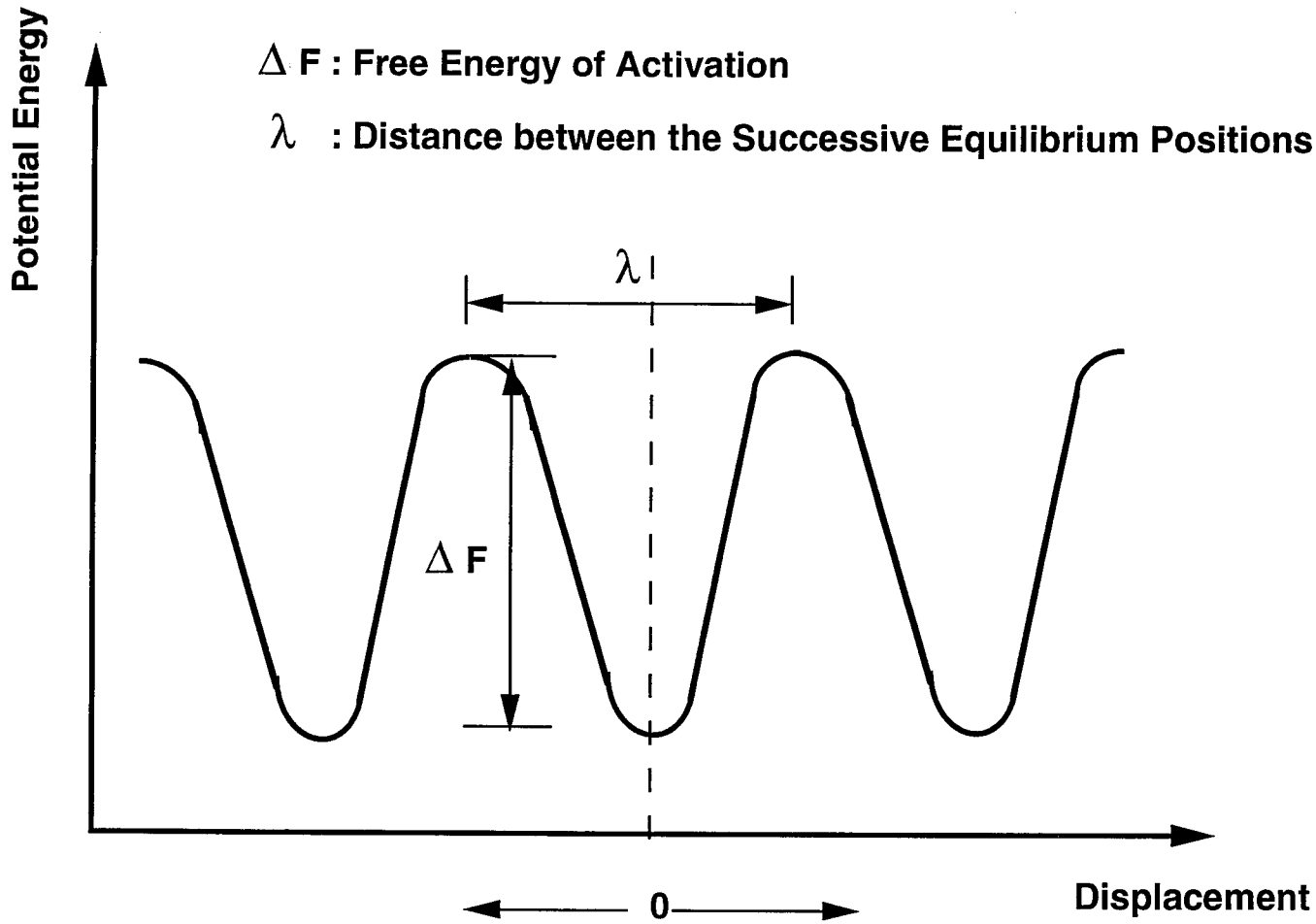

Figure (2.9) Energy bariers and activation energy.

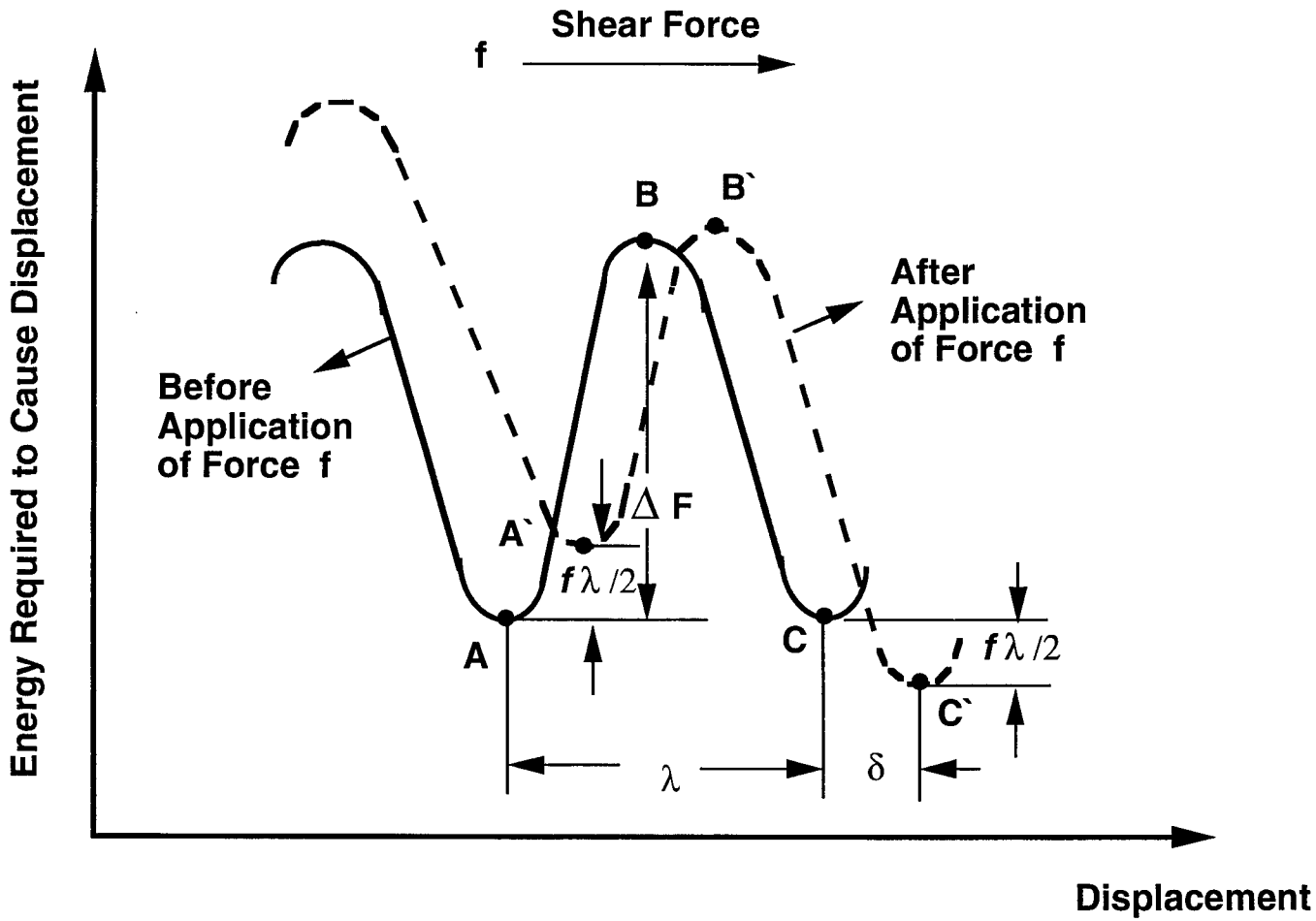

Figure (2.10) The effect of a shear force on energy barriers.

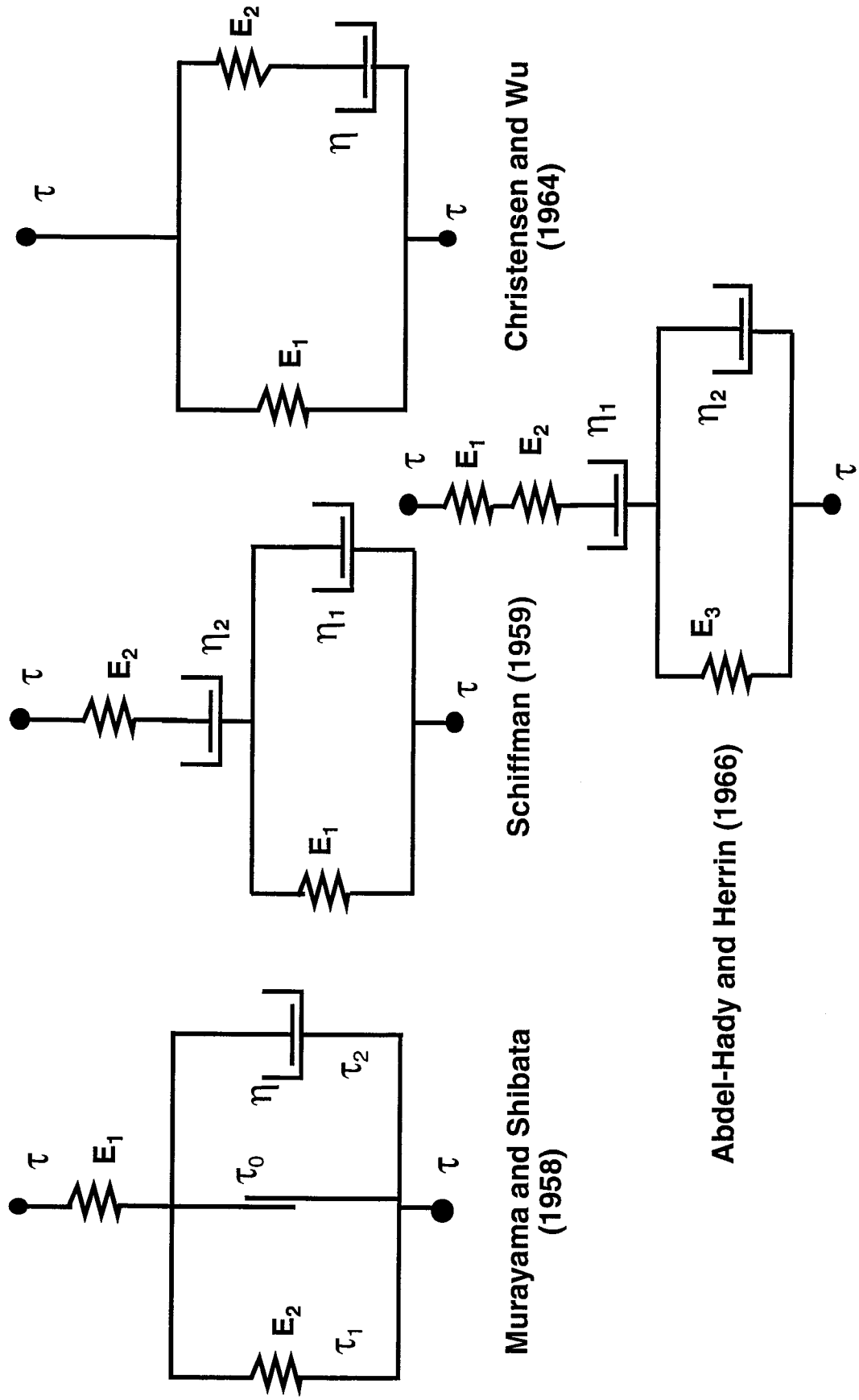

Figure (2.11) Different rheological models proposed for characterization of the stress-strain-time behaviour of soil.

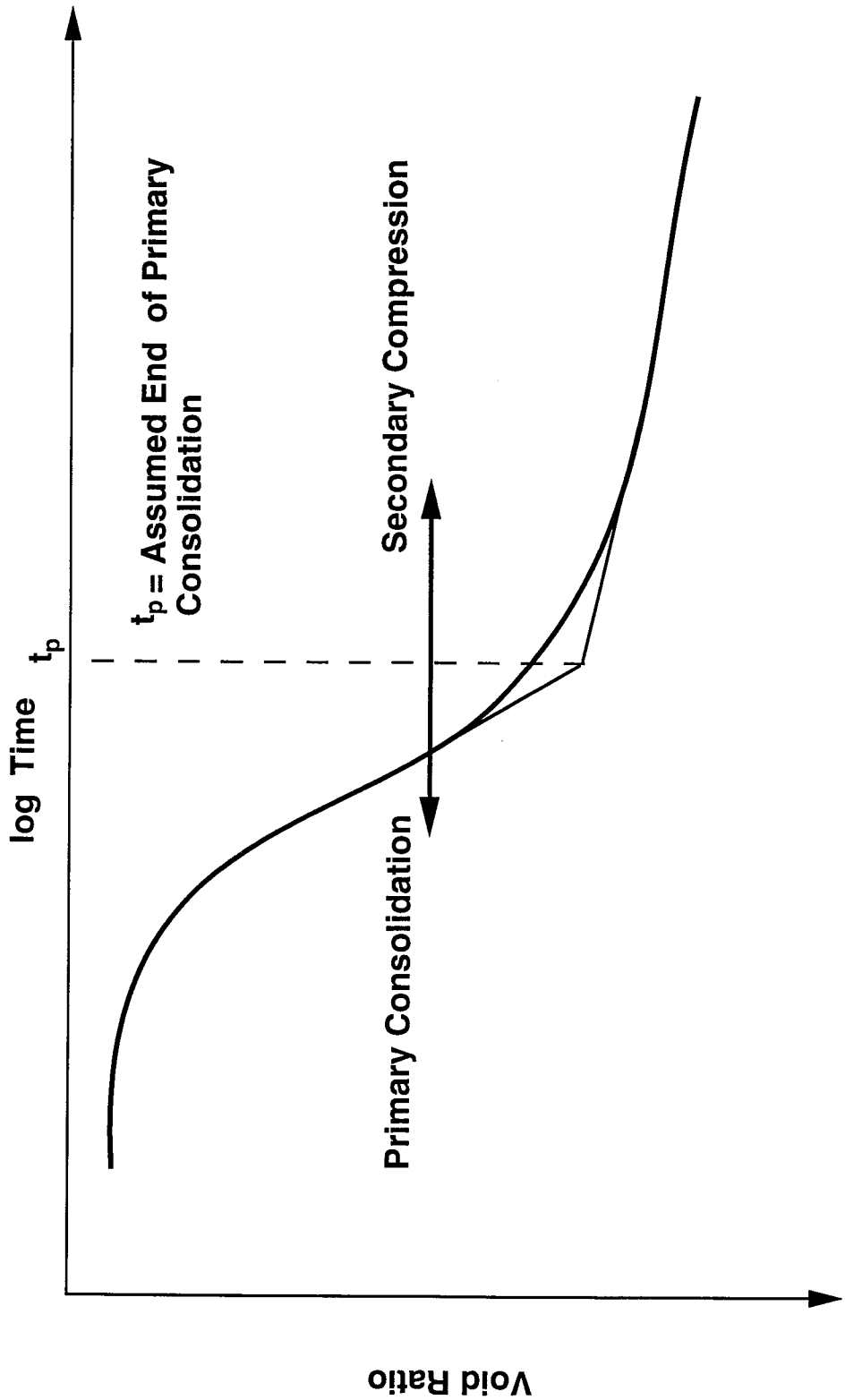

Figure (2.12) Idealize relationship between void ratio and logarithm of time showing primary consolidation and secondary compression.

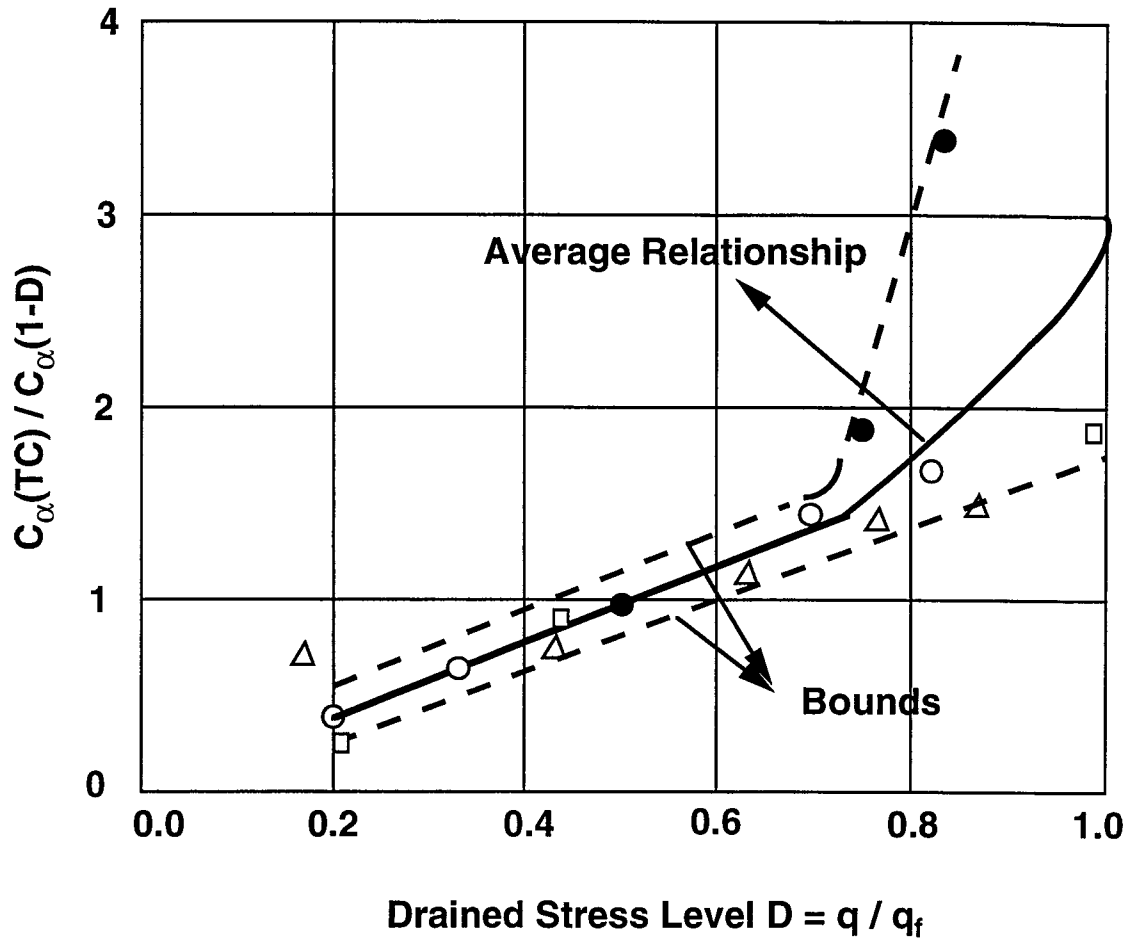

SYMBOL	RESEARCHERS	CLAY	PI %
●	Barden (1969)	Remoulded Frodsham Clay *	——
□	Bishop and Lovenbury (1969)	Normally Consolidated Pancone Clay (Pisa)	47
△	Bishop and Lovenbury (1969)	Over Consolidated London Clay (Hendon)	47
○	Murayama and Shibata (1961)	Normally Consolidated Osaka Clay *	43

* refers to an assumed drained creep strength, q_f

Figure (2.13) Variation of coefficient of consolidation with deviatoric stress level (modified after Fuleihan and Ladd (1976)).

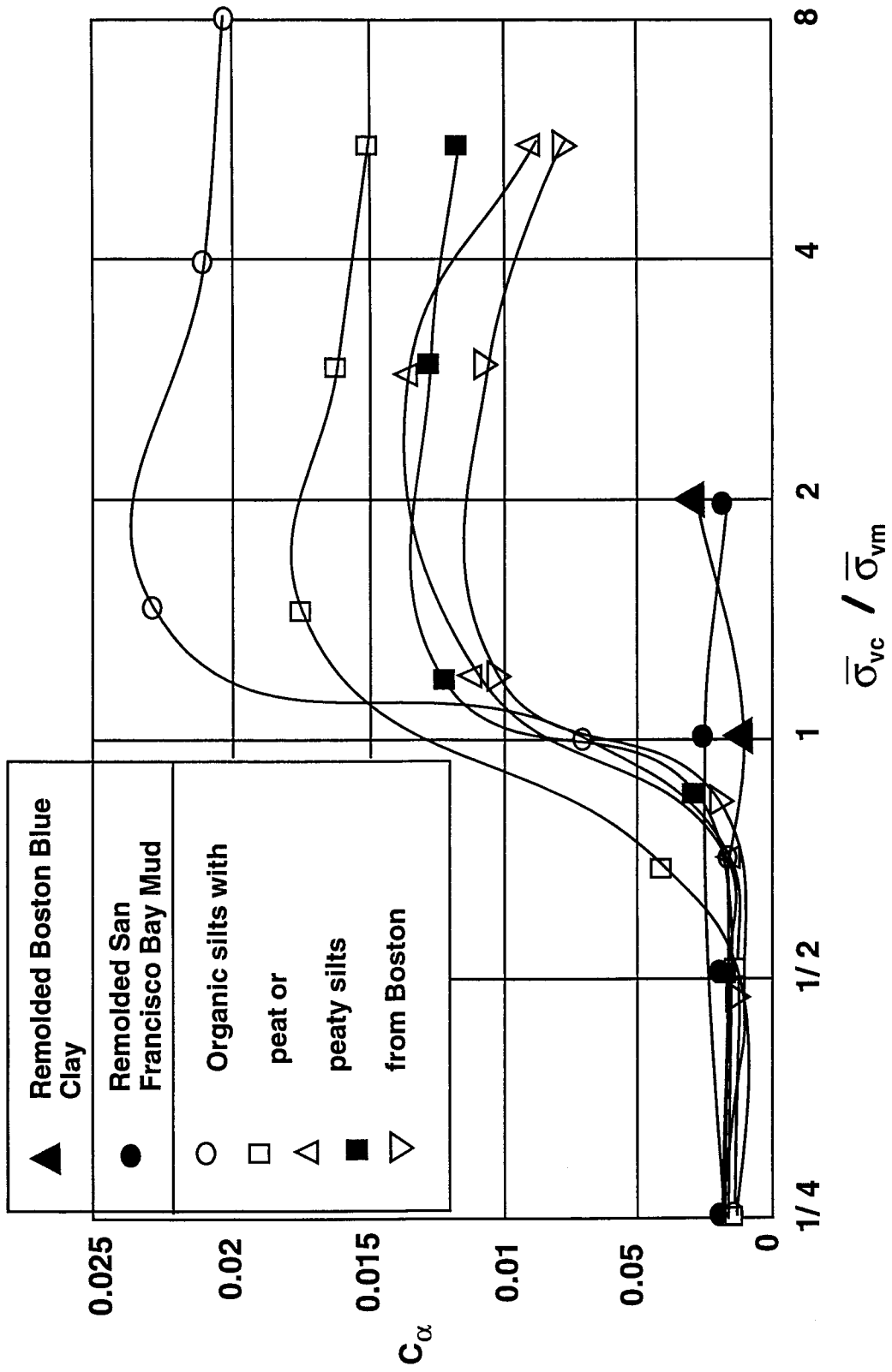

Figure (2.14) Effect of precompression on rate of secondary compression (modified after Ladd and Preston (1965)).

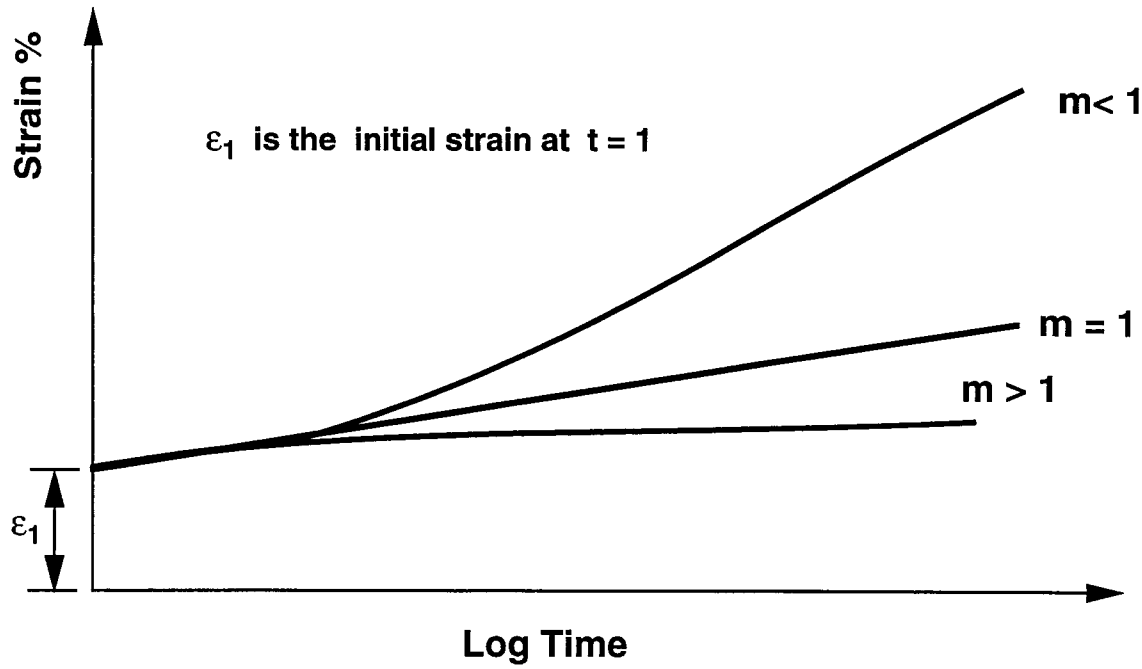

Figure (2.15a) Schematic representation of Singh-Mitchell creep function.

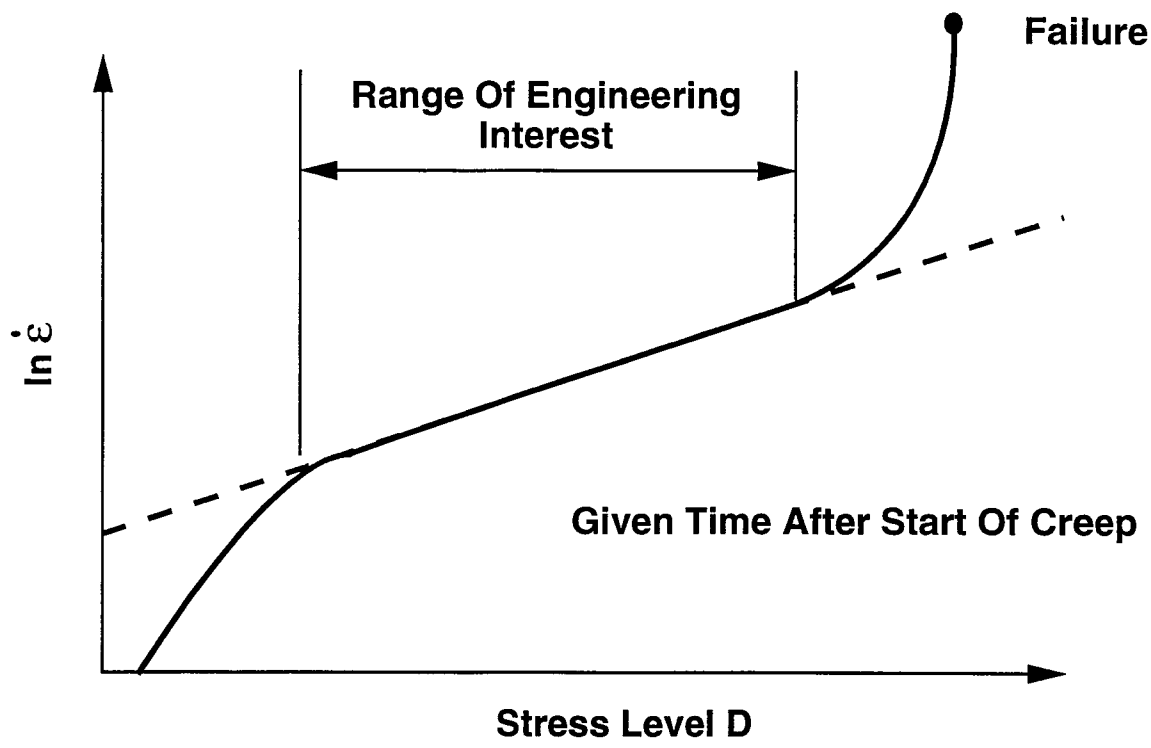

Figure (2.15b) Influence of deviatoric stress level on creep strain rate.

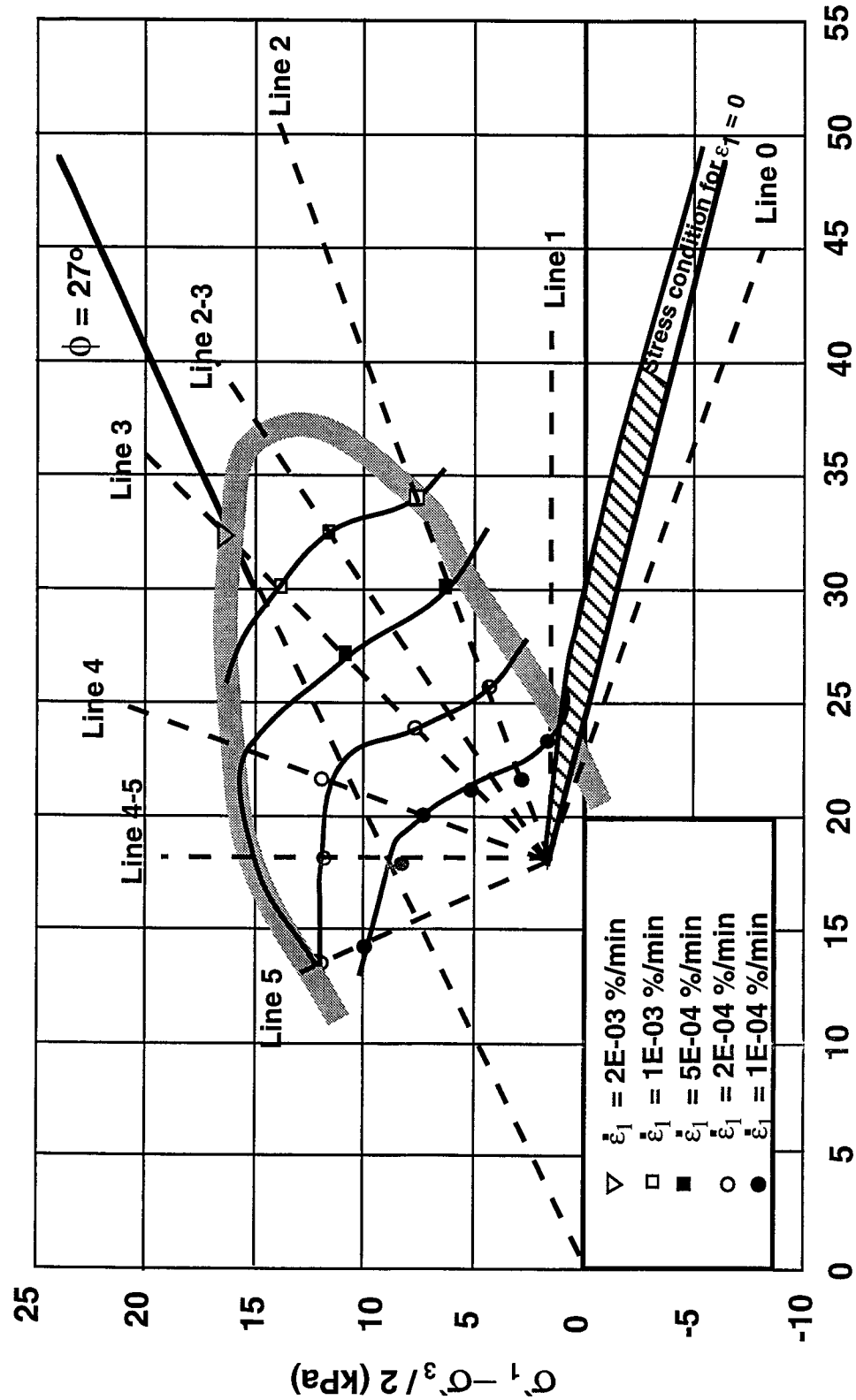

Figure (2.16) Lines of equal shear strain rates in the stress space for drained and undrained creep tests, overconsolidated Saint-Alban clay (modified after Tevanas et al. (1978)).

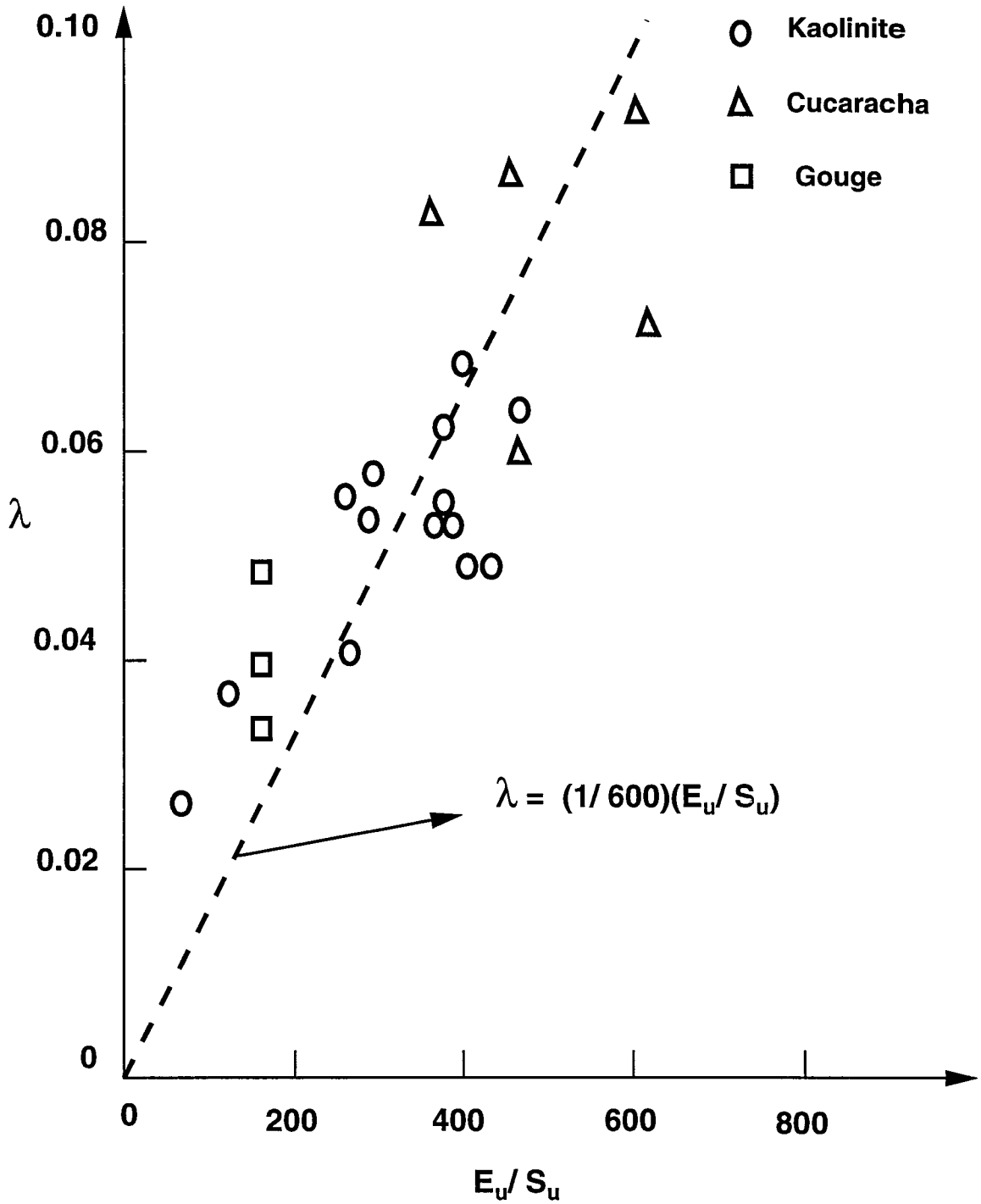

Figure (2.17) Relationship between λ and E_u/S_u (modified after Mesri et al. (1981)).

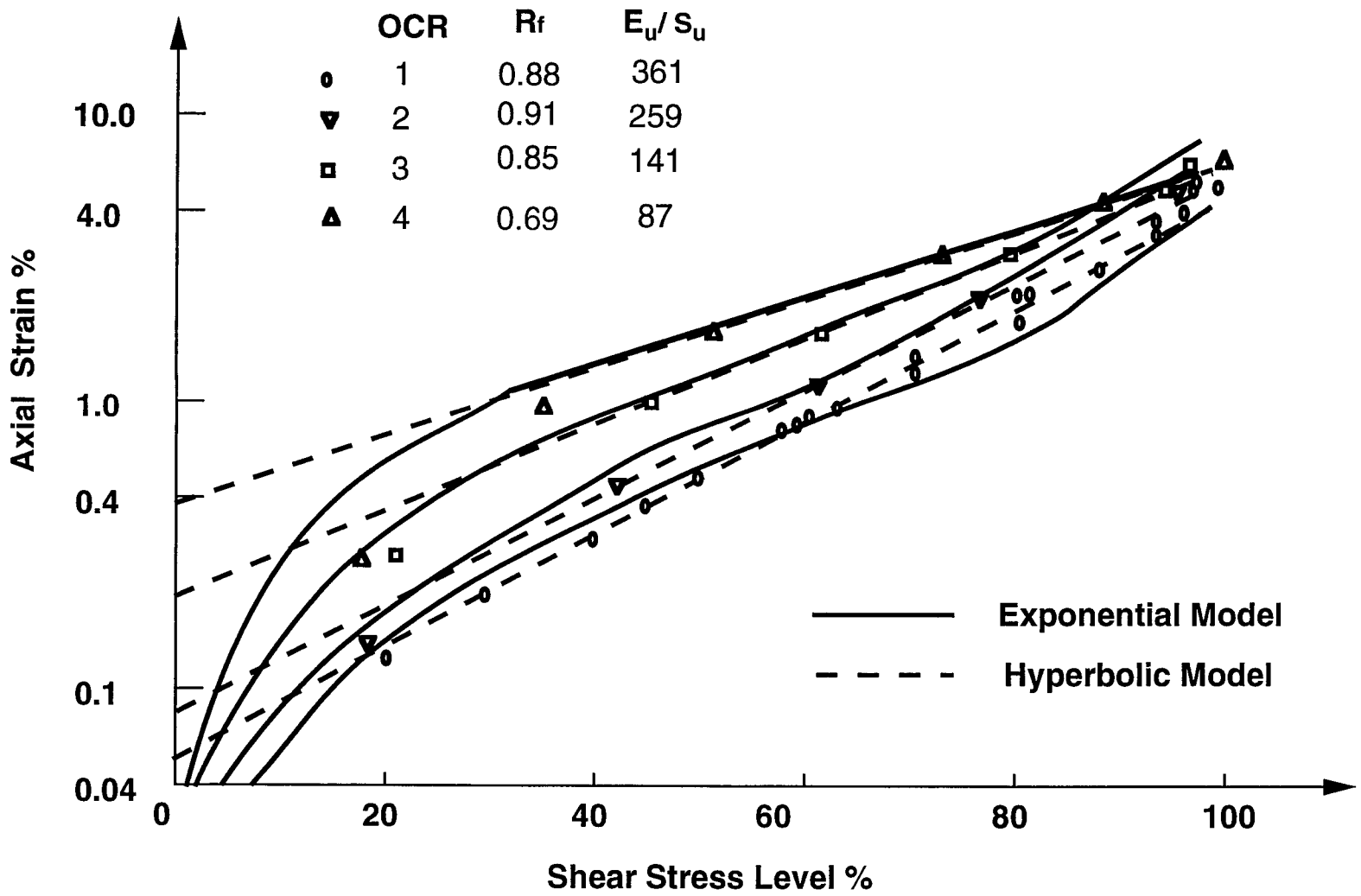

Figure (2.18) Exponential and hyperbolic modelling of constant load test on kaolinite at t_1= 60 min (modified after Mesri et al. (1981)).

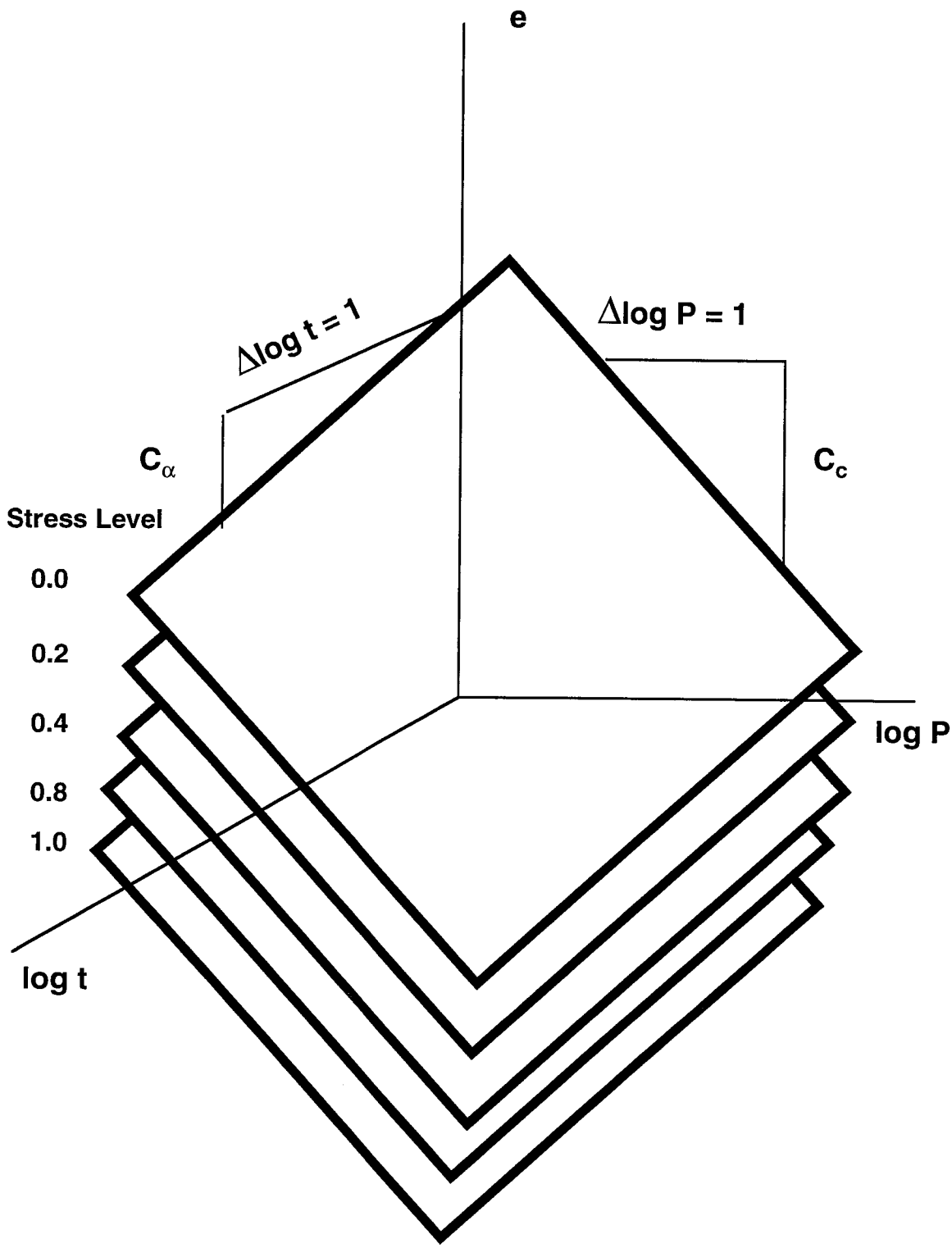

Figure (2.19) Kavazanjian's general volumetric model (modified after Kavazanjian (1978)).

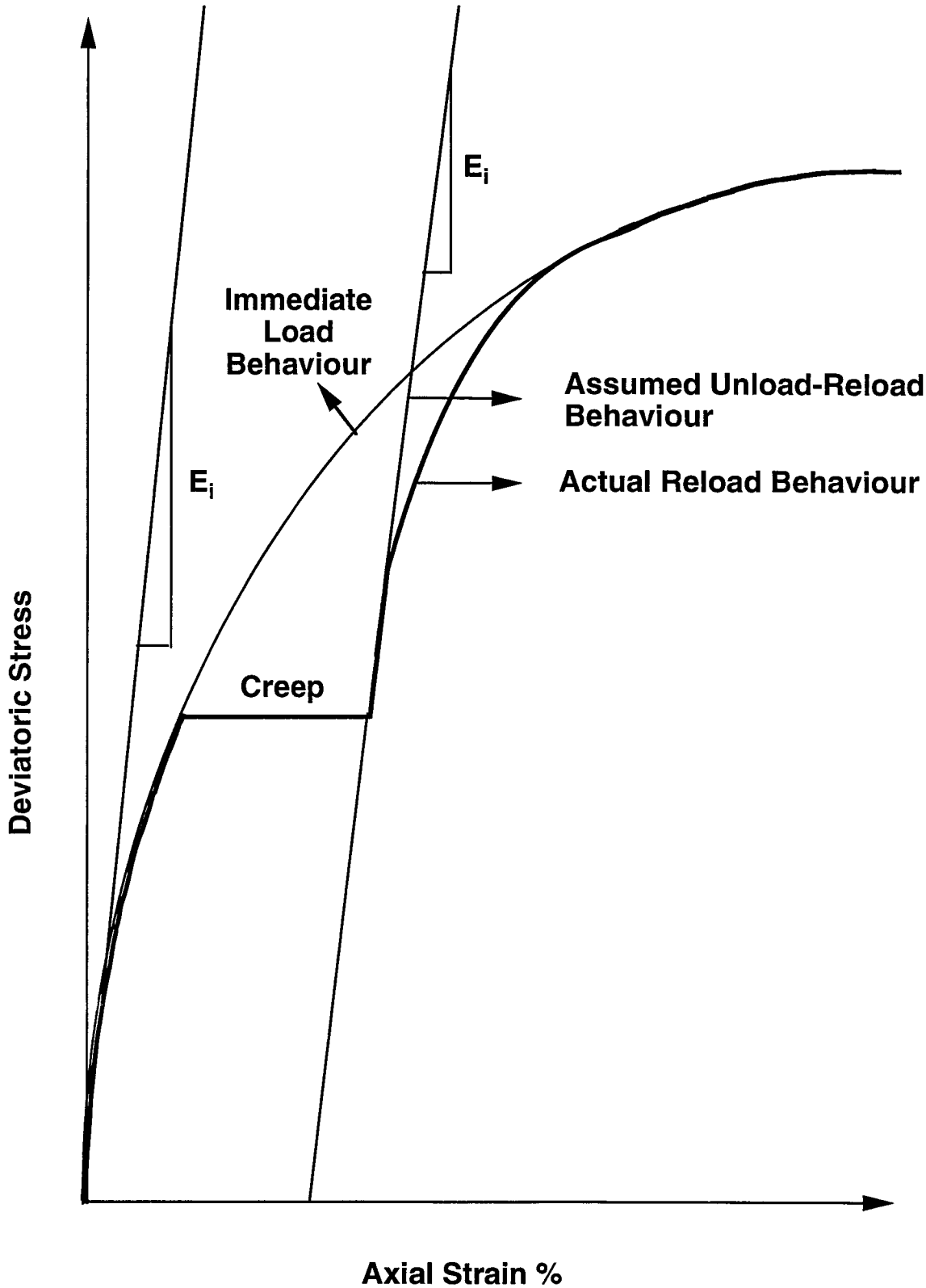

Figure (2.20) Kavazanjian's general deviatoric model (modified after Kavazanjian (1978)).

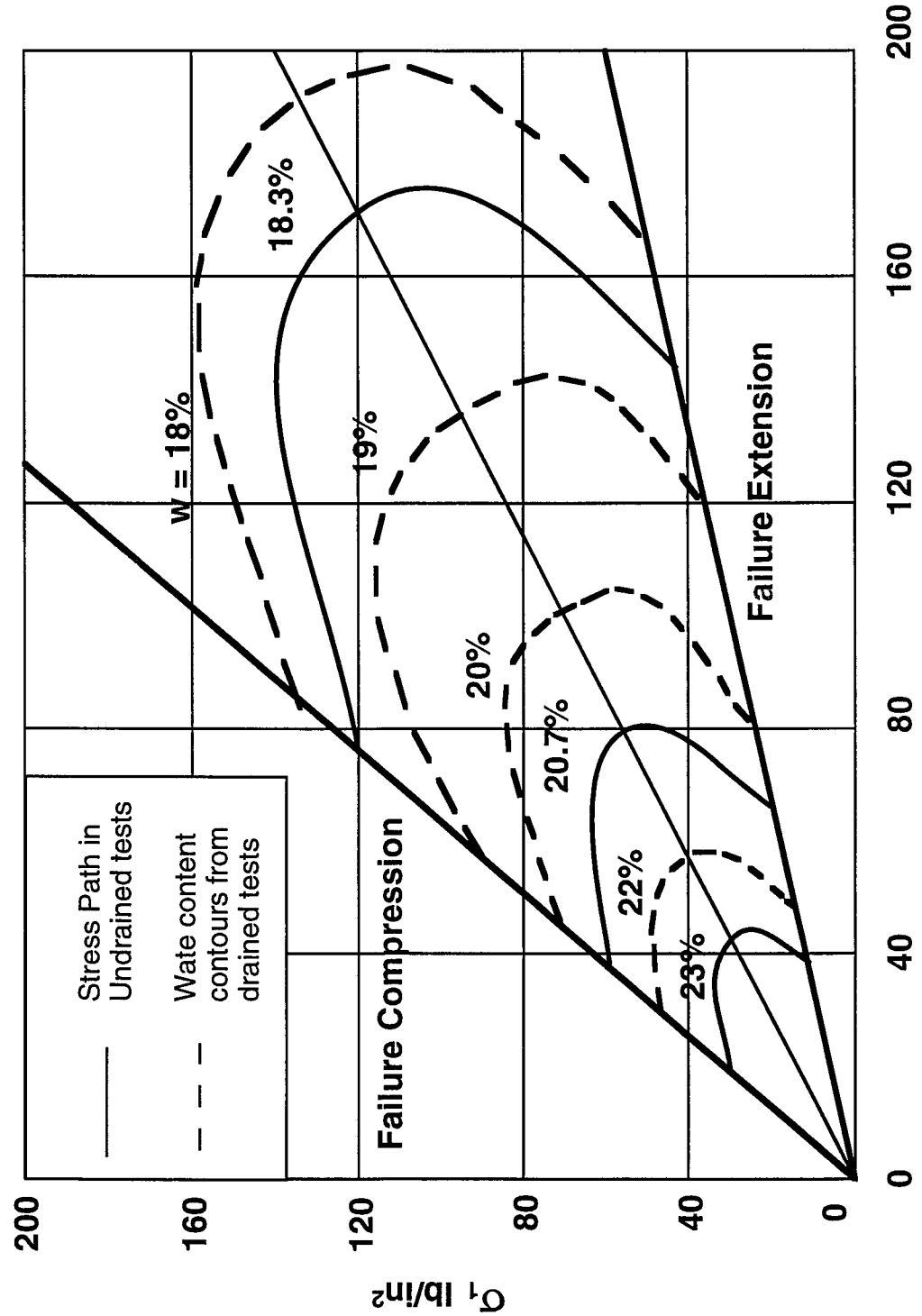

Figure (2.21) Triaxial test results on remoulded clay samples (modified after Henkel D.J. (1960)).

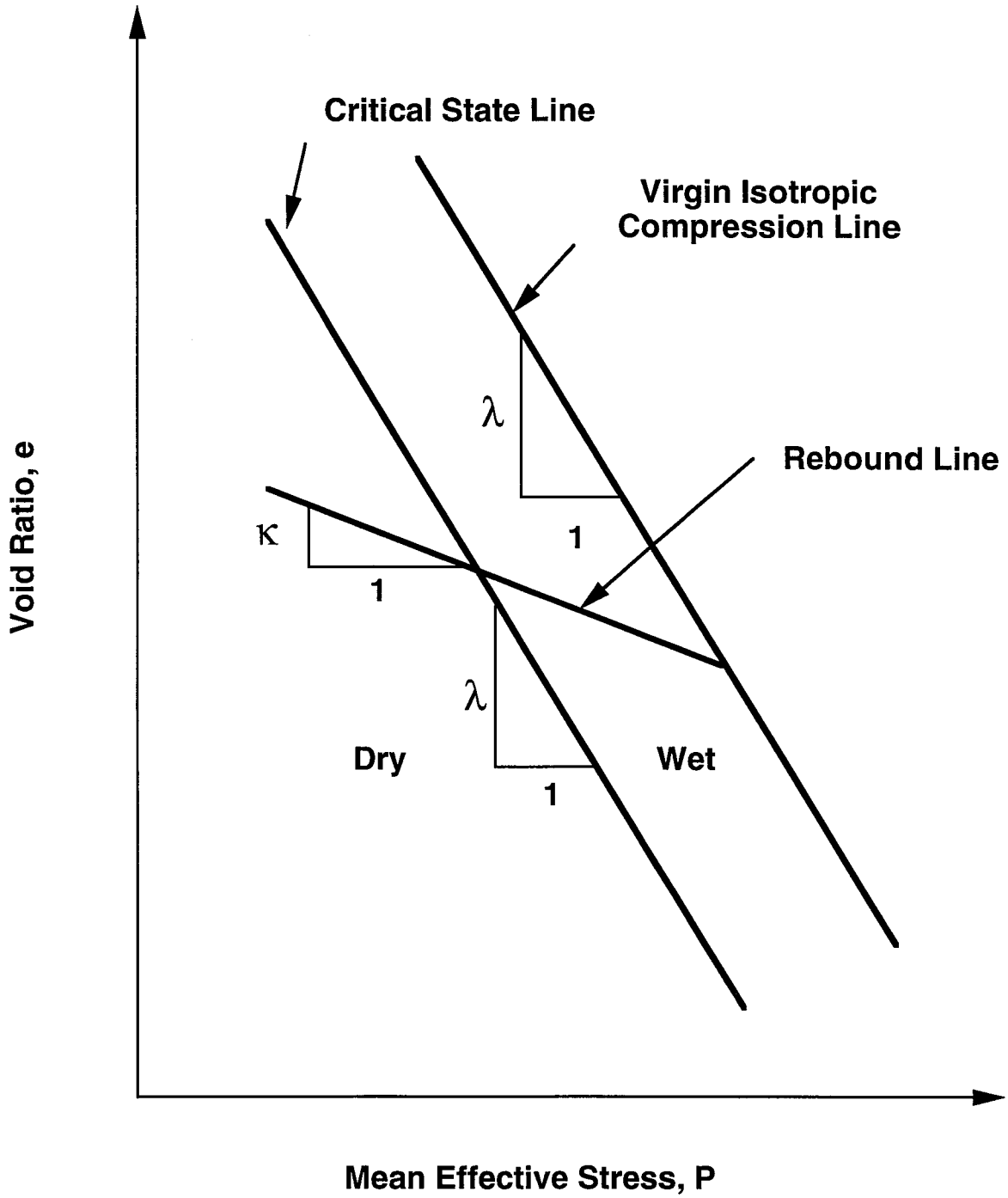

Figure (2.22) Consolidation curves on e-ln P space.

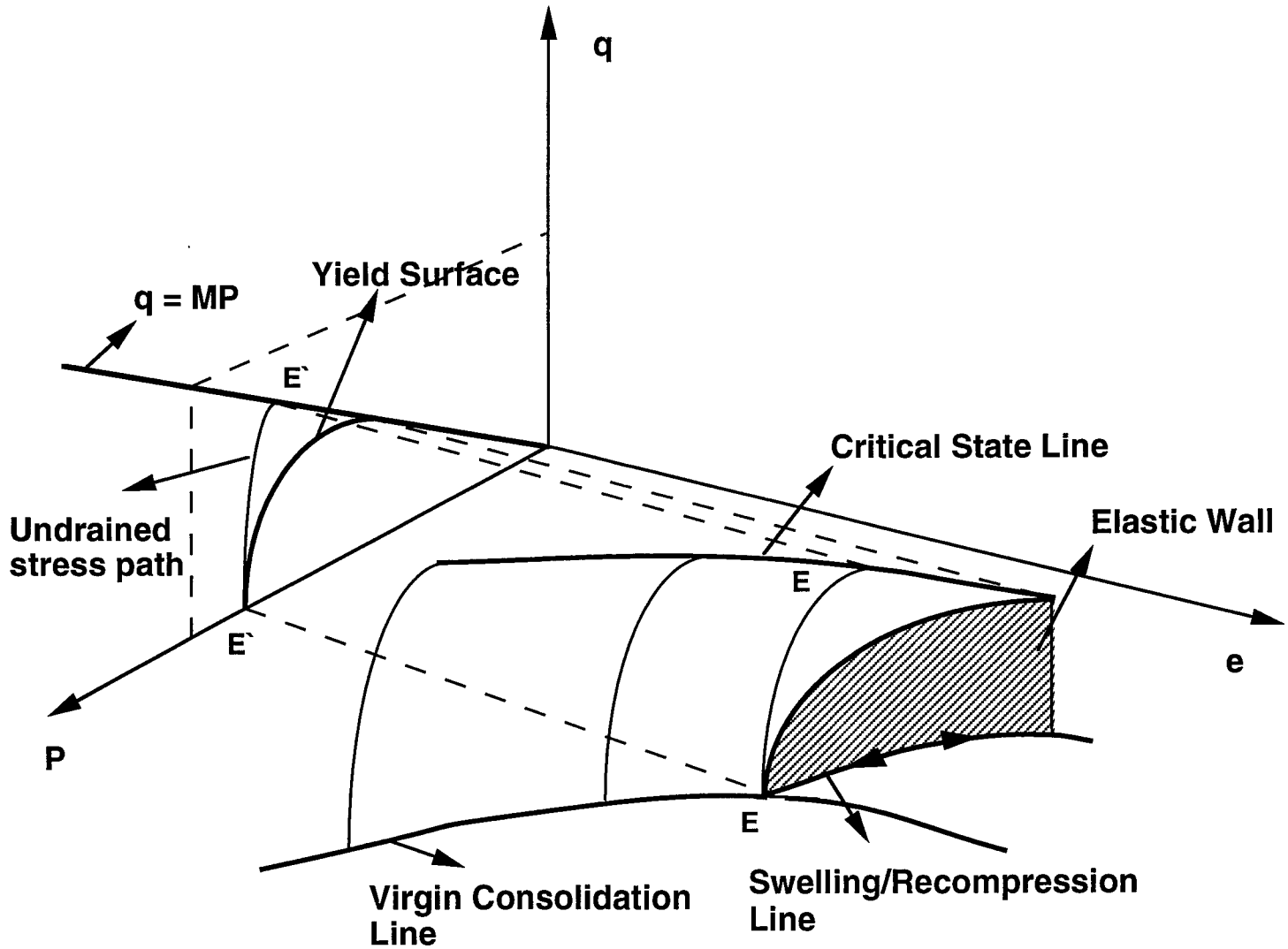

Figure (2.23) The state boundary surface.

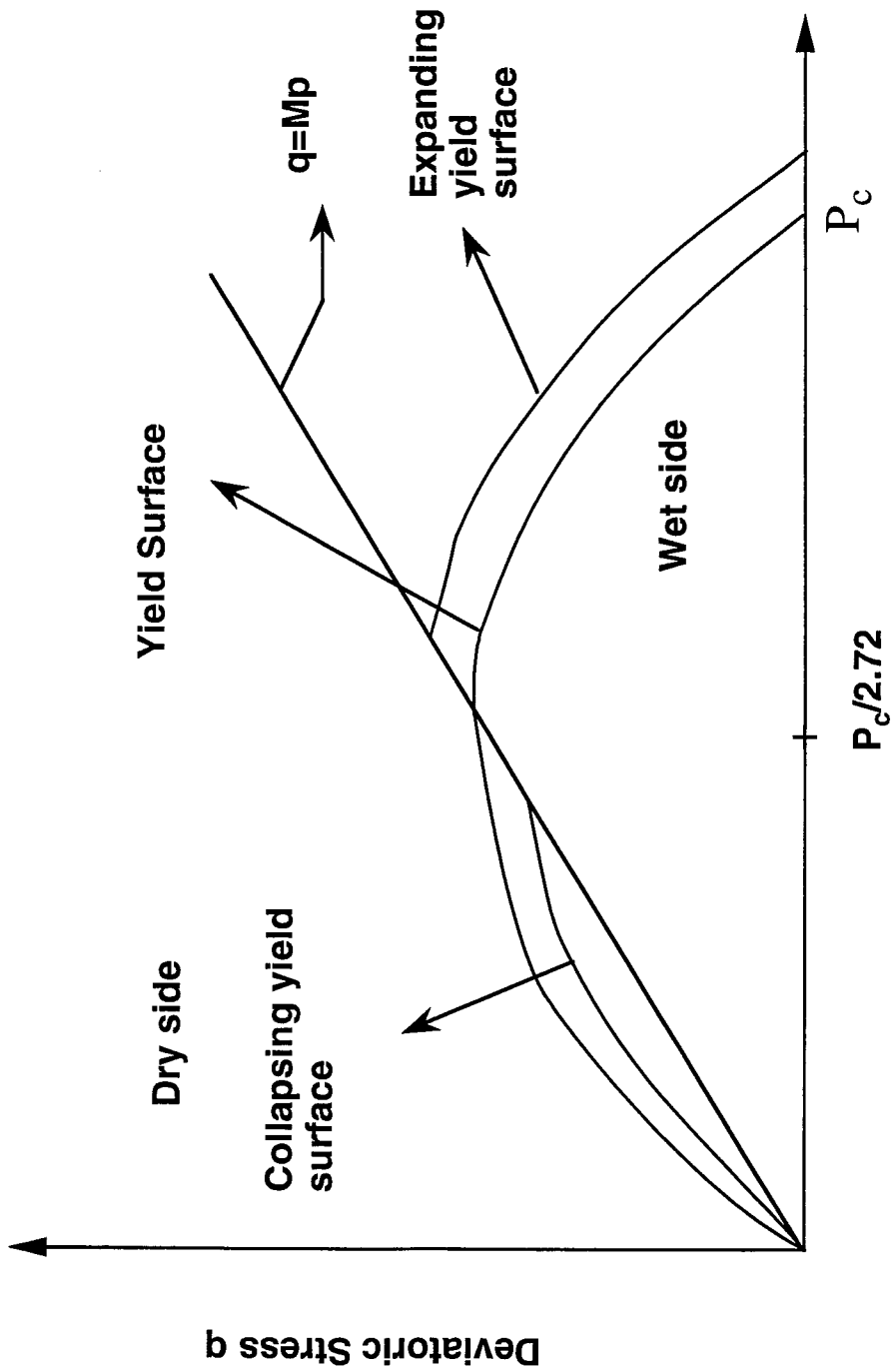

Figure (2.24) Yield surface for original cam-clay model.

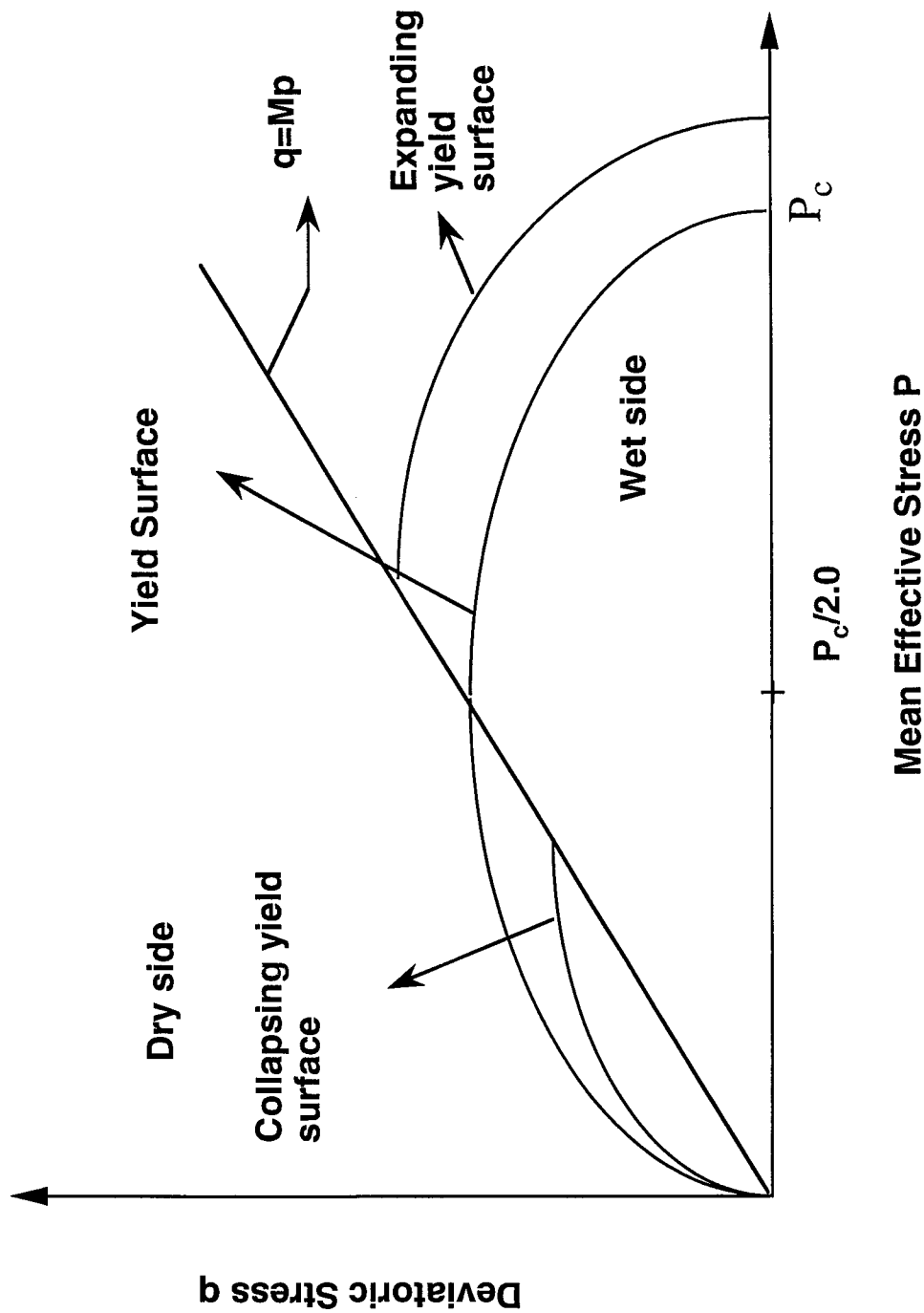

Figure (2.25) Yield surface for modified cam-clay model.

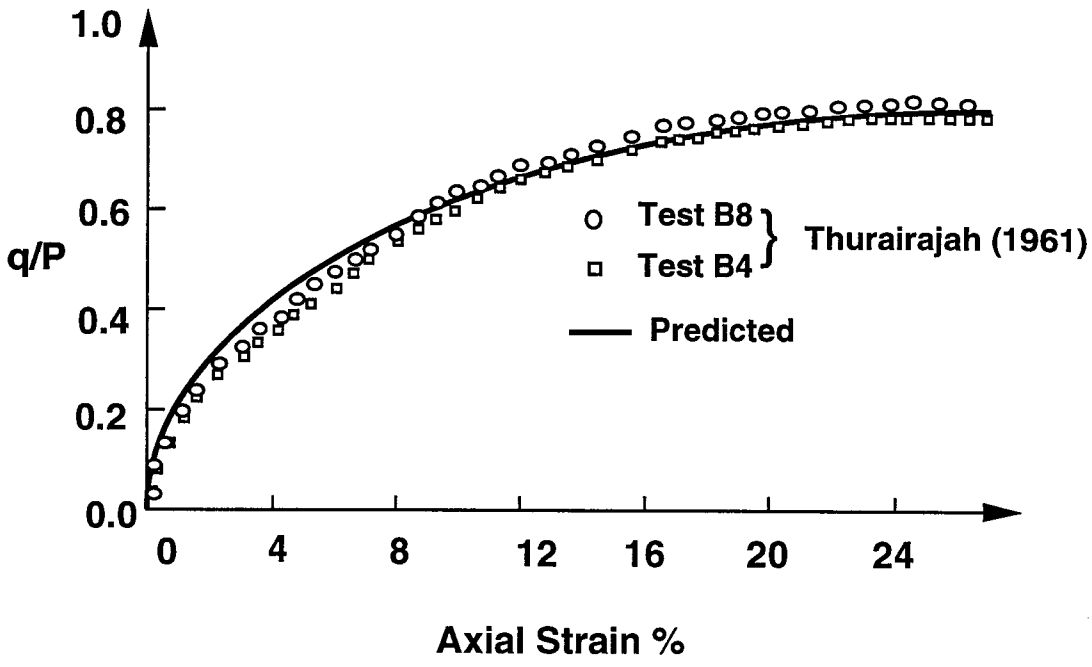

(a)

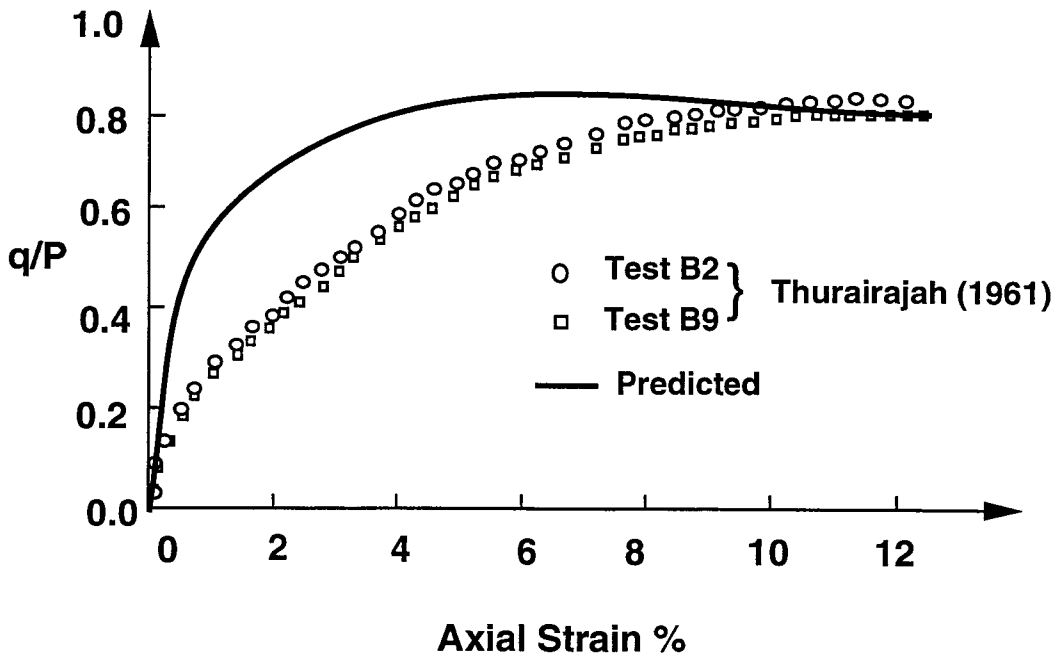

(b)

Figure (2.26) Comparison of experimental and theoretical stress-strain relationship for Kaolin a) drained tests, b) undrained tests (modified after Burland (1965)).

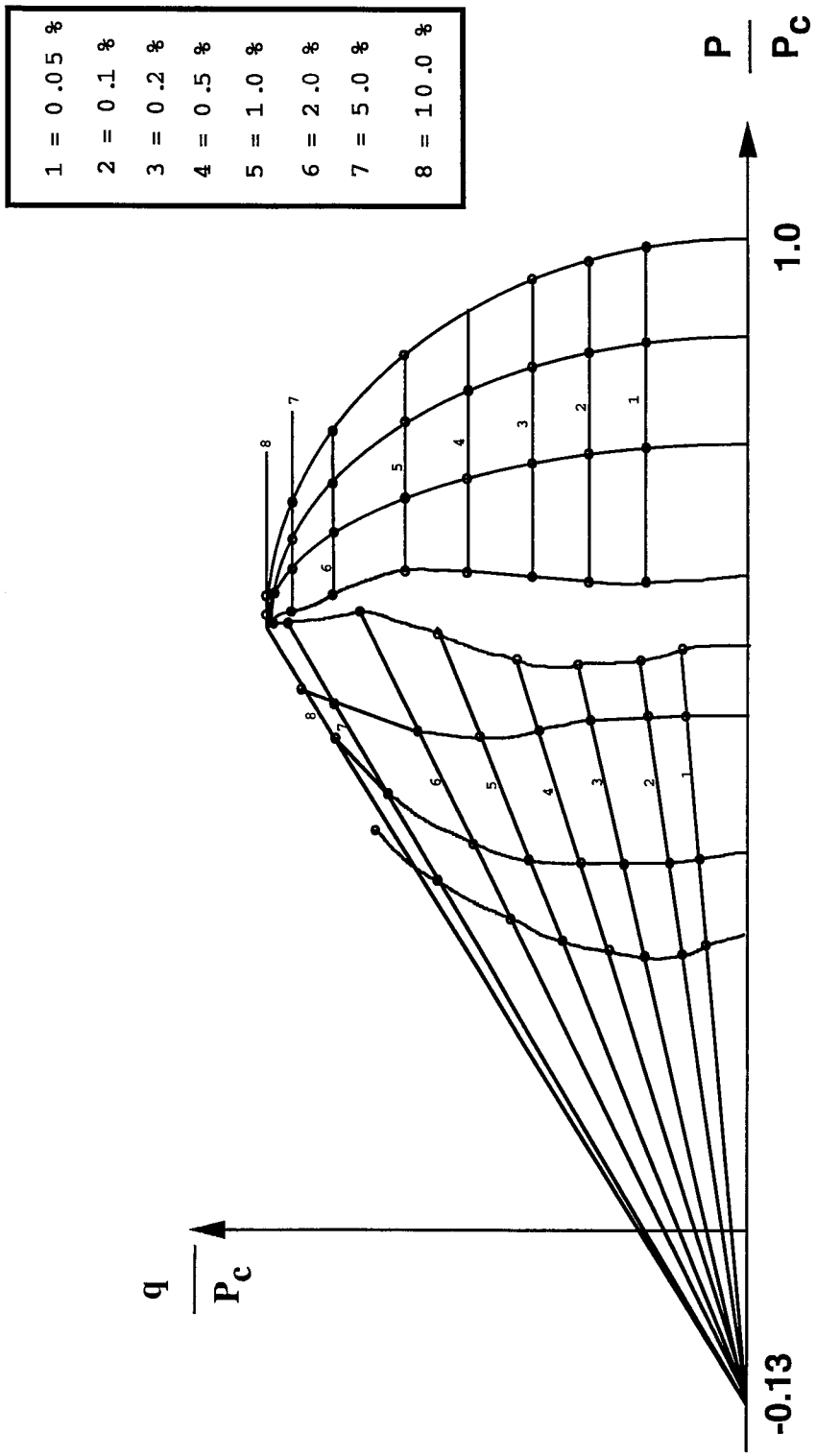

Figure (2.27) Stress paths and strain contours for undrained triaxial tests on Kaolin (modified after Loudon (1967)).

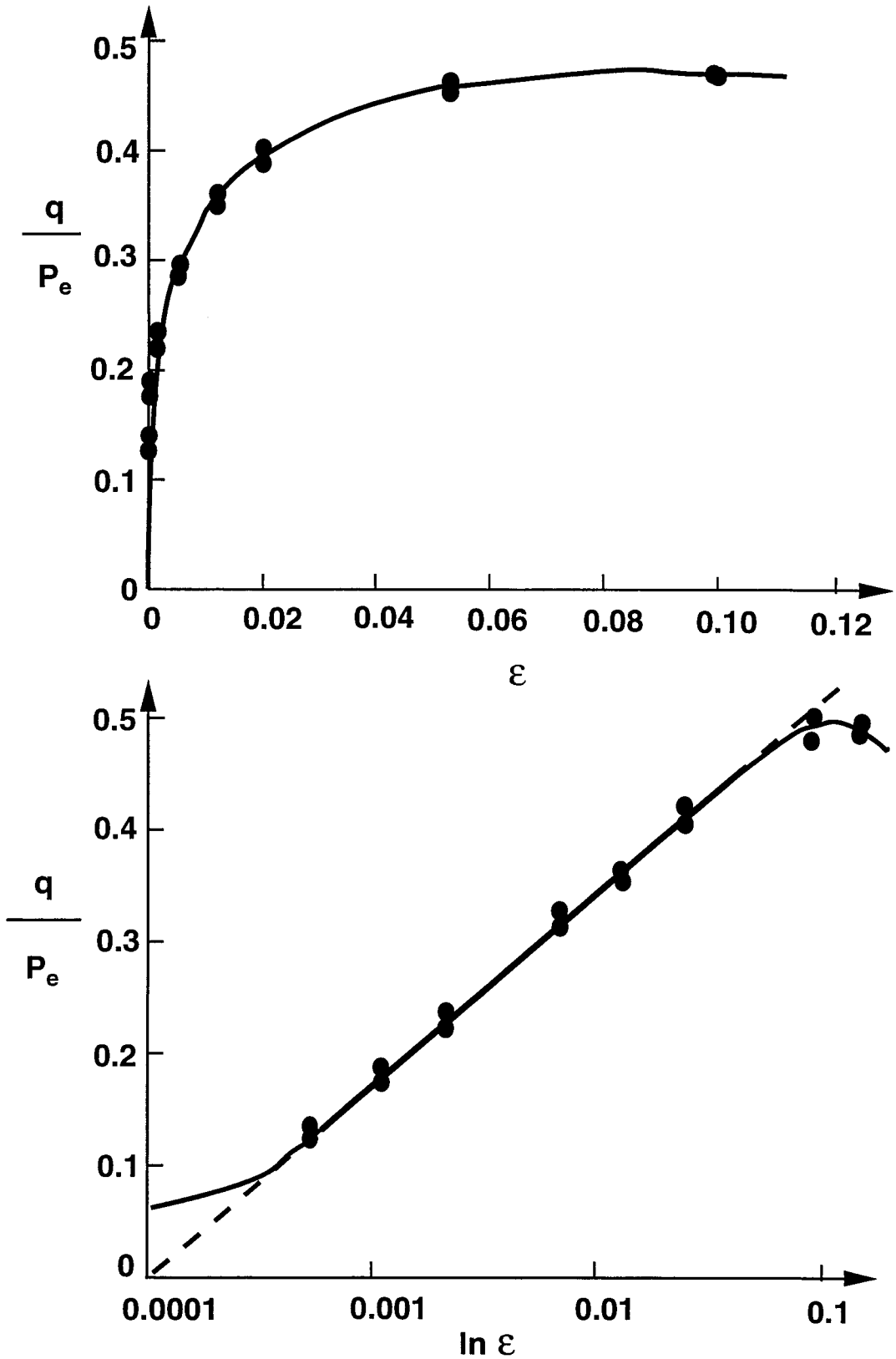

Figure (2.28) Relationship governing spacing of strain contours on wet side of critical state (modified after Loudon (1967)).

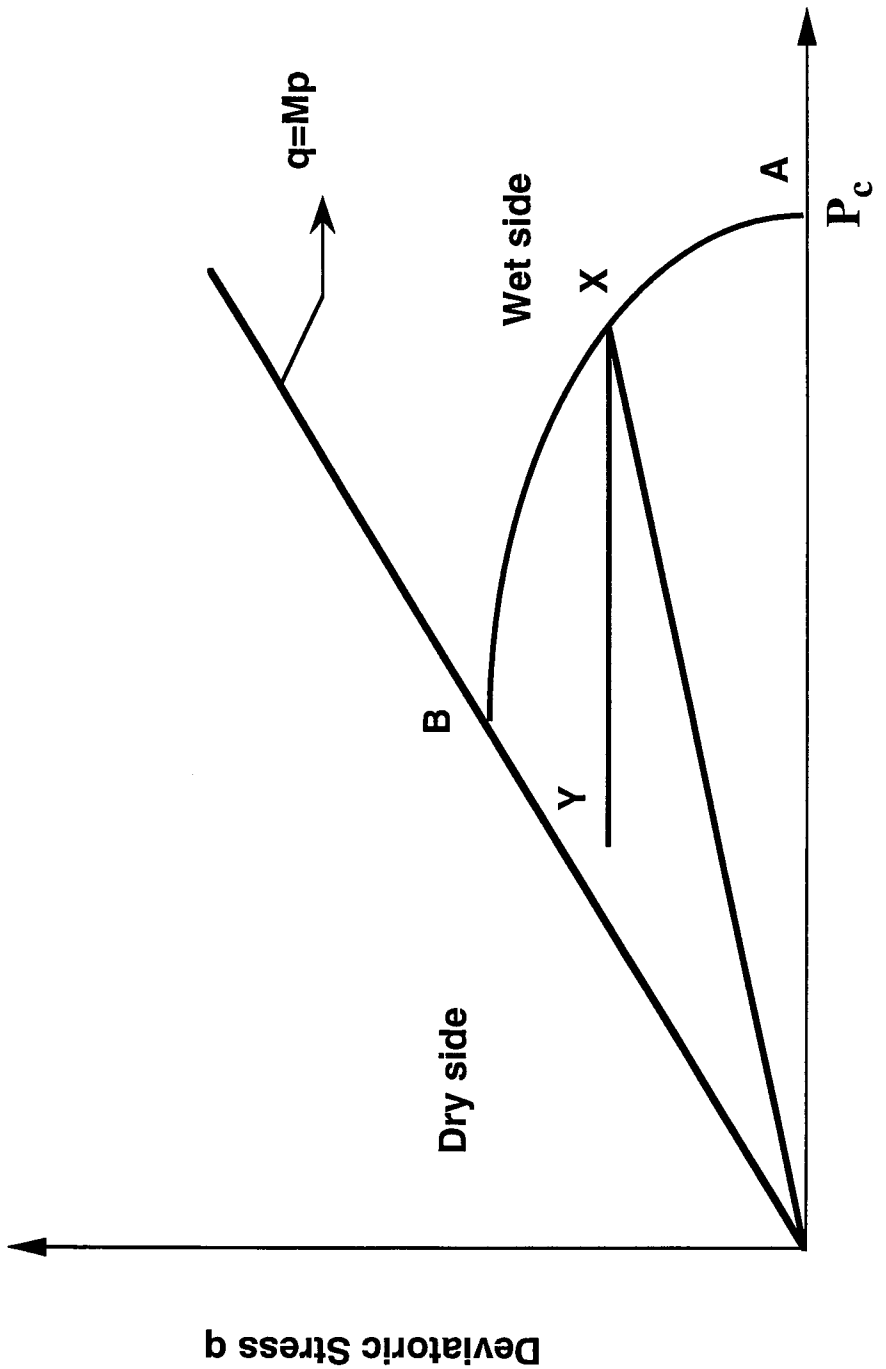

Figure (2.29) Horizontal yield surface for modified cam-clay model.

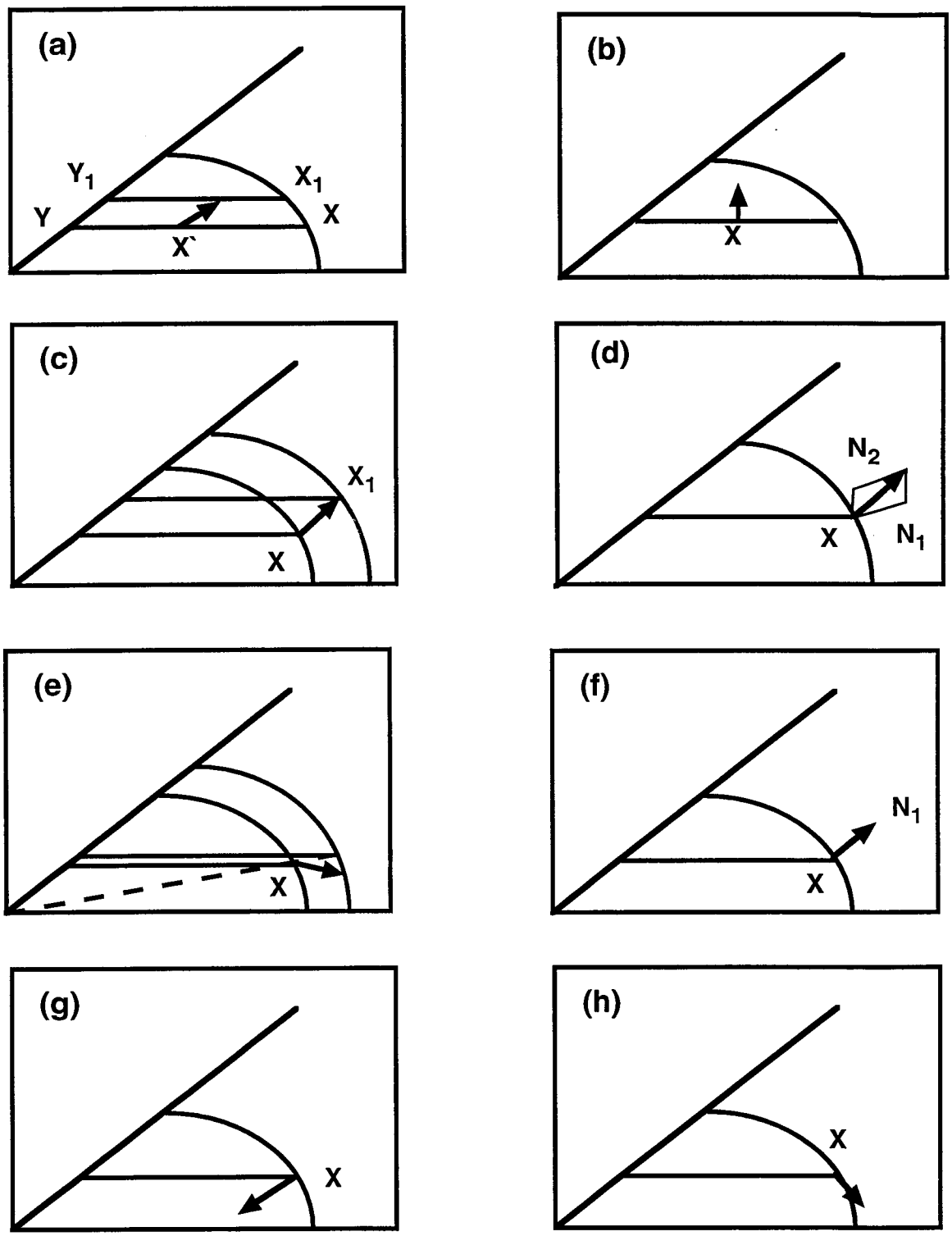

Figure (2.30) Development of plastic shear distortion beneath the state boundary surface (modified after Borja (1984)).

References:

Abdel Hadi, O.N., and Herrin, M. 1966. Characteristics of soil-asphalt as a rate process. ASCE Journal of the Highway Division, **92**(HW1): 49-69.

Barden, L. 1965. Consolidation of clay with non-linear viscosity. Geotechnique, **25** : 345-362.

Bishop, A.W. and Lovenbury, H.T. 1969. Creep characteristics of two undisturbed clays. Proceedings, 7th International Conference on Soil Mechanics and Foundation Engineering, Mexico City, Mexico, 1969. Vol. 1. pp. 29-37.

Bjerrum, L. 1967. Engineering geology of Norwegian normally consolidated marine clays as related to settlements of buildings. Geotechnique, **17**: .83-117.

Borja, R.I. 1984. Finite element analysis of the time-dependent behaviour of soft clays. Ph.D. thesis, Stanford University, California.

Borja, R.I., Hsieh, H.S., and Kavazanjian, E. Jr. 1990. Double-yield-surface model. II: Implementation and verification. ASCE Journal of the Geotechnical Engineering Division, **116**(GT9):1402-1421.

Burland, J.B. 1965. The yielding and dilation of clay. Correspondence Geotechnique, **15**: 211-214.

Christensen, R.W., and Wu, T.H. 1964. Analysis of clay deformation as a rate process. ASCE Journal of Soil Mechanics and Foundation Engineering Division, **90**(SM6): 125-157.

de Ambrosis, L.P. 1974. Settlement of foundation due to creep. Ph.D. thesis, University of Sydney, Australia.

de Josselin, de Jong G. 1968. Consolidation models conssisting of an assembly of viscous elements of a cavity channel network. Geotechnique, **18**: 195-228.

Duncan, J.M., and Chang, C.Y. 1970. Non-linear analysis of stress and strain in soils. ASCE Journal of Soil Mechanics and Foundation Engineering Division, **96**(SM5): 1629-1653.

Duncan, J.M., Bryne, P., Wong, K.S., and Mabry, P. 1980. Strength, stress-strain and bulk modulus parameters for finite element analyses of stresses and movements in soil masses. Geotechnical Engineering Report, No. UCB/GT/80-01. Department of Civil Engineering, University of California, Berkeley.

Eyring, H. 1936. Viscosity, plasticity and diffusion as example of absolute reaction rates. Journal of Chemical Physics, **4**: 283-291.

Feda, J. 1989. Interpretation of creep of soils by rate process theory. Geotechnique, **39**: 667-677.

Foss, I. 1969. Secondary settlements of buildings in Drammen, Norway. Proceedings, 7th International Conference on Soil Mechanics and Foundation Engineering,Mexico City, Mexico, 1969. Vol. 2. pp. 99-106.

Glasstone, S., Laidler, K. and Eyring, H. 1941. The theory of rate processes. McGraw Hill Book Co., New York.

Henkel, D.J. 1960. The relationship between the effective stresses and water content in saturated clays. Geotechnique, **10**: 41-54.

Hsieh, H.S. 1987. A non-associative cam-clay plasticity model for the stress-strain-time behaviour of soft clays. Ph.D. thesis, Stanford University, California, U.S.A..

Holzer, T.L., Hoeg K., and Arulanandan, K. 1973. Excess pore pressure during undrained creep. Canadian Geotechnical Journal, **10** (1): 12-24.

Hvorslev, M.J. 1960. Physical components of shear strength of cohesive soils. ASCE, Research Conference on Shear Strength of Cohesive Soils, Boulder, Colorado, June 1960. pp. 169-273.

Janbu, N. 1963. Soil compressibility as determined by oedometer and triaxial tests. Proceedings, 1st European Conference on Soil Mechanics and Foundation Engineering, Wiesbaden, West Germany, October 1963. Vol. 1. pp. 19-25.

Kavazanjian, E. Jr. 1978. A general stress-strain-time formulation for soils. Ph.D. thesis, University of California, Berkeley.

Kavazanjian, E. Jr., and Mitchell, J.K. 1977. A general stress-strain-time formulation for soils. Proceedings, Specialty Session 9, 9th International Conference on Soil Mechanucs and Foundation Engineering, Tokyo, Japan, 1977. pp. 113-120.

Kavazanjian, E. Jr., Mitchell, J.K., and Bonaparte R. 1980. Stress-deformation predictions using a general phenomenological model. Position paper for the NSF/NSERC workshop on Limit Equilbrium, Plasticity and Generalized Stress-Strain in Geotechnical Engineering, McGill University, Montreal, Canada, 28-30 May 1980. pp. 461-491.

Keedwell, M.J. 1984. Rheology and soil mechanics. Elsevier, London.

Kondner, R.L. 1963 . Hyperbolic stress-strain response: Cohesive soils. ASCE Journal of Soil Mechanics and Foundation Engineering Division, **89** (SM1): 115-144.

Kuhn, M.R. and Mitchell, J.K. 1963. New prespectives on soil creep. ASCE Journal of Geotechnical Engineering Division, **119** (GT3): 507-524.

Ladd, C.C. and Foott, R. 1974. New design procedure for stability of soft clays. ASCE Journal of Geotechnical Engineering Division, **100** (GT7): 763-786.

Ladd, C.C. and Preston, W.B. 1965. On the secondary compression of saturated clays. Research report R65-59, Research in Earth Physics, Phase Report No. 6, Department of Civil Engineering, MIT, Cambridge, Massachusetts.

Leonards, G.A. and Girault, P. 1961. A study of the one dimensional consolidation test. Proceedings, 5th International Conference on Soil Mechanics and Foundation Engineering, London, England, 12-24 August 1961. Vol. 1. pp. 213-218.

Leonards, G.A. and Ramiah, B.K. 1959. Time effects in the consolidation of clays. ASTM, STP 254. pp. 116-130.

Loudon, P.A. 1967. Some deformation characteristics of Kaolin. Ph.D. thesis, Cambridge University, England.

Mesri, G. 1973. Coefficient of secondary compression. ASCE Journal of Soil Mechanics and Foundation Engineering Division, **99** (SM1): 123-137.

Mesri, G. and Goldewski, P.M. 1977. Time and stress compressibility relationship. ASCE Journal of Geotechnical Engineering Division, **103** (GT5): 417-430.

Mesri, G., Febres, C.E., Shield, D.R., and Castro, A. 1981. Shear stress-strain-time behaviour of clays. Geotechnique, **31**: 537-552.

Mitchell, J.K. 1964. Shearing resistance of soil as a rate process. ASCE Journal of Soil Mechanics and Foundation Engineering Division, **90** (SM1): 29-61.

Mitchell, J.K. 1993. Fundamentals of soil behaviour. Second edition, John Wiley and Sons Inc., New York.

Mitchell, J.K., Campanella, R.G. and Singh, A. 1968. Soil creep as a rate process. ASCE Journal of Soil Mechanics and Foundation Engineering Division, **94** (SM1): 231-53.

Murayama, S., and Shibata, T. 1958. On the rheological characters of clay, part 1. Disaster Preventation Research Institute, Koyoto University. Bulletin **26**.

Murayama, S., and Shibata, T. 1961. Rheological properties of clays. Proceedings, 5th International Conference in Soil Mechanics and Foundation Engineering, Paris, France, July 17-22 1961. Vol. 1. pp. 269-273.

Murayama, S., and Shibata, T. 1964. Flow and stress relaxation of clays. Rheology and Soil Mechanics Symposium of the International Union of Theoretical and Applied Mechanics, Grenoble, France, 1-8 April 1964. pp.99-129.

Poulos, H.G., de Ambrosis, L.P., and Davis, E.H. 1976. Method of calculating long-term creep settlements. ASCE Journal of Geotechnical Engineering Division, **102** (GT7): 787-804.

Roscoe, K.H., and Burland, J.B. 1968. On the generalized stress-strain behaviour of "wet" clay. Engineering plasticity. *Edited by* J.Heyman and F.A. Leckie. Cambridge University Press, Cambridge, England.

Roscoe, K.H., and Schofield, A.N. 1963. Mechanical behaviour of an idealized wet clay. Proceedings, 1st European Conference on Soil Mechanics and Foundation Engineering, Wiesbaden, West Germany, October 1963. pp. 47-54.

Roscoe, K.H., Schofield, A.N., and Turairajah, A. 1963. Yielding of clays in state wetter than critical. Geotechnique, **13**: 211-246.

Schofield, A. and Wroth , C.P. 1968. Critical state soil mechanics. McGraw Hill Book Co., England.

Schiffman, R.L. 1959. The use of visco-elastic stress-strain laws in soil testing. ASTM special technical publication No. 254. pp. 131-155.

Singh A. 1966. Creep phenomena in soils. Ph.D. thesis, University of California, Berkeley.

Singh, A., and Mitchell, J.K. 1968. Generalized stress-strain-time function for soil. ASCE Journal of Soil Mechanics and Foundation Engineering Division, **94**(SM1): 21-46.

Soydemir, C., and Schmid, W.E. 1970. Deformation and stability of viscoelastic soil media. ASCE Journal of Soil Mechanics and Foundation Engineering Division, **96** (SM6): 2081-2098.

Tavenas, F., Leroueil, S., and Roy, M. 1978. Creep behaviour of an undisturbed lightly overconsolidated clay. Canadian Geotechnical Journal, **15**: 402-423.

Taylor, D.W. 1942. Research on consolidation of clays. Report Serial No. 82, Department of Civil Engineering, MIT, Cambridge, Massachusetts.

Taylor, D.W. 1948. Fundamentals of soil mechanics. John Wiley and Sons Inc., New York.

Terzaghi, K. 1941. Undisturbed clay samples and undisturbed clays. Journal of the Boston Society of Civil Engineering, **15** (3): 645-660.

Walker, L.K. 1969. Secondary compression in the shear of clays. ASCE Journal of Soil Mechanics and Foundation Engineering Division, **95** (SM1):167-188.

Wroth, C.P., and Loudon, P.A. 1967. The correlation of strains within a family of triaxial tests on overconsolidated samples of Kaolin. Proceedings, 1st Geotechnical Conference on Shear Properties of Natural Soils and Rocks, Oslo, Norway, June, 1967. Vol. 1, pp.159-163.

Wu, T.H., Resindez, D., and Neukirchner, R.J. 1966. Analysis of consolidation by rate process theory. ASCE Journal of Soil Mechanics and Foundation Engineering Division, **92** (SM6): 229-248.

Wu, T.H., El Rafai, A.N., and Hsu, J.R. 1978. Creep deformation of clays. ASCE Journal of Geotechnical Engineering Division, **104** (GT1): 61-76.

CHAPTER 3

AN EFFECTIVE STRESS MODEL FOR CREEP OF CLAY[1]

3.1 INTRODUCTION:

Constitutive equations which model accurately the behaviour of soils are essential if reliable numerical predictions of performance are to be achieved for practical geotechnical problems. In recent years considerable attention has been directed towards the study of stress-strain-time aspects of soil to investigate the influence of time and rate of strain on strength and deformation behaviour (Murayama and Shibata 1961; Christensen and Wu 1964 ; Singh and Mitchell 1968; Borja and Kavazanjian 1985). Examples of such study consider creep and stress relaxation tests. Because most of the geotechnical problems involve the application of sustained loads, creep has been studied more extensively than stress relaxation (Murayama and Shibata 1961 ; Singh and Mitchell 1968 ; Kavazanjian and Mitchell 1980 ; Hsieh et al 1990 ; Borja et al 1990). Unfortunately these studies suffer two limitations: either the problem of creep has been dealt with as a theoretical exercise to propose a rheological model, or they were carried out for a numerical simulation of laboratory or field tests, which are simple in terms of boundary conditions and stress paths in comparison with those that arise in realistic geotechnical projects such as dams, dykes and tunnels.

To study the problem of creep in the field, here, the authors describe a numerical scheme to simulate the time-dependent behaviour of cohesive soil expressed in terms of the

---

[1] A version of this chapter has been submitted for publication to the Canadian Geotechnical Journal: Morsy, M.M., Chan, D.H., Morgenstern, N.R. 1994. An effective stress model for creep of clay.

effective stresses. This scheme is used to analyze quantitatively the creep behaviour of the foundation of the Tar Island Dyke located in Fort McMurray, Alberta, Canada (Morsy 1994).

In this chapter, a comprehensive numerical model for the time-dependent behaviour of normally to lightly over-consolidated soft clays is described. The model, which is a double yield surface model, was first developed by Hsieh (1987). The constitutive equations were cast in a manner to conform with a unified phenomenological model for the stress-strain-time behaviour of soft clays developed by Kavazanjian and Mitchell (1980). The parameters used in the model are all readily obtainable from standard laboratory tests, which are familiar to most geotechnical engineers, and in some cases may be obtained from correlation with index properties of the soil.

In addition to describing the model , the finite element formulation used in the finite element code PISA^{TM} (Chan and Morgenstern 1992) to simulate numerically the time-dependent behaviour (creep) of the cohesive soil is presented. In order to perform a finite element analysis in terms of effective stresses, the pore pressure must be evaluated in the whole soil domain. A numerical scheme proposed by DeAlencar (1988) to incorporate the pore pressure into the finite element analysis based on field observations is adopted in the proposed time-dependent scheme. The pore pressure in the soil domain is interpolated from the available field measurements (DeAlencar et al. 1992). The effectiveness of the interpolation technique is illustrated by a field example, which shows the capability of the technique in calculating the pore pressure distribution within the soil domain based on a limited amount of piezometer measurements .

Two stress integration techniques are introduced based on the return mapping schemes for the double-yield surface model. A numerical example is used to demonstrate and compare the global accuracy and stability of the two techniques.

The validity of the constitutive model is evaluated by performing in a preliminary manner a numerical simulation of stress controlled drained creep triaxial tests on clay samples from the Tar Island area (Watts 1980).

3.2 THREE DIMENSIONAL STRESS-STRAIN-TIME MODEL FOR WET CLAY:

3.2.1 Double yield surface model:

The constitutive model presented here is based on the double-yield surface model proposed by Hsieh (1987). The formulation employed in the model is consistent with Kavazanjian and Mitchell's (1980) postulate that the total deformation of cohesive soil can be separated into four interdependent volumetric and deviatoric, time-independent and time-dependent components.

The model employs the concept of "double-yield criteria", shown in Figure (3.1), which is defined by the ellipsoid of the Modified Cam-clay model (MCCM) and the Von Mises cylinder inscribed in the ellipsoid.

[3.1] $$F = F(\sigma'_{ij}, P_c) = \frac{q^2}{M^2} + P(P - P_c) = 0,$$

[3.2] $$G = G(\sigma'_{ij}, q_c) = q - q_c = 0,$$

where

F is the yield function based on MCCM yield criterion;
G is the yield function based on Von-Mises yield criterion;
σ'_{ij} are the effective stress components;
P is the mean normal stress = $\frac{\sigma'_1 + \sigma'_2 + \sigma'_3}{3}$;
q is the deviator stress = $\frac{1}{\sqrt{2}}\sqrt{(\sigma'_1 - \sigma'_2)^2 + (\sigma'_2 - \sigma'_3)^2 + (\sigma'_3 - \sigma'_1)^2}$;
$\eta = q/P$;
M is the slope of the critical-state line in the P-q plane;
P_c is the isotropic preconsolidation pressure;
q_c is the shear yield stress based on the Von-Mises yield criterion.

In this model, the total strain-rate tensor $\dot{\varepsilon}$ is decomposed in the following manner (Borja and Kavazanjian 1985; Hsieh et al. 1990; Borja et al. 1990):

[3.3] $$\dot{\varepsilon} = \dot{\varepsilon}^e + \dot{\varepsilon}^P_F + \dot{\varepsilon}^P_G + \dot{\varepsilon}^t,$$

where superscripts e and P denote the time-independent elastic and plastic parts, respectively; superscript t denotes the time-dependent (creep) part; and subscripts F and G refer to the MCCM ellipsoid and Von Mises cylinder yield surfaces, respectively.

The elastic part of the time-independent components of equation (3.3) is evaluated by applying:

1) the generalized Hooke's Law;

2) the elastic stress-strain-tensor C^{e}_{ijkl} requires at least two independent material properties:

a) The elastic bulk modulus K^{e} has the accepted form:

[3.4] $$K^{e} = \frac{1+e}{\kappa} P,$$

where

e is the current void ratio;

κ is the recompression index, in natural logarithm scale.

b) The elastic shear modulus μ^{e} is obtained by assuming the trace of the modified Cam-clay yield surface on the q-γ plane, Figure (3.2),(the deviator stress-axial strain plane in the triaxial stress condition) is a hyperbola of the form,

[3.5] $$q = \frac{\gamma P_c}{a + b\gamma} R_f \ ,$$

where

$\gamma = \frac{\sqrt{2}}{3}\sqrt{(\varepsilon_1 - \varepsilon_2)^2 + (\varepsilon_2 - \varepsilon_3)^2 + (\varepsilon_3 - \varepsilon_1)^2}$ is the deviator strain;

a, b are the hyperbolic stress-strain parameters;

$R_f = \frac{(\sigma_1 - \sigma_3)_{failure}}{(\sigma_1 - \sigma_3)_{ultimate}}$ is the failure ratio.

The elastic shear modulus is back calculated from the initial tangent modulus of the hyperbola curve by :

[3.6] $$\mu^e = \frac{P_c R_f}{3a} .$$

The immediate plastic deformation is evaluated based on the current stress state with respect to the double-yield surface, which leads to four cases:

a) Semi-plastic process on the F surface:
F is the only surface which is involved in the deformation process. In this case the soil is considered to be normally consolidated with respect to F but overconsolidated with respect to G;

b) Semi-plastic process on the G surface:
G is the only surface which is involved in the deformation process. In this case the soil is to be considered normally consolidated with respect to G but overconsolidated with respect to F;

c) Fully plastic process:
Both the F and G surfaces are both involved in the deformation process;

d) Elastic process:
The soil is overconsolidated with respect to both surfaces F and G. The deformation process becomes purely elastic.

Kavazanjian and Mitchell (1980) considered that the time-dependent strain rate tensor can be divided into distinct but interdependent, volumetric $\dot{\varepsilon}_v^t$ and deviatoric $\dot{\varepsilon}_d^t$ components:

[3.7] $$\dot{\varepsilon}^t = \dot{\varepsilon}_v^t + \dot{\varepsilon}_d^t .$$

They postulated that these creep strain rate tensors can be determined using the following phenomenological volumetric and deviatoric expressions for creep (Taylor 1948; and Singh and Mitchell 1968).

[3.8] $$\dot{\varepsilon}_v^t = \frac{\Psi}{(1+e)t_v} ,$$

[3.9] $$\dot{\varepsilon}_d^t = A\exp(\overline{\alpha}\overline{D})[\frac{(t_d)_i}{t_d}]^m \ ,$$

where

ψ is the secondary compression coefficient, in natural logarithm scale;
e is the void ratio;
exp is the exponential;
t_v is the volumetric age, relative to an initial reference time $(t_v)_i$;
$(t_v)_i$ is the instant volumetric time, usually set to unity;
A, $\overline{\alpha}$,m are the Singh-Mitchell creep parameters;
$(t_d)_i$ is the instant deviatoric time, usually set to unity;
t_d is the deviatoric age relative to $(t_d)_i$;
$\overline{D} = \frac{(\sigma_1 - \sigma_3)}{(\sigma_1 - \sigma_3)_{ult}}$ is the deviatoric stress level.

The total creep strain rate tensor is evaluated by employing a non-associated flow rule for both the equivalent volumetric and deviatoric yield surfaces associated with the state parameters P and q. It is only necessary to determine the size of these potential functions as $P_o = P + \frac{q^2}{M^2 P} \le P_c$ for the ellipsoid F and $q_o = q \le q_c$ for the cylinder G. By forcing the creep strain rate to satisfy the secondary compression law for volumetric creep and the Singh-Mitchell law for the deviatoric creep simultaneously, the creep strain rate can be expressed as:

[3.10] $$\dot{\varepsilon}^t = \frac{\psi}{3(1+e)t_v} I + \sqrt{\frac{3}{2}} A\exp(\overline{\alpha}\overline{D})[\frac{(t_d)_i}{t_d}]^m \hat{n},$$

where

I is the second-order identity tensor;
$\hat{n} = \frac{\sigma'}{\|\sigma'\|}$;
$\| \ \|$ denotes the Euclidean norm.

The above constitutive model requires thirteen parameters. Seven parameters for completing material definition in the absence of creep are : virgin compression index C_c, recompression index C_r, angle of internal friction ϕ, void ratio e_a at unit preconsolidation

pressure, the hyperbolic stress-strain parameters a, b and R_f. Six more parameters are required for creep: secondary compression coefficient C_α, the Singh-Mitchell creep parameters A,α and m and the reference times $(t_v)_i$ and $(t_d)_i$ (usually set to unity).

3.2.2 Implementation of the numerical model in finite element code PISA™:

The double-yield surface model is implemented in the finite element code **PISA™** (Program for Incremental Stress Analysis) developed at the University of Alberta (Chan and Morgenstern 1992). The program is capable of performing one, two, and three dimensional linear and non-linear elastic as well as elasto-plastic analyses involving various yield criteria. In this study, the program capability is extended to include the time-dependent creep analysis.

3.3 THE NUMERICAL ALGORITHM OF THE DOUBLE YIELD SURFACE MODEL:

3.3.1 Finite element effective stress model:

In performing a finite element analysis to obtain the deformation response of a geotechnical structure, there are two approaches, namely the total and effective stress approaches. Ideally the analysis should be performed in term of effective stresses. In carrying out an effective stress analysis, it is necessary to calculate the pore pressure in the soil for the entire domain.

There are several approaches to determine the in-situ pore pressure as shown in Figure (3.3). One approach is to determine the pore pressure in the soil domain assuming steady seepage conditions govern the generation and dissipation of pore pressure in the soil domain. Another approach is to use empirical and semiempirical relations to determine the pore water pressure profile in the soil domain due to external loads. The most popular approach is to couple the deformation of the soil with the generation and dissipation of pore pressure. All these approaches require the determination of consolidation and seepage characteristics of the materials. Accurate predictions of pore pressure are often difficult due to difficulties in determining the permeabilities of the soils, in defining the boundary conditions of the problem and in locating macro and micro features, such as fissures and joints, which can significantly affect the flow of water and the rate of consolidation.

A different approach was proposed by De Alencar (1988) to avoid the problems of pore pressure prediction, is to prescribe the pore pressure in the soil provided that pore pressure measurements are available. In this approach the pore pressure is interpolated at each integration point[2] in the finite element mesh based on the field measurements. This approach is adopted in the present study.

In common with most finite element analysis, we start with the virtual work equilibrium statement. Consider a soil structure shown schematically in Figure (3.4) occupying a domain Ω and bounded by surface Γ, with strain tensor $\{\varepsilon\}$, and with stress field $\{\sigma\}$, the sum of the external and internal virtual work of the structure will be zero for any virtual displacement and strain, $\{\delta u\}$ and $\{\delta\varepsilon\}$, satisfying the compatability condition. Thus

$$[3.11] \qquad \int_{\Omega}\{\delta\varepsilon\}^{T}\{\dot{\sigma}\}d\Omega - \int_{\Omega}\{\delta u\}\{\dot{\bar{b}}\}d\Omega - \int_{\Gamma_{\sigma}}\{\delta u\}^{T}\{\dot{\bar{t}}\}d\Gamma = 0.$$

In the above equation $\{\ \}$ denotes the vector quantity, while $[\ ]$ denotes the matrix quantity and $\{\ \}^{T}$ or $[\ ]^{T}$ denotes the transpose of a vector or a matrix, respectively, and the dot denotes rate or incremental quantity. Also $\{\dot{\bar{b}}\}$ denotes prescribed body forces, $\{\dot{\bar{t}}\}$ prescribed boundary traction on boundary Γ_{σ} and it is implicitly assumed that $\{\delta u\} = 0$ on Γ_{u}. For compatibility of strains, the displacements are related to strains by a linear differential operator,

$$[3.12] \qquad \{\varepsilon\} = [L]\{u\},[L]^{T} = \begin{bmatrix} \frac{\partial}{\partial x} & 0 & 0 & 0 & \frac{\partial}{\partial z} & \frac{\partial}{\partial y} \\ 0 & \frac{\partial}{\partial y} & 0 & \frac{\partial}{\partial z} & 0 & \frac{\partial}{\partial x} \\ 0 & 0 & \frac{\partial}{\partial z} & \frac{\partial}{\partial y} & \frac{\partial}{\partial x} & 0 \end{bmatrix}.$$

We can rewrite equation (3.11) as,

$$[3.13] \qquad \int_{\Omega}\{\delta u\}^{T}[L]^{T}\{\dot{\sigma}\}d\Omega - \int_{\Omega}\{\delta u\}^{T}\{\dot{\bar{b}}\}d\Omega - \int_{\Gamma_{\sigma}}\{\delta u\}^{T}\{\dot{\bar{t}}\}d\Gamma = 0.$$

We assume a trial expansion of $\{u\}$ in term of known shape functions [N] as,

---

[2] The interpolation technique is presented in Appendix A.

[3.14] $$\{u\} = [N]\{a\},$$

where $\{a\}$ is the nodal displacement vector. Substituting into equation (3.13) we have:

[3.15] $$\{\delta a\}^T\left(\int_\Omega [N]^T[L]^T\{\dot{\sigma}\}d\Omega - \int_\Omega [N]^T\{\dot{\bar{b}}\}d\Omega - \int_{\Gamma\sigma}[N]^T\{\dot{t}\}d\Gamma\right) = 0.$$

From equation (3.15) we have the standard equilibrium equation, by equating the expression inside the brackets to zero:

[3.16] $$\int_\Omega [N]^T[L]^T\{\dot{\sigma}\}d\Omega - \int_\Omega [N]^T\{\dot{\bar{b}}\}d\Omega - \int_{\Gamma\sigma}[N]^T\{\dot{t}\}d\Gamma = 0,$$

or

$$\int_\Omega [B]^T\{\dot{\sigma}\}d\Omega - \{\dot{\bar{F}}\} = 0,$$

with

$$[B] = [L][N] \quad ; \quad \{\dot{\bar{F}}\} = \int_\Omega [N]^T\{\dot{\bar{b}}\}d\Omega + \int_{\Gamma_\sigma}[N]^T\{\dot{t}\}d\Gamma.$$

As the pore water pressure is taken as a known quantity , so an effective stress analysis can be carried out. The procedures for incorporating pore water pressures in the finite element analysis can be found in the existing literature, Christian (1968); Byrne (1976); Zienkiewicz and Humpheson (1977); and Chan and Morgenstern (1989). To complete the formulation the constitutive relations for the material have to be introduced, we have:

[3.17] $$\{\dot{\sigma}\} = \{\dot{\sigma}'\} + \{m\}\dot{p},$$

[3.18] $$\{\dot{\sigma}'\} = [C^e]\{\dot{\varepsilon}^e\},$$

where

$\{\dot{\sigma}\}$ is the total stress increment;
$\{\dot{\sigma}'\}$ is the effective stress increment;
$\{m\}^T = \langle 1,1,0,1,0,0\rangle$;
$\dot{p}$ is the pore pressure increment;
$[C^e]$ is the elastic stress-strain matrix;
$\{\dot{\varepsilon}^e\}$ is the elastic strain increment.

From equations (3.10), (3.17), and (3.18) we have,

$$[3.19] \qquad \{\dot{\sigma}\} = [C^e]\left\{\dot{\varepsilon} - \dot{\varepsilon}_F^P - \dot{\varepsilon}_G^P - \dot{\varepsilon}^t\right\} + \{m\}\dot{p}.$$

On substituting in equation (3.16), we have thus

$$[3.20] \qquad [K]\{a\} - \int_\Omega [B]^T\{\dot{\sigma}^t\}d\Omega - \{\dot{\bar{F}}\} + \int_\Omega [B]^T\{m\}\dot{p} = [K]\{a\} - \{\dot{V}\} = 0,$$

where

$$\{\dot{V}\} = \int_\Omega [B]^T[\bar{C}]\{\dot{\sigma}^t\}d\Omega + \{\dot{\bar{F}}\} - \int_\Omega [B]^T\{m\}\dot{p},$$

$$[K] = \int_\Omega [B]^T[\bar{C}][B]d\Omega,$$

where $[\bar{C}]$ is the elasto-plastic stress-strain matrix which depends explicitly on the stress state of the soil element with respect to the yield surfaces (see Appendix B); and $\{\dot{\sigma}^t\}$ is the stress relaxation rate and it is evaluated based on the stress state of the soil with respect to the double-yield surfaces (see Appendix B).

Equations (3.10),(3.19), and (3.20) present a discretized system of ordinary differential equations from which a solution can be obtained in a time stepping manner according to the following procedures:

a) Starting from known values of $\{\sigma^n\}, \{a^n\}, \{\varepsilon^n\}$ and $\{\bar{F}^n\}$ at a time instant t^n, where superscript n denotes quantity evaluated at time t^n. Compute the time-dependent strain rate tensor $\{\dot{\varepsilon}^t\}^n$ using equation (3.10).

b) Time-step length is determined according to the variable scheme(Zienkiewicz and Cormeau, 1974) using the following equation :

$$[3.21] \qquad \Delta t_n = \tau\left[\frac{\varepsilon_{ij}^n}{\dot{\varepsilon}_{ij}^n}\right]_{min}^{\frac{1}{2}},$$

where

τ is the time increment parameter, the value must be specified by the user. For an explicit scheme, it is in the range of 0.01 to 0.15;

ε_{ij}^{n} is the component of the strain tensor at step n;

$\dot{\varepsilon}_{ij}^{n}$ is the component of the strain rate tensor at step n;

min. is the minimum value of Δt_n (time step) which is taken over all integration points in the clay layer.

c) Calculate the increment pseudo load $\{\Delta V^n\}$,

[3.22] $$\{\Delta V^n\} = \int_\Omega [B^n]^T [\overline{C}^n]\{(\Delta\sigma^t)^n\}d\Omega + \{\Delta\overline{F}^n\} - \int_\Omega [B^n]^T \{m\}\Delta p^n ,$$

[3.23] $$\{(\Delta\sigma^t)^n\} = \int_{t_n}^{t_n+\Delta t_n} \{(\dot{\sigma}^t)^n\}dt ,$$

where Δ denotes incremental quantities determined over time step Δt_n. While $\{\Delta\overline{F}^n\}$ represents the change in loads during the time interval Δt_n. In the majority of the problems encountered in engineering, the load increments are applied as discrete steps thus $\{\Delta\overline{F}^n\}$=0 for all time steps other than the first step within an increment and Δp^n is the change in pore water pressure through the time step Δt_n.

d) Calculate the nodal displacement increment $\{\Delta a^n\}$ and the strain increment $\{\Delta\varepsilon^n\}$ occurring during the time step Δt_n as following:

[3.24] $$\{\Delta a^n\} = [K]^{-1}\{\Delta V^n\},$$

where

$$[K] = \int_\Omega [B^n]^T [\overline{C}^n][B^n]d\Omega ,$$

[3.25] $$\{\Delta\varepsilon^n\} = [B^n]\{\Delta a^n\}.$$

e) Calculate the total stress increment for time increment Δt_n :

[3.26] $$\{\Delta\sigma^n\} = [\overline{C}^n]\{\Delta\varepsilon^n\} - \{(\Delta\sigma^t)^n\}.$$

f) At time t_{n+1} , the soil element state is updated from:

[3.27]
$$\{\sigma^{n+1}\} = \{\sigma^n\} + \{\Delta\sigma^n\},$$
$$\{u^{n+1}\} = \{u^n\} + \{\Delta u^n\},$$
$$\{\varepsilon^{n+1}\} = \{\varepsilon^n\} + \{\Delta\varepsilon^n\}.$$

The process from a) to f) is repeated through a certain number of iterations to improve the estimated time-dependent strain, displacement and stress fields .

For each time step, the pore pressure at the integration points of the finite element mesh are determined from the field measurements corresponding to that time step. The following interpolation technique was proposed by De Alancar et al. (1992) to calculate the pore pressure as follows:

1) An initial pore pressure distribution is assumed for the entire domain. In the case of a finite element analysis, this means that an initial set of values are assigned at each integration point of the mesh. The initial pore pressure distribution may be specified by the user based on the knowledge of the water table.

2) Based on the pore pressure distribution, the pore pressure at the piezometers locations are calculated using a weighting scheme (see Appendix A).

3) The errors between the calculated and the observed pore pressure at the piezometers locations are determined and compared with a specified tolerance.

4) If the errors at the piezometer locations are larger than the specified tolerance, a correction is applied to the pore pressure distribution.

5) Steps 2, 3, and 4 are repeated until the errors in the calculated pore pressure are sufficiently small.

As the number of piezometers may be limited and may not completely define the pore pressure distribution for the entire domain, it is sometimes necessary to provide additional

pore pressure information based on the boundary conditions of the problem and knowledge of the ground water regime. This can be done by adding fictitious piezometers and determining a pore pressure distribution to conform with this new information. It is often assumed that the pore water pressure within any loading step is equal to the value at the beginning of the loading step. If substantial changes in pore pressure is observed between each loading step an average pore pressure can be used.

3.3.2 Verification of the interpolation technique:

To illustrate the interpolation technique for the determination of the pore pressure within the soil foundation. Consider the field problem shown in Figure (3.5), which is the soil foundation beneath berm 319 in Tar Island Dyke, station 56+00. The dyke foundation consists of a clay layer overlying a sand layer. The dyke is constructed mainly of sand. The initial pore pressure distribution is hydrostatic. The raising of the dyke crest from elevation 325 to 330 meters caused a generation of pore pressure in the clay layer beneath berm 319 as recorded by three piezometers installed at different elevations in the clay layer . Under these circumstances it is expected that the pore pressure values in the sand layer would remain unchanged due to the free draining characteristic of the sand.

Fictitious piezometers are placed at the upper and lower interfaces between the sand layers and the clay layer. The initial pore pressure distribution is assumed hydrostatic in the clay layer. Then the pore pressure is calculated for the entire clay layer using the procedure described earlier. The results are plotted in Figure (3.6), which shows the interpolated pore pressure at selected depths and the measured pore pressure at the tip of the piezometers in the clay layer. The plot shows an excellent agreement between the measured and the interpolated pore pressures.

3.3.3 Stress integration algorithm:

3.3.3.1 Overview:

In the context of a finite-element plasticity analysis, the solution of boundary value problems requires the use of a numerical integration procedure for describing the incremental evolution of stresses and hardening parameters. In general, one seeks a

numerical integration algorithm which is both convergence and stable over a range of physically reasonable step sizes. Convergence means that the algorithm converges to a prescribed tolerance level and produces nearly identical stress solutions when the step size is divided into smaller subincrements. Stability means that even with a reasonably large step size, convergent solutions can still be achieved. In addition an efficient algorithm that converges rapidly is most desirable, especially considering the large number of loading steps that are required to simulate the construction sequences of a real structure, with each loading step requiring an iterative algorithm treatment for more accurate results.

Several explicit and implicit integration schemes are being used for elasto-plastic computations. Explicit integration schemes usually require the evaluation of the elastoplastic transition through the calculation of a contact stress on the yield surface and a scaling factor for the plastic multiplier. This procedure often breaks down in cases of complex stress and loading conditions since it can produce undesirable phenomena such as negative plastic flow when the plastic multiplier numerically becomes negative. They are also computationally inefficient especially for complex yield surfaces that require an iterative procedure for finding the scaling factor and contact stresses. Further refinements of these algorithms can be achieved by subdividing the step size into smaller increments (Owen and Hinton, 1986). However, the algorithm is only first-order accurate and conditionally stable (Prevost, 1987).

For rate-independent plasticity the "return mapping algorithm" provides an efficient and robust integration scheme for the rate constitutive equations. This procedure amounts to a "discrete" enforcement of the consistency condition and has been suggested first by Wilkins (1964) for the Von-Mises yield criterion. Krieg and Krieg (1976) extended the return algorithm to the case of linear isotropic and kinematic hardening rules, while Simo and Taylor (1985) further extended it to nonlinear hardening rules in conjunction with a formulation for development of consistent tangent moduli. Borja and Seung (1990) tested two stress integration algorithms in the case of the modified Cam clay yield surface. The first one was the closest point projection algorithm for an associative flow rule while the second one was the central return mapping for a non-associative flow rule. Both formulations show remarkable solution accuracy and stability. The closest point and the central return algorithms are depicted schematically in Figure (3.7).

3.3.3.2 Return mapping algorithm for the double-yield surface model:

In the case of the double-yield surface model, different return mapping schemes have been used in the analysis according to the stress state of the soil element with respect to the double yield surface.

In the case of the semi-plastic process on the F surface, that is the F surface is the only surface involved in the plastic deformation process, the closest point projection scheme (Borja and Seung 1990) is used in the stress integration.

In the case of the semi-plastic process on the G surface , that is the G surface is the only surface involved in the plastic deformation process, the radial return mapping is used in the stress mapping as shown in Figure (3.8).

In the case of the fully plastic process, both the F and G surfaces are involved in the plastic deformation process. A return mapping technique is required to relocate the stress state defined by $\left(P_{n+1}^{tr}, q_{n+1}^{tr}\right)$, which lies outside the elastic region enclosed by the double yield surface, in order to coincide with the point of intersection between the two yield surfaces (P,q). The authors propose two return mapping techniques. Each one is composed of two schemes of return mapping as follows:

a) In the first technique, shown in Figure (3.9), the radial return algorithm is used to relocate the stress state $\left(P_{n+1}^{tr}, q_{n+1}^{tr}\right)$ to point 2 on the G surface. The second step is to use the closest point algorithm to find the closest distance of point 3 (trial stress state) on the F surface. Then the two steps are repeated several times until the final trial stress state coincides with the point of intersection (P,q) according to the specified tolerance. This technique is named the closest point radial mapping technique.

b) In the second technique, shown in Figure (3.10), the radial return algorithm is used to relocate the stress state $\left(P_{n+1}^{tr}, q_{n+1}^{tr}\right)$ to point 2 on the G surface. The second step is to use the hydrostatic return mapping scheme to move the stress state along the G surface with respect to the F surface until the stress state coincide with the intersection point (P,q) according to the specified tolerance. The technique is named the hydrostatic radial mapping technique.

3.3.3.4 Numerical example:

Two fortran subprograms named CLRAPMT and HYRAMT were written to investigate the performance of the closest point radial mapping and the hydrostatic radial mapping techniques. The two subprograms were linked to the nonlinear finite element code PISA^{TM} (Chan and Morgenstern 1992) to test the performance of both techniques. In program PISA^{TM} the iterations are terminated according to the following convergence criteria:

1) Displacement criterion:

$$\frac{\left\|\Delta \underline{U}^{i}\right\|}{\left\|{}^{t+\Delta t}\underline{U}\right\|} \leq \varepsilon_u \qquad [3.28]$$

where

$\left\|\Delta \underline{U}^{i}\right\|$ is the increment of displacement norm at iteration i ;

$\left\|{}^{t+\Delta t}\underline{U}\right\|$ is the total displacement norm at time t+Δt;

$\|\underline{U}\| = \sqrt{\sum_{i=1}^{n}(U_i)^2}$ (n is the number of elements in U_i);

and

ε_u is the displacement tolerance specified by the user.

2) Force criterion :

$$\frac{\left\|{}^{t+\Delta t}\underline{R} - {}^{t+\Delta t}\underline{R}^{i}\right\|}{\left\|{}^{t+\Delta t}\underline{R} - {}^{t}\underline{R}\right\|} \leq \varepsilon_f \qquad [3.29]$$

where

$\left\|{}^{t+\Delta t}\underline{R}\right\|$ is the nodal force vector at time t + Δt ;

$\left\|{}^{t+\Delta t}\underline{R}^{i}\right\|$ is the nodal force vector after i iterations;

$\left\|{}^{t}\underline{R}\right\|$ is the nodal force vector at tome t;

and

ε_f is the force tolerance specified by the user.

The displacement and the force tolerances are set to 10^{-3}. All computations were performed using 64-bit word for double precision floating point calculations in a RISC6000 workstation operating under the AIX system at the University of Alberta.

In the numerical example used to test the two return mapping techniques, a triaxial soil sample is subjected to a confining pressure of 750 KPa and then it is subjected to a uniform axial pressure of 1000 KPa. The example is considered as an axisymmetric problem. The finite element mesh, Figure (3.11), is composed of 4 four node quadrilateral element with a 2X2 Gaussian integration rule employed for each element. The confining pressure is applied in two time steps. The axial pressure is applied in one, five, ten, and twenty equal steps. Stresses were integrated using subprograms RACLPMT and RAHYMT and the solution obtained from these two techniques were compared.

Tables (3.1) and (3.2) demonstrate the accuracy of the two stress integration algorithms and show that the five and twenty step solutions give nearly identical results for both schemes with only a 5% difference, although more iterations per time step are required by the case of five time steps.

Tables (3.1) and (3.2) also show the average number of iterations required for convergence for each of the two integration techniques and the total CPU time required for execution. Both techniques required the same number of iterations to converge for a given step size. The hydrostatic radial mapping technique required , not surprisingly, only about 9.5 to 11.3 percent of the CPU time required by the closest point radial mapping technique . Based on the comparison, the authors adopt the hydrostatic radial mapping technique for the stress integration in the case of the fully plastic process on both the F and G surfaces.

3.4 PRELIMINARY VERIFICATION OF THE DOUBLE YIELD SURFACE MODEL:

3.4.1 Drained creep triaxial tests:

In the laboratory, two sets of stress controlled incremental drained triaxial tests were carried out on samples of the foundation clay beneath the Tar Island Dyke (TID), referred to as the Tar Island Clay (TIC), Watts (1980). Each set consists of three samples, each

consolidated under different isotropic consolidation pressures. The samples in one set were prepared with the bedding plane horizontal and were numbered T1, T2, and T4. The samples in the other set were prepared with the bedding planes inclined at an angle of 45° and were numbered I1, I2, and I3.

All samples were consolidated isotropically to a pressure above the average preconsolidation stress of 650 KPa, determined from the oedometer tests. The final isotropic consolidation pressures during the application of shear stresses were varied from 740 KPa to 1500 KPa between samples which allowed an investigation of the influence of normal effective stress and water content on the creep behaviour. All the creep tests were stress controlled in order to simulate field conditions beneath the Tar Island Dyke founded on this clay (Mittal and Hardy 1977).

3.4.2 Test results:

The results of the triaxial tests are shown in Figures (3.12) and (3.13). The results are plotted in the conventional manner of deviatoric stress versus axial strain. The stresses and strains at the beginning and at the end of each load increment are joined by straight lines. The load increment durations vary from 10 to 230 hours. This straight line path represents the stress-strain path followed by the sample during the test. A smooth curve is also drawn through the final stress-strain point of each extended increment. The smooth lines represent the long term stress-strain behaviour of the clay. All samples failed along distinct shear planes and as with all stress controlled tests, failure was catastrophic.

3.4.3 Numerical simulation:

In order to simulate the two sets of the drained creep triaxial tests, a finite element model composed of four eight-node elements is employed as shown in Figure(3.14). These elements were prestressed to the same isotropic effective pressure in the laboratory tests. Then the elements were sheared following the same stress-time history as the laboratory test.

Table (3.3) summarizes the double yield surface parameters for the TID clay. The parameters were determined from a laboratory program carried out by Watts (1980). The parameters C_c, C_r, e_a and C_α were determined from the results of isotropic triaxial tests. In the case of the hyperbolic parameters because there were no data available from isotropic

consolidation undrained triaxial tests, these parameters were calculated theoretically (Appendix C). The angle of internal friction was determined from triaxial compression tests. The Singh-Mitchell parameters A,α, and m were determined from drained triaxial creep tests.

Two types of analysis were carried, a time-independent analysis and a time-dependent analysis. The results of the numerical simulations are plotted in Figure (3.15) for horizontal bedding sample T4 and Figures (3.16) and (3.17) for inclined samples I1 and I3.

For the horizontal bedding sample T4, the inclusion of the creep in the model yields the most accurate prediction for both the axial strains and the vertical displacements. In the case of the inclined bedding samples I1 and I3, the inclusion of creep in the model improved the results of the analysis and shows excellent agreement with the laboratory results.

3.5 CONCLUSIONS:

In the absence of extensive reliable shear stress-strain-time observations on a variety of natural soils and under a wide range of loading conditions, the existing creep models for soils should be viewed as *ad hoc* generalizations necessitated by the immediate need for analysis of engineering problems and interpretation of laboratory and field observations. The authors have extended the numerical model developed by Hsieh (1987) capable of simulating the time-dependent behaviour (creep) of cohesive soil in the three dimensions to include field observed pore water pressures in order to model creep deformation in terms of effective stress. The double-yield surface model uses two well known phenomenological relations (Taylor 1948, Singh and Mitchell 1968) to evaluate creep deformation. The model is incorporated in a finite element numerical scheme. The scheme is characterized by the following features:

(a) the prediction of the stress-strain-time behaviour of cohesive soil uses the classical plasticity theory and phenomenological creep rate relationships that are well established in geotechnical engineering;

(b) the material parameters used in the model are well understood by geotechnical engineers in term of their physical meanings. The determination of these parameters requires traditional consolidation and triaxial tests;

(c) the determination of the pore pressure distribution within the soil domain and its use as input data in the numerical analysis reduces the complexity of the finite element analysis using the effective stress approach.

This numerical scheme has been implemented in a finite element code PISA^{TM} and shown to be a practical approach for numerical simulation of the time-dependent behaviour of field problems with complex boundary conditions.

The authors introduce two techniques for the stress integration algorithm for the double yield surface model based on the return mapping technique. The two techniques are tested numerically and found to be numerically stable and accurate. The numerical test allows the authors to compare between the two techniques in terms of the number of iterations and CPU time required for the convergence of the numerical example. The hydrostatic radial technique is chosen for the analysis because of greater efficiency.

The double-yield surface model has been used to simulate a set of drained creep triaxial tests for the TID clay(Watts 1980). The results of the finite element analysis shows that:

(a) creep deformation is found to be a major component of the overall deformation of the TID clay;

(b) the double-yield surface models represents accurately the stress-strain-time behaviour of the TID clay.

The procedures used developed by De Alencar et al. (1992) to interpolate pore pressures within a soil mass based on limited field measurements are an efficient means for conducting effective stress analyses.

Table 3.1. Accuracy and stability test results of the hydrostatic radial mapping technique.

Number of time steps	Ave. no. of iterations per time step	Vertical displacement (meters)[a]	CPU (sec)
1	#[b]	#[b]	#[b]
5	8.8	-0.24522E-02	4
10	7.3	-0.25294E-02	6
20	6	-0.25668E-02	11

[a]The vertical displacement is calculated at the center of the triaxial sample.

[b]did not converge after 25 iterations.

Table 3.2. Accuracy and stability test results of the closest point radial mapping technique.

Number of time steps	Ave. no. of iterations per time step	Vertical displacement (meters)[a]	CPU (sec)
1	#[b]	#[b]	#[b]
5	8.8	-0.24522E-02	38
10	7.3	-0.25294E-02	53
20	6	-0.25668E-02	116

[a]The vertical displacement is calculated at the center of the triaxial sample.

[b]did not converge after 25 iterations.

Table 3.3. Double-yield surface model material parameter for Tar Island Dyke clay.

Parameter	Symbol	Value
Virgin compression index	C_c	0.10665
Recompression index	C_r	0.03
Secondary compression coefficient	C_α	0.0031
Hyperbolic stress-strain parameters	a,b, and R_f	0.0032,1.398, 0.89
Singh-Mitchell creep parameters	A,α,and m	0.052%/day,2.47,1.12
Angle of internal friction	ϕ	26.49
Void ratio at P_c = 1 KPa	e_a	0.8909
Instant volumetric and deviatoric time	$(t_v)_i$, $(t_d)_i$	1 day, 1 day

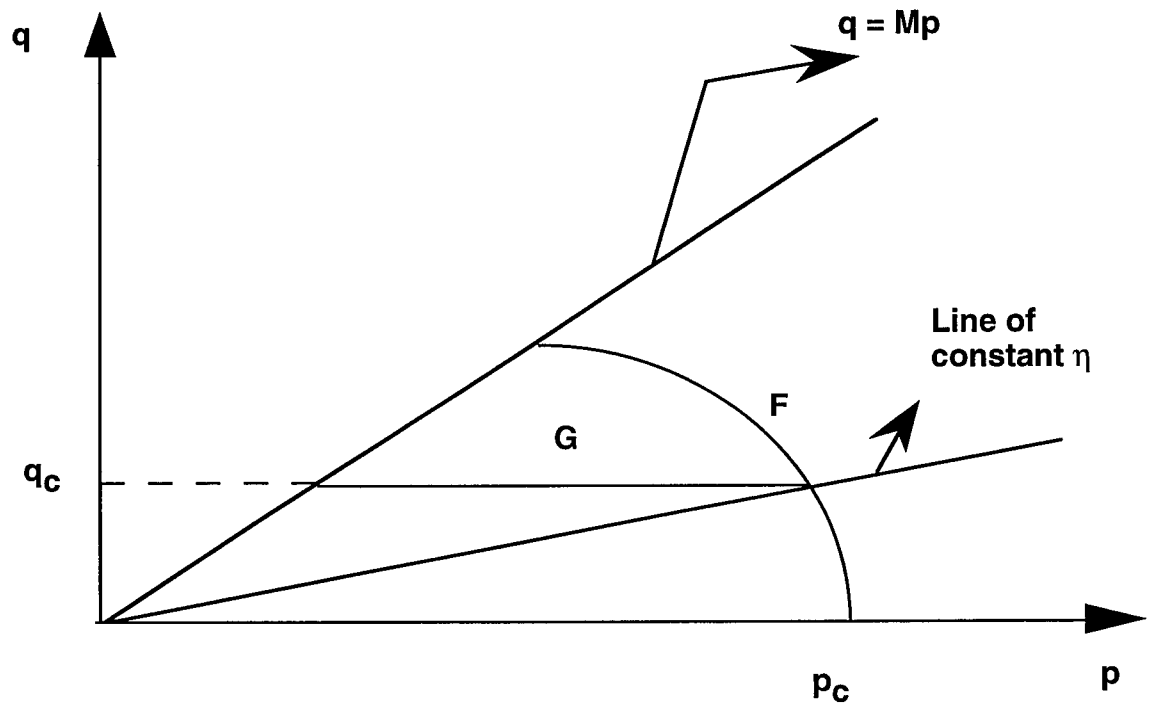

Figure (3.1) Projection of double yield surfaces on P-q plane.

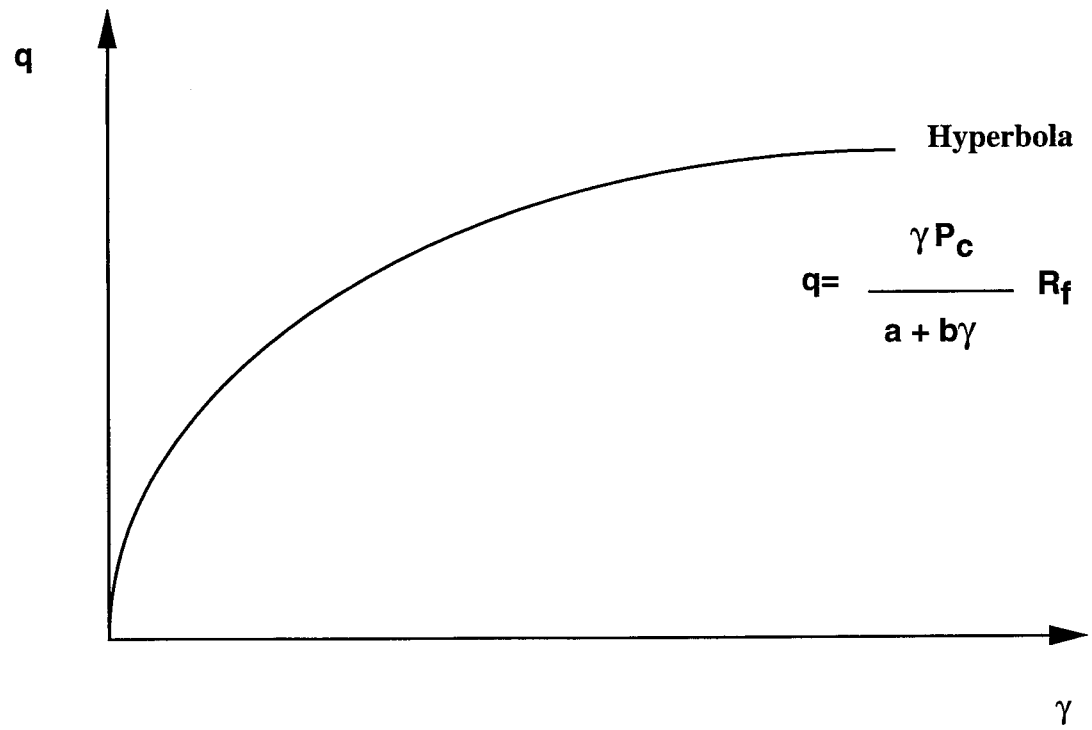

Figure (3.2) Trace of MCCM yield surface on the P-γ plane.

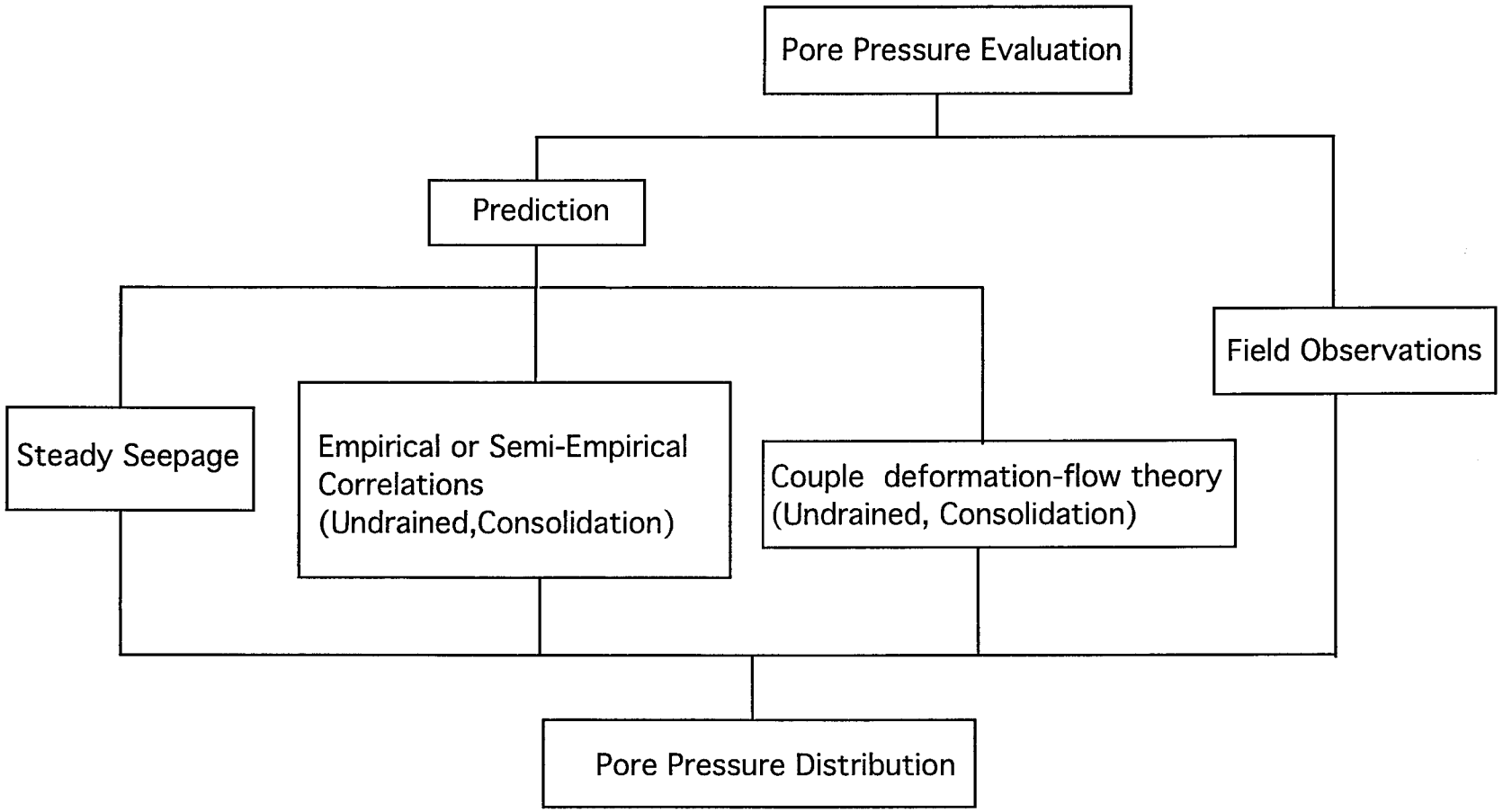

Figure (3.3) Methods of pore pressure evaluation (De Alencar(1988)).

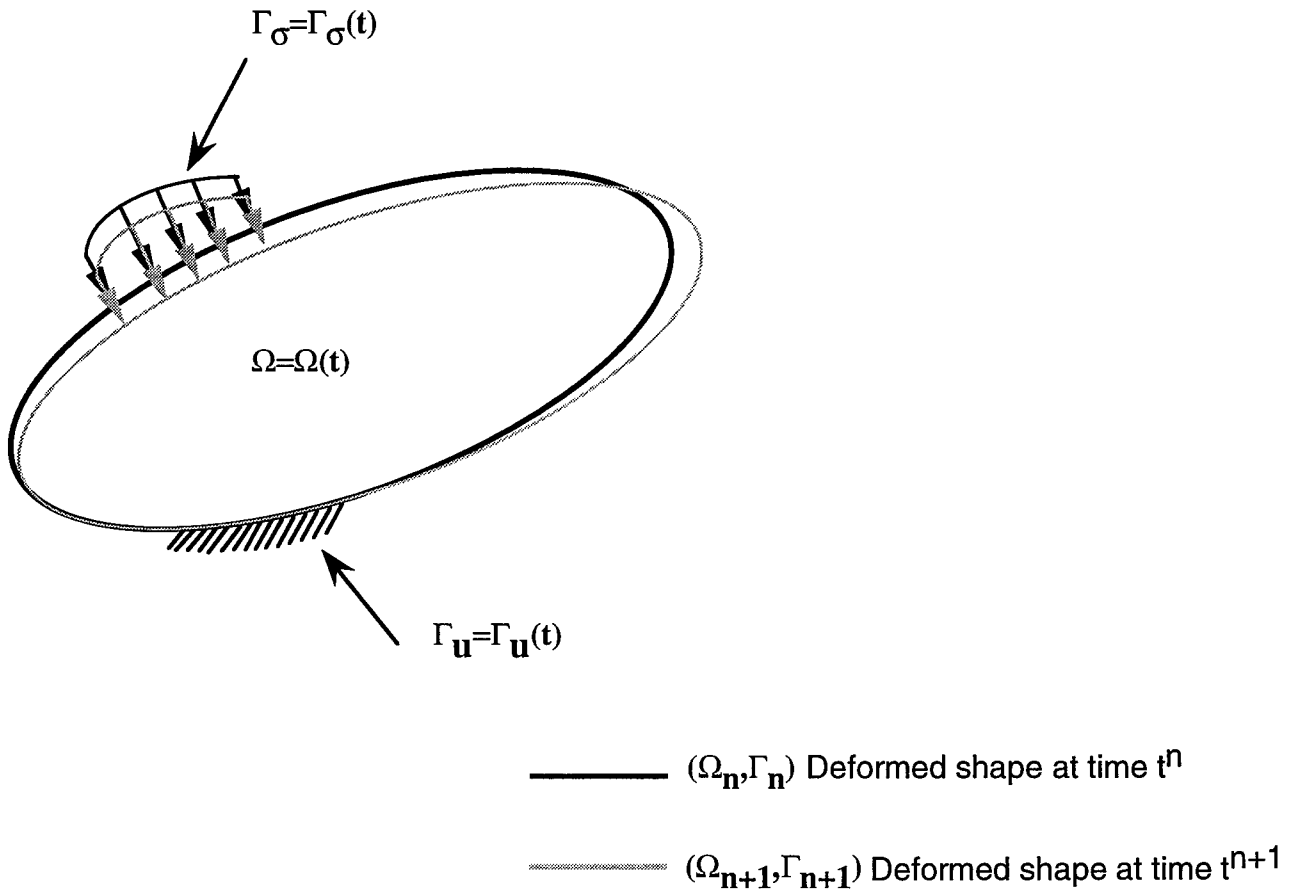

Figure (3.4) Schematic illustration of time-varying problem domain and boundaries.

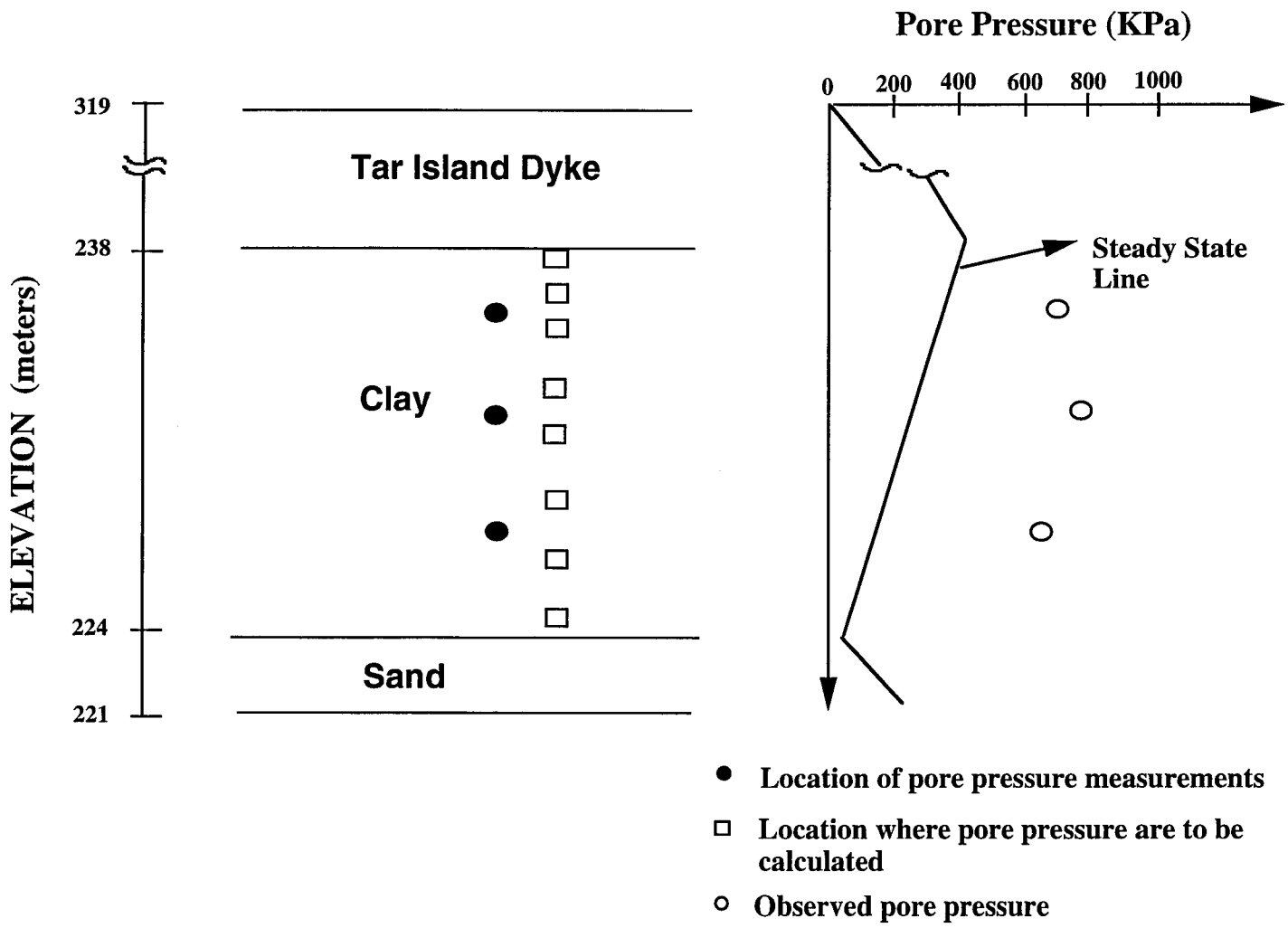

Figure (3.5) Example of pore pressure calculation.

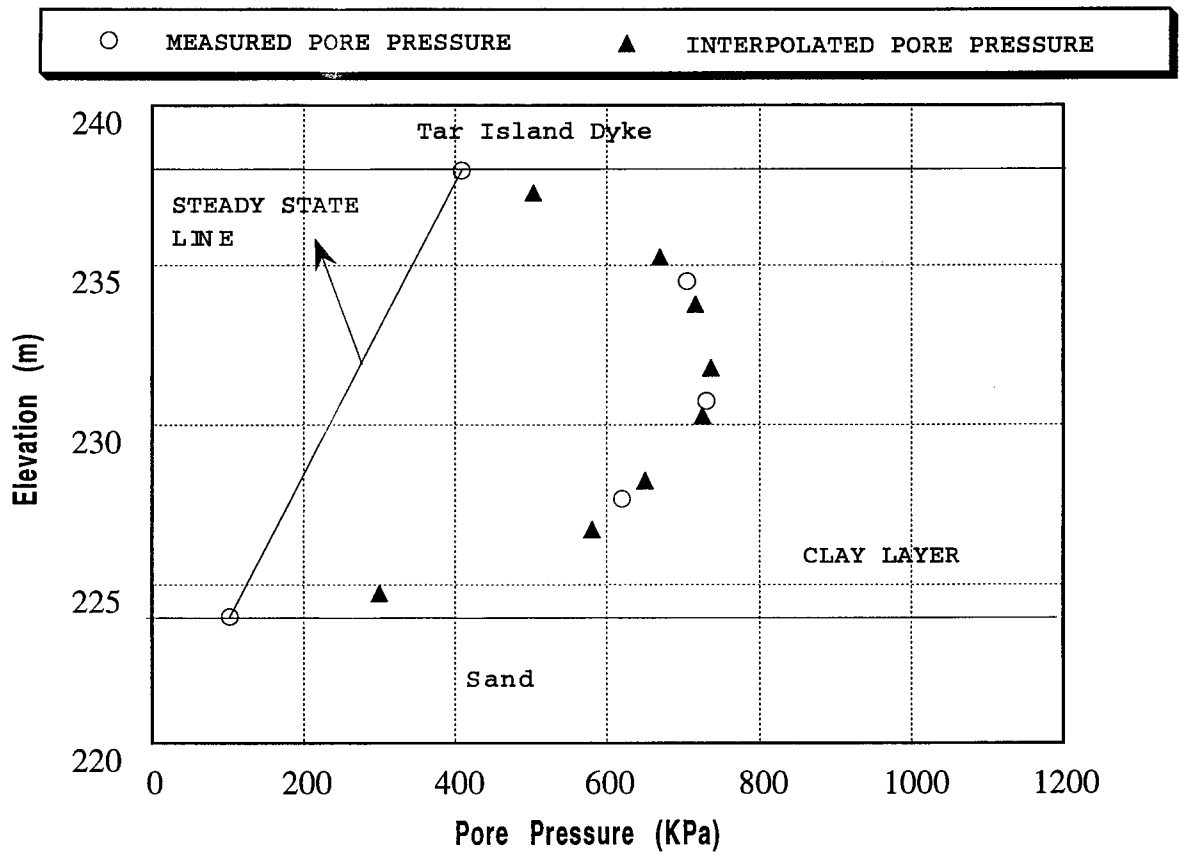

Figure (3.6) Comparison between interpolated and measured pore pressure.

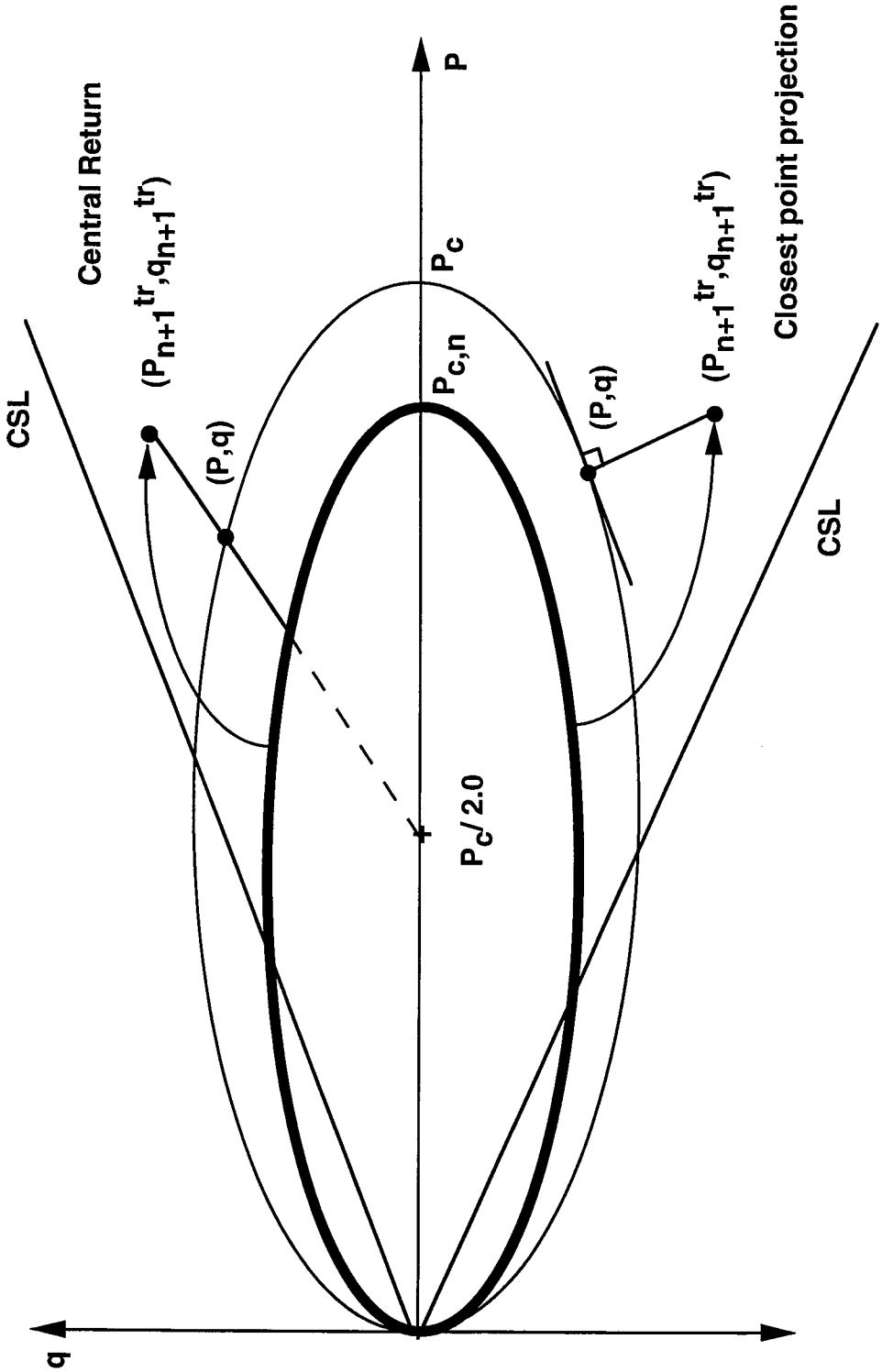

Figure (3.7) Central return and closest point projection mapping schemes (modified after Borja and Seung (1990)).

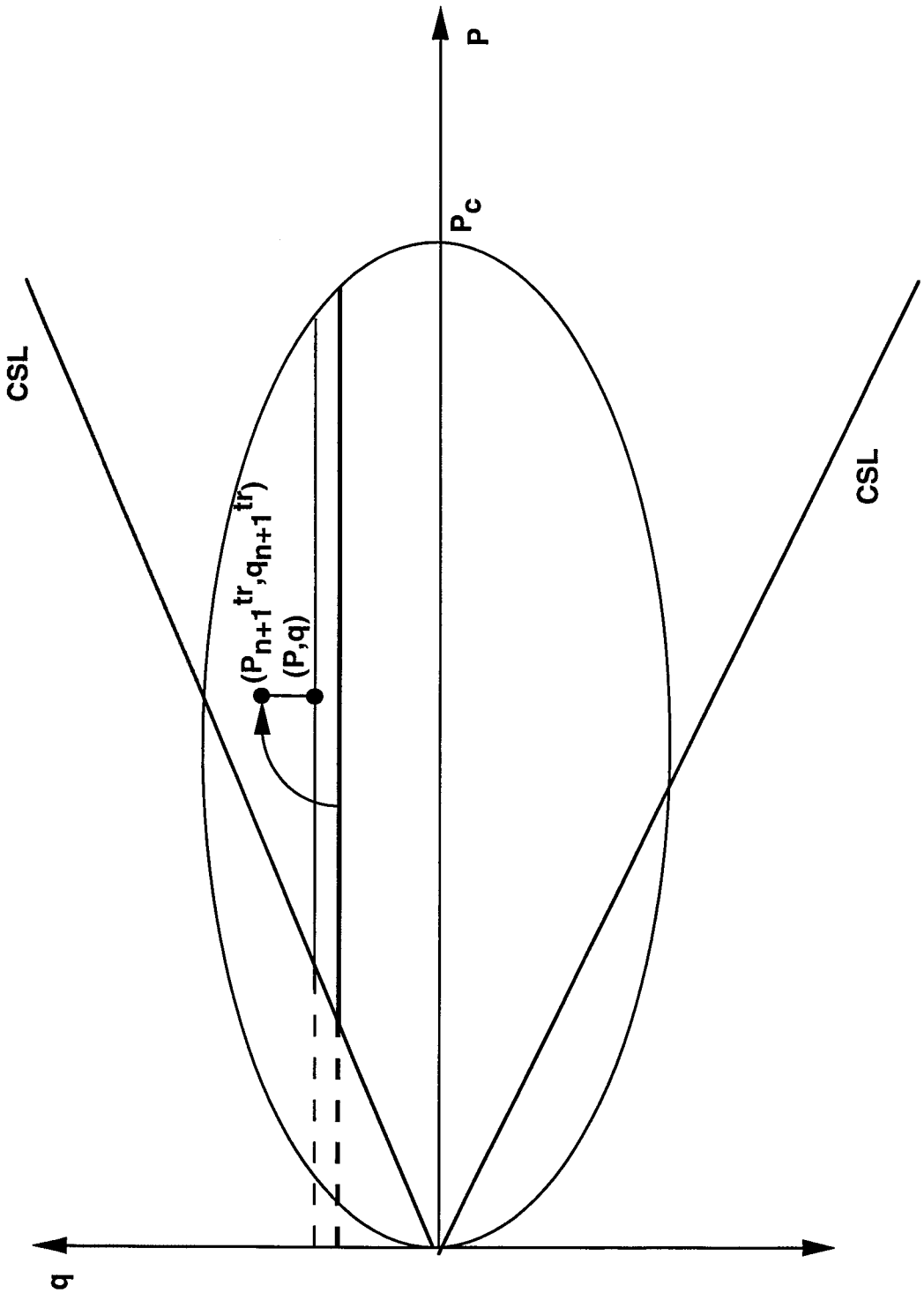

Figure (3.8) Radial return mapping schemes for the Von-Mises surface.

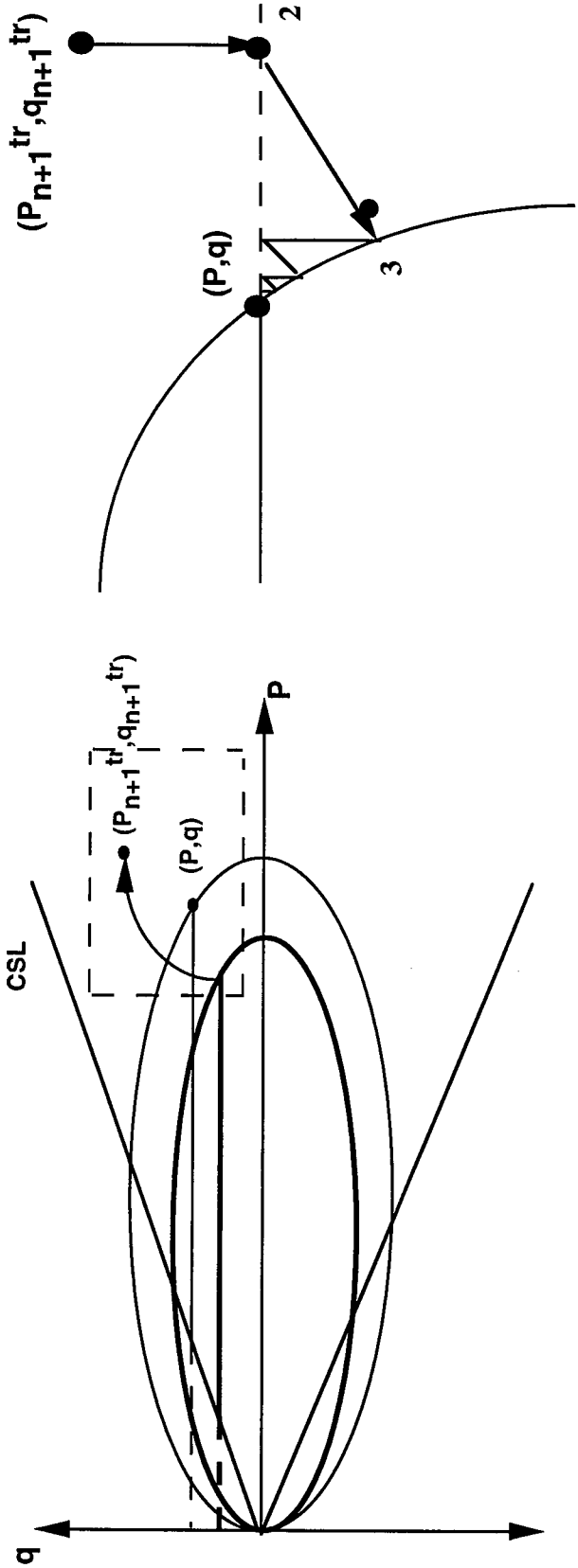

Figure (3.9) Closest point radial return mapping technique for the double yield surface.

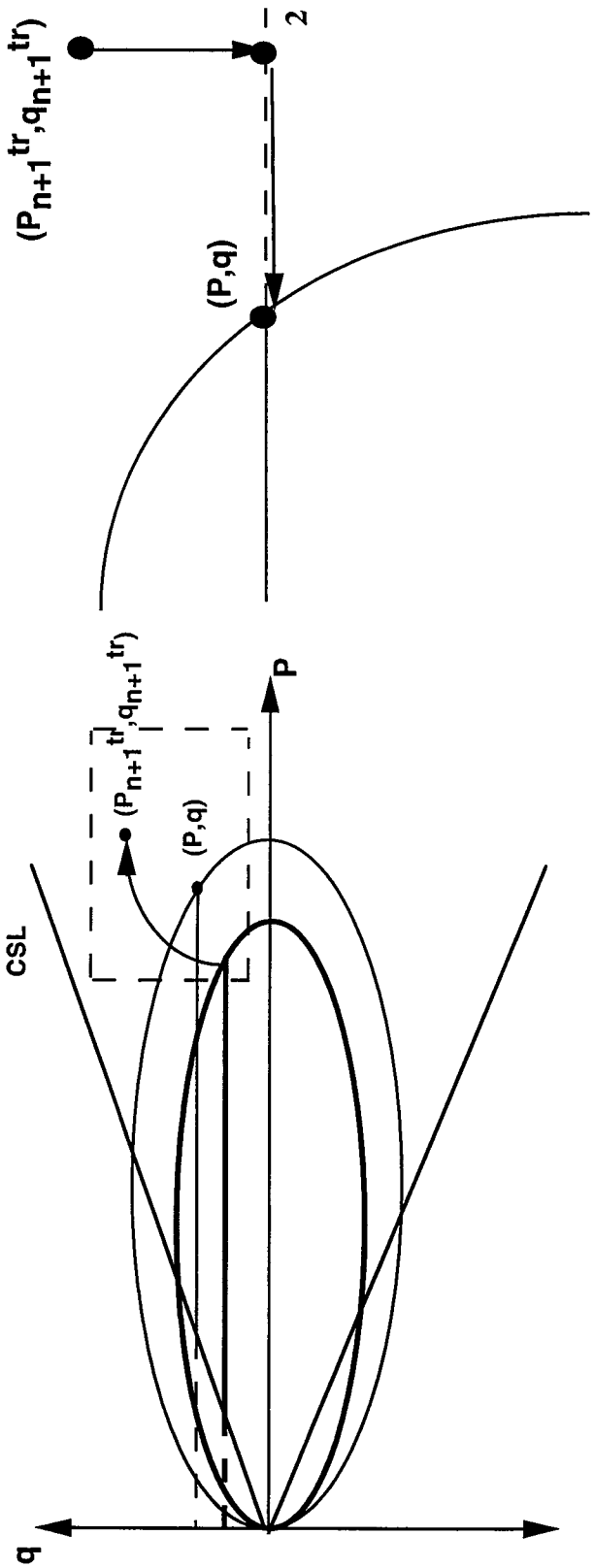

Figure (3.10) Hydrostatic radial return mapping technique for the double yield surface.

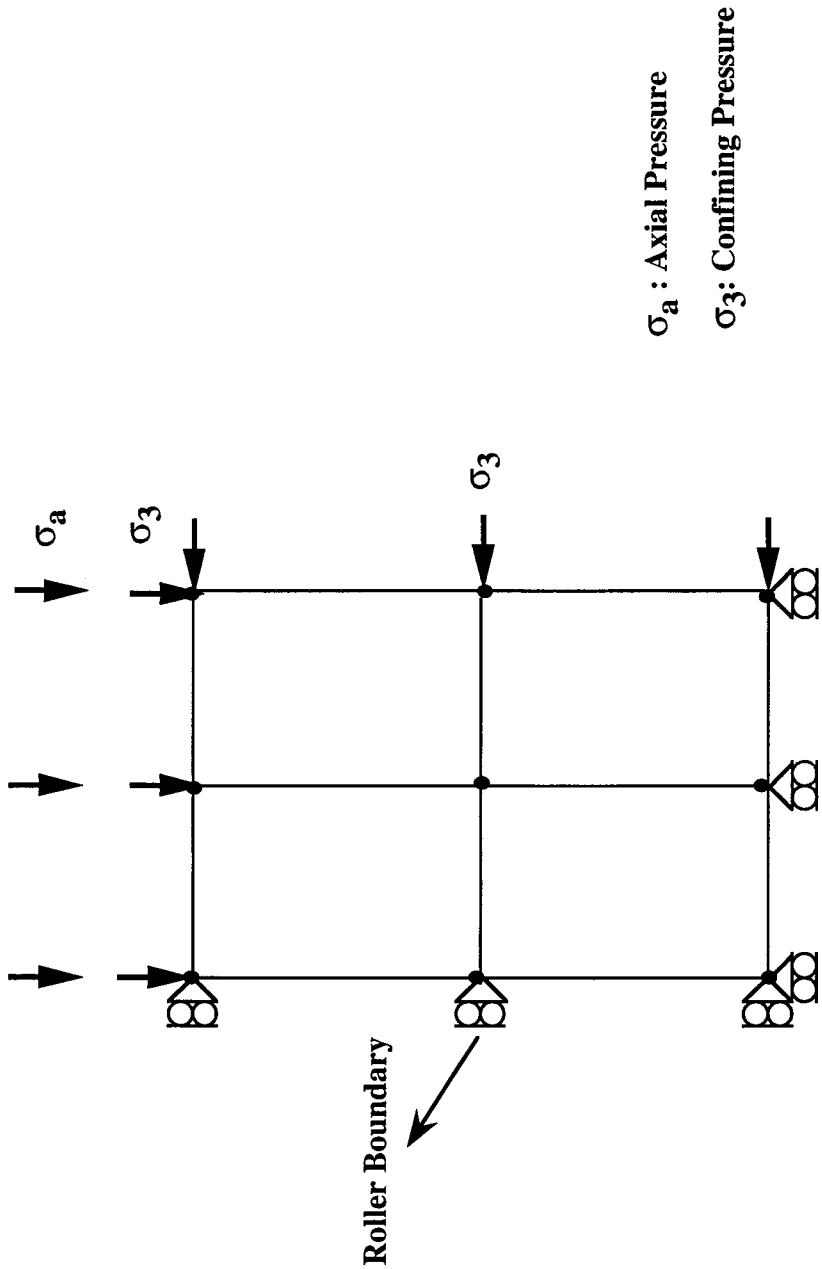

Figure (3.11) Finite element mesh of the numerical example.

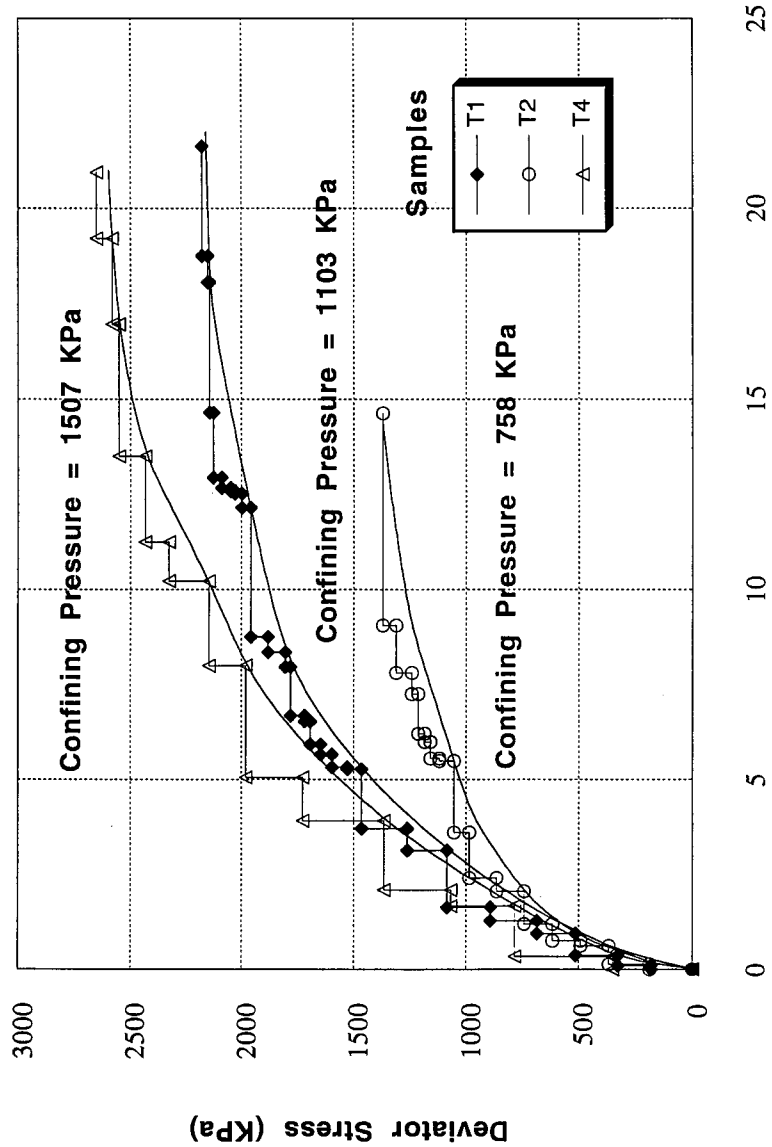

Figure (3.12) Results of the triaxial tests on samples T1, T2, and T4.

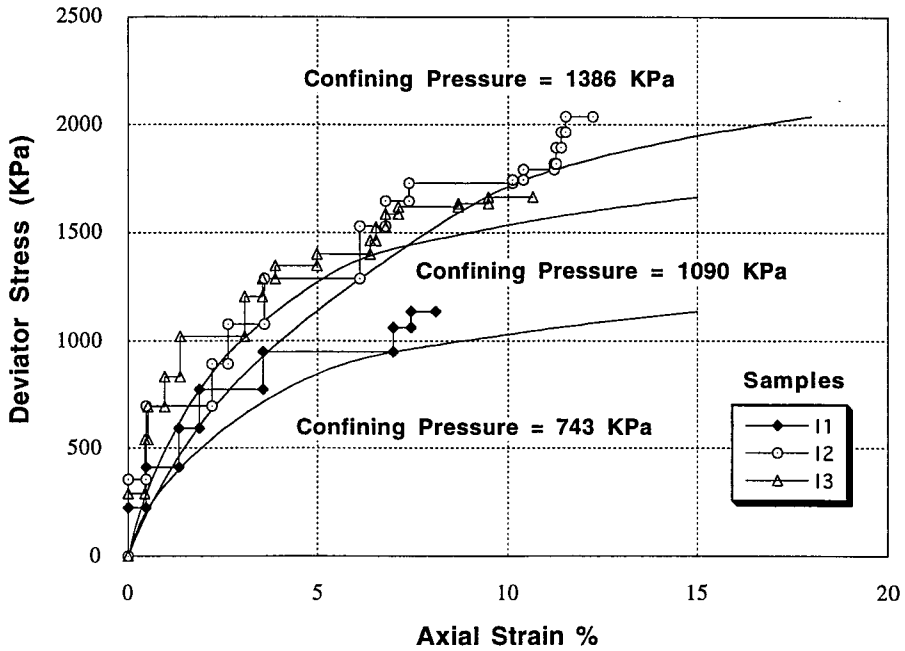

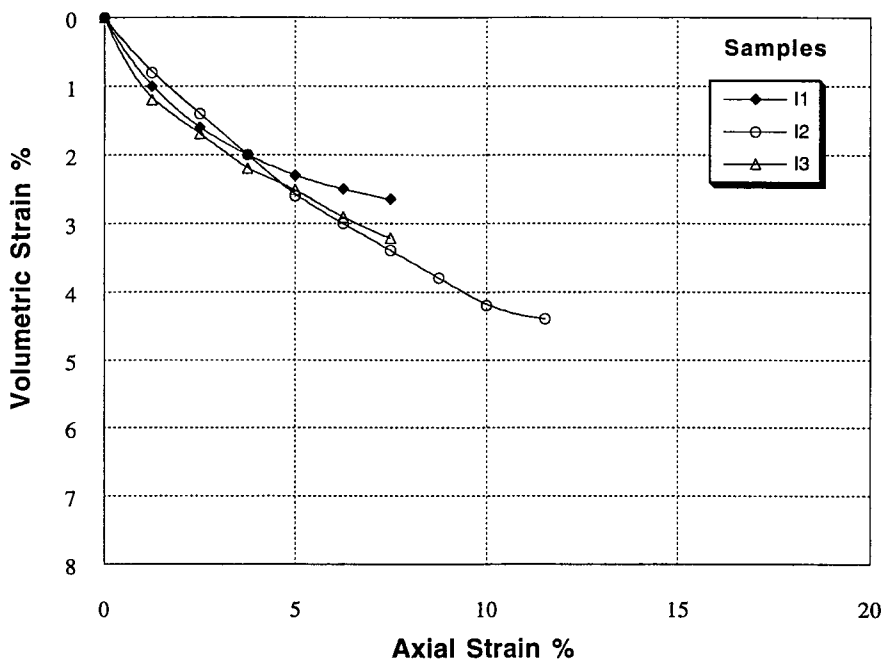

Figure (3.13) Results of the triaxial tests on samples I1,I2, and I3.

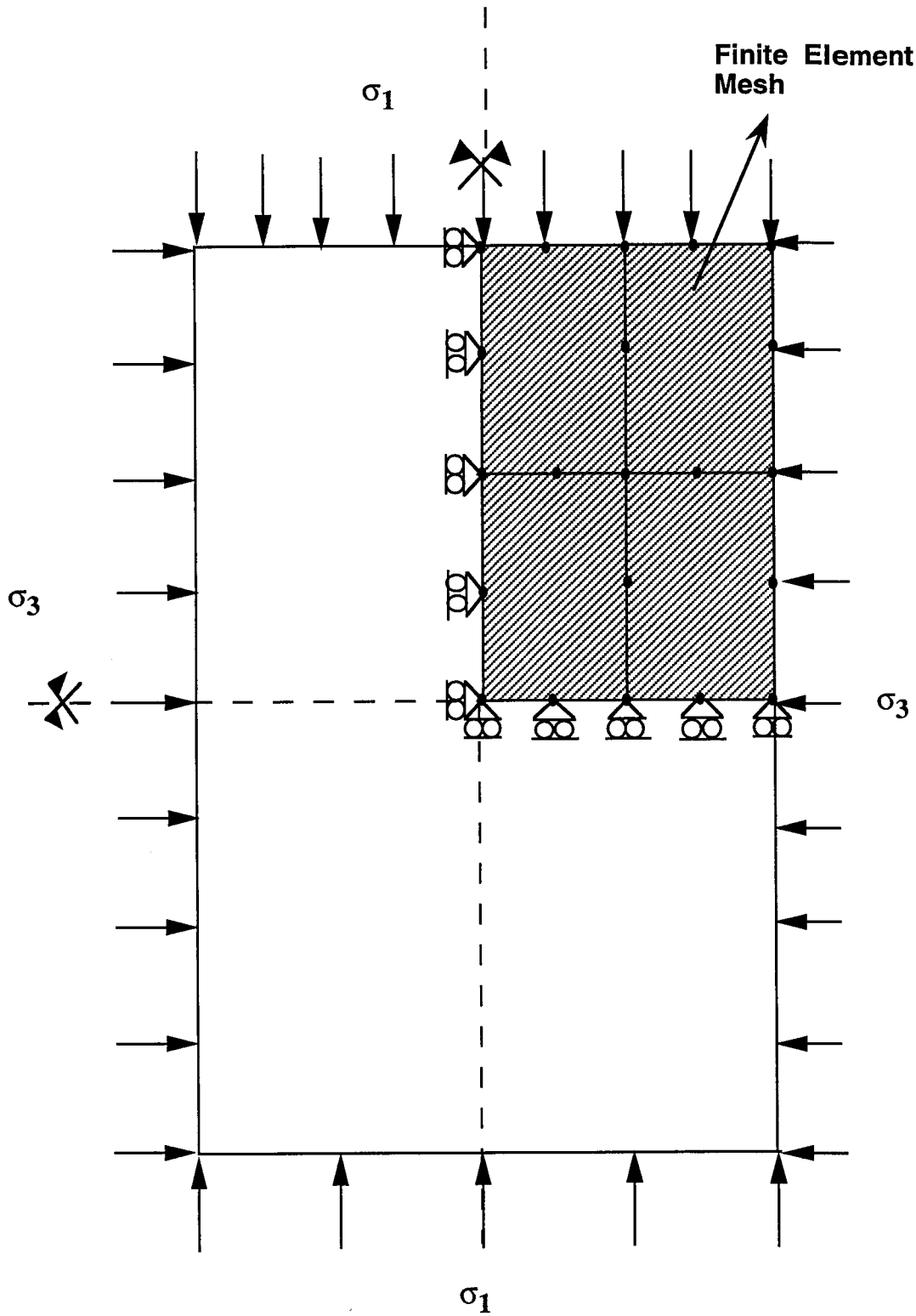

Figure (3.14) Numerical simulation of triaxial test on TID clay sample.

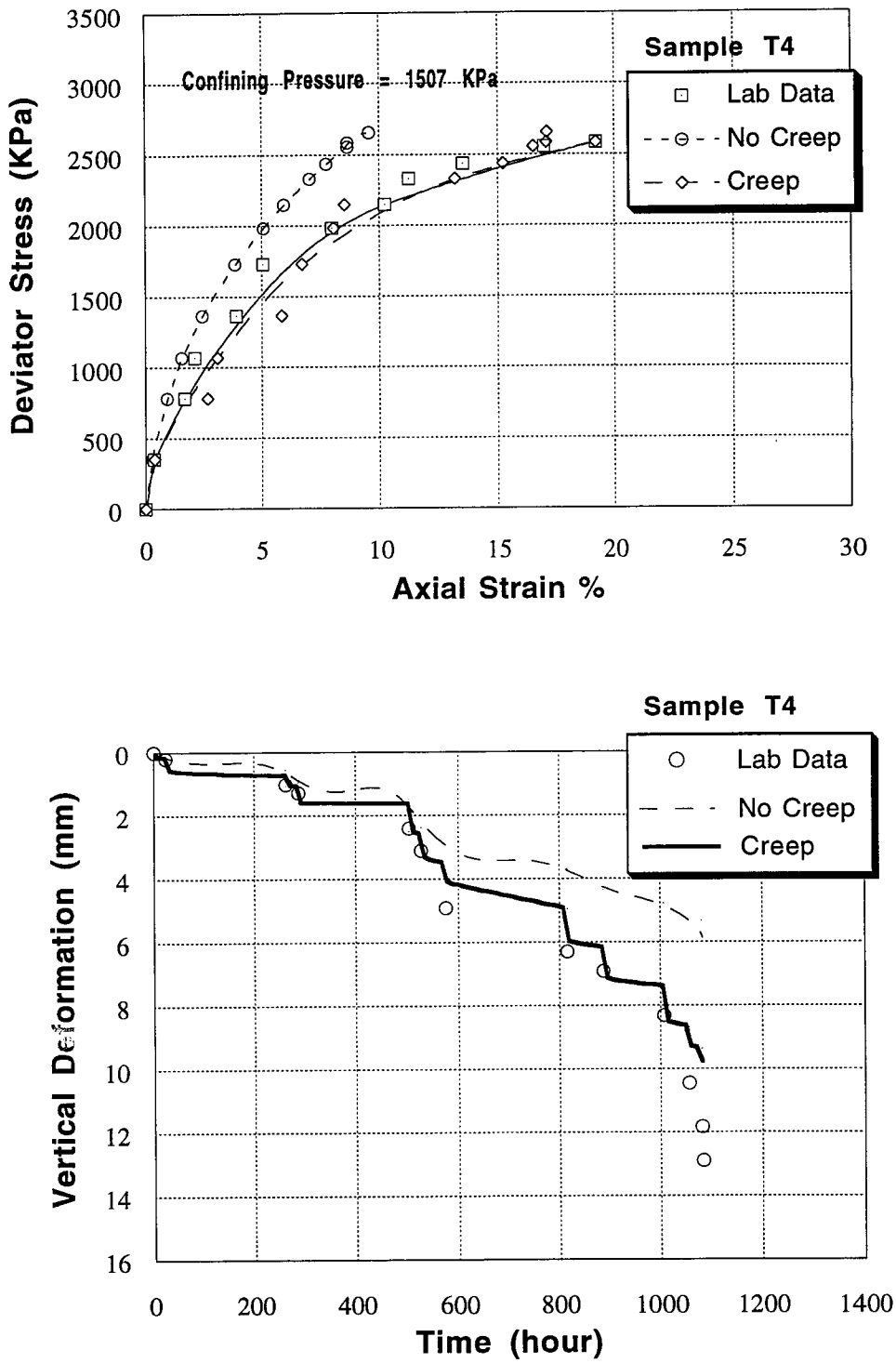

Figure (3.15) Numerical simulation of Horizontal sample T4.

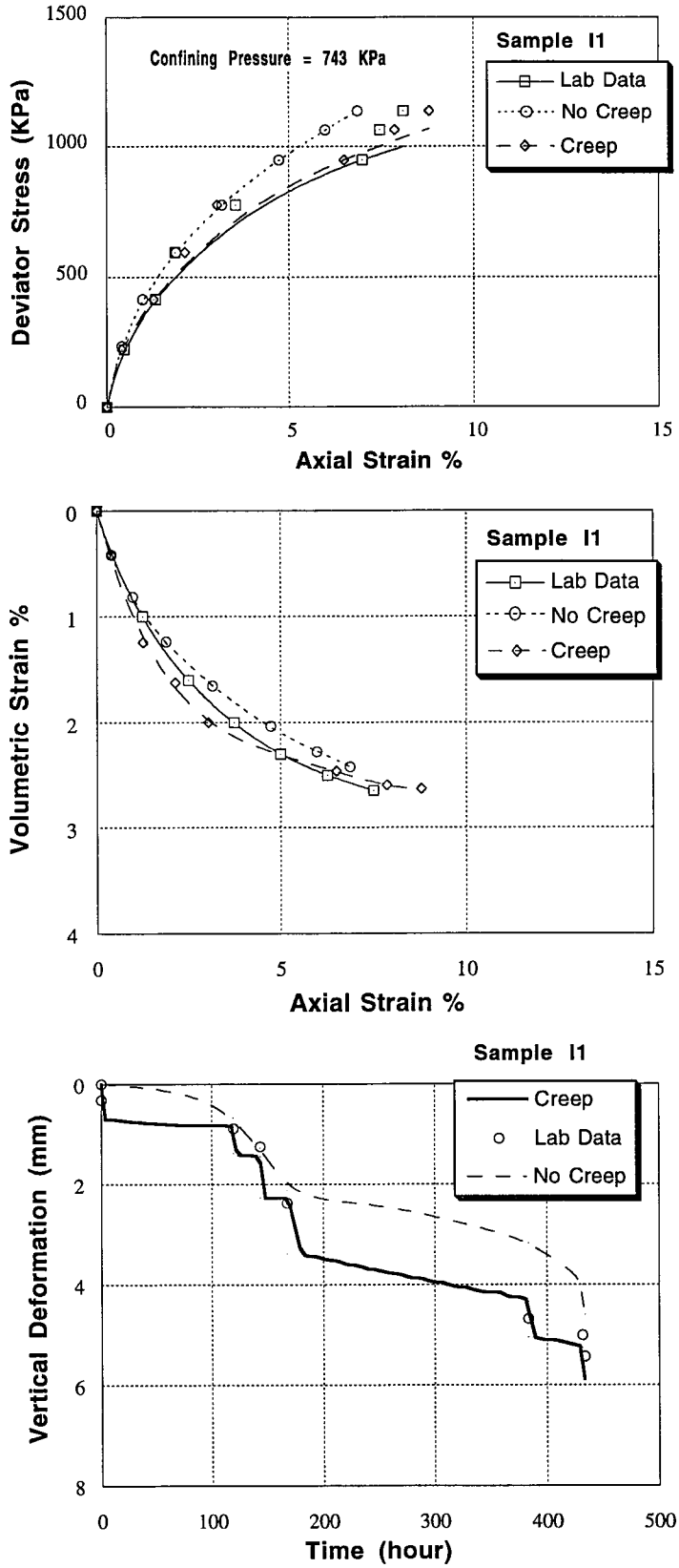

Figure (3.16) Numerical simulation of Inclined sample I1.

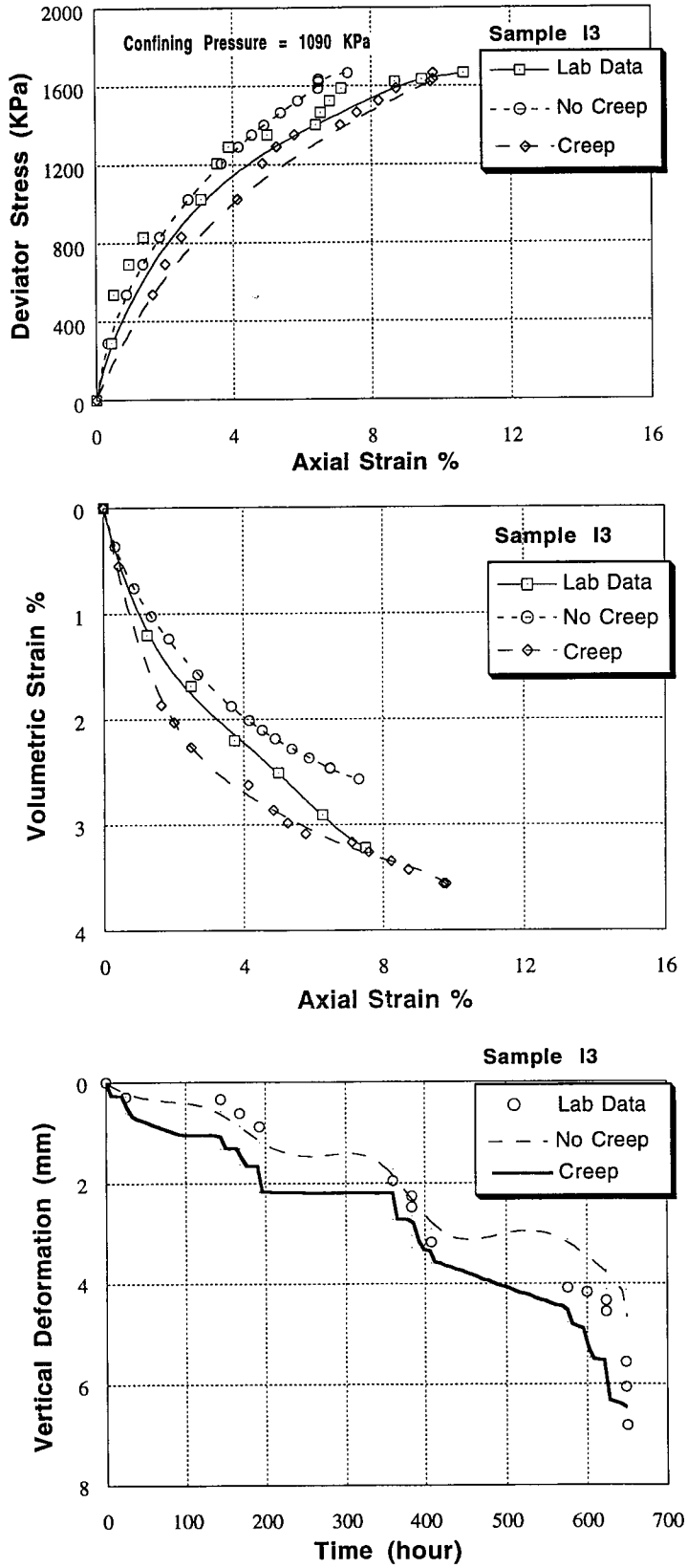

Figure (3.17) Numerical simulation of Inclined sample I3.

References:

Atkinson, J.H., and Bransby, P.L. 1978. The mechanics of soils: An introduction to critical soil mechanics. McGraw-Hill, London.

Bathe, K.J., 1982. Finite element procedure in engineering analysis. Prentice Hall Inc.

Bishop, A.W. and Henkel, D.J. 1962. The measurements of soil properties in the triaxial test. Arnold, London.

Bjerrum, L. 1967. Engineering geology of Norwegian normally consolidated marine clays as related to settlements of buildings. Geotechnique, **17**: .83-117.

Borja, R.I., and Kavazanjian, E.Jr. 1985. A constitutive model for the stress-strain-time behaviour of 'wet' clays". Geotechnique, **35**: 283-298.

Borja, R.I., and Lee, S.R. 1990. Cam-clay plasticity, Part I: Implicit integration of elasto-plastic comstitutive relations. Computer Methods in Applied Mechanics and Engineering, **78**: 49-72.

Borja, R.I., Hsieh, H.S., and Kavazanjian, E. Jr. 1990. Double-yield-surface model. II: Implementation and verification. ASCE Journal of the Geotechnical Engineering Division, **116**(GT9):1402-1421.

Byrne, P.M. 1976. Effective stress finite element slope analysis. Proceedings, 29th Canadian Geotechnical Conference,Vancouver, British Coloumbia, 1976. Session 8, pp. 35-55.

Chan, D.H. and Morgenstern, N.R. 1989. An effective stress approach for undrained analysis. Proceedings, 3rd International Symposium on Numerical Models in Geomechanics, Niagra Falls, Canada, May 1989. pp. 740-750.

Chan, D.H. and Morgenstern, N.R. 1992. User manual of program PISA. University of Alberta, Edmonton, Alberta, Canada.

Christian, J.T.1968. Undrained stress distribution by numerical methods. ASCE Journal of Soil Mechanics and Foundation Engineering Division, **94**(SM6): 1333-1345.

Christensen, R.W., and Wu, T.H. 1964. Analysis of clay deformation as a rate process. ASCE Journal of.Soil Mechanics and Foundation Engineering Division, **90**(SM6): 125-157.

De Alencar, J.A. 1988. Deformation of dams on sheared foundations. Ph.D. thesis, University of Alberta, Edmonton, Alberta, Canada.

De Alencar, J.A., Chan, D.H., and Morgenstern, N.R. 1992. Incorporation of measured pore pressure in finite element analysis. Proceedings, 45th Canadian Geotechnical Conference, Toronto, Ontario, 26-28 October, 1992. pp. 62-1 - 62-10.

Duncan, J.M., and Chang, C.Y. 1970. Non-linear analysis of stress and strain in soils. ASCE Journal of Soil Mechanics and Foundation Engineering Division, **96**(SM5): 1629-1653.

Hsieh, H.S. 1987. A non-associative cam-clay plasticity model for the stress-strain-time behaviour of soft clays. Ph.D. thesis, Stanford University, California, U.S.A..

Kavazanjian, E. Jr., and Mitchell, J.K. 1980. Time-dependent deformation behaviour of clays. ASCE Journal of the Geotechnical Engineering Division, **106**(GT6): 611-630.

Kondner, R.L. 1963 . Hyperbolic stress-strain response: Cohesive soils. ASCE Journal of Soil Mechanics and Foundation Engineering Division, **89** (SM1): 115-144.

Krieg, R.D. and Krieg, D.B. 1976. Accuracies of numerical solution methods for the elastic perfectly plastic model. Journal of Pressure Vessel Technology, ASME, **99**: 510-515.

Mesri, G., Febres, C.E., Shield, D.R., and Castro, A. 1981. Shear stress-strain-time behaviour of clays. Geotechnique, **31**: 537-552.

Mittal, H.K., and Hardy, R.M. 1977. Geotechnical aspects of Tar sand tailings dyke.ASCE, Proceedings of the conference on geotechnical practice of disposal of solid waste materials, Ann Arbor, Michigan, June 13-15, 1977. pp. 327-347.

Morsy, M.M. 1994. Effective stress modeling of creep behaviour of clay. Ph.D. thesis, University of Alberta, Edmonton, Alberta, Canada.

Morsy, M.M., Chan, D.H., and Morgenstern, N.R. 1993. Numerical simulation of drained creep deformation of Tar-Island dyke clay. Proceedings, International Conference on Soft Soil Engineering, Guangzhou, China, November 8-11, 1993. pp. 190-195.

Murayama, S., and Shibata, T. 1961. Rheological properties of clays. Proceedings, 5th International Conference in Soil Mechanics and Foundation Engineering, Paris, France, July 17-22, 1961. Vol. 1 pp. 269-273.

Prevost, J.H. 1987. Modelling behaviour of geomaterials. *In* Geotechnical Modelling and Applications. *Edited by* S.M. Sayed. Gulf puplishing company, Huston.

Roscoe, K.H., and Burland, J.B. 1968. On the generalized stress-strain behaviour of "wet" clay. Engineering plasticity. *Edited by* J.Heyman and F.A. Leckie. Cambridge University Press, Cambridge, England.

Roscoe, K.H., Schofield, A.N., and Turairajah, A. 1963. Yielding of clays in state wetter than critical. Geotechnique, **13**: 211-246.

Simo, J.C. and Taylor, R.L. 1983. Consistent tangent operators for rate-independent elastoplasticity. Computer Methods in Applied Mechanics and Engineering, **48**: 101-118.

Singh, A., and Mitchell, J.K. 1968. Generalized stress-strain-time function for soil. ASCE Journal of Soil Mechanics and Foundation Engineering Division, **94**(SM1): 21-46.

Taylor, D.W. 1948. Fundamentals of soil mechanics. John Wiley and Sons, New York, N.Y.

Tavenas, F., Leroueil, S., and Roy,M. 1978. Creep behaviour of an undisturbed lightly overconsolidated clay. Canadian Geotechnical Journal, **15**: 402-423.

Watts, B.D. 1980. Lateral creep deformations in the foundation of a high dam. M.Sc. thesis, University of Alberta, Edmonton, Alberta, Canada.

Wilkins, M.L. 1964. Calculation of elastic-plastic flow. Chapter 3. *In* Methods of Computational Physics. Acadamic press, NewYork.

Wroth, C.P., and Loudon, P.A. 1967. The correlation of strains within a family of triaxial tests on overconsolidated samples of Kaolin. Proceedings, 1st Geotechnical Conference on Shear Properties of Natural Soils and Rocks, Oslo, Norway, June, 1967. Vol. 1, pp.159-163.

Zienkiewicz, O.C. amd Cormeau, I.C. 1974. Viscoplasticity, plasticity and creep in elastic solids - an unified numerical approach. International Journal of Numerical Methods in Engineering, **8**: 821-845.

Zienkiewicz, O.C. and Humpheson, C. 1977. Viscoplasticity: A generalized model for description of soil behaviour. *I n* Numerical Methods in Geotechnical Engineering.*Edited by* S.Desai and J.T. Christian. McGraw-Hill Book Company, pp. 116-147.

CHAPTER 4

NUMERICAL SIMULATION OF DRAINED CREEP DEFORMATION OF TAR-ISLAND DYKE CLAY[1]

4.1 INTRODUCTION:

Saturated clays, like most engineering materials, undergo shear deformations that are time dependent. Although manifestations of such behavior have been recognized and sometimes accounted for in practice, little systematic treatment of clay response under generalized time loading histories has been pursued.

Clayey soils are found in almost all regions in Canada. Situated in northern Alberta, Canada, the 92 m. high Great Canadian Oil Sand Tar Island Dyke is constructed on soft clay on the west bank of the Athabasca river near Fort McMurray. The time dependent lateral deformations of the clay foundation were monitored by several inclinometers over a period of twenty years. Based on the nature of the lateral deformations and the piezometer readings in the clay foundation, it is postulated that the movements are the result of drained creep deformation (Mittal and Hardy 1977).

To study the creep behaviour of clay, a series of incremental drained creep triaxial tests were performed at the University of Alberta on samples from the foundation of Tar Island Dyke (Watts 1980). In this paper, a numerical simulation of laboratory tests was carried out using a recently developed constitutive model for the stress-strain-time behavior of cohesive soils. The model employs two yield surfaces, the Modified Cam-Clay ellipsoid (Roscoe and Burland 1968), and the Von Mises cylinder inscribed in the

---

[1] A version of this chapter was presented in the 1st International Conference on Soft Soil Engineering (Guangshou, China, November 1993) as: Morsy, M.M., Chan, D.H., and Morgenstern, N.R. 1993. Numerical simulation of drained creep deformation of Tar-Island dyke clay.

Cam-Clay ellipsoid (Hsieh et al. 1990). In this model the parameters required for material characterization are few and obtainable from conventional laboratory tests. The constitutive model is coded into a finite element program PISA^{TM} (Program for Incremental Stress Analysis) developed at the University of Alberta.

4.2 GEOLOGY AND GEOTECHNICAL PROPERTIES OF THE TAR ISLAND DYKE CLAY:

The Tar Island Dyke (TID) clay was mainly formed by sedimentation in an abandoned meander of the Athabasca river. The major source of sediment of the meander was suspended silt and clay from overbank flows when the Athabasca river flooded. There is also evidence of essentially still water deposition in the form of numerous calcium carbonate shells throughout the deposits (Watts 1980).

The TID clay is very stiff, medium to highly plastic and contains variable amounts of silt, sand, organic material, coal fragments and calcium carbonate shell material. Approximately 30 percent was clay size material with the majority of the remainder in the silt size range. Horizontal bedding is evident throughout the entire soil horizon. Bedding planes are marked by organic material concentrated in thin dark seams less than 10 cm thick at irregular intervals.

Soil samples were obtained fourteen years after commencement of dyke construction, when the height of the dyke reached 90 meters. The plasticity index of the material ranged from 20 to 30 percent and the liquid limit from 44 to 54 percent. The average natural water content of the samples being tested was approximately 27 percent which is significantly less than the natural water content of approximately 45 percent before dyke construction. The difference in water content, of course, reflects consolidation of the clay due to the imposed dyke load.

4.3 TEST PROGRAM AND PROCEDURES:

Drained triaxial creep tests were performed on two sets of samples (Watts 1980). Each set consisted of three samples, each consolidated under different isotropic consolidation pressure. The samples in one set were prepared with the bedding plane horizontal and were numbered T1, T2 and T4. The samples in the other set were prepared with the bedding plane inclined at an angle of 45^{o} and were numbered I1, I2 and

I3. All samples were consolidated isotropically to pressures above the average preconsolidation stress of 650 KPa, determined from odeometer tests. The final isotropic consolidation pressures during application of shear stress varied from 740 KPa to 1500 KPa between samples which allowed an investigation of the influence of normal effective stress or water content on the creep behaviour.

All the creep tests were stress controlled tests in order to simulate the field conditions associated with the construction of the Tar Island Dyke.

4.4 TEST RESULTS:

The results of the triaxial tests are shown in Figures (4.1) and (4.2). The stresses and strains at the beginning and the end of each load increment are joined by straight lines. This straight line path represents the stress-strain path followed by the sample during the test. A smooth line is also drawn through the final stress-strain point of each extended increment. The smooth line represent the long term stress-strain behaviour of the clay.

All samples failed along distinct shear planes and as with all stress controlled tests, failure was catastrophic. It is known that the TID clay was strain weakening, but it was not possible to evaluate this characteristic in a stress controlled test.

4.5 CONSTITUTIVE MODEL

The constitutive model presented here is based on the concept of decomposition of total strain into an immediate (time-independent) part and a delayed (time-dependent) part in a generalized three-dimensional framework (Bjerrum 1967; Borja and Kavazanjian 1985; and Hsieh et al. 1990), see Figure (4.3). In modelling the time independent component, the ellipsoidal modified Cam-clay volumetric yield surface F and an interdependent horizontal deviatoric yield surface G beneath the ellipsoid are used.

[4.1] $$F = F(\sigma', P_c) = \frac{q^2}{M^2} + P\,(P - P_c) = 0,$$

[4.2] $$G = G\,(\sigma', q_c) = q - q_c = 0,$$

where

σ' : effective stress components;

P : mean normal stress $= \frac{\sigma'_1 + \sigma'_2 + \sigma'_3}{3}$;

q : deviatoric stress $= \frac{1}{\sqrt{2}} \sqrt{(\sigma'_1 - \sigma'_2)^2 + (\sigma'_2 - \sigma'_3)^2 + (\sigma'_3 - \sigma'_1)^2}$;

η : stress ratio on the yield surface F;

M : slope of the critical -state line in the P-q plane;

P_c : preconsolidation pressure;

q_c : radius of Von Mises cylinder.

The time dependent part in this model consists of a volumetric creep component (Taylor 1948) and a deviatoric creep component (Singh and Mitchell 1968):

[4.3] $$\dot{\varepsilon}_v = \frac{\psi}{(1+e)t_v},$$

[4.4] $$\dot{\varepsilon}_d = Ae^{\overline{\alpha}\overline{D}}\left(\frac{(t_d)_i}{t_d}\right)^m,$$

where

$\dot{\varepsilon}_v$: volumetric strain rate;

$\dot{\varepsilon}_d$: deviatoric strain rate;

ψ : secondary compression coefficient, in logarithmic scale;

e : void ratio as well as the Euler's number 2.71828;

t_v : volumetric age, relative to an initial reference time $(t_v)_i$;

$(t_v)_i$: instant volumetric time, usually set to unity;

$A, \overline{\alpha}, m$: Singh-Mitchell creep parameters;

$(t_d)_i$: instant deviatoric time, usually set to unity;

t_d : deviatoric age relative to $(t_d)_i$;

$\overline{D}$: $\frac{(\sigma_1 - \sigma_3)}{(\sigma_1 - \sigma_3)_{ult}}$ is the deviator stress level.

Based on this phenomenological model, the total strain-rate tensor can be decomposed into four components:

[4.5] $$\dot{\varepsilon} = \dot{\varepsilon}^{e} + \dot{\varepsilon}_{F}^{P} + \dot{\varepsilon}_{G}^{P} + \dot{\varepsilon}^{t} ,$$

where superscripts e and p denote the time independent elastic and plastic components, respectively; superscript t denotes the time dependent (creep) component; and subscripts F and G refer to the appropriate ellipsoidal and cylindrical yield surfaces, respectively.

The strain rate components of equation (4.5) are evaluated by applying:

(a) The generalized Hooke's law to evaluate the elastic component.

(b) For the immediate plastic component, it is evaluated according to the stress state as follows:

(i) Semi-plastic process on F surface, in the event that F is the only surface involved in the deformation process. In this case the soil is to be considered normally consolidated with respect to F but overconsolidated with respect to G.

(ii) Semi-plastic process on G surface, in the event that G is the only surface involved in the deformation process. In this case the soil is to be considered normally consolidated with respect to G but overconsolidated with respect to F.

(iii) Fully plastic process, in the event that both the F and G surfaces are both involved in the deformation process.

(c) The total creep strain rate is evaluated by employing a flow rule for both volumetric and deviatoric yield surfaces and by forcing the creep strain rate to satisfy the secondary compression law for volumetric creep and the Singh-Mitchell law for the deviatoric creep simultaneously expressed as:

[4.6] $$\dot{\varepsilon}^{t} = \frac{\Psi}{3(1+e)t_{v}} I + \sqrt{\frac{3}{2}} A e^{\bar{\alpha}\bar{D}} \left[\frac{(t_{d})_{i}}{t_{d}} \right]^{m} \hat{n} ,$$

where

I : second-order identity tensor;

$$\hat{n} = \frac{\sigma'}{\|\sigma'\|} .$$

4.6 MODEL PARAMETERS:

The constitutive model proposed herein requires thirteen constants. Seven parameters for complete material definition in the absence of creep are: virgin compression index C_c, recompression index C_r, angle of internal friction ϕ, void ratio e_a at unit preconsolidation, the hyperbolic stress-strain parameters a, b and R_f. If creep effects are considered, six more constants are required: secondary compression coefficient C_α, Singh-Mitchell creep parameters A, m and $\bar{\alpha}$, and reference times $(t_v)_i$ and $(t_d)_i$. Table (4.1) summarizes the model parameters for the TID clay. The parameters C_c, C_r , e_a and C_s were computed from the results of isotropic triaxial tests (Taylor 1948; and Atkinson and Bransby 1978).

The hyperbolic parameters a, b and R_f and angle of internal friction ϕ were determined from isotropically consolidation undrained triaxial tests (Bishop and Henkel 1962). Figures (4.4a) and (4.4b) show the results of the creep drained triaxial test of sample I1 in axes time vs. strain rate and stress level vs. strain rate, respectively. These test results, and the test results of other samples, were used to obtain the average values of Singh-Mitchell parameters $\bar{\alpha}$,A, and m (Singh and Mitchell 1968; and Mesri et al. 1981).

The $(t_v)_i$ and $(t_d)_i$ were chosen to be one day based on the results of the drained creep triaxial tests. In the initial portion of the time vs. strain rate plot shown in Figure (4.4a), the strain rate decreases continuously in a non-linear manner. This strain accounts for both the consolidation and the creep effects. In the later part of the curve, the strain rate decreases continuously in a linear fashion and this is believed to be due entirely to the drained creep effect.

4.7 COMPARISON BETWEEN THE THEORETICAL AND EXPERIMENTAL RESULTS:

In order to simulate the two sets of the creep drained triaxial tests a mesh of four eight-nodes elements were employed. These elements were prestressed to the same

isotropic effective pressure in the laboratory tests. Then the elements were sheared following the same stress-time history of the laboratory test.

Two types of analysis were carried out, a time independent analysis and a time dependent analysis. The results of the numerical simulations are shown in Figure (4.5) for horizontal bedding sample T4 and Figures (4.6) and (4.7) for inclined samples I1 and I3.

For the horizontal bedding sample T4, the inclusion of the creep in the model yields the most accurate prediction for both the axial strain and vertical deformations. In the case of the inclined bedding samples I1 and I3, the inclusion of the creep in the model improved the results of the analysis and show excellent agreement with the laboratory results.

4.8 CONCLUSIONS:

From the results of the laboratory tests and the numerical analysis, the following conclusions can be made:

1) Creep deformation was found to be a major component of the overall deformation of the TID clay.

2) The double yield surface model is shown to provide an accurate prediction of the stress-strain-time behaviour of the TID clay.

Table 4.1 Model Parameters For Tar Island Dyke.

Parameter	Symbol	Value
Virgin Compression Index	C_c	0.10665
Recompression Index	C_r	0.03
Secondary Compression Coefficient	$C\alpha$	0.0031
Hyperbolic Stress-Strain Parameters	a, b, R_f	0.0032,1.398,0.89
Singh-Mitchell Creep Parameters	A, $\bar{\alpha}$,m	0.052%/day,2.47,1.12
Angle Of Internal Friction	ϕ	26.49
Void Ratio At Pc = 1 KPa	e_a	.8909
Instant Volumetric And Deviatoric Time	$(t_v)_i$, $(t_d)_i$	1 day , 1 day

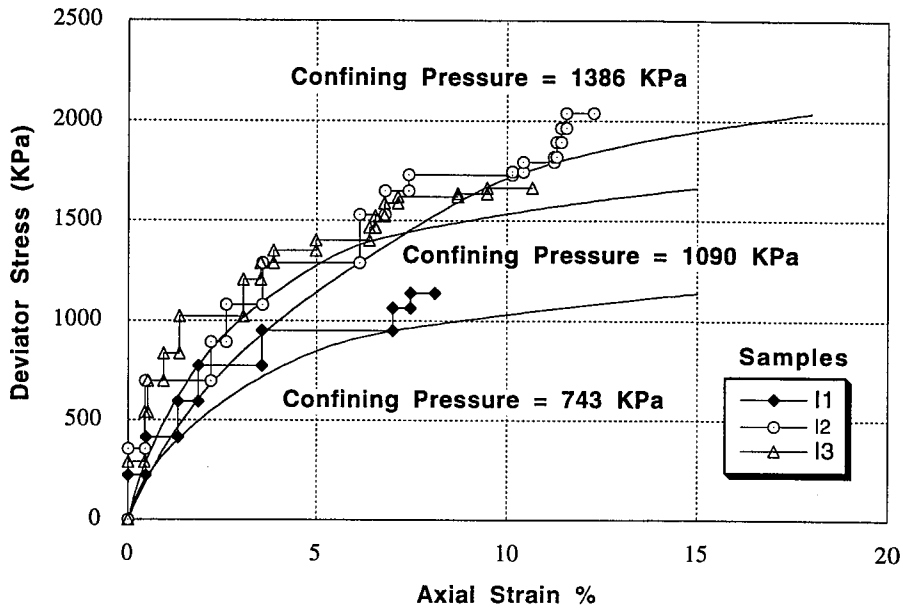

Figure (4.1a) Deviator stress vs. axial strain.

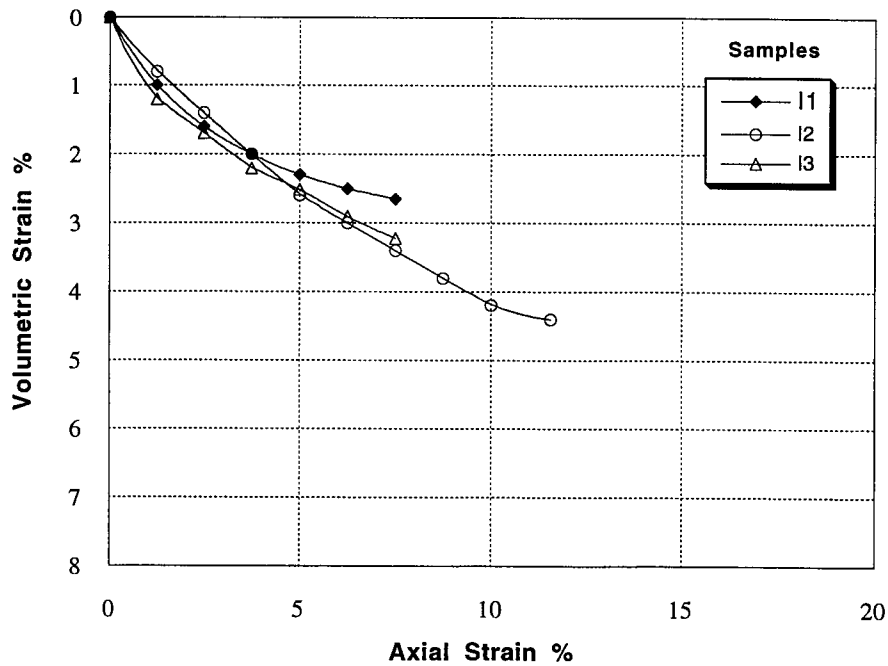

Figure (4.1b) Volumetric strain vs. axial strain.

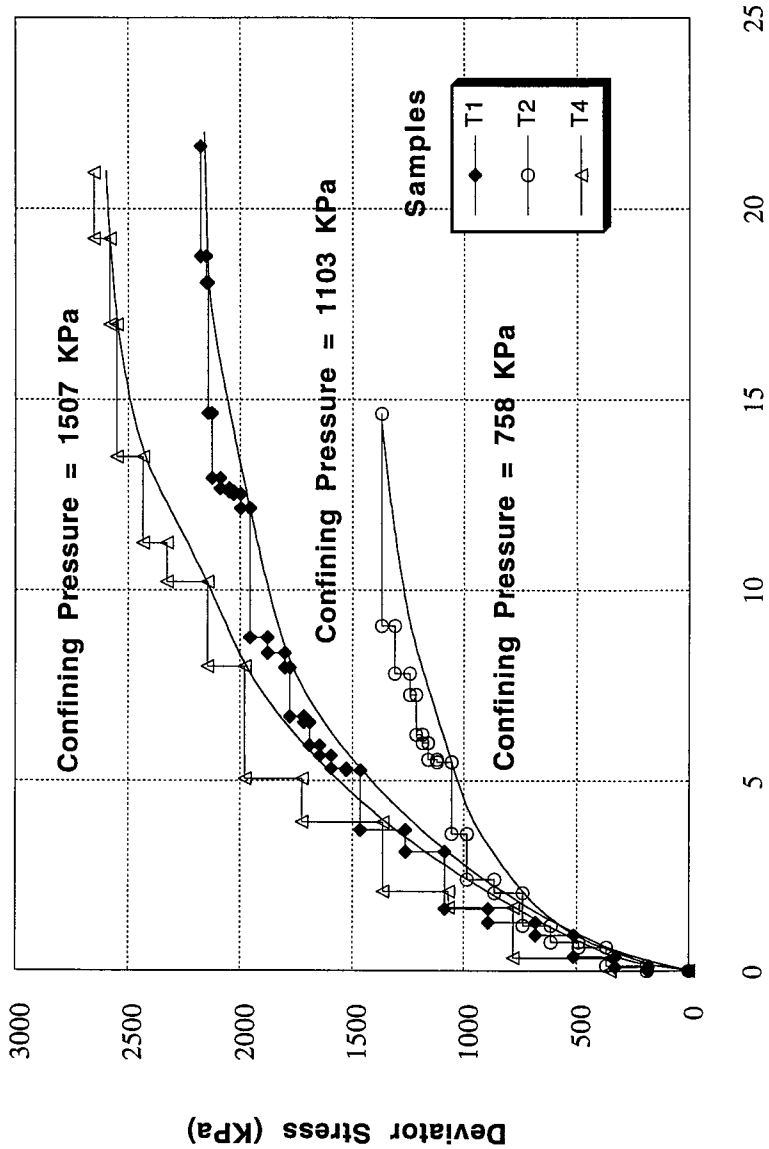

Figure (4.2) Deviator stress vs. axial strain.

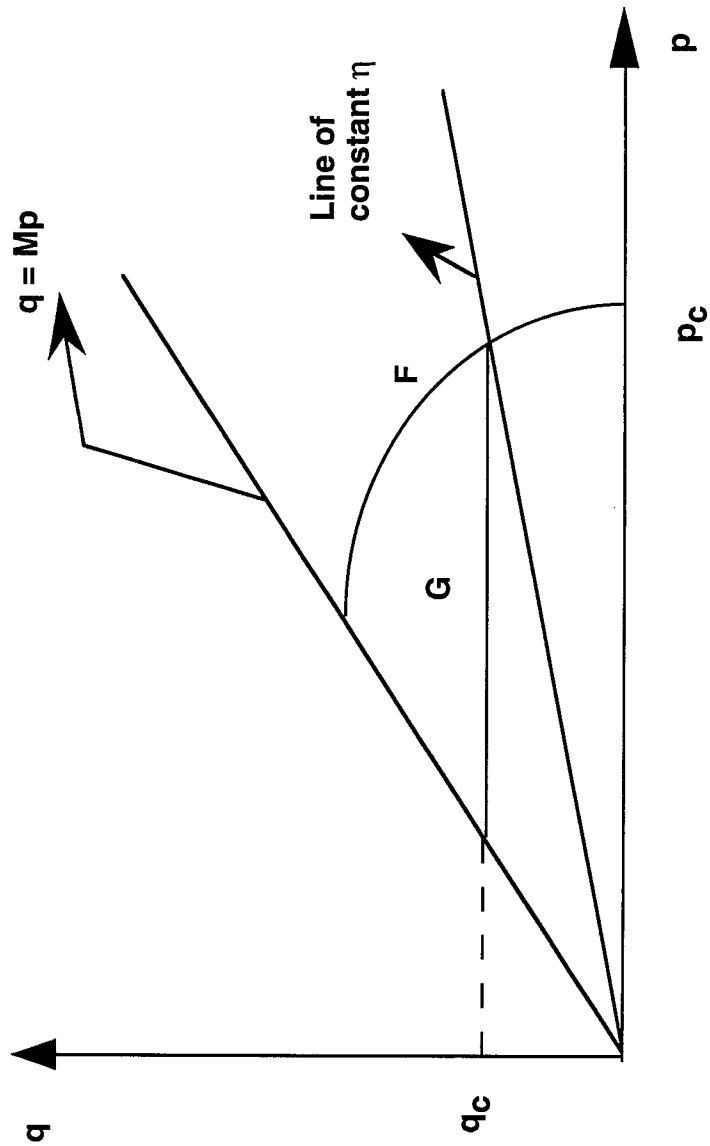

Figure (4.3) Projection of double yield Surface on P-q plane

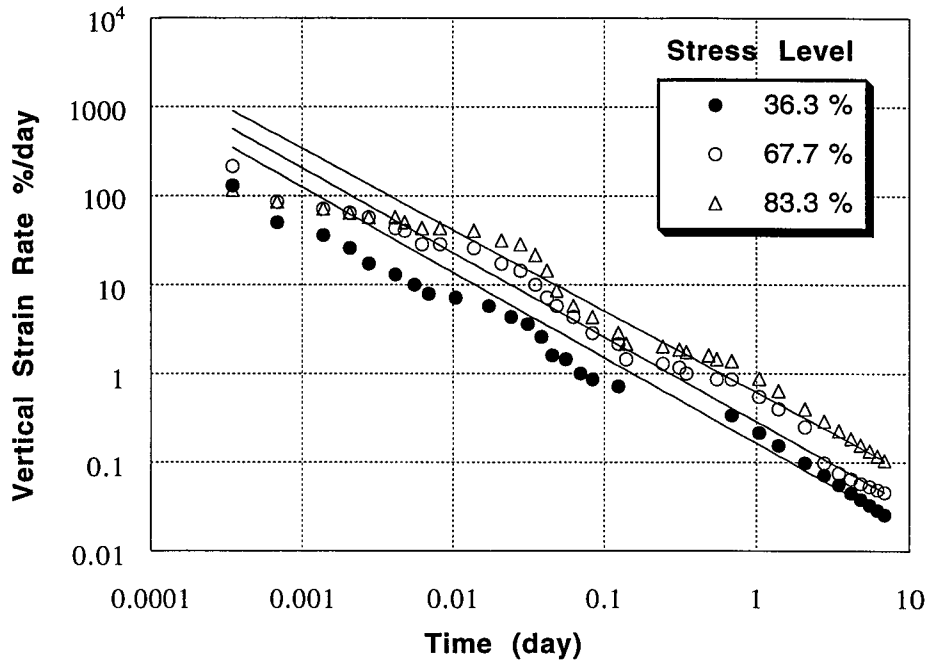

Figure (4.4a) Vertical strain vs. time for I1.

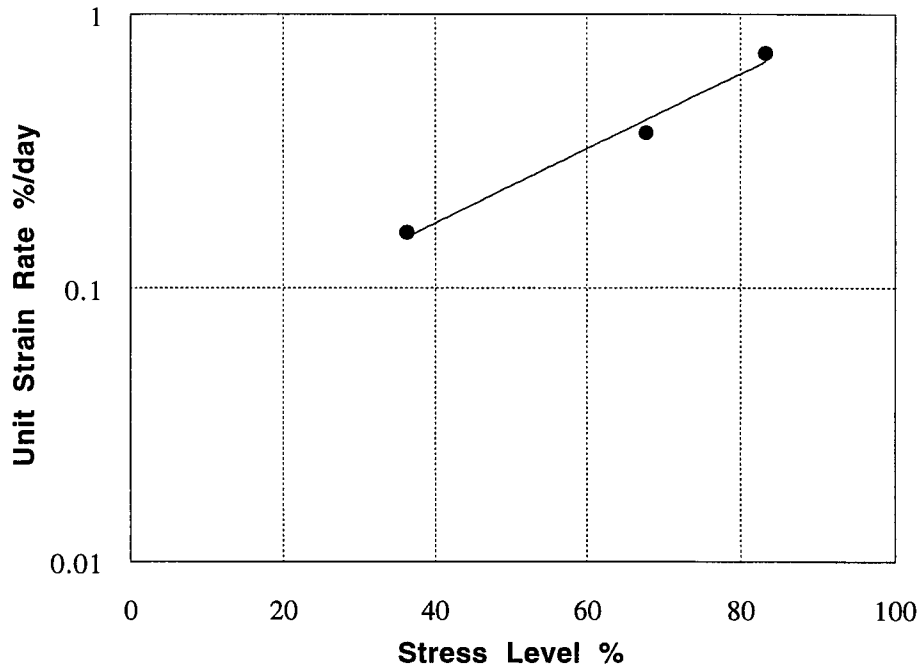

Figure (4.4b) Unit strain vs. stress level for I1.

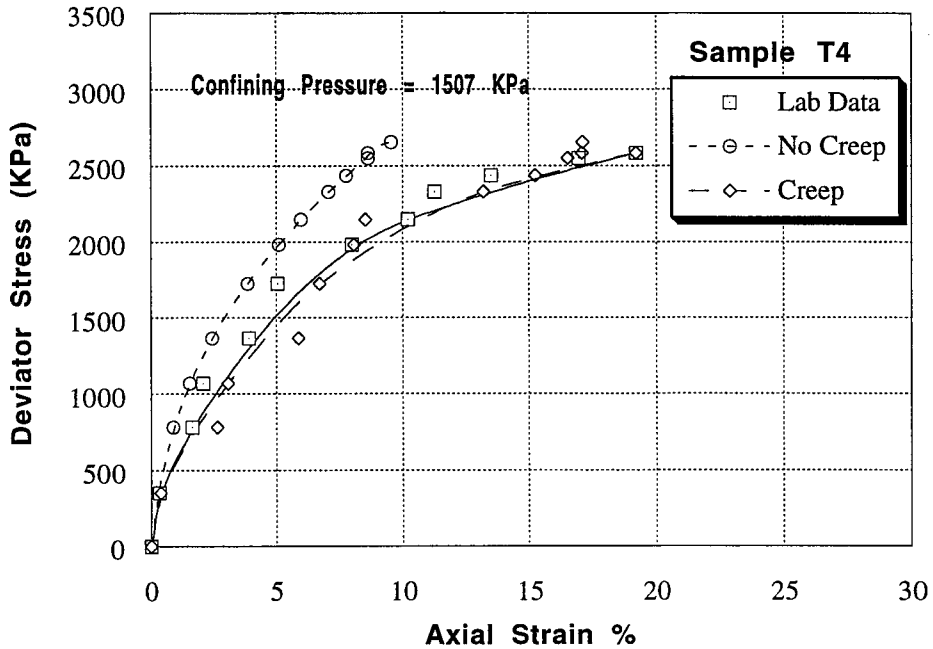

Figure (4.5a) Deviator stress vs. axial strain.

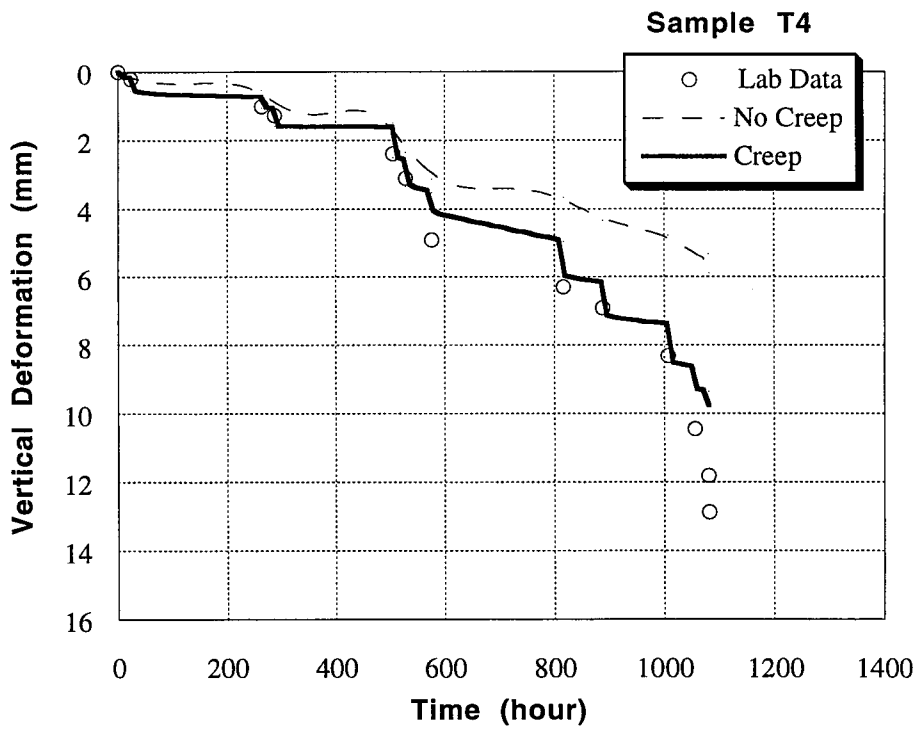

Figure (4.5b) Vertical deformation vs. time.

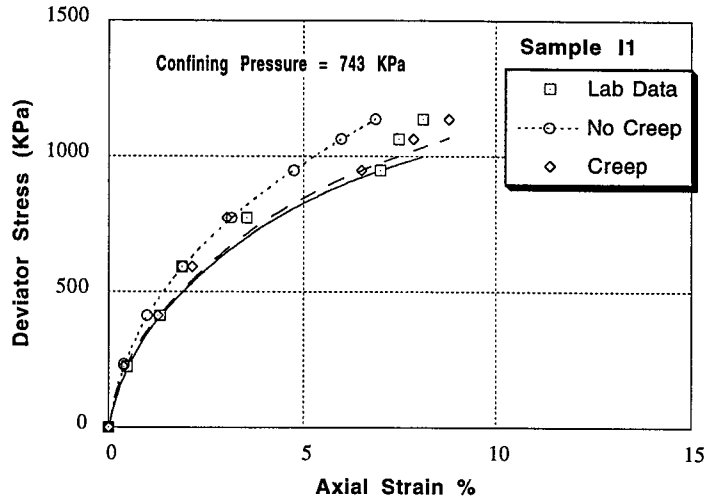

Figure (4.6a) Deviator stress vs. axial strain.

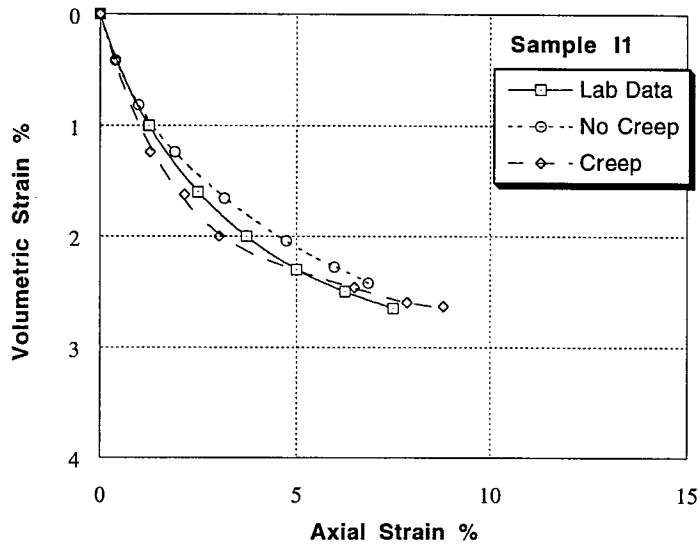

Figure (4.6b) Volumetric strain vs. axial strain.

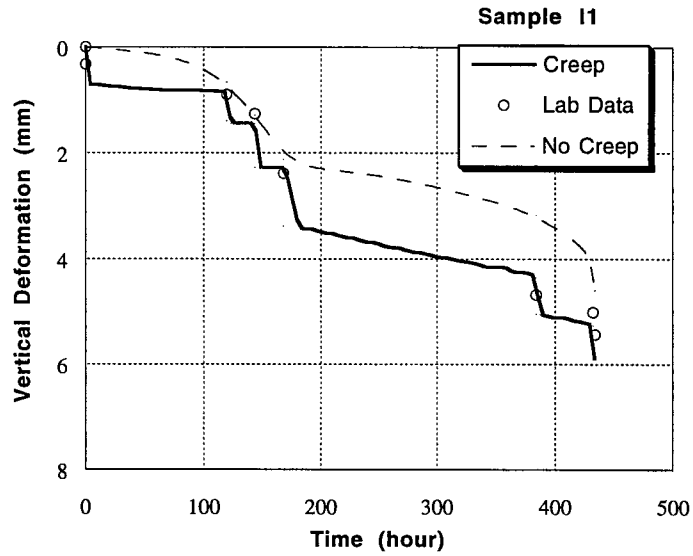

Figure (4.6c) Vertical deformation vs. time.

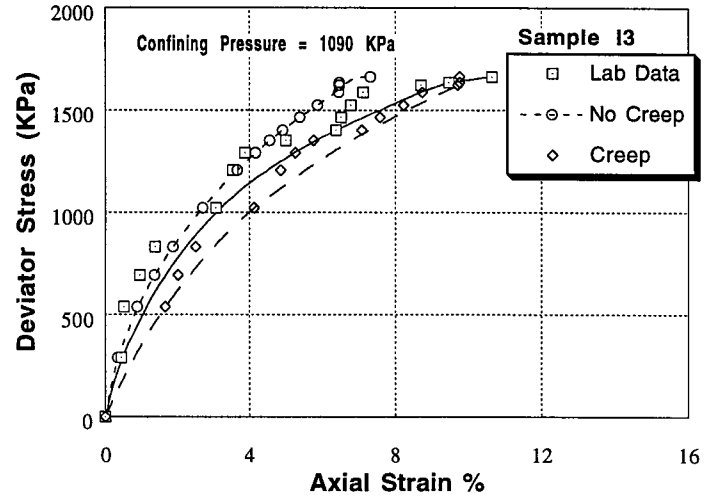

Figure (4.7a) Deviator stress vs. axial strain.

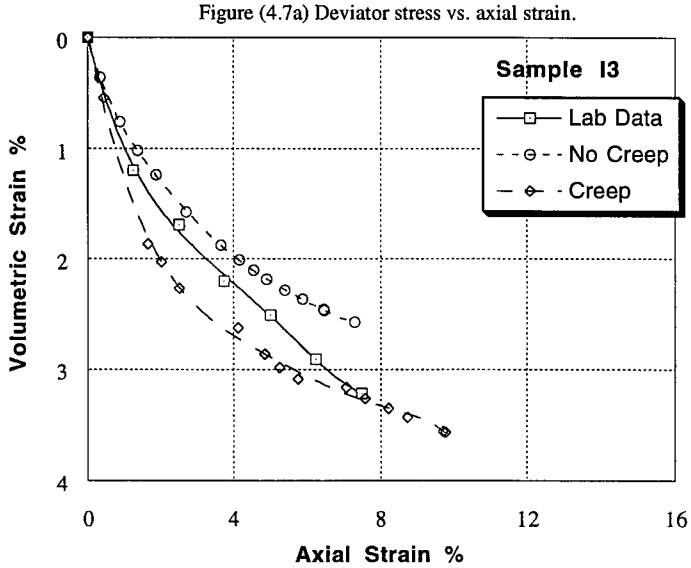

Figure (4.7b) Volumetric strain vs. axial strain.

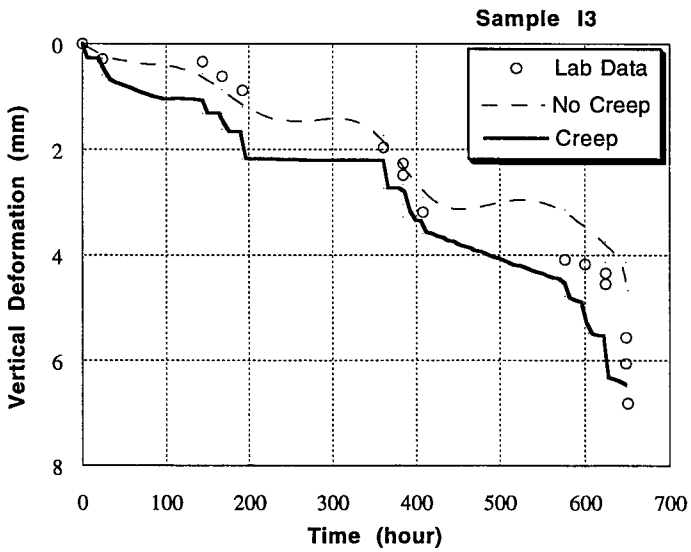

Figure (4.7c) Vertical deformation vs. time.

References:

Atkinson, J.H., and Bransby, P.L. 1978. The mechanics of soils: An introduction to critical soil mechanics. McGraw-Hill, London.

Bishop, A.W. and Henkel, D.J. 1962. The measurements of soil properties in the triaxial test. Arnold, London.

Bjerrum, L. 1967. Engineering geology of Norwegian normally consolidated marine clays as related to settlements of buildings. Geotechnique, **17**: .83-117.

Borja, R.I., and Kavazanjian, E.Jr. 1985. A constitutive model for the stress-strain-time behaviour of 'wet' clays". Geotechnique, **35**: 283-298.

Borja, R.I., and Lee, S.R. 1990. Cam-clay plasticity, Part I: Implicit integration of elasto-plastic comstitutive relations. Computer Methods in Applied Mechanics and Engineering, **78**: 49-72.

Borja, R.I., Hsieh, H.S., and Kavazanjian, E. Jr. 1990. Double-yield-surface model. II: Implementation and verification. ASCE Journal of the Geotechnical Engineering Division, **116**(GT9):1402-1421.

Hsieh, H.S., Kavazanjian, E. Jr., and Borja, R.I. 1990. Double-yield surface model.I:Theory. ASCE Journal of the Geotechnical Engineering Division, **116**(GT9): 1381-1401.

Mesri, G., Febres, C.E., Shield, D.R., and Castro, A. 1981. Shear stress-strain-time behaviour of clays. Geotechnique, **31**: 537-552.

Mittal, H.K., and Hardy, R.M. 1977. Geotechnical aspects of Tar sand tailings dyke.ASCE, Proceedings of the conference on geotechnical practice of disposal of solid waste materials, Ann Arbor, Michigan, June 13-15, 1977. pp. 327-347.

Roscoe, K.H., and Burland, J.B. 1968. On the generalized stress-strain behaviour of "wet" clay. Engineering plasticity. *Edited by* J.Heyman and F.A. Leckie. Cambridge University Press, Cambridge, England.

Singh, A., and Mitchell, J.K. 1968. Generalized stress-strain-time function for soil. ASCE Journal of Soil Mechanics and Foundation Engineering Division, **94**(SM1): 21-46.

Taylor, D.W. 1948. Fundamentals of soil mechanics. John Wiley and Sons, New York, N.Y.

Watts, B.D. 1980. Lateral creep deformations in the foundation of a high dam. M.Sc. thesis, University of Alberta, Edmonton, Alberta, Canada.

CHAPTER 5

SIMULATION OF CREEP DEFORMATION IN THE FOUNDATION OF TAR ISLAND DYKE[1]

5.1 INTRODUCTION :

Tar Island Dyke (TID) is located on the west bank of the Athabasca River near Fort McMurray, Alberta. The dyke is slightly over three kilometers long, and by the end of 1984, it was approximately 92 m high. The dyke as originally planned in 1964 was to be a low structure, about 12 m high, constructed of compacted earth fill. The purpose of the dyke was to retain the tailings produced by the GCOS (Great Canadian Oil Sands Ltd., now Suncor) during the early years of operation until a mined out area became available for tailings storage.

In 1964, a site investigation carried out for the construction of TID showed that the general stratigraphy in the Tar Island area was composed in part of variable thickness of soft silt and/or clay to a maximum of 16 m underlain by a layer of sand and gravel resting on limestone bedrock. In 1966 GCOS found that due to unanticipated processing difficulties more storage was required in the Tar Island area and studies began with the objective of raising the dyke to a much greater height, using tailings sand as the main construction material, instead of constructing a conventional earth fill dyke to store tailings which would be more expensive. TID was the first full scale commercial operation in the recovery and refining of oil from the vast oil sands in Canada. Because of the nature of the fluid components of the tailings, failure of such a structure with subsequent spilling of the retained tailings into the Athabasca river, would have a major detrimental effect on the environment.

---

[1]A version of this chapter has been submitted for publication to the Canadian Geotechnical Journal: Morsy, M.M., Morgenstern, N.R., and Chan, D.H. 1994. Simulation of creep deformation in the foundation of Tar island dyke.

In January 1975, Alberta Environment appointed a Design Review Panel to review the design and performance of the dyke and to comment on the advisability of granting future requests to raise the dyke. Since 1975, the dyke and its foundation have been subjected to continuous and extensive geotechnical monitoring. Many piezometers and inclinometers were installed. The outcome of the measurements are discussed in this paper. Significant movements in the clay layer were observed during the construction of the dyke, especially between stations 56+00 and 65+00. Based on the nature of the lateral deformations and piezometer readings in the clay layer, it was postulated that the movements in the foundation were a result of creep. The sustained nature of this creep required an enhanced degree of vigilance to assure dyke safety.

In 1980, Watts performed a series of incremental drained creep triaxial tests on clay samples from the foundation of TID to study the creep behaviour and the factors affecting it. The results of Watts's study are utilized here as a basis for the numerical analysis of the time-dependent behaviour of the TID foundation.

The effect of time on the deformation behaviour of soft clays, in the case of drained creep, has been the subject of numerous investigations (Murayama and Shibata 1961; Singh and Mitchell 1968; Tavenas et al. 1978; Mesri et al. 1981; and Leroueil et al. 1985). Unfortunately these investigations have been limited in that the problem of creep has been dealt with essentially as a theoretical exercise aimed at the validation of various rheological models and the creep has rarely been evaluated in field problems.

TID represents a unique opportunity to study numerically the influence of creep deformation of soft clay in terms of effective stresses. The results will help fill an important gap in the generalized description of creep phenomena in soft clays.

In this paper, the numerical model proposed by Morsy et al. (1994) is applied to simulate the performance of TID over 25 years. The results of the finite element analysis of Section 56+00, Cell 4, are compared with the field measurements, which show the importance of the inclusion of creep effects in order to develop a comprehensive understanding of the time-dependent behaviour of the clay beneath TID.

5.2 OVERVIEW OF TAR ISLAND DYKE (TID):

The purpose of this section is to present a brief overview of the construction history, foundation conditions and instrumentations of TID . A summary of the remedial measures used to improve the stability of the dyke in 1988 is also provided.

Most of the material used in this section can be found in papers by Mittal and Hardy (1977), Chen et al (1983) and from the data provided by the designers of Tar Island Dyke, Hardy Associates Ltd. (1978), Hardy BBT Ltd. and HBT AGRA Limited.

As shown in Figure (5.1), Tar Island Dyke consists of six cells in which tailings have been placed to provide containment for Pond One. Cells 3 and 4 have been chosen to be the main area in this study because the dyke in both cells is founded on a layer of weak clay generally varying in thickness between 3 and 16 m. The field measurements show that this layer has experienced significant continuing deformations at several locations.

5.2.1 Construction history:

The construction of a 12 m high conventional earth fill dyke to store the tailing began in 1965 and continued intermittently until 1967 when it became apparent that the volume of tailings was greater than anticipated and that the continued construction of a conventional earth fill dyke to store the tailings would be prohibitively expensive. Since 1968, the dyke has been raised with hydraulically placed sand tailings according to the upstream method of cell construction, which has been described by Mittal and Hardy (1977).

In this method, the tailings stream is sluiced into construction cells oriented parallel to the dyke centerline. During the sluicing operation pad dozers are used to spread and compact the sand placed in the cells, forming a compacted shell. In winter months when the construction of the cells is not feasible, the tailings stream is discharged upstream of the compacted shell. The coarse sand fraction settles out to form a beach with a 2 to 3 percent slope. The water and fine tails fractions of the tailings stream flow into the pond.

The dyke consists of a compacted downstream zone and an uncompacted upstream zone which retain a pond as shown in Figure (5.2). The downstream face of the dyke has

an overall slope of three horizontal to one vertical. There are access berms at approximately 13 m vertical intervals. Seepage through the dyke is controlled by blanket drains composed of plant coke. All seepage collected in the drains is returned to the pond.

By the end of 1980 the dyke reached a height of 87 m. During 1984, the TID crest was raised to a height of 92 m which led to the shearing of inclinometer S81-101C (Berm 303 m) near the contact of the foundation clay and the underlying sand and gravel. A field program was carried out to examine the clay foundation and slickensides were detected. In 1988, a remedial measures program was completed and the main construction activities involved the construction of a toe berm, excavation of the dyke crest, and the relocation of the dyke crest inside the pond to reduce the shear strain rate in the foundation and thus improve the stability of the dyke.

5.2.2 Geology of the site and soil stratigraphy:

The geology of the Tar Island area has been discussed by Watts (1980). TID rests on the active flood plain of the Athabasca river. The abutments of the dyke are the Athbasca River valley walls which are composed of the Clearwater Formation shale and the McMurray Formation oilsand. The common stratigraphic sequence in the general area consists of recent river deposits overlying Pleistocene glacial materials which rests unconformably on the Cretaceous Clearwater and McMurray Formations. They, in turn , unconformably overlie the Devonian Limestone.

The meandering incised Athabasca river has completely eroded all Pleistocene and Cretaceous sediments in the area. The local foundation stratigraphy consists of muskeg overlying a recent deposit of silt and clay which overlies a layer of sand resting on the Devonian Limestone. Cobbly gravel is usually found just above the sand/limestone contact.

The original foundation investigations for the dyke were undertaken in 1964 and 1965. Since then there have been numerous site investigations. An isopach map of the silt and clay deposit based on the 1964 and 1965 borehole logs is shown in Figure (5.3). The thickness of silt and clay encountered in selected boreholes drilled in 1975 are also shown on the isopach map. It is noted in Figure (5.3) that the thickness of the clay deposit is at its maximum at stations 56+00 and 65+00.

The silt and clay deposit originated by sedimentation in an abandoned meander of the Athabasca River. The basal sands represents an Athabasca River bed load sediment which was deposited prior to a complete cutoff of the meander.

The major source of sediment to the meander was undoubtedly suspended silt and clay from overbank during the flooding of the Athabasca River. This genesis implies that the deposit should be coarser at its margins and finer further away. There is also evidence of essentially still water deposition in the form of numerous calcium carbonate shells throughout the deposit.

5.2.3 Geotechnical properties of silt and clay deposit:

The deposit consists of interbedded silt and clay with occasional sand lenses. Silt and sand predominate towards the margins of the deposit. Based on thirty-four grain size analyses on 1964 and 1965 samples, the deposit has an average of twenty percent sand, sixty-three percent silt and seventeen percent clay. It also contains variable amounts of coal fragments, calcium carbonate shell material and organic material.

Index properties of the foundation clay from 1964 and 1975 laboratory and field testing program are summarized in Table (5.1). The Liquid Limit of the deposit varies from forty-four percent to fifty-five percent and the Plasticity Index varies from twenty percent to thirty seven percent. Soil samples were obtained in 1980, fourteen years after commencement of dyke construction, when the height of the dyke reached about 89 m. The average natural water content of the samples was approximately twenty-seven percent which is significantly less than the natural water content of approximately forty -five percent before dyke construction. The difference in water content reflects the consolidation of the clay due to the imposed dyke load.

Before construction of the dyke the deposit was medium stiff with undrained strengths ranging from 45 kPa to 90 kPa. The undrained strength over effective stress ratio was 0.45, which showed that the clay was lightly overconsolidated before the construction of the dyke. The undrained strength has increased with time as the deposit consolidates under the weight of the dyke.

The effective friction angle for the foundation clay has been obtained from both conventional triaxial and direct shear tests. It varies between 24 and 27 degrees with an average value of 26.5 degrees and a residual angle of 14 degrees.

5.2.4 Foundation iInstrumentation:

Tar Island Dyke is heavily instrumented. Piezometers are used to monitor seepage in the tailings sand and in the foundation. Foundation piezometers are concentrated at stations 56+00 and 65+00 where the clay deposit is the thickest. Numerous inclinometers have been installed to monitor the lateral deformation of the clay deposit at these two stations since 1976. Vertical deformation of the clay deposit is not monitored directly but is periodically estimated from changes in water content and thickness of the layer as well as from the measured excess pore pressure in the clay layer. Figure (5.4) shows the location of the instrumentation existing in cells 3 and 4.

Piezometers :

The measurements from the piezometers at station 56+00 at the 277 m and the 291 m berms are illustrated in Figures (5.5) and (5.6). The readings from the 303 m and 319 m berms are shown in Figures (5.7) and (5.8). On every pore pressure plot a 'steady-state' line is shown. This line represents the theoretical pore pressure in the clay layer when consolidation is completed based on a downward flow situation. The steady-state line is determined assuming the pore pressure at the base of the clay layer is equal to that in the sand and gravel layer which is governed by the water level of the Athabasca river. The pore pressure at the top of the clay layer is governed by the seepage regime in the tailings sand and has been determined from piezometer readings or estimated by extrapolation of the piezometer readings within the dyke.

It can be seen from Figures (5.5) and (5.6) that the clay deposit from the 291 m berm downstream was essentially fully consolidated in 1980. From Figures (5.7) and (5.8), the clay deposit beneath the 303 m and 319 m berms still had excess pore pressures and was consolidating.

Inclinometers:

A number of inclinometers have been installed in the dyke since 1976 to monitor the lateral movements of the foundation. The readings for five inclinometers numbered

SI79-108, SI76-105, SI79-109 and SI78-101 have been selected for the analysis, and are shown in Figures (5.9) to (5.12).

The base of all inclinometers is founded in the limestone to provide a fixed reference point for calculation of lateral movements at different depths. At each depth, two readings are taken in the A and the B directions. The average value of the A readings and the B readings are multiplied by the instrument constant to give the horizontal displacement in each of the A and the B directions. The vector sum of the A and B displacement is then computed to give the maximum horizontal displacement, irrespective of orientation, at each depth. In this calculation step, the maximum displacement is in the section normal to the longitudinal axis of the dyke.

The shear strain is calculated in a similar manner and is given by :

[5.1] $$\gamma = \mathrm{Arcsin}(X \bullet C) * 100\%,$$

where

γ is the shear strain;

X is the difference of the vector sum of the average values of the two components of the SI readings between two consecutive measuring points on the probe;

C is the Instrument constant.

From the inclinometers plots, the horizontal movements in the clay layer are characterized by:

i) The plot of cumulative deflection shows an essentially linear increase in the magnitude of movements from the bottom to the top of the clay layer. There were no sudden increase is evident in shear displacements at any depth due to a defined failure plane.

ii) The rate of cumulative lateral movement is the maximum at the sand/clay interface (i.e. at the top of the clay layer) , while it is the minimum at the clay and basal sand interface.

Vertical deformation:

Three different techniques are used to calculate the vertical deformation of the clay layer. They are:

1) Settlement based on elevation changes:
   Comparing the relative elevation of foundation clay layers found in the original borehole before the construction of the dyke (1964 field program) with those in the hole logs drilled at different construction stages of TID.

2) Inferred settlement based on water content:
   Settlement of the clay layer was estimated based on the changes in the water content in the clay layer assuming that the clay is saturated and that all changes in water content are the consequence of vertical settlement.

3) Calculated settlement:
   Settlement of the clay can be estimated using consolidation theory such as the classical Terzaghi one dimensional theory using the observed excess pore pressure.

The average settlement of the clay layer up to 1983, based on elevation comparison was estimated to be 3.36 to 3.96 m . Based on the water content change it varies from 2.74 to 3.66 m and based on consolidation calculations, it varies from 3.35 to 3.96 m.

5.2.5 Slickensides:

Prior to 1984, the clay layer had experienced continuing deformation, but it was concluded that the peak strength parameters still governed the overall stability of the critical section at cells 3 and 4.

During 1984, the dyke crest was raised from 87 m to 92 m. It was noted that inclinometer S81-101C (Berm 303) sheared near the contact of the foundation clay and the underlying sand and gravel. It was found that the shear strain increased from 0.5% to 4.5% in five months, and the rate of shear strain through the five months was 9.6%/year. This led to the examination of the clay layer foundation to check whether there was visual

evidence of shearing of the clay which would lead to a reevaluation of the stability of the dyke based on residual strength.

Between January 1985 and February 1987, a total of 15 test holes were drilled at the critical section, cells 3 and 4, to investigate the extent of the slickensides. The location of the test holes and the location of slickensides observed are shown in Figure (5.13).

Based on visual inspection of the samples, the slickensides were found at different elevations in various boreholes. There was no evidence to indicate the presence of a discrete slip surface across the boreholes at a particular elevation. Also, there was no correlation between the elevation of the recorded maximum shear strains and the elevation of the observed slickensides. In general, the slickensides observed are poorly developed or immature, tending to be inclined or undulating in a horizontal or sub-horizontal plane. The undulating character of all the slickensides suggests that the movements associated with the formation of the slickensides are of limited magnitude.

Based on the results of the visual inspection of the clay samples in 1985 and 1987 field programs, it was suggested that more than one process may have contributed to the formation of the slickensides :

a) Surface construction traffic:

High wheel loading has caused local shear failure and development of slickensides at the upper surface of the foundation clay.

b) Differential consolidation:

Shear straining due to differential consolidation of the clay foundation could induce slickensides. Differential consolidation arises due to non-uniform loading beneath the slope of the dyke and the non-uniform thickness of the foundation clay. The slickensides induced by differential consolidation may occur at all depths throughout the clay.

c) Shear stress :

The shear stresses induced beneath the slopes of the dyke are the major contributing factor to the shear strains in the foundation clay. However, it is not possible to differentiate the influence of shear stresses from other processes

on the basis of incomplete development of the observed slickensides described above. Nevertheless, the shear stresses would tend to advance the development of any slickensides initiated by construction traffic near the surface of foundation clay. The shear stresses would act in conjunction with differential consolidation in the initiation and development of slickensides.

5.2.6 Remedial measures program:

Based on the data and findings of the two field programs, a remedial measures program was carried out which comprised of two parts as shown in Figure (5.14):

1) An excavation at the dyke crest down to elevation 319 m.

and

2) Construction of a stabilization berm at the dyke toe to elevation 264 m.

Through 1988, the remedial measures program for the critical section of TID was successfully completed. The completed construction work included the following (Figure 5.15):

a) Relocation of the dyke crest 305 m inside the pond at elevation 321 m.

b) Excavation of tailings sand from the crest region down to elevation 321 m.

c) Construction of a toe berm to elevation 251 m using sand excavated from the dyke crest.

Six lines of instrumentation were installed at the toe of the TID to monitor the stability of the toe berm during construction. Figure (5.16) presents a typical section through the instrument lines showing the primary instrumentation monitored during the 1988 berm construction.

Piezometer measurements indicate low excess pore pressure was generated in the foundation clay by toe berm loading. Piezometric levels returned to pre-construction levels within two months after completion of the toe berm.

upstream of the toe berm, as shown in Table (5.2). The results also reveal that the shear strain rates had been reduced by an average rate of 43% through 1989-1990. Overall, the remedial measures improved the stability of TID and reduced the creep rates.

Since the 1988 remedial measures program have achieved the goal of reducing the shear strain rate in the clay foundation, the 1989 program to raise the toe berm further to elevation 264 m and further cutting of the crest to 318 m was abandoned.

5.3 MECHANISM OF FOUNDATION MOVEMENT BENEATH TID:

In 1980, Watts carried out a study to evaluate the nature of the TID foundation movements over the previous four years (1976 to 1980). The study was composed of two parts; the first was the evaluation of the field measurements in term of piezometers and inclinometers records and the second was a laboratory program to study the drained creep deformation of the TID foundation clay.

The main results from this evaluation of the field data are summarized in the following:

i) TID clay becomes normally consolidated due to the dyke construction. It has deformed vertically and horizontally due to the continued construction of the dyke since 1965.

ii)The insitu piezometer records in 1980 indicate that the clay was fully consolidated downstream of the 291 m berm and that significant excess pore pressures are dissipating upstream of this berm.

iii) The time dependence of the horizontal shear strain may either be a consequence of creep or of lateral consolidation. The creep mechanism is considered to be the dominant mechanism causing the time-dependent shear strains since:

a) Horizontal shear straining is occurring in portions of the foundation where any excess pore pressure have already dissipated. This is apparent in the top and bottom portion of the clay deposits and in the full thickness of the clay deposits downstream of the 291 m berm.

bottom portion of the clay deposits and in the full thickness of the clay deposits downstream of the 291 m berm.

b) A mechanism of horizontal consolidation necessitates compression in the horizontal direction. However horizontal normal strains are in order of 0.04 % which is insignificant compared to the horizontal shear strains of 1 to 4 % over the same time period.

Based on these findings, Watts (1980) carried out drained creep oedometer and drained triaxial creep tests on undisturbed clay samples at different sample orientations, cell pressures and stress levels. Figure (5.17) shows the plots of the logarithm of axial strain rates versus the logarithm of time for a horizontal bedding sample and an inclined bedding sample. The plots show that the axial creep strain rate decreases according to a power law with time. The average value of the power law exponent m is 1.12 and is independent of the sample orientation and stress level.

Also, the triaxial test results show that the axial creep strain rate is an exponential function of the applied deviator stress level. This result together with the power law dependence of strain rate on time fulfill the requirements of a Singh-Mitchell (1968) model for creep strain.

From 1980 to 1987, the height of the TID was raised from elevation 325 m to 330 m (92 m high). This did not create excess pore pressure in the entire domain of the clay foundation. The toe berm constructed in 1988, created excess pore pressure at the toe region. This excess pore pressure was dissipated completely in two months time. Thus, it is evident that tcreep is occurring under partially drained conditions and can be interpreted in term of effective stresses.

5.4 FORMULATION OF THE NUMERICAL MODEL OF TID:

The construction of the dyke is simulated using a two dimensional plane strain finite element model. The finite element mesh shown in Figure (5.18), is composed of 700 6-node triangular and 8-node quadrilateral isoparametric elements. The analysis involves the construction of the dyke from 1965 to 1984 and the construction of the toe berm in 1987. Figure (5.19) shows the dyke crest elevation and pond level rise with time and the idealized construction stages for the analysis.

The foundation stratigraphy for the model is an idealized version of that at station 56+00. The sand/limestone interface forms the lower boundary of the finite element domain and was assigned a zero, vertical and horizontal displacement boundary condition. The left boundary of the grid was chosen to be 700 m from the toe of the dyke so that it would not affect the deformation in the area downstream of the dyke. The right boundary was placed at the center of the river for the same reason. Both boundaries were assigned zero horizontal displacement boundary conditions.

An effective stress approach is used to analyze the time-dependent deformation of the clay layer (Morsy et al. 1994). In this case history, effective stresses in the clay layer are functions of the increase of the dyke loading, the rise of the pond elevation and the dissipation of excess pore pressure with time.

In constructing the numerical model, the followings are taken into account:

a) the construction sequence of the dyke over 25 years;

b) the generation of pore pressure in the foundation due to the increase of the dyke load and changes of phreatic surface and pond level with time;

c) the dissipation of pore pressure in the foundation clay with time;

d) the time-dependent deformation in the clay foundation which is governed by the creep mechanism expressed in terms of effective stresses.

Due to the stress path dependence of the material behaviour, a realistic loading sequence is a fundamental requirement for obtaining reasonable results. In the analysis, the loading sequence is composed of an initial "switch-on-gravity" step in order to generate a pre-existing stress field with respect to the dyke construction. Then, subsequent layer by layer construction is simulated corresponding to a certain period of construction according to the idealized construction stages shown in Figure (5.20).

5.4.1 Material modeling:

Sand and gravel layer:

Insignificant deformation has been observed in this material. It was assumed, therefore, that it behaves in a linearly elastic manner. The material parameters correspond to a medium density sand. Table (5.3) shows the material parameters of the sand and gravel layer.

Clay layer:

The time-dependent behaviour of the foundation clay is modeled using a recently proposed constitutive model (double-yield surface model) for the stress-strain-time behaviour of cohesive soil by Hsieh et al (1990). The soil parameters used to model the TID clay are shown in Table (5.4). The model parameters were determined from a laboratory program, which studied the drained creep behaviour of TID clay (Watts 1980).

The index parameters C_c, C_r, C_α and e_a were determined as average values of the results of conventional one dimensional consolidation tests. The hyperbolic parameters a, b, and R_f were calculated based on realistic assumptions (see Appendix D) , since there were no data available from isotropic consolidated undrained triaxial compression tests. The angle of internal friction was obtained as an average value of the results of triaxial and direct shear tests. The Singh-Mitchell parameters A, α and m were determined as an average values of the results of drained creep triaxial tests.

Compacted and beach sand:

The hyperbolic model is chosen for both soils based on the characteristic behaviour of medium and loose density sandy material. Table (5.5) summarizes the linearly elastic and the hyperbolic model parameters for both the compacted and loose beach sand.

5.4.2 Incorporation of measured pore pressure in the effective stress analysis of TID:

An effective stress approach was necessary to analyze the creep behaviour of the foundation of TID. According to the numerical scheme used in the analysis (De Alancar

1988; and Morsy et al. 1994), the pore pressure distribution in the dyke and its foundation should be prescribed at different stages of construction.

Pore pressure in the sand and gravel layer:

Piezometers that have been installed in the sand and gravel layer below the clay foundation since 1975 show that the piezometric levels consistently match the elevation of the Athabasca River.

The prescribed pore pressures at the integration points in the finite element mesh are calculated as hydrostatic pore pressures resulted from the average river elevation (234.5 m).

Pore pressure in compacted and beach sand:

The general form of the phreatic surface in the dyke can be specified by data obtained from open stand pipe and inferred from piezometer data. Figure (5.20) shows the average phreatic surface specified for each stage of construction based on stand pipes and piezometer records.

From the records of the piezometers installed in the compacted and beach sand, it is found below each berm that the field measurements can be joined together with a straight line, considering zero pore pressure at the phreatic surface. This straight line implies that pore pressures within the tailings sand are substantially less than hydrostatic and appear to be uniformly distributed. The pore pressure at the integration points is calculated considering zero pore pressure at the phreatic surface and an average hydraulic gradient equal 0.28, a value determined from field measurements, using the following equation :

[5.2] $$P_w = \gamma_w * h * (1 - i),$$

where

P_w is the pore pressure at the integration point ;

h is the difference in elevation between the phreatic surface and the integration point;

i is the hydraulic gradient;

γ_w is the unit weight of water.

Pore pressure in foundation clay:

Piezometric levels in the foundation clay layer in the vicinity of Station 56+00 have been investigated since 1975. The pore pressure generation and dissipation are functions of the dyke load and time. For each step in the finite element analysis, the pore pressure at the integration points are interpolated from the available field measurements through this step, according to the interpolation technique proposed by De Alancar et al. (1992) .

Figures (5.21) to (5.23) show a comparison between the interpolated pore pressure at the integration points and the measured pore pressure in the clay layer at different locations. There is excellent agreement between measured and interpolated values.

5.5 THE ANALYSIS OF TAR ISLAND DYKE:

Visco-elasto-plastic finite element analyses were carried out to investigate the time-dependent stress-strain behaviour of the dyke foundation over twenty five years of construction and operation.

The analyses were carried out using the finite element code PISA™ (Program for Incremental Stress Analysis) developed at the University of Alberta. This program is capable of performing one, two, and three dimensional linear and non-linear elastic as well as elasto-plastic analysis involving various yield criteria. For the analysis of TID, the program capability is been extended to include visco-elasto-plastic analysis (Morsy 1994).

In order to carry out a time-dependent non-linear finite element analysis using an effective stress approach, the following data should be prescribed as input for each stage of the numerical analysis of TID:

a) the pore pressure regime for the entire domain, which are interpolated from the average measured pore pressures (De Alencar et al. 1992);

b) based on the average phreatic surface in the dyke for each stage, the bulk density of each element in the finite element mesh is redefined based on its position with respect to the phreatic surface;

c) the loading process is modeled by placement of a layer, each layer corresponds to a certain stage. In each stage, a layer is initially placed as a linear elastic material with a low modulus of deformation representing the placement process. In subsequent stages, the material is modeled by a hyperbolic model. The technique is used because the deformation modulus according to the hyperbolic model is a function of the confining stress. When the material is first placed the confining stress is very low (or zero at the surface) what would mean a very low or zero confining modulus, which causes a numerical unstability problem if the hyperbolic model is used when the layer is initially placed instead of the linear elastic model;

d) in each stage of construction, the time-dependent deformation is calculated over the idealized time period for each stage. The time period for each stage is specified in term of years.

5.5.1 Discussion of the results:

In this section, the results of the numerical analysis are presented and compared with the field measurements.

5.5.1.1 Vertical deformation:

As discussed earlier, the measured vertical settlement had been calculated based on the change of elevation at the top and bottom of the clay layer with time from boreholes at berm 291 m. Figure (5.24) shows that the analysis is in excellent agreement with the measured vertical deformations until 1972 and then it deviates gradually from the field data with a steady decrease resulting in a discrepancy of about 19 % at 1983.

In order to overcome this discrepancy, the value of C_c has been increased to 0.32 (since the range of the virgin compression index (C_c) is between 0.23 to 0.36). Figure (5.24) shows that the new value of C_c yields very satisfactory results. The predicted values of the vertical displacements match the field measurements with slight

overprediction at 1983 of about 2%. The value of C_c is fixed at 0.32 for the entire analysis.

5.5.1.2 Horizontal deformation:

The results for the years 1980 and 1987 are compared with the field measurements, at different locations in the clay foundation, as shown in Figures (5.25) to (5.27). It is observed that the shapes of the curves as well as the values of the horizontal displacements are in good agreement with the field values.

It is seen in Figure (5.25) that the shape of the calculated displacement curves beneath berm 251 m are in reasonable agreement with the horizontal displacements measured by inclinometers SI76-105 and SI83-105. The only exception is at the interface between the dyke and the foundation. In 1980, the field horizontal displacements are underestimated by an average of 30%, while in 1987 this percentage increases slightly to 32%.

Beneath berm 277 m, see Figure (5.26), an excellent agreement is obtained between the calculated and measured horizontal displacements in 1980 at inclinometer SI76-102. In the upper half of the clay layer the field horizontal displacements are overestimated by 5% on average, while in the lower half of the clay layer, the field horizontal displacements are underestimated by 8% on average. Both the measured and calculated horizontal displacements are in excellent agreement in terms of curve shape along the clay layer.

At berm 291 m, Figure (5.27), the calculated and measured horizontal displacements are in very good agreement with magnitudes as well as the shape of the curve. In 1987, the field values are overpredicted by about 10% on average.

5.5.1.3 Shear strain:

Both measured and calculated shear strains at selected locations and depths downstream of berm 291 m. are plotted versus time in Figures (5.28) to (5.31). The calculated shear strains are the horizontal shear strains. On each figure the average shear strain rate for a certain period of time is calculated based on measured and calculated values.

Toe:

In Figure (5.28), the shear strain beneath the original toe at elevation 235.87 m is plotted. From the plot, it is seen that the construction of the toe berm caused a sudden increase in the shear strain by 0.80% over six months during the construction of the berm. After the completion of the construction of the berm the shear strain rate was reduced to 0.13%/year.

Both the measured and calculated shear strains are in good agreement. The calculated values coincide with the measured shear strains between December 1979 to December 1982 and also after the construction of the toe berm. From December 1982 to June 1988, the predicted values underestimate the shear strains by an average of 22%.

Berm 251 m:

In Figure (5.29), both the measured and the calculated shear strains show how the construction of the toe berm reduces the shear strain rate beneath berm 251 m by 50% (the calculated values) and by 65% (the measured values). Between December 1975 and December 1982, the calculated values overpredicted the measured shear strains by 20% on average, while from December 1982 to December 1991 the measured shear strains are underpredicted by 17% on average.

Berm 277 m:

Figure (5.30) shows that both the calculated and measured shear strains are in excellent agreement. Both show that the construction of the toe berm reduced the shear strain rate beneath berm 277 m by approximately 50%. The calculated values underpredict the measured shear strain from December 1979 to December 1991 by 15% on average.

Berm 291 m:

Figure (5.31) indicates that both the measured and calculated shear strains are in excellent agreement . The measured and the calculated shear strain rate before and after the construction of the toe berm are nearly equal.

Figure (5.31) indicates that both the measured and calculated shear strains are in excellent agreement . The measured and the calculated shear strain rate before and after the construction of the toe berm are nearly equal.

From the piezometer measurements, it is evident that downstream of berm 291 m drained creep is the dominant mechanism which controls the deformation taking place in the clay foundation. Without the inclusion of creep deformations in the numerical model, it would not be possible to account for the development of the observed displacement with time and to explain the effect of the construction of the toe berm on the shear strain rate in the dyke foundation.

5.6 CONCLUSIONS:

The analysis of the creep deformation of the foundation of station 56+00, cell 4, of TID provides valuable experience in modeling this class of problems which involves complicated geological conditions, in addition to significant time-dependent deformation of the foundation over 25 years of complicated stage construction procedures.

The numerical scheme used by the authors in the finite element analysis of the TID provides a simple and powerful tool for the design process of this class of problems according to the observational method, as it is characterized by:

a) the parameters required to model the time-dependent material behaviour are obtainable from traditional triaxial and consolidation tests;

b) the pore water pressure regime within the dyke and its foundation, at any stage of construction and operation, is calculated based on the available measurements in term of piezometers and standpipe data and used as input data in the analysis;

c) the scheme helps the geotechnical engineers to avoid the problem of accurate prediction of the change of the pore pressure regime in the soil domain, at any stage of construction, as a function of time due to external loads, dissipation, and change in the elevation of the phreatic surface.

The satisfactory agreement between the measured and the calculated vertical and horizontal displacements and shear strain shows the importance of the inclusion of the creep in the numerical model, to realistically represent the stress-strain behaviour of cohesive soil.

The time-dependent analysis of Tar Island Dyke is considered to be a step toward a more complete understanding of the effect of creep on the time-dependent behaviour of cohesive soils under the effects of complex boundary conditions in the field. The simplicity of the numerical scheme proposed and the excellent agreement of the results of the analysis with the field measurements will help persuade designers ,in future, to analyze for creep effects where appropriate.

Table 5.1. Index properties of foundation clay.

Index Properties	Symbol	Number Of Test	Range Of Value	Average Value	Remarks
Insitue Void Ratio %	e_o	4	0.656 - 1.424	1.255	1964 Testing Program.
Natural Water Content %	W %	49	32% - 75%	45.1%	1964 Testing Program
Liquid Limit %	W_L %	13	44% - 55%	49.5%	1964 Testing Program.
Plastic Limit %	W_P %	13	23% - 31%	27%	1964 Testing Program.
Specific Gravity	G	5	2.69 - 2.92	2.76	1964 and 1975 TestingProgram.
Saturated Unit Weight (KN/m^3)	γ_{sat}	-	-	17.3	$\gamma_{sat} = (G+e)/(1+e) * \gamma_{wat.}$
Compression Index	C_c	6	0.23 - 0.36	0.28	1964 and 1975 TestingProgram.
Cofficient Of Consolidation cm^2/sec	C_v	8	1E-02 - 2E-04	1E-03	1964 and 1975 TestingProgram.

Table 5.2 SI shear strain rates upstream of toe berm before and after the 1988 remedial measures.

Inclinometer Number (SI)	Berm	SI Shear Strain Rate (%/year)		% Reduction in Shear Strain Rate
		1985-1988	1989-1990	
S85-101D	303	0.13	0.03	77
S85-102A	277	0.15	0.07	53
S76-104	251	0.17	0.08	53
S83-105A	251	0.15	0.09	40
S79-109	291	0.10	0.06	40
S85-111	303	0.13	0.04	69
S85-112	277	0.12	0.11	8
S85-113	264	0.14	0.10	29
S85-114	251	0.20	0.08	60
S85-115	264	0.13	0.06	54
S85-117	264	0.14	0.13	7
Average		0.14	0.08	43

Table 5.3. Material parameters for sand and gravel layer

Parameter	Symbol	Value
Modulus Of Elasticity	E	40,000
Poisson Ratio	ν	0.3
Bulk Density (KN/m^3)	γ_b	19.7

Table 5.4. Material parameters for clay layer

Parameter	Symbol	Value
Virgin compression index	C_c	0.28
Virgin recompression index	C_r	0.03
Void ratio at Pc=1.0 KPa	e_a	0.852
Angle of internal friction	ϕ	26.0
Hyperbolic parameter	a	.0048
Hyperbolic parameter	b	1.57
Correction Factor	R_f	.89
Secondary compression coefficient	$C\alpha$	.0032
Singh-Mitchell creep parameters	A	.0257 %/year
Singh-Mitchell creep parameters	$\overline{\alpha}$	2.47
Singh-Mitchell creep parameters	m	1.12
Bulk Density (KN/m^3)	γ_b	17.9
Dry Density (Kn/m^3)	γ_d	12.3

Table 5.5. Material parameters for compacted and beach sand

Parameter	Symbol	CTS1[a]	CTS2[b]	BTS1[c]	BTS2[d]
Elastic Modulus	E	40,000	____	20,000	____
Poisson Ratio	ν	0.3	0.3	0.3	0.3
Initial Modulus	K	____	2000	____	1000
Exponent	n	____	0.54	____	0.54
Friction Angle	ϕ	____	36	____	30
Correction Factor	R_f	____	0.9	____	0.9
Bulk Density (KN/m^3)	γ_b	19.7	19.7	19.7	19.7
Dry Density (KN/m^3)	γ_d	15.3	15.3	15.3	15.3

[a]CTS1 : Compacted tailing sand using linear elastic model when layer is added.

[b]CTS2 : Compacted tailing sand using the hyperbolic model.

[c]BTS1 : Beach tailing sand using linear elastic model when layer is added.

[d]BTS2 : Beach tailing sand using the hyperbolic model.

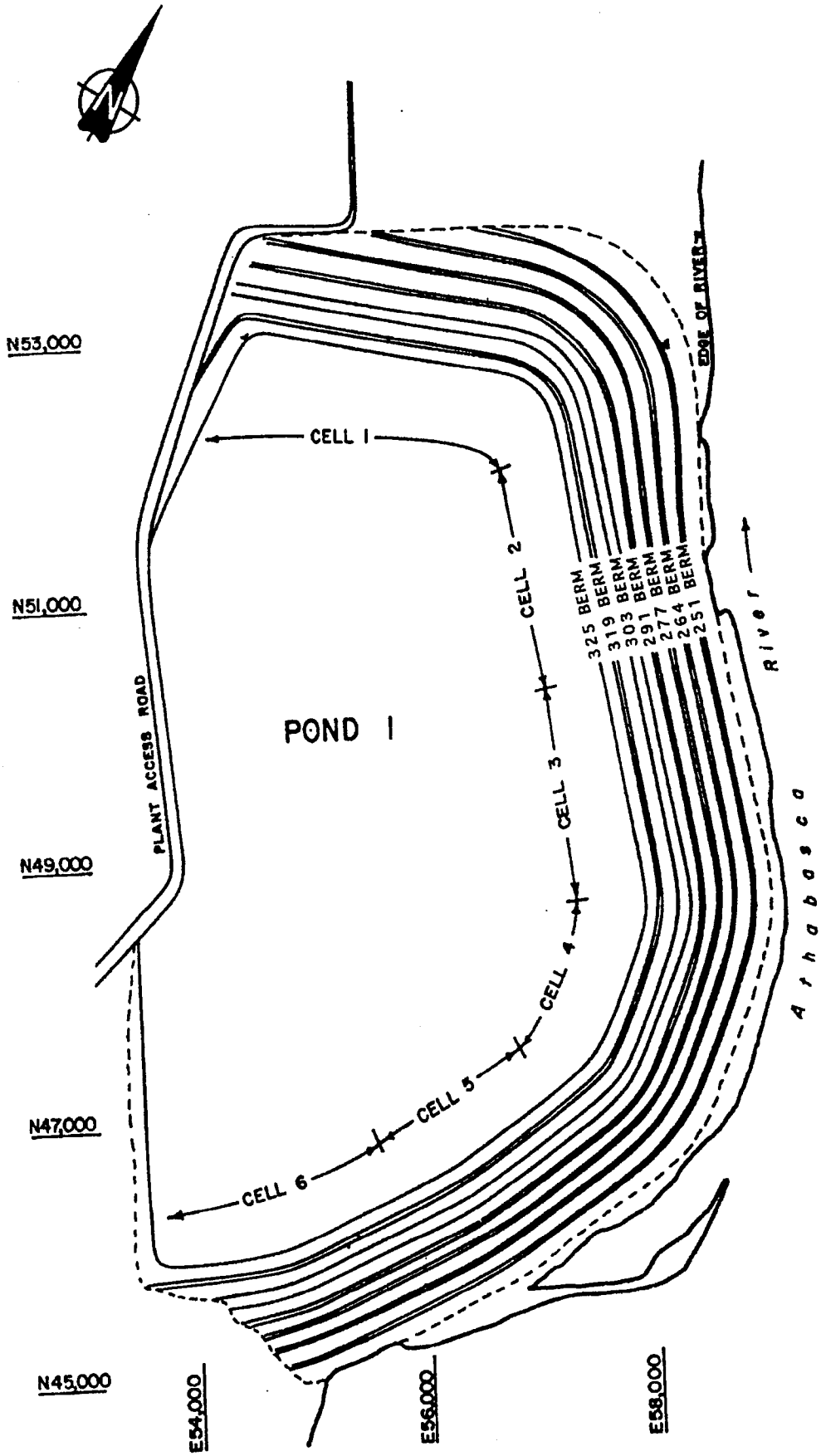

Figure (5.1) Plan view of Tar island dyke(modefied after Watts (1980)).

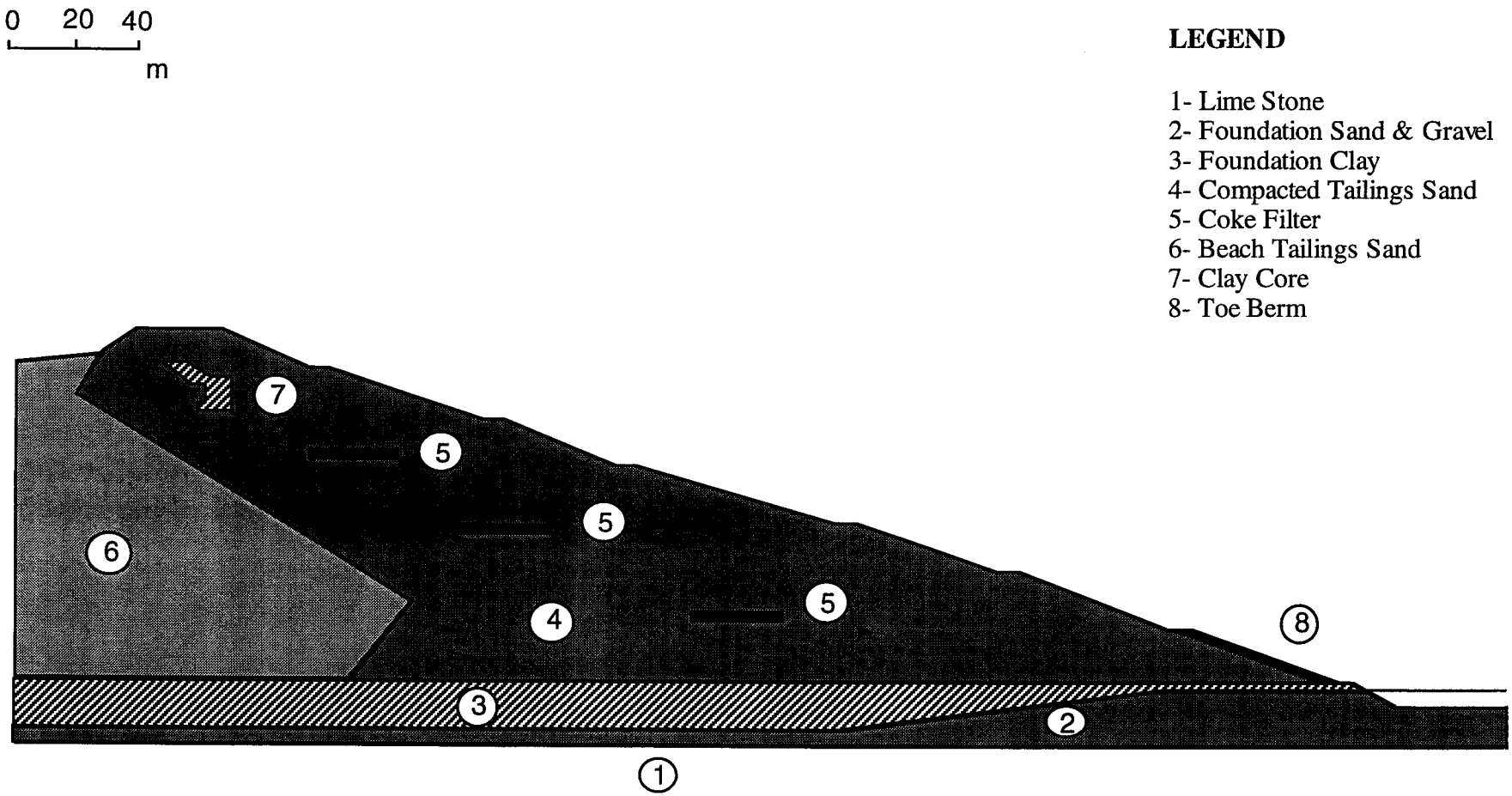

Figure (5.2) Typical section through Tar island dyke.

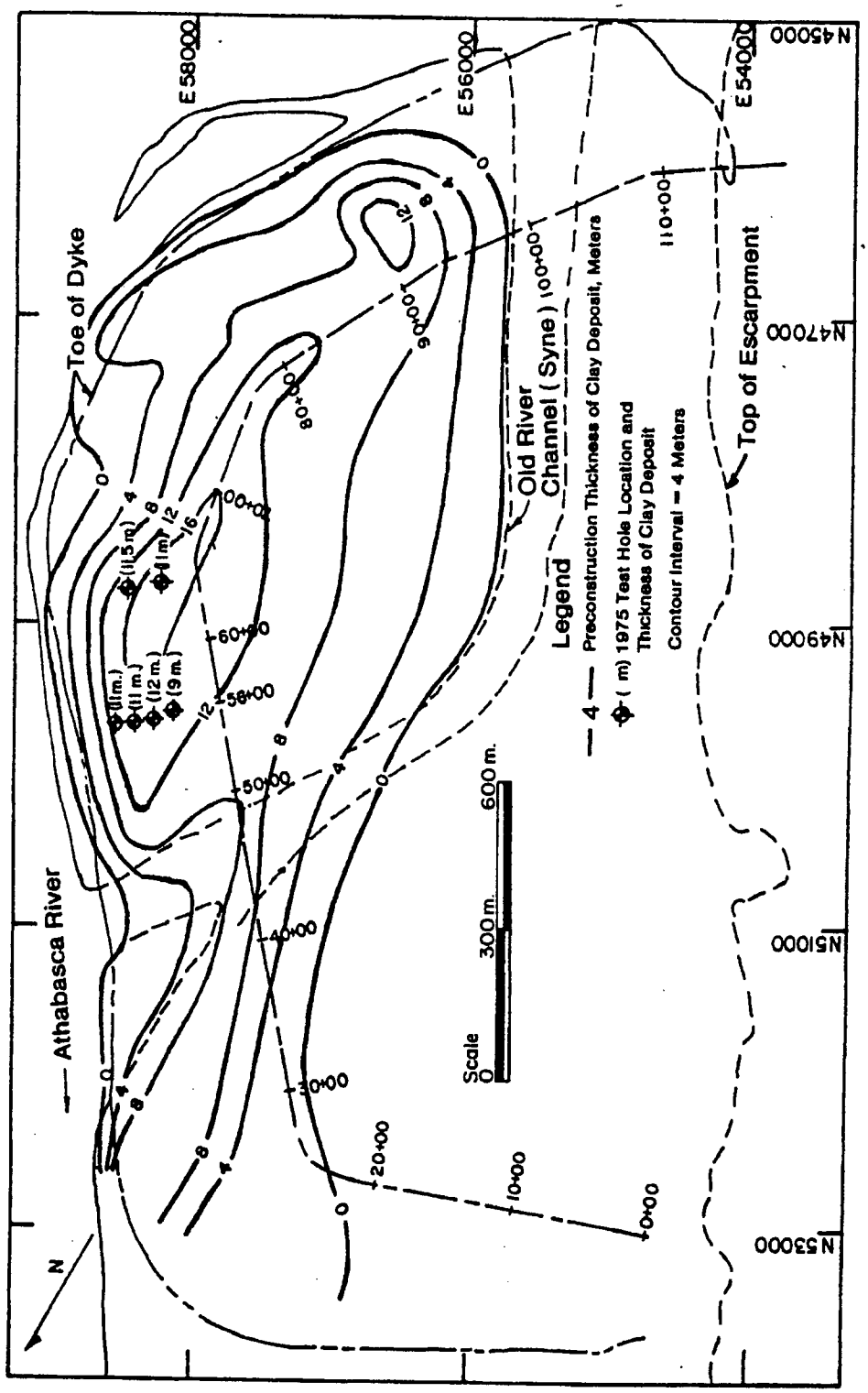

Figure (5.3) Isopach map of clay and silt deposit

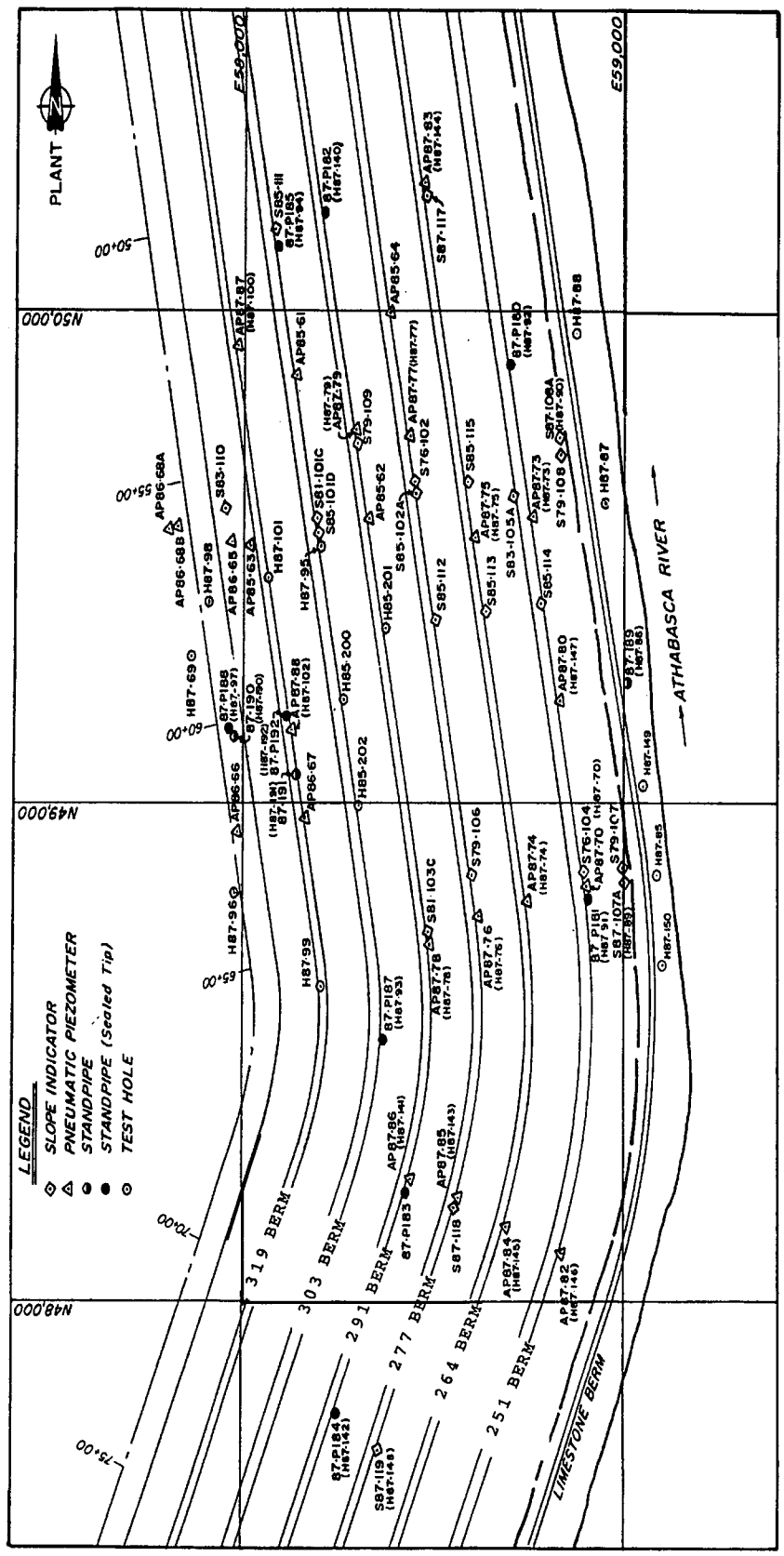

Figure (5.4) Location of boreholes and instrumentation for geotechnical investigation, December 1987.

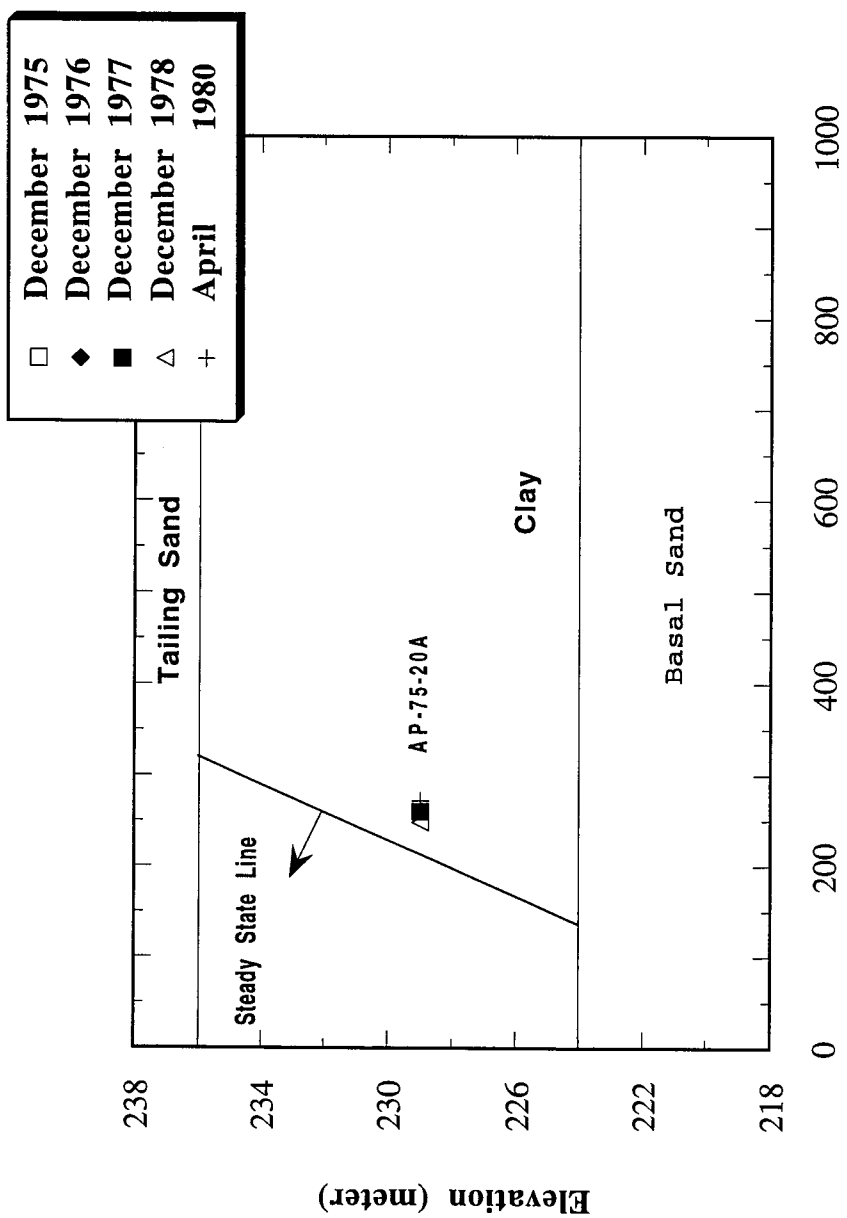

Figure (5.5) Summary of foundation pore pressure for berm-277

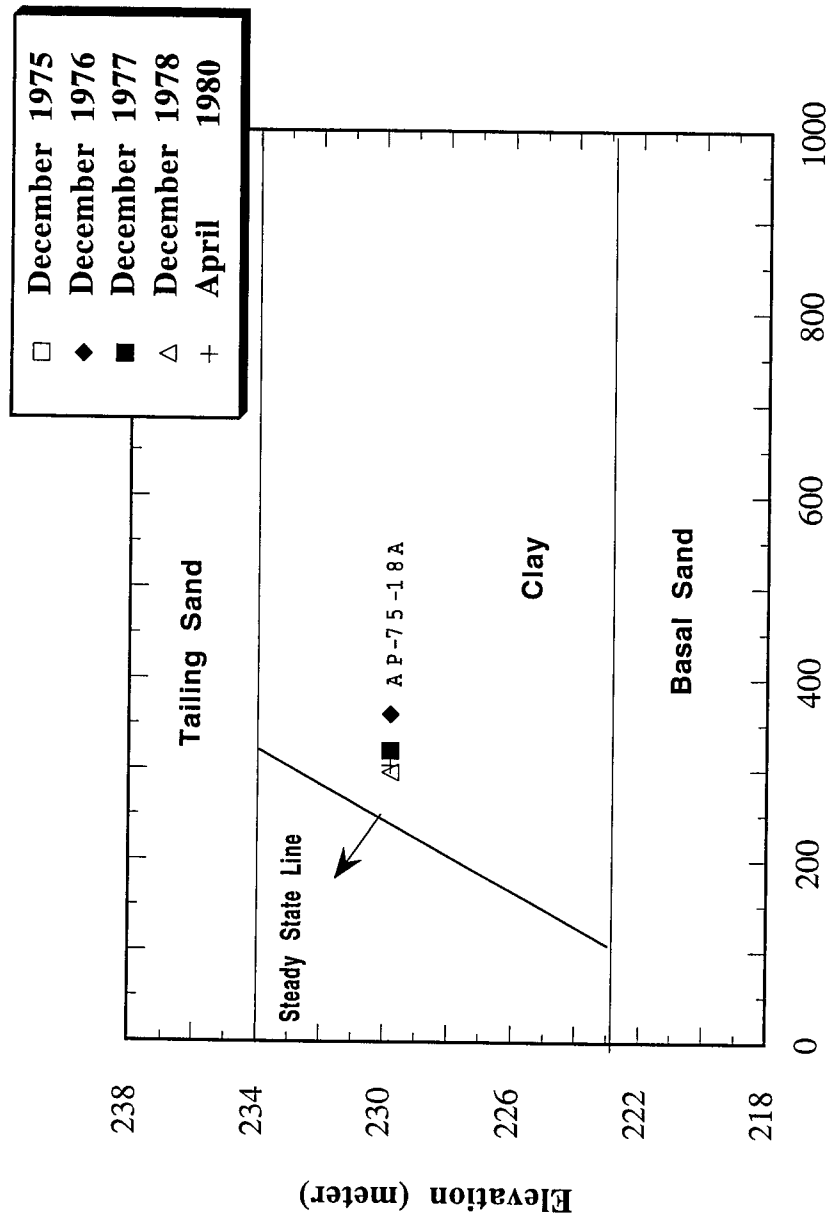

Figure (5.6) Summary of foundation pore pressure for berm-291

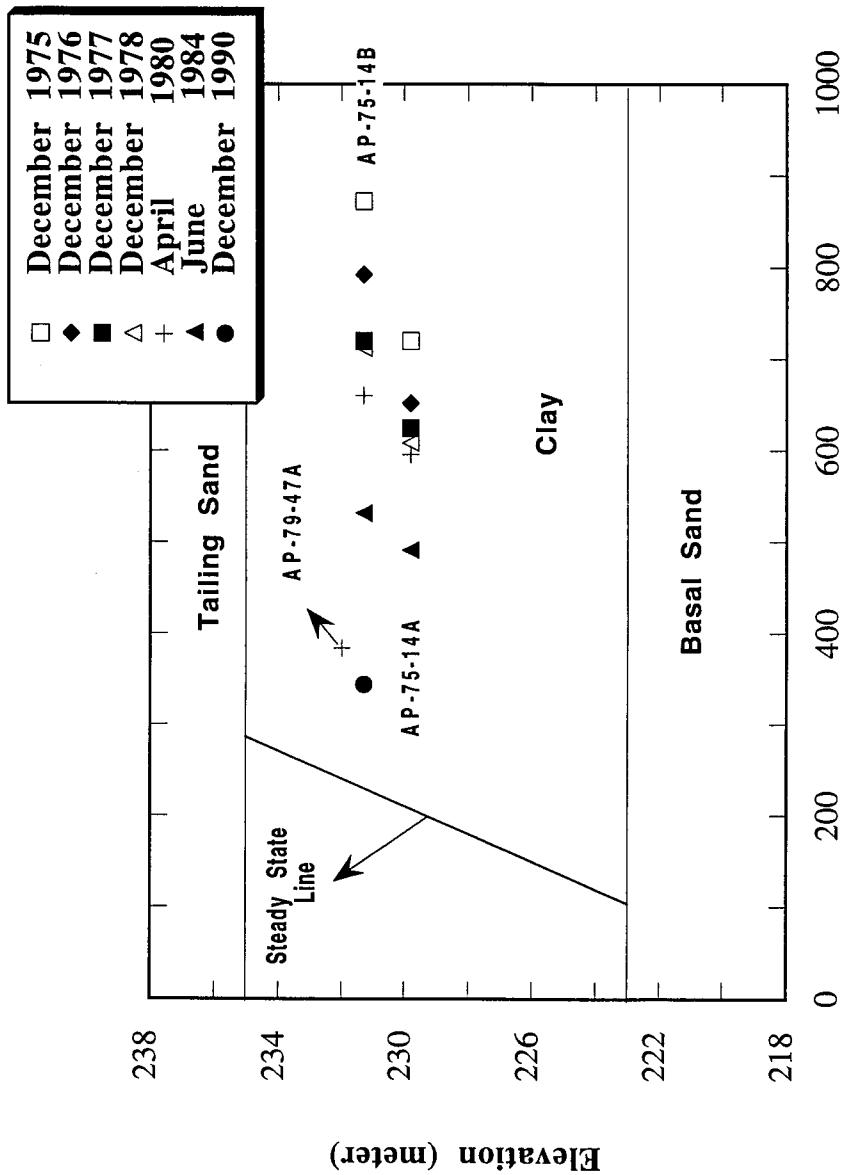

Figure (5.7) Summary of foundation pore pressure for berm-303

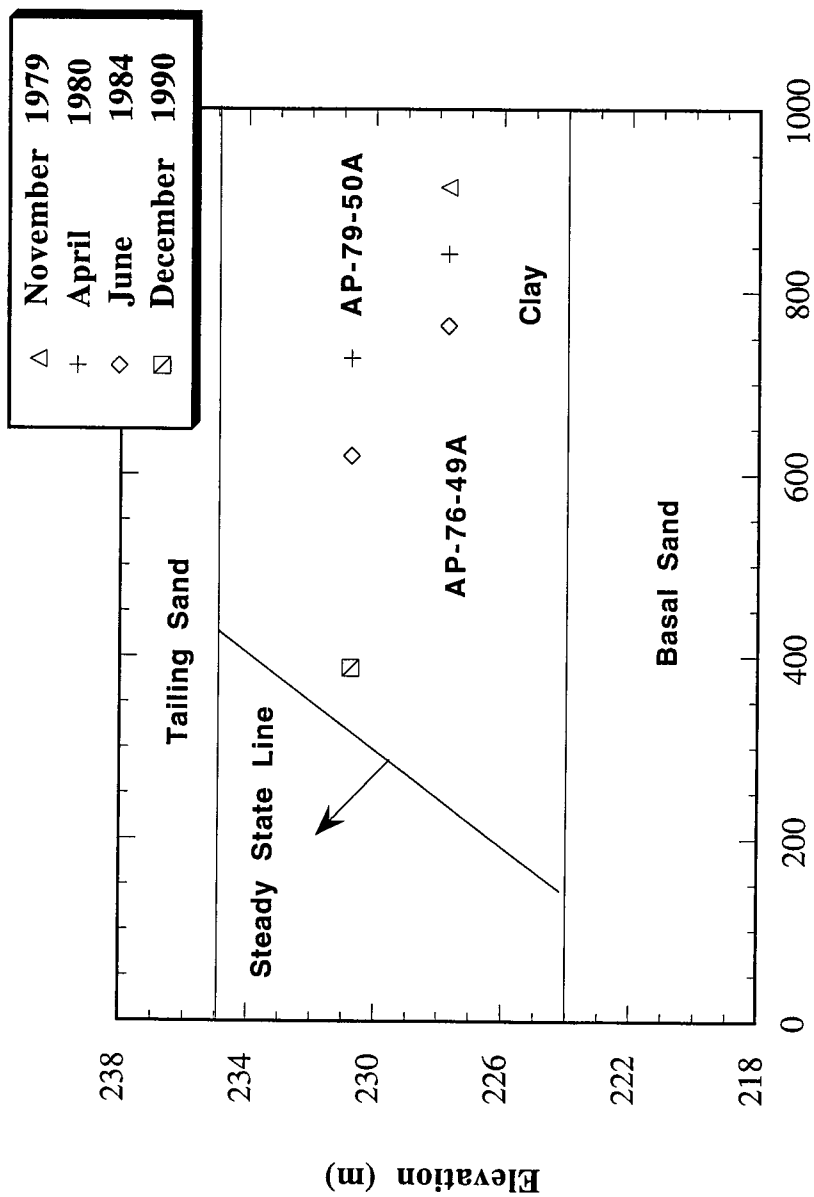

Figure (5.8) Summary of foundation pore pressure for berm-319

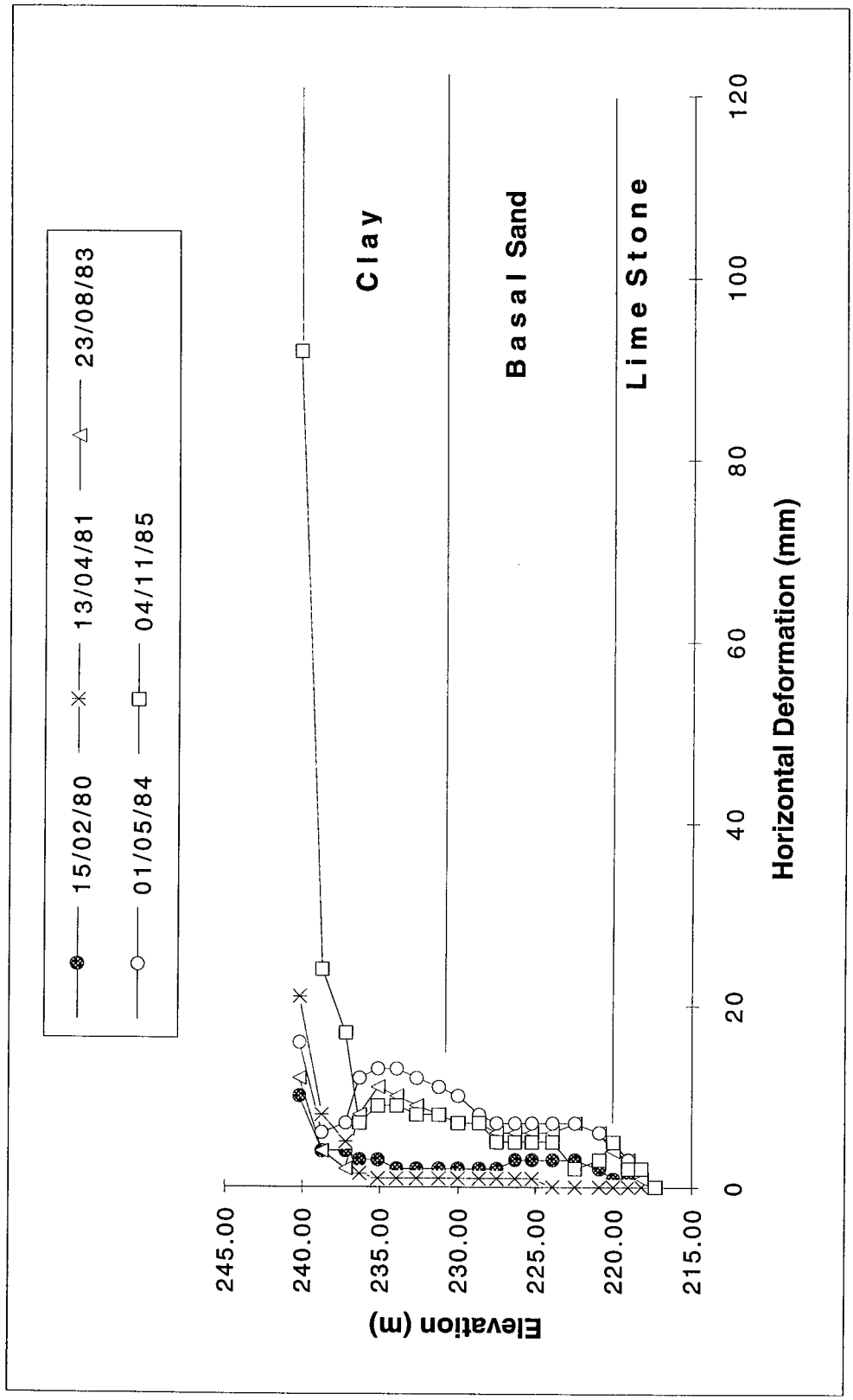

Figure (5.9) Inclinometer SI-79-108, Toe.

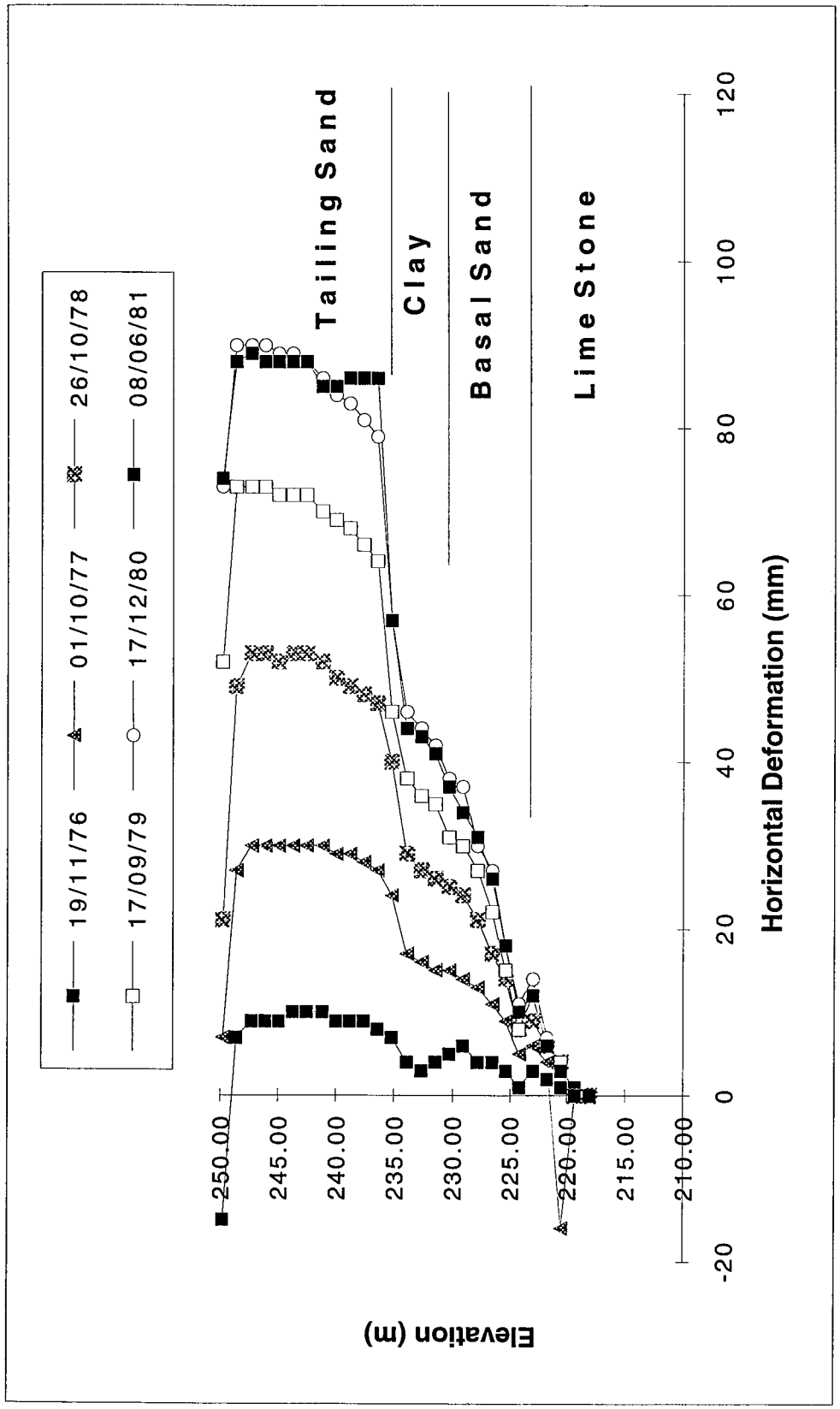

Figure (5.10) Inclinometer SI-76-105, Berm 251.

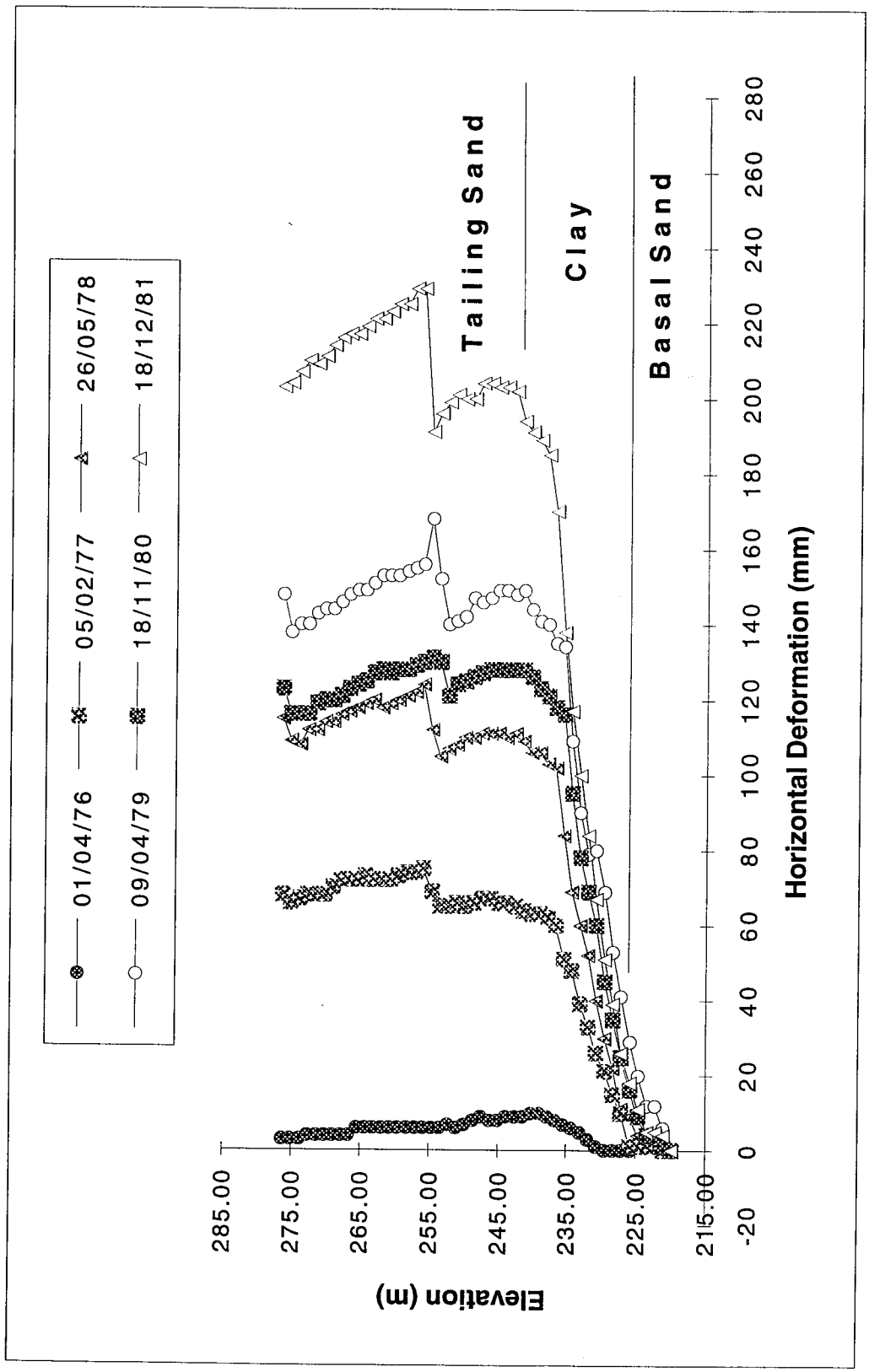

Figure (5.11) Inclinometer SI-76-102, Berm 277.

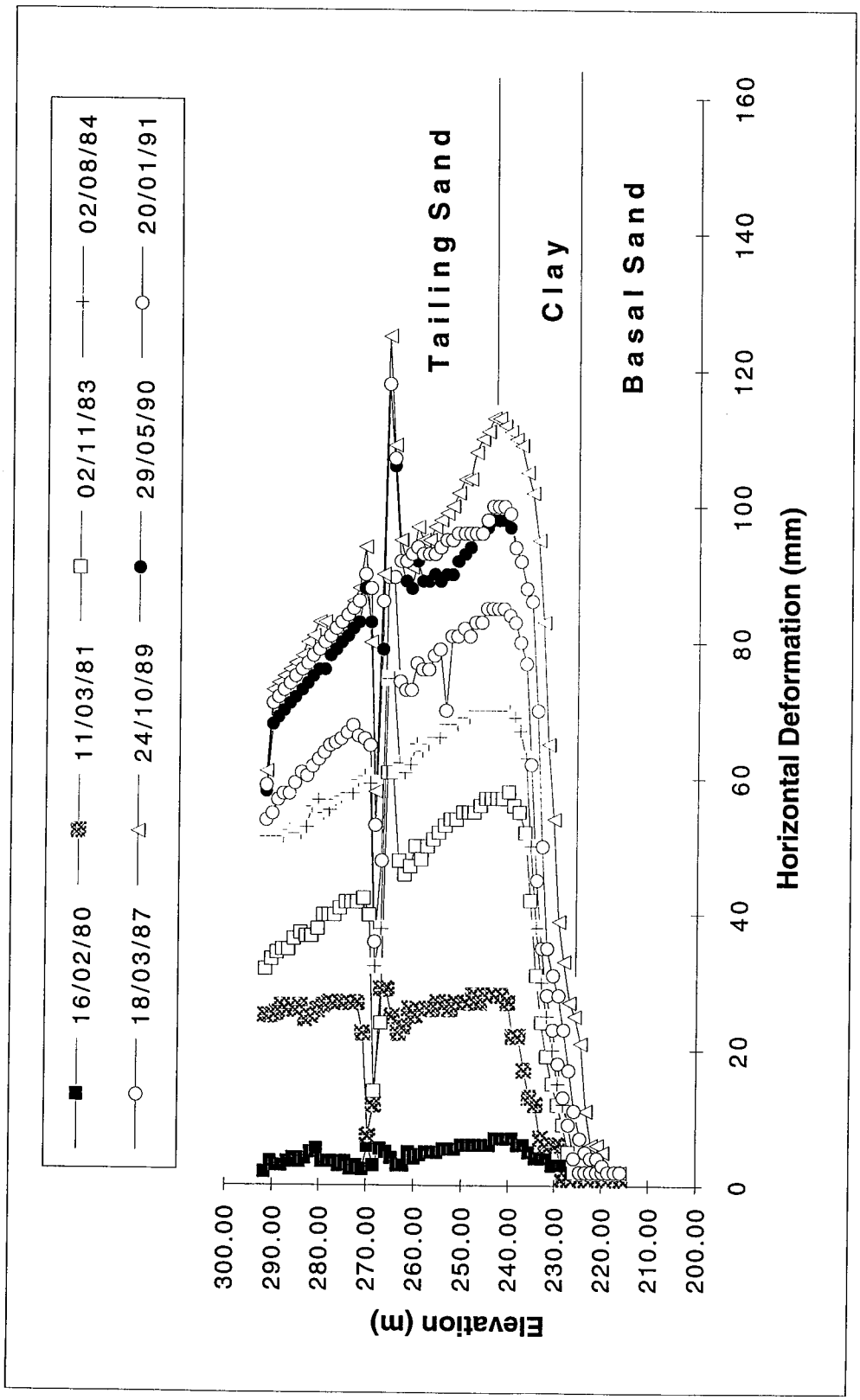

Figure (5.12) Inclinometer SI-79-109, Berm 291.

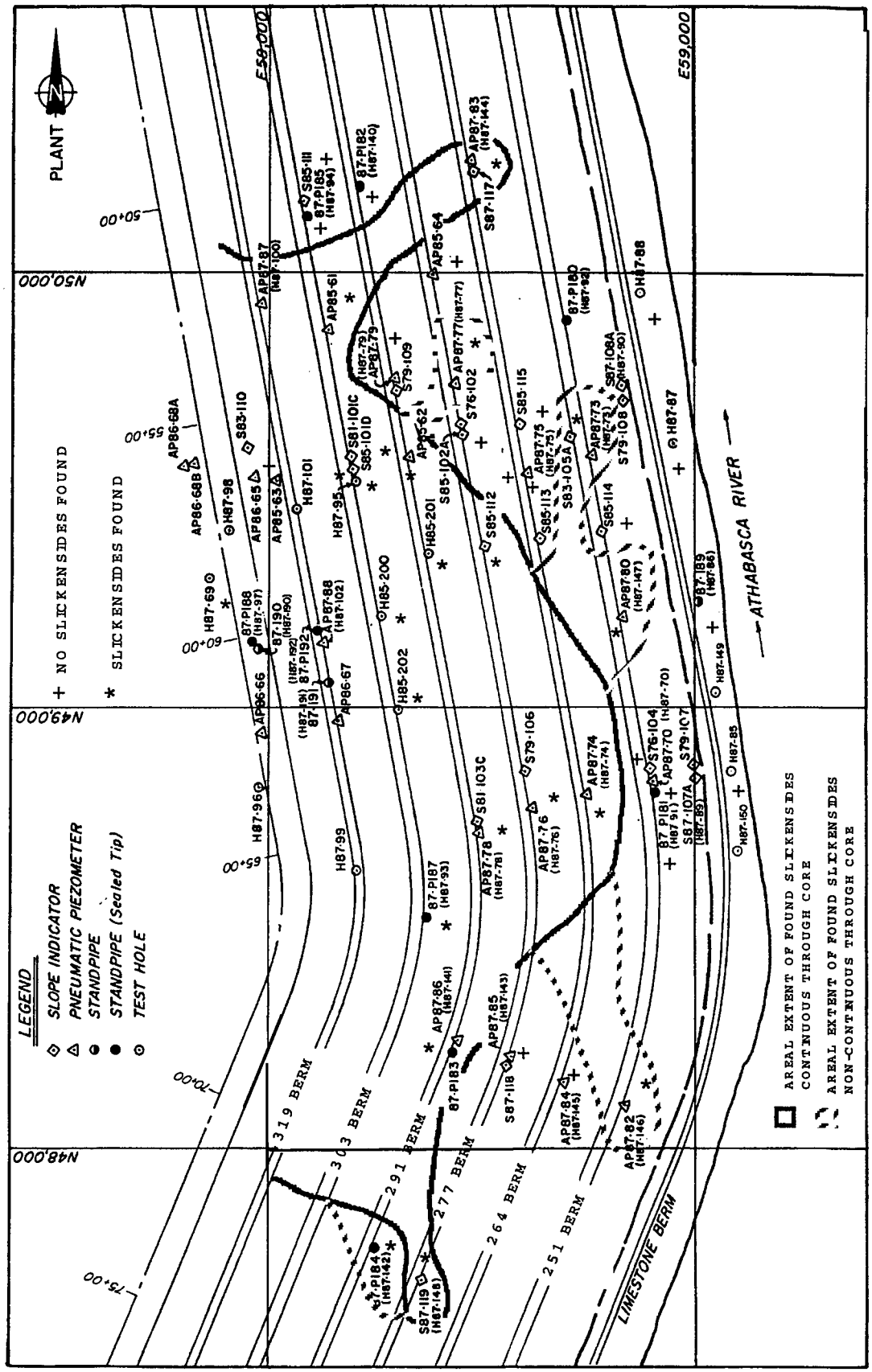

Figure (5.13) Location of slickensides found in foundation clay.

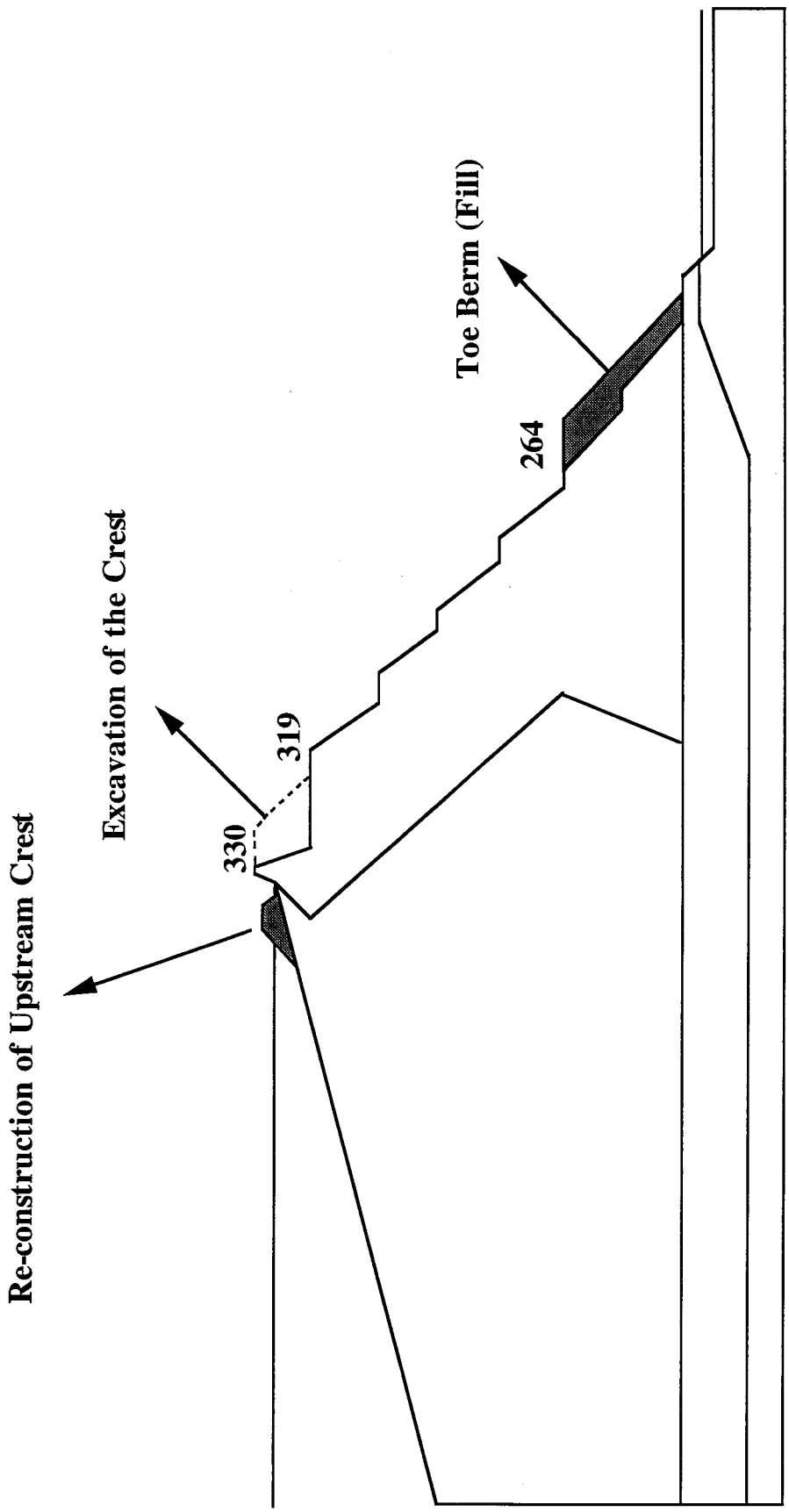

Figure (5.14) Proposed remedial measures program.

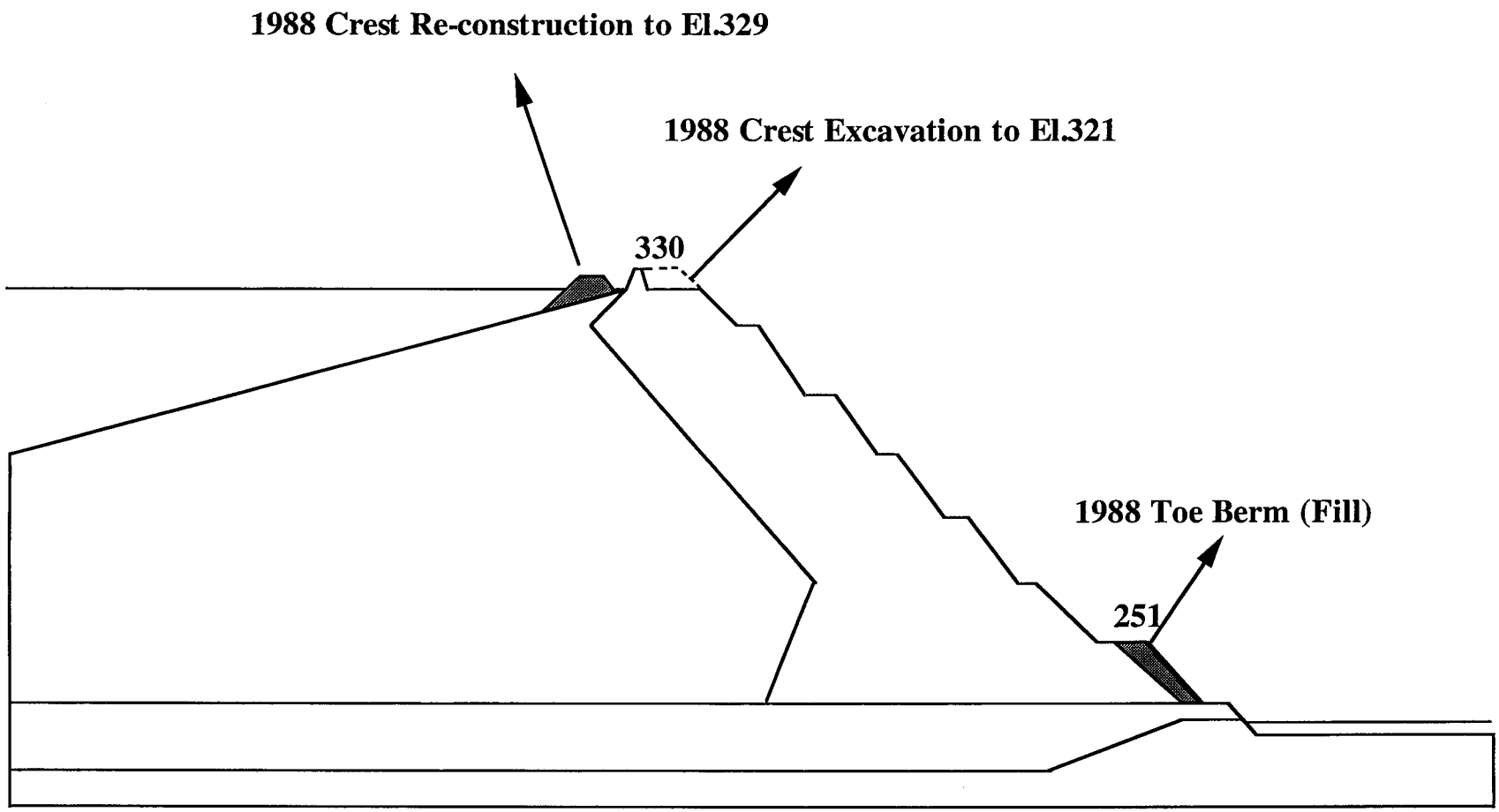

Figure (5.15) 1988 remedial measures program.

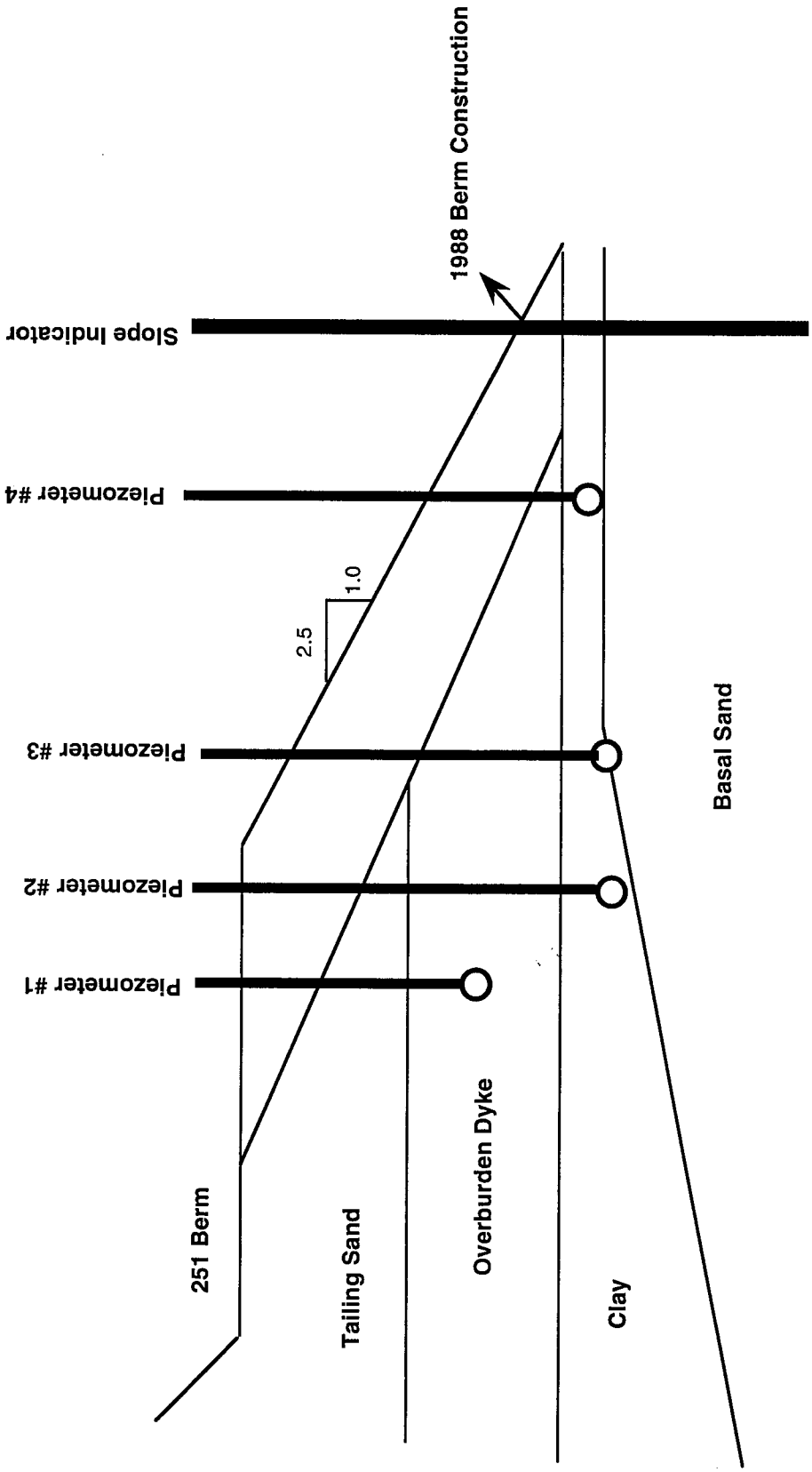

Figure (5.16) Primary instrumentation monitored during 1988 berm construction.

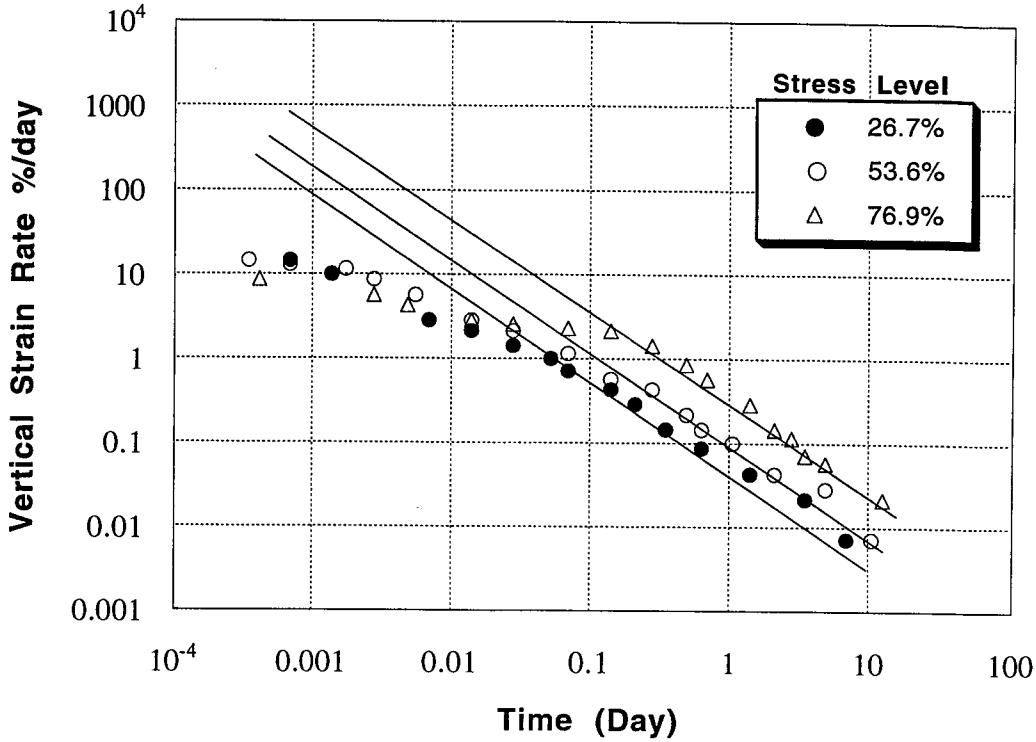

Figure (5.17a) Vertical strain rate vs. time for horizontal bedding samples.

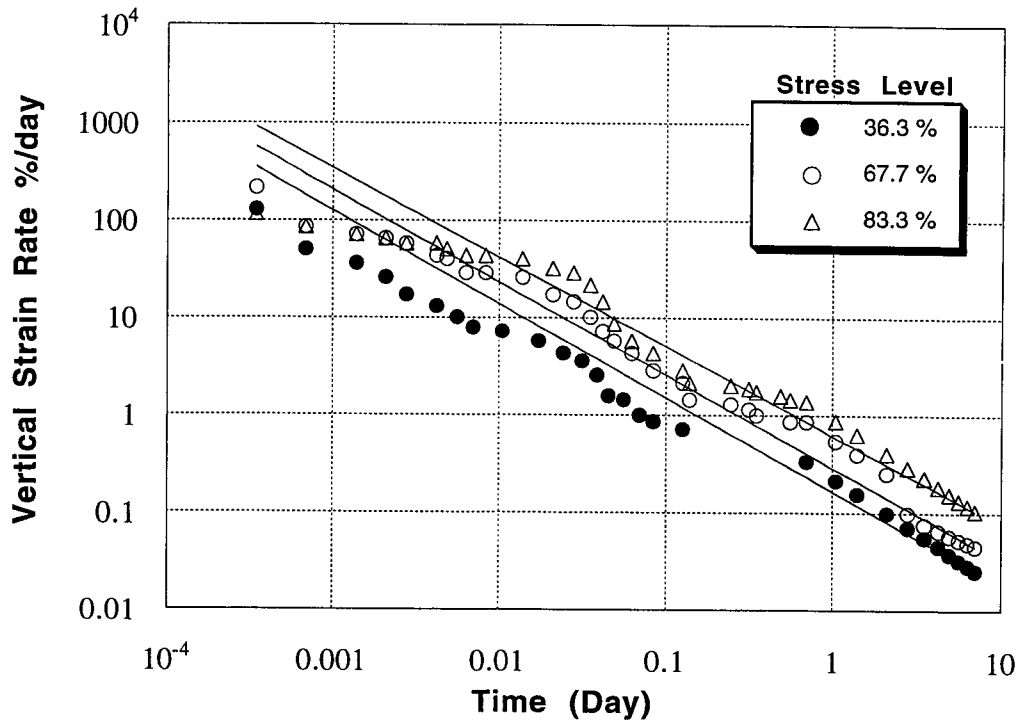

Figure (5.17b) Vertical strain rate vs.time for inclined bedding samples.

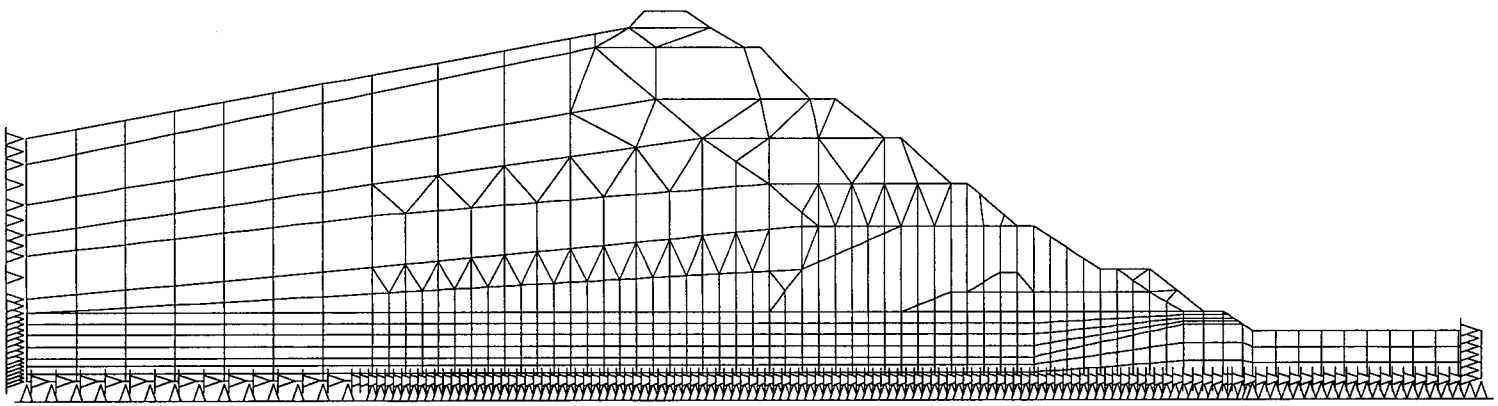

Figure (5.18) Finite element idealization of the Tar island dyke.

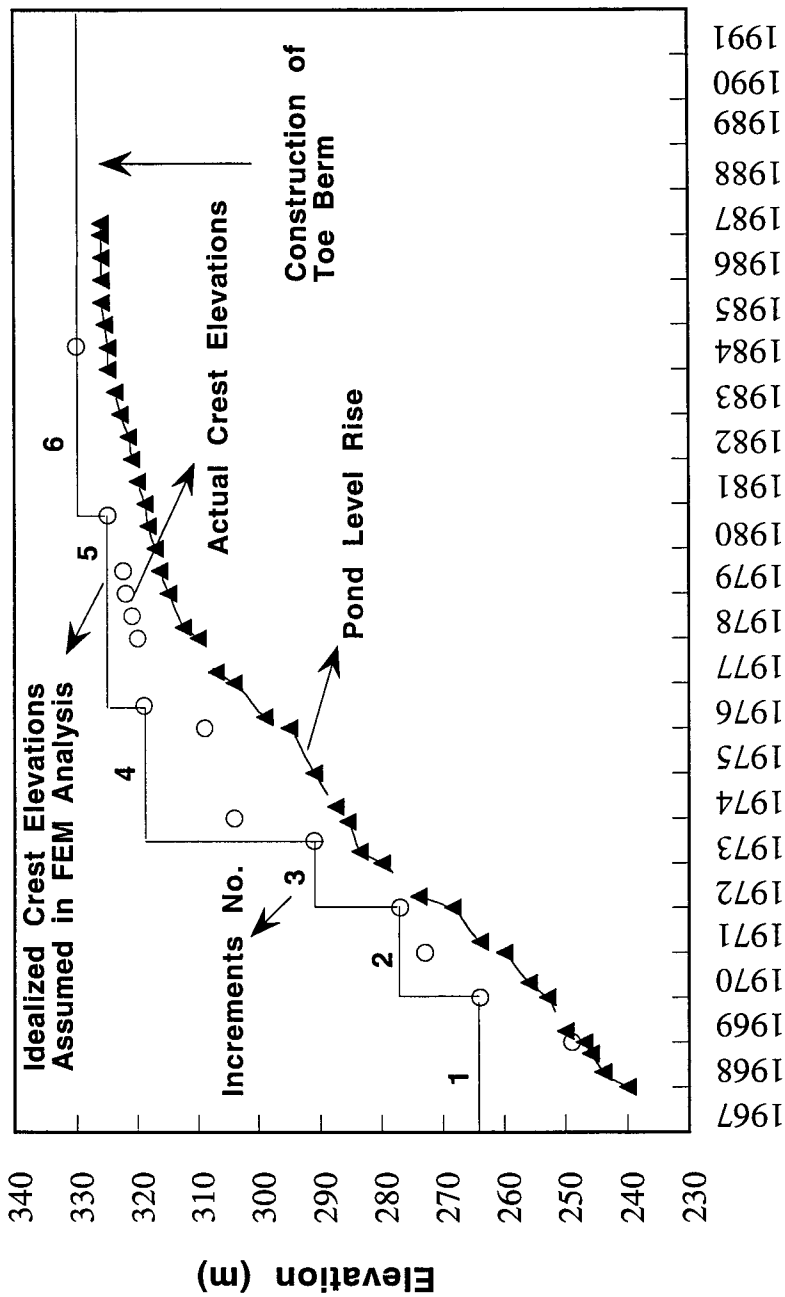

Figure (5.19) Dyke crest and pond level rise with time.

Foundation Stage :

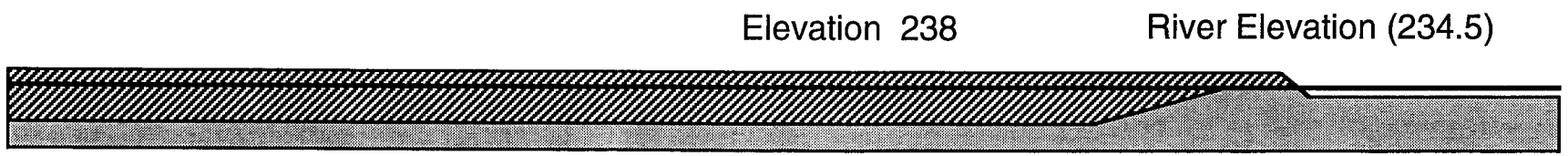

Stage One :

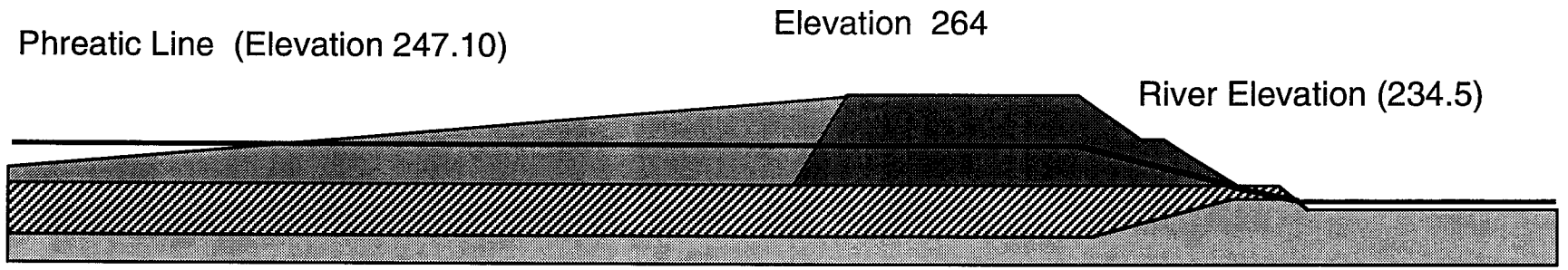

Construction Period: January 1967 - Decmember 1969

Figure (5.20) Idealized construction stages of TID for the finite element analysis.

Stage Two :

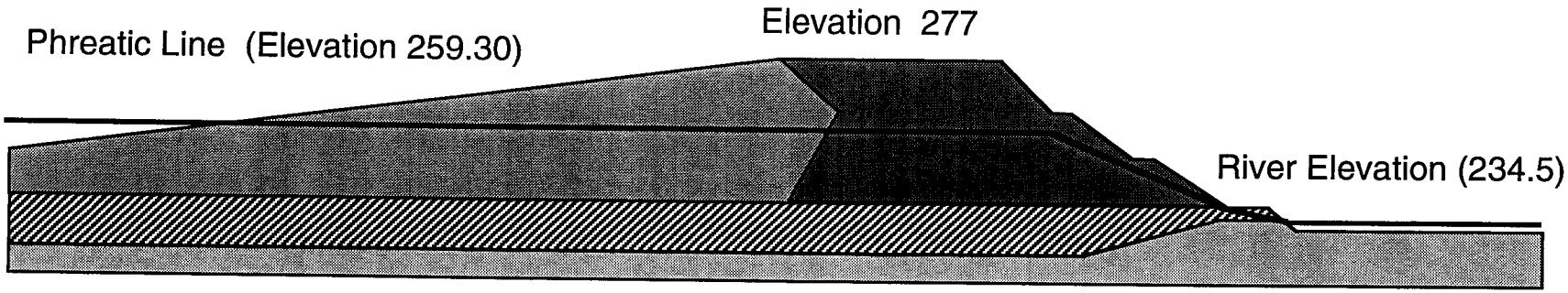

Construction Period: Decmember 1969 - December 1971

Stage Three :

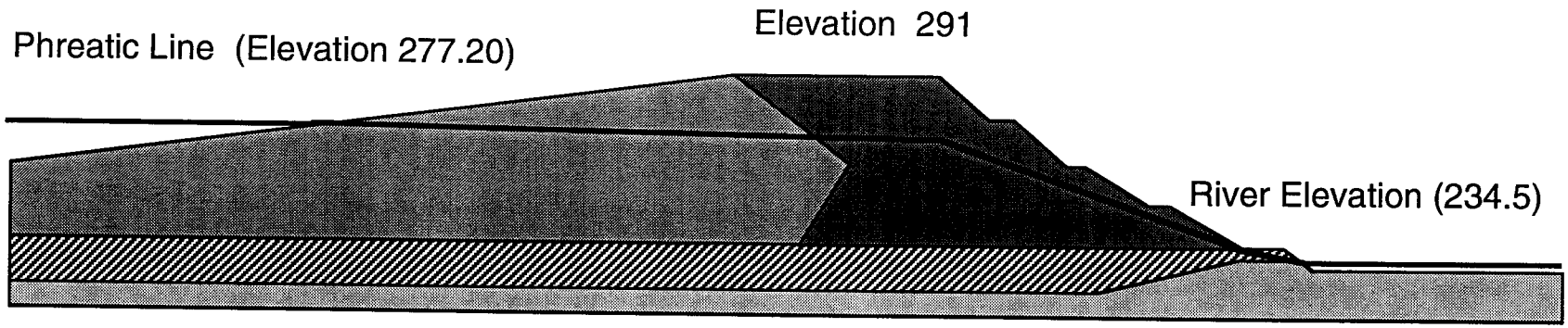

Construction Period: December 1971 - June 1973

Figure (5.20 cont.) Idealized construction stages of TID for the finite element analysis.

Stage Four :

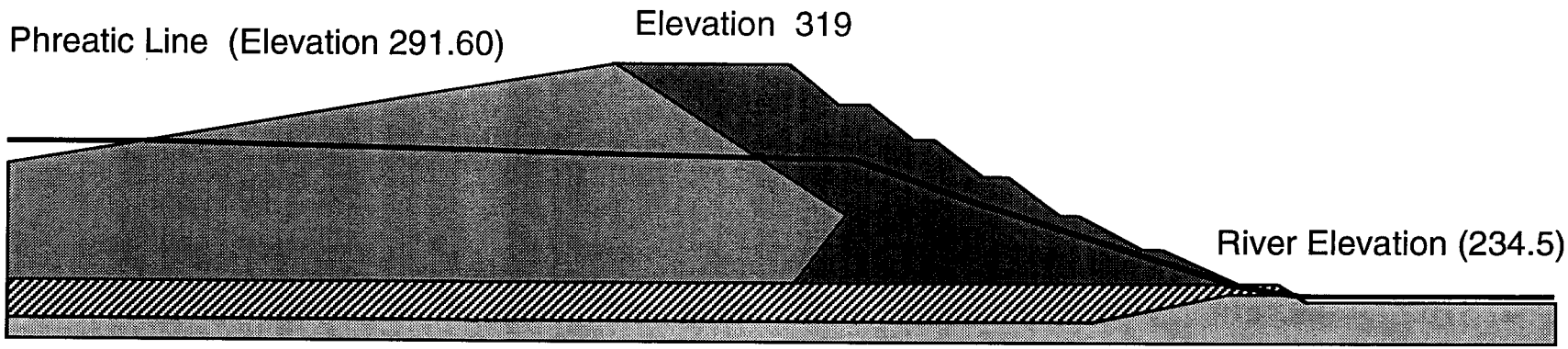

Construction Period: June 1973 - June 1976

Stage Five :

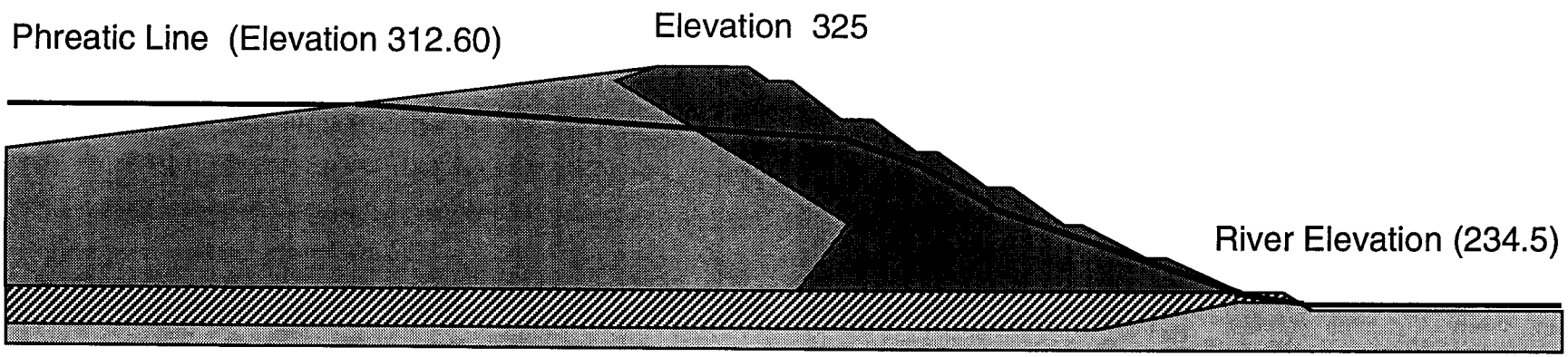

Construction Period: June 1976 - September 1980

Figure (5.20 cont.) Idealized construction stages of TID for the finite element analysis.

Stage Six :

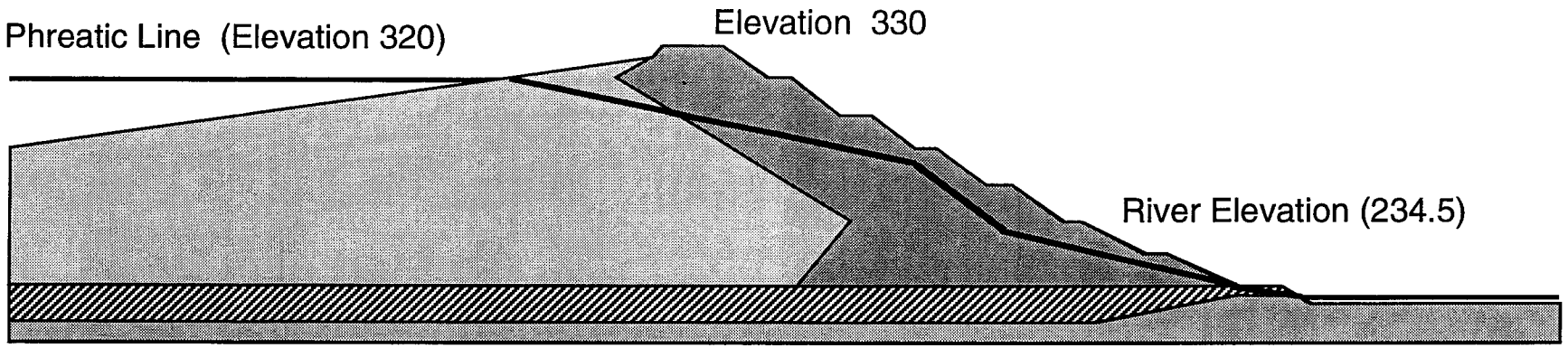

Construction Period: September 1980 - December 1987

Remedial Measures Stage :

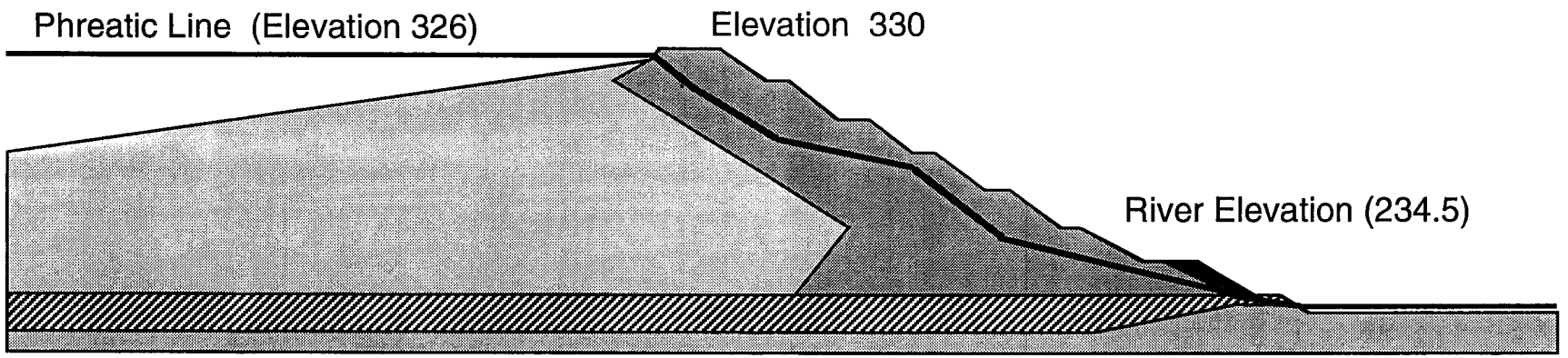

Construction Period: December 1987 - December 1992

Figure (5.20 cont.) Idealized construction stages of TID for the finite element analysis.

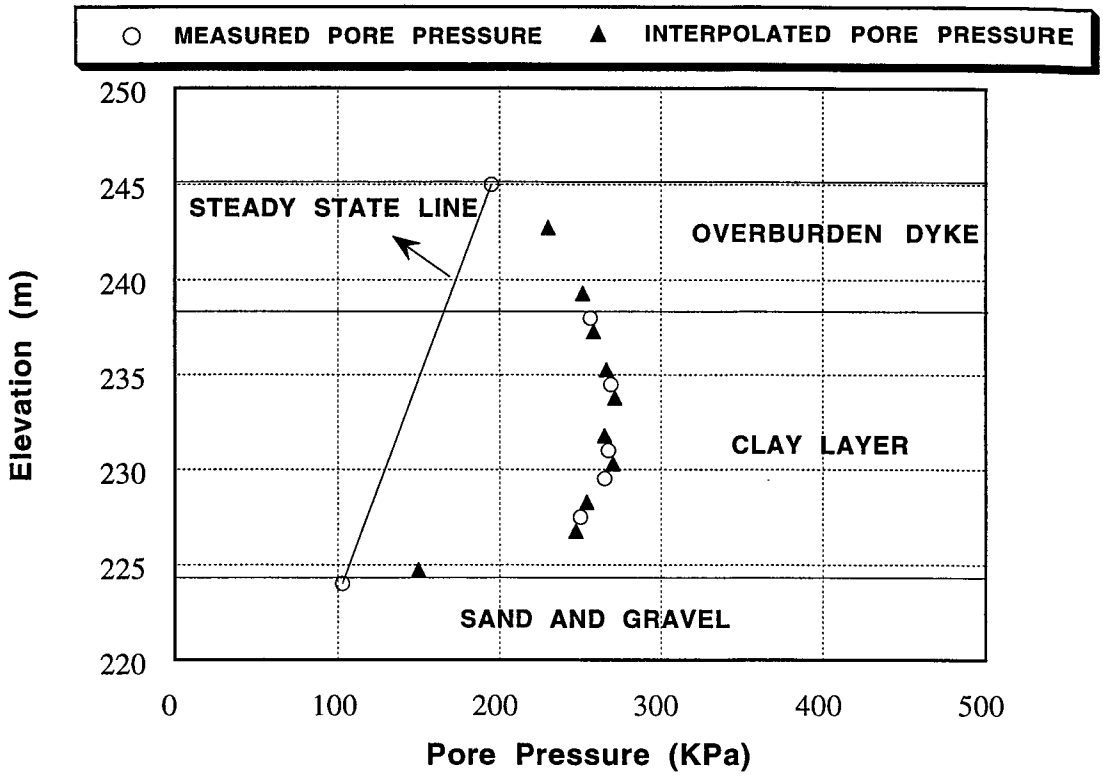

Figure (5.21a) Comparison between measured and interpolated pore pressure at berm 277 in August/1978

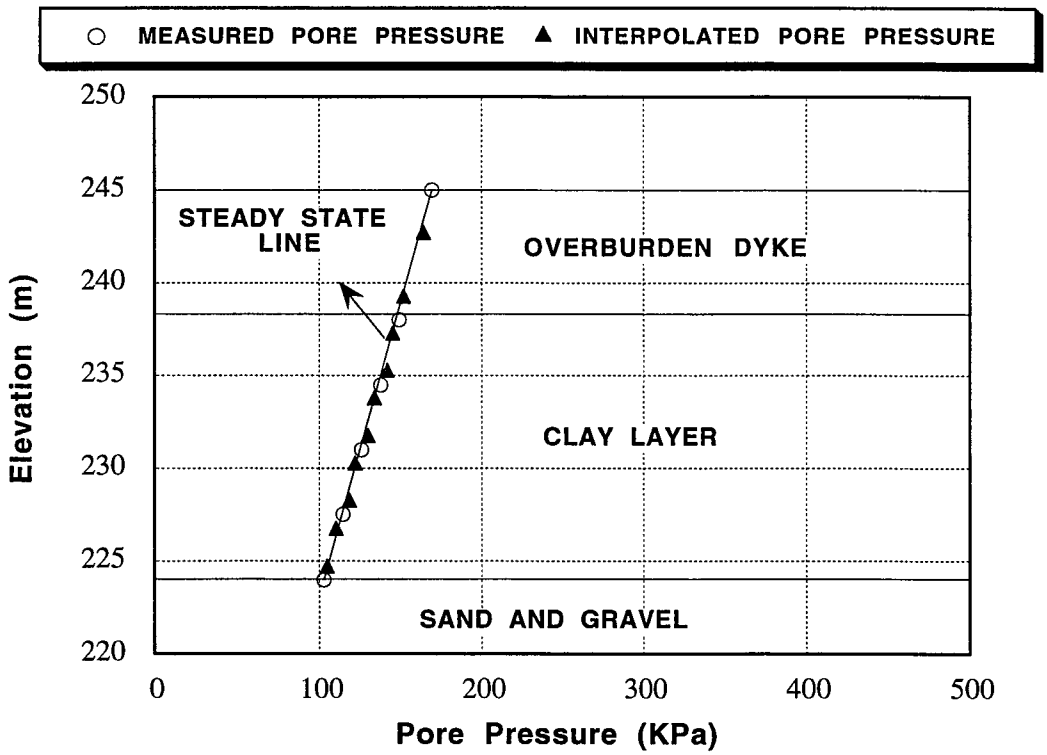

Figure (5.21b) Comparison between measured and interpolated pore pressure at berm 277 in December/1984

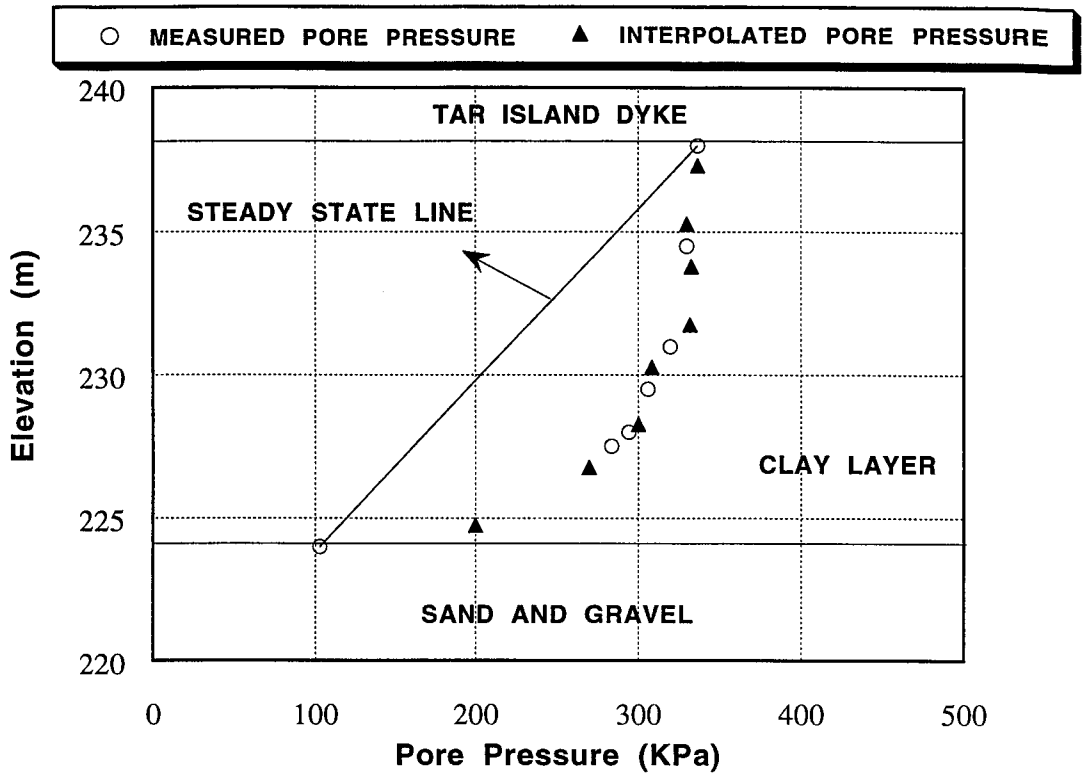

Figure (5.22a) Comparison between measured and interpolated pore pressure at berm 291 in August/1978.

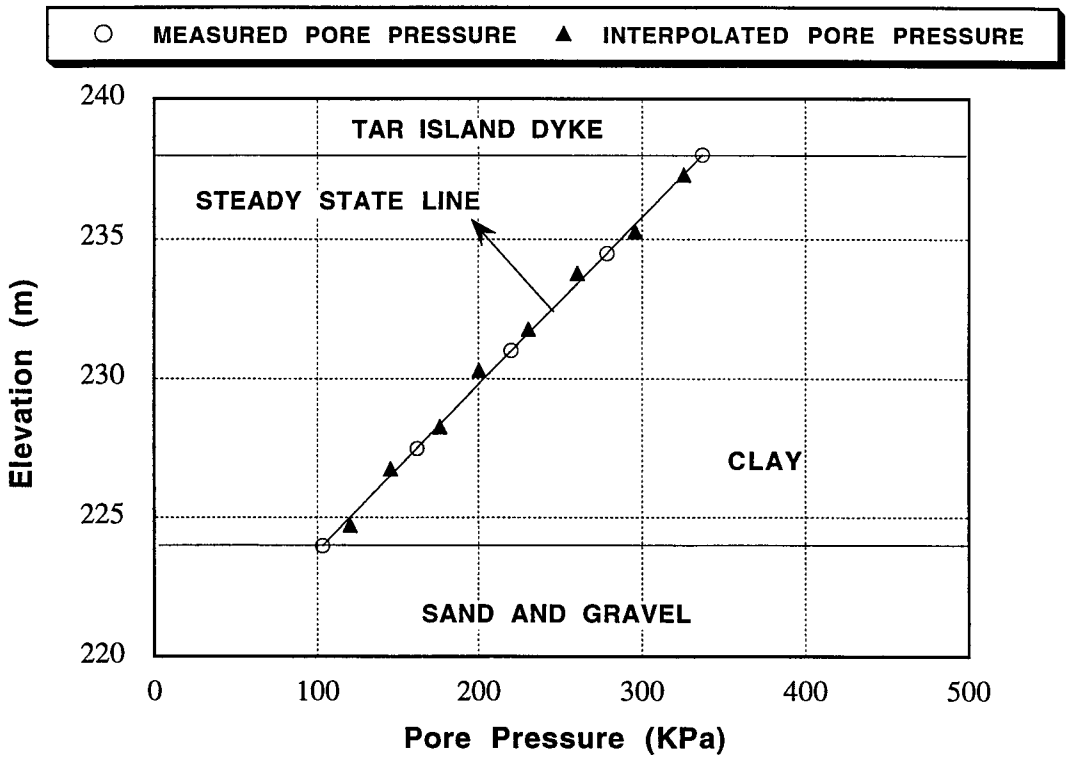

Figure (5.22b) Comparison between measured and interpolated pore pressure at berm 291 in December/1984.

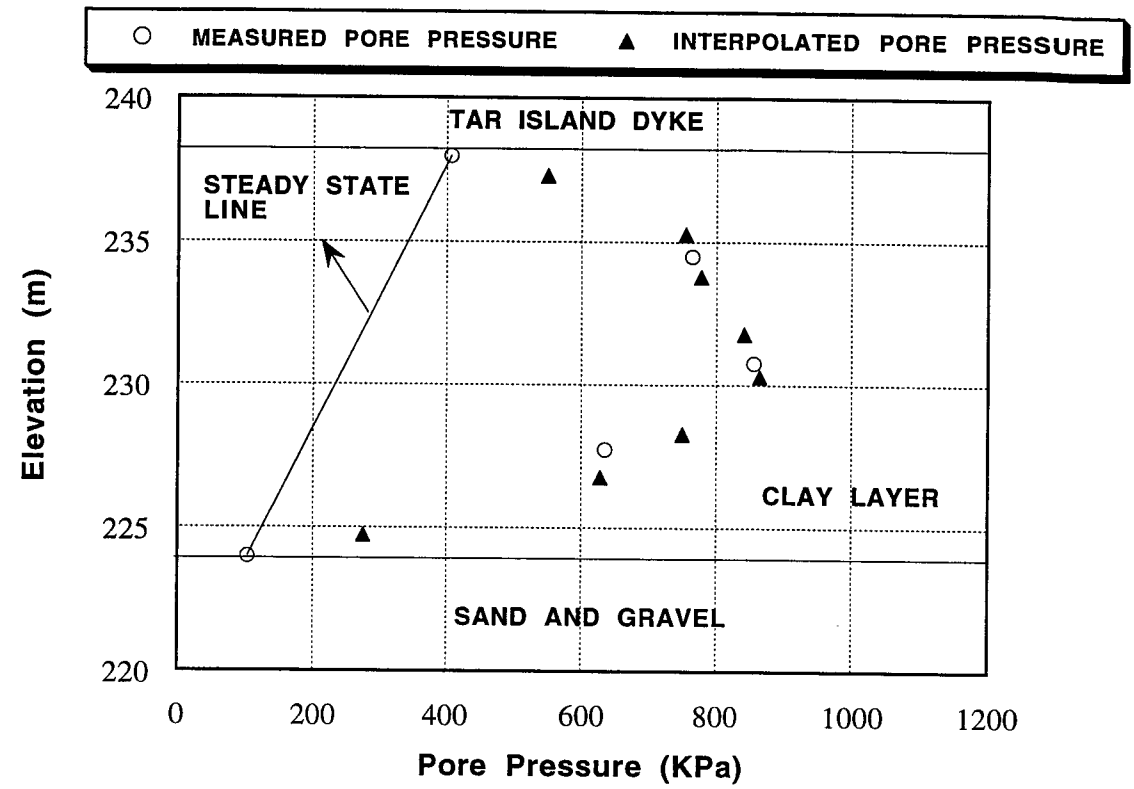

Figure(5.23a) Comparison between interpolated and measured pore pressure at berm 319 in August/1978.

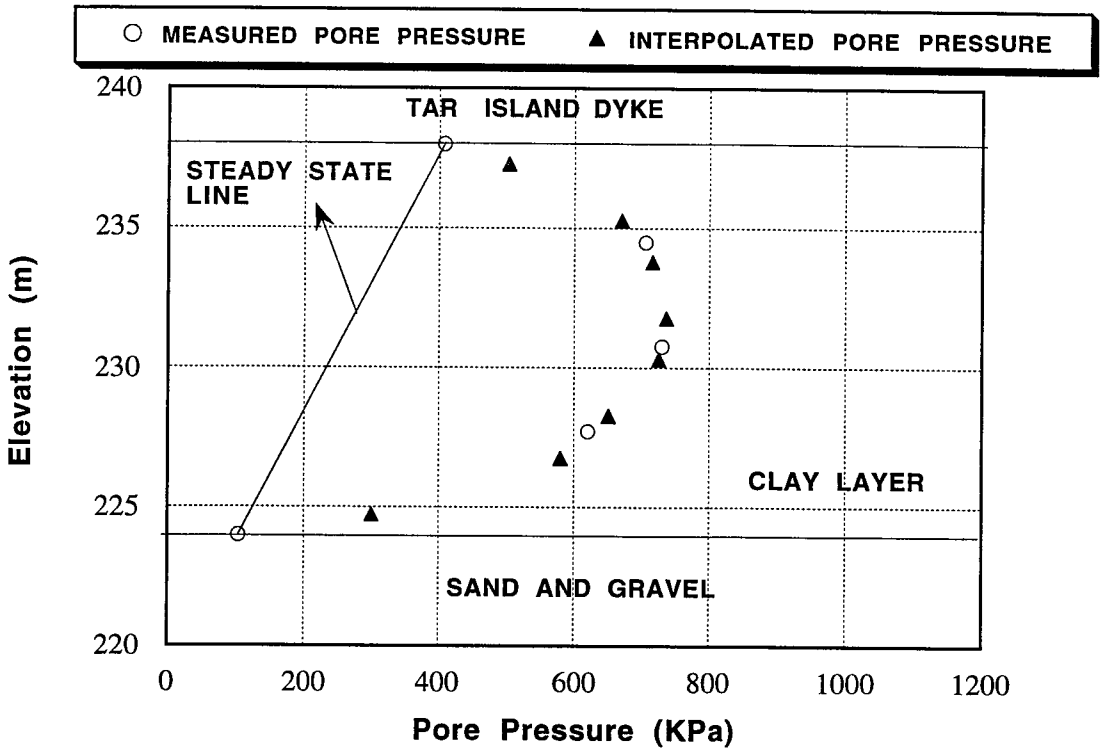

Figure(5.23b) Comparison between interpolated and measured pore pressure at berm 319 in December/1984.

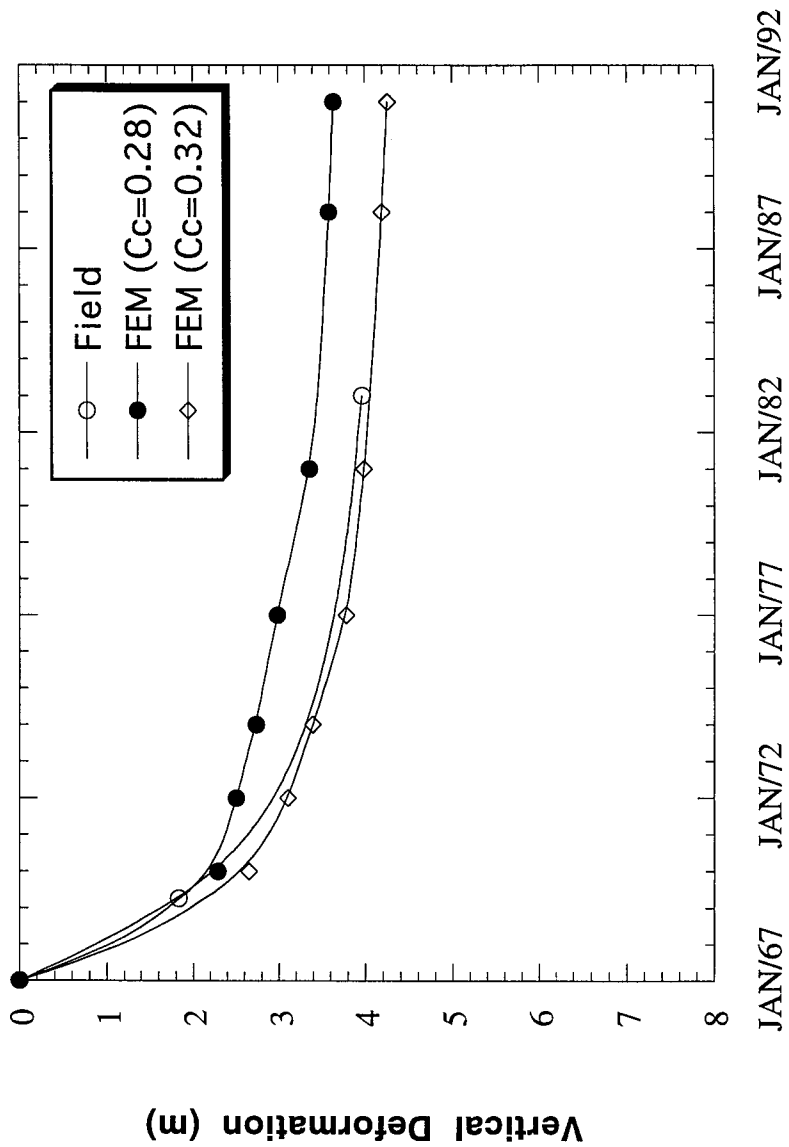

Figure (5.24) Vertical deformation beneath TID.

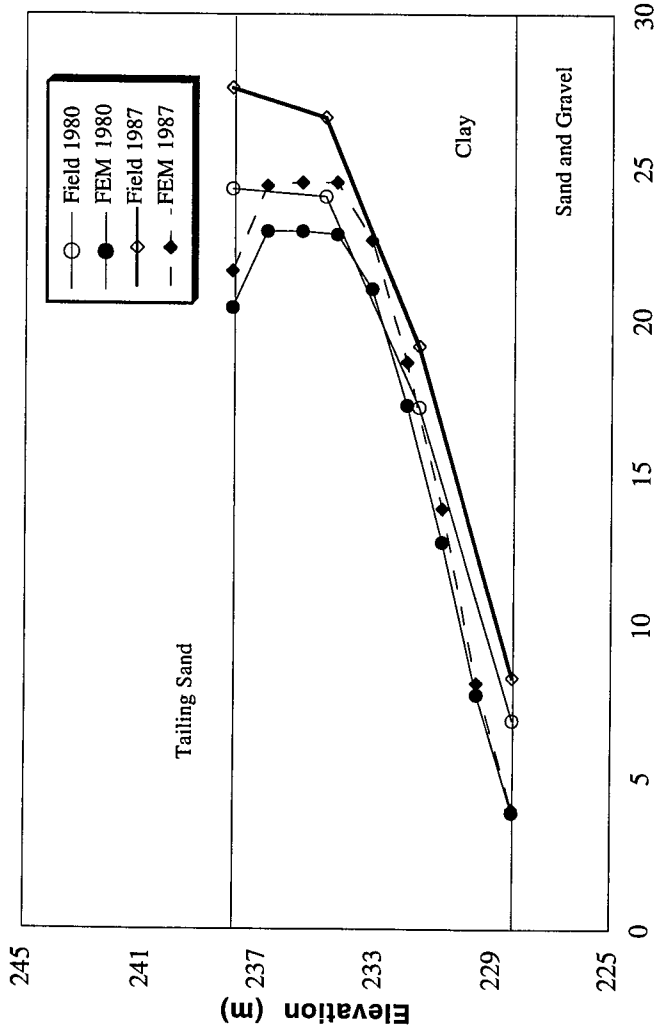

Figure (5.25) Total horizontal deformation at berm 251.

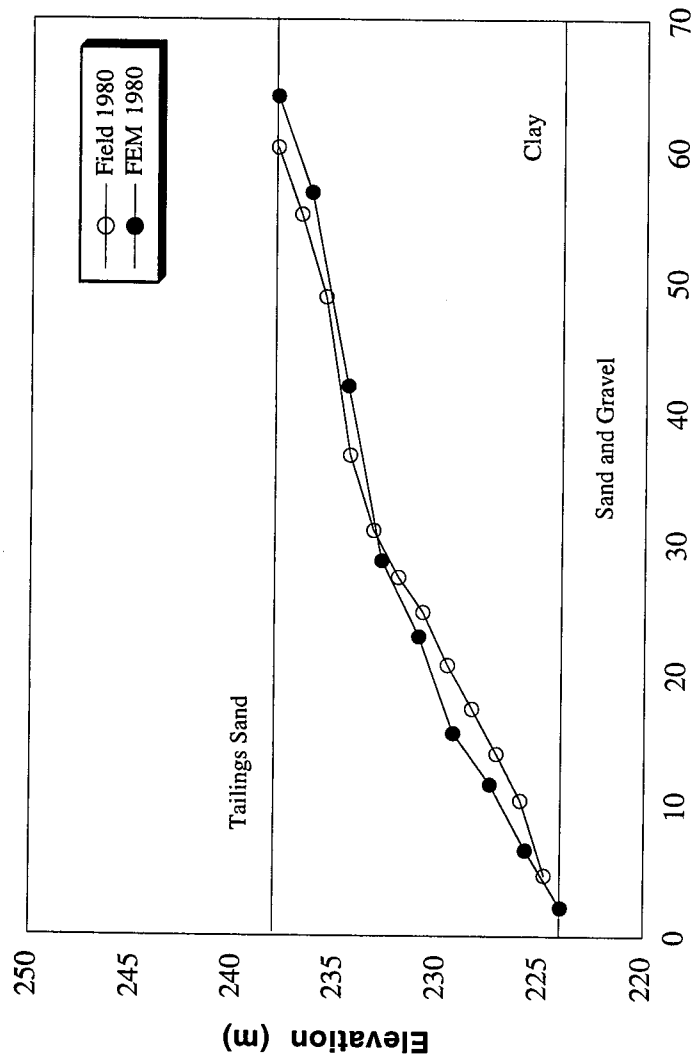

Figure (5.26) Total horizontal deformation at berm 277.

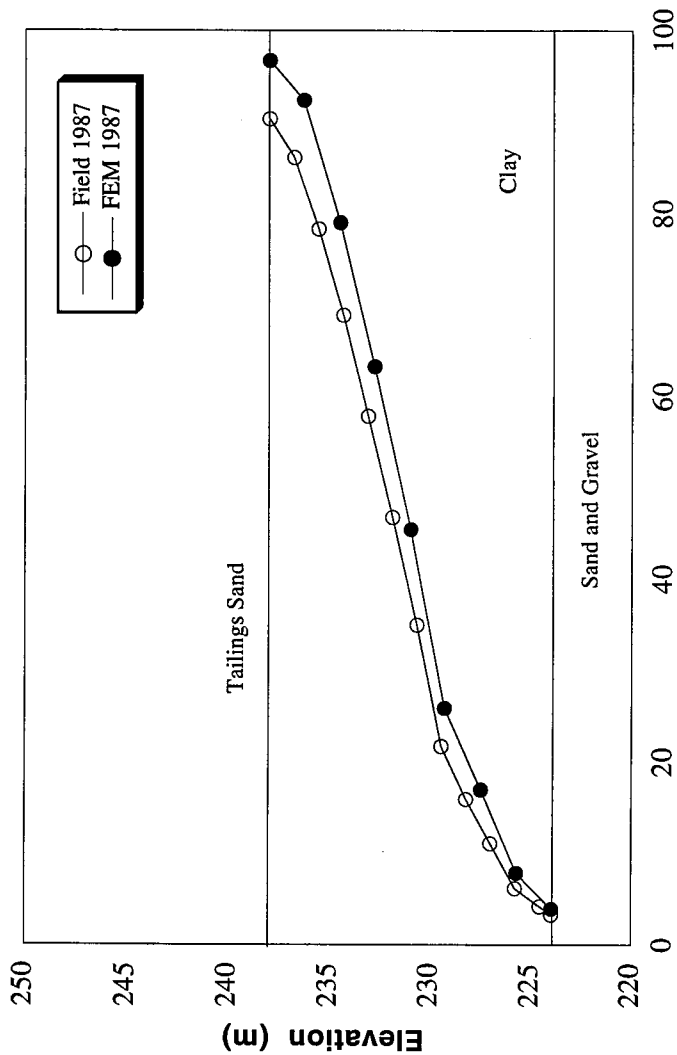

Figure (5.27) Total horizontal deformation at berm 291.

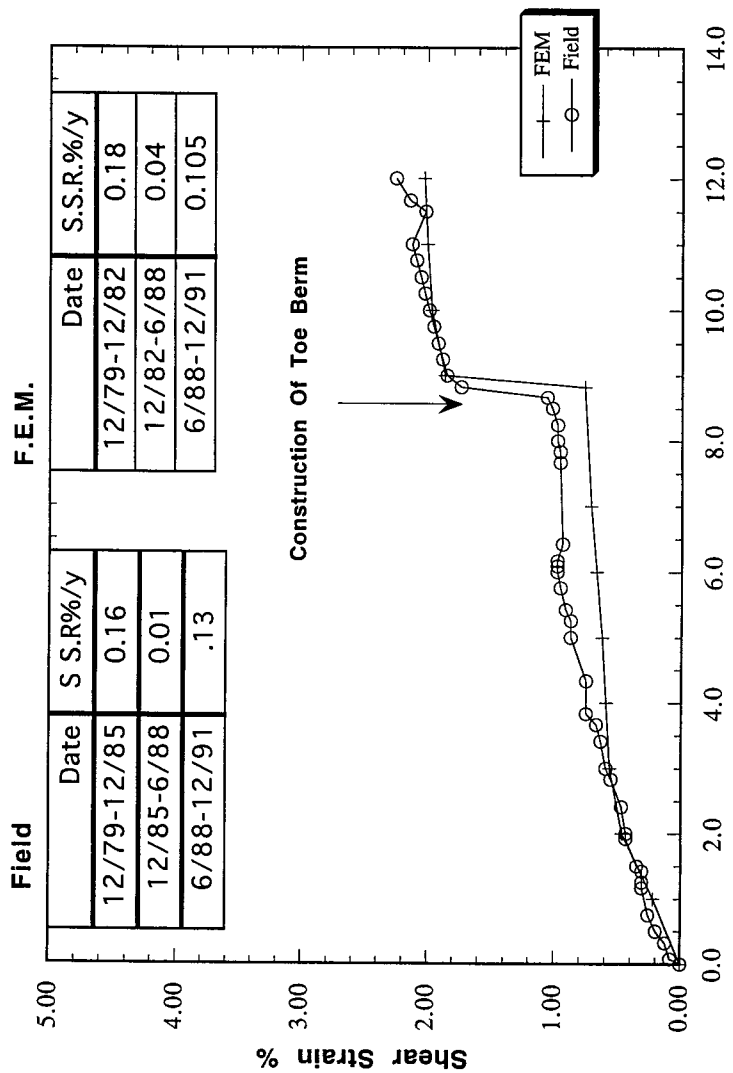

Figure (5.28) Shear Strain Vs. Time At Toe
(SI79-108,SI87-108A,Elev=235.87 m)

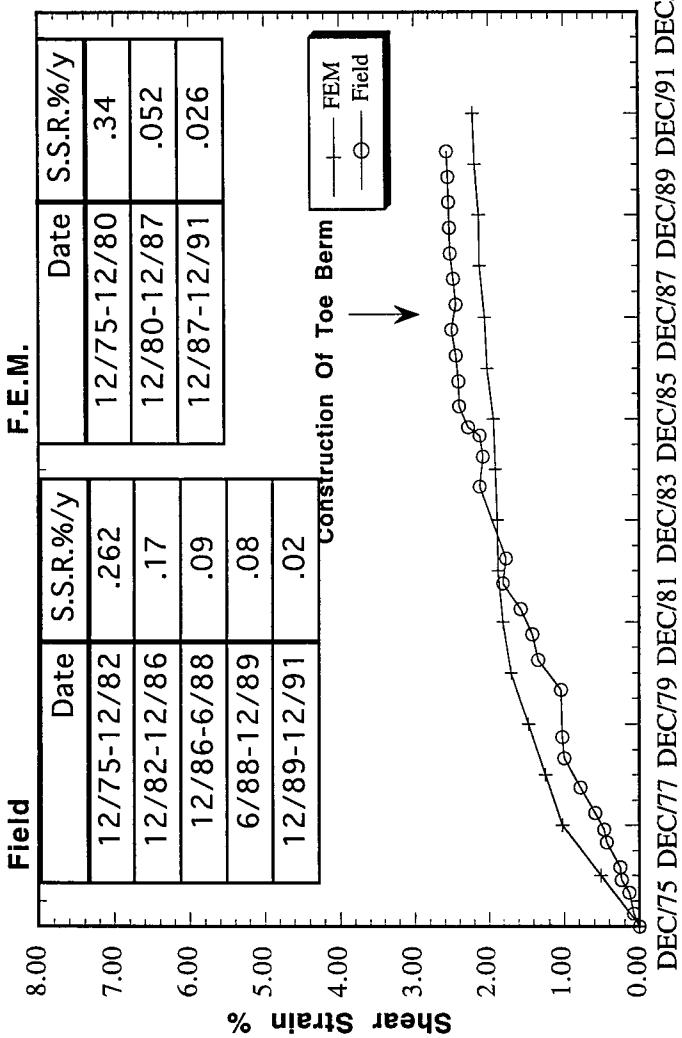

Figure (5.29) Shear Strain Vs. Time For Berm 251
(SI76-104,Elev. 234.93 m)

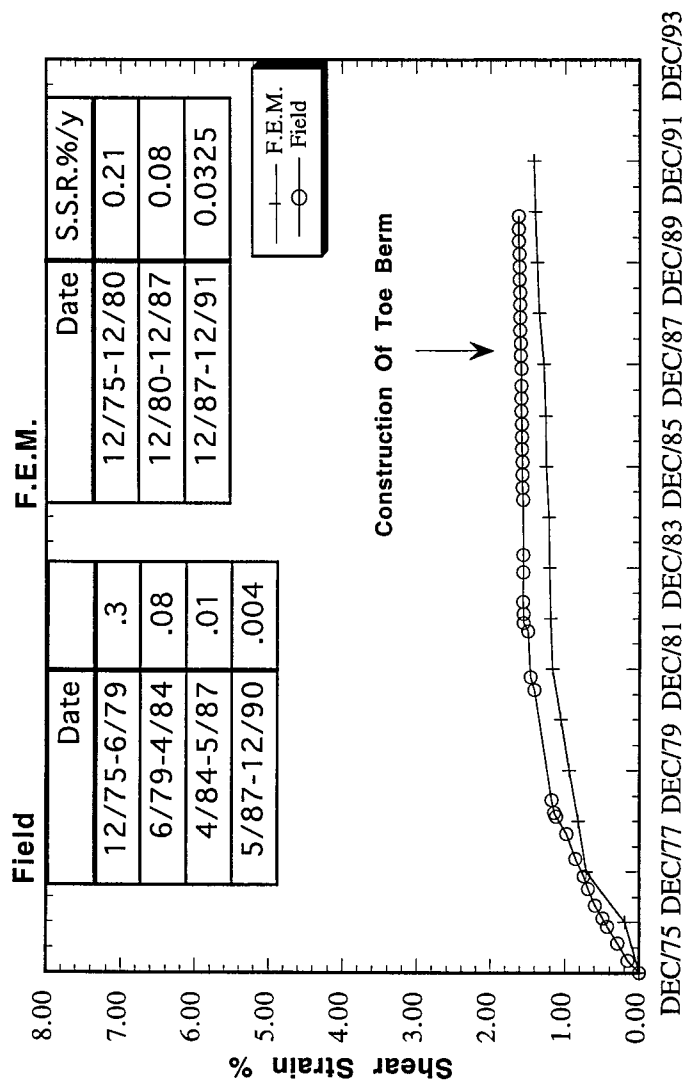

Figure (5.30) Shear Strain Vs. Time For Berm 277
(SI76-102,SI85-102A,Elev.=230.0 m)

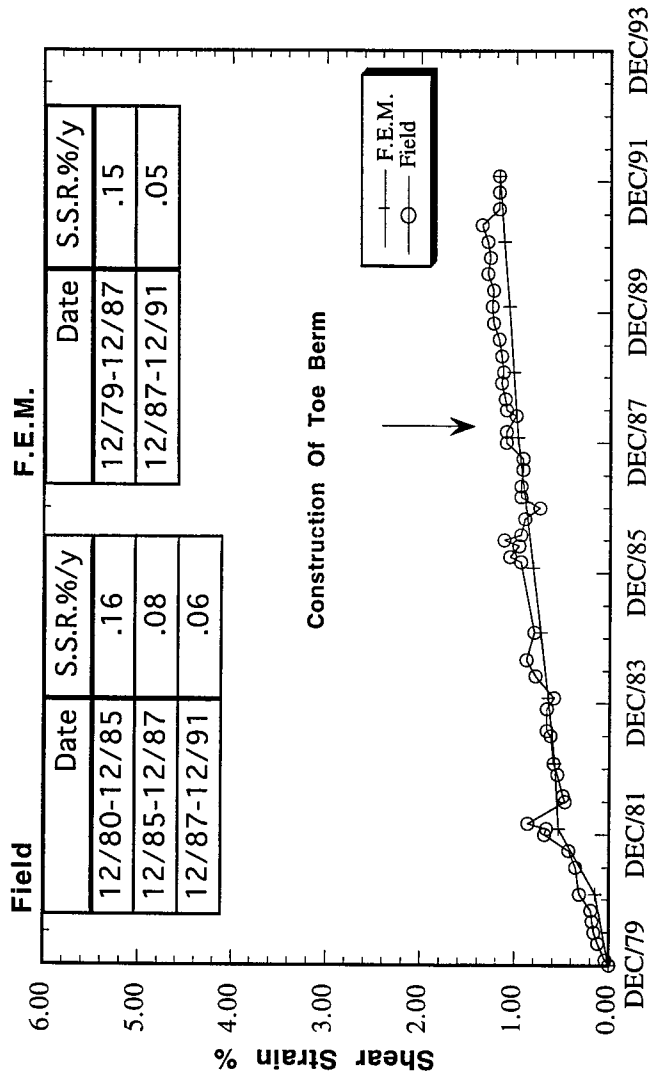

Figure (5.31) Shear Strain Vs. Time For Berm 291
(SI79-109,Elev.=235.7 m.)

References:

Akai, K., Adachi, T., and Ando, N. 1975. Existance of a unique stress-strain-time relation of clays. Soil and Foundation, **15** (1): 1-16.

Bishop,A.W. and Henkel,D.J. 1962. The measurements of soil properties in the triaxial test. Second edition, Arnold, London.

Borja,R.I., Hsieh,H.S., and Kavazanjian,E.,Jr. 1990. Double-yield-surface model. II:Implementation and verification. ASCE Journal of the Geotechnical Engineering Division, **116**(GT9): 1402-1421.

Chan,D.H. and Morgenstern,N.R. 1992. User Manual of program PISA. University of Alberta, Edmonton, Alberta.

Chen, W.K., Martschuk, J., and McRoberts, E.C. 1983. Performance of Tar Island Dyke. Proceeding of the 7th Panamerican Conference on Soil Mechanics and Foundation Engineering, Vancouver, Canada, June 1983. Vol. 2. pp. 553-566.

De Alencar, J.A. 1988. Deformation of dams on sheared foundations. Ph. D. thesis, University of Alberta, Edmonton, Alberta.

De Alencar, J.A., Chan, D.H. and Morgenstern, N.R. 1992. Incorporation of measured pore pressure in finite element analysis. Proceeding of 45th Canadian Geotechnical Conference, Toronto, Ontario, 26-28 October,1992. pp. 62-1 - 62-10.

Duncan, J.M. and Chang, C.Y. 1970. Non-linear analysis of stress and strains of soils. ASCE Journal of Soil Mechanics and Foundation Engineering, **96** (SM5): 1629-1653.

Kondner, R.L. 1963. Hyperbolic stress-strain response: Cohesive soils. ASCE Journal of Soil Mechanics and Foundation Engineering, **89** (SM1): 115-144.

Leroueil, S., Kabbaj, M., Tavenas, F., and Bouchard, R. 1985. Stress-strain-time behaviour rate relation for the compressibility of sensitive natural clays. Geotechnique, **35** : 537-552.

Mesri,G., Febres, C.E., Shield, D.R., and Castro, A. 1981. Shear stress-strain-time behaviour of clays.Geotechnique, **31**: 537-552.

Mittal, H.K., and Hardy, R.M. 1977. Geotechnical aspects of a Tar Island Dyke. ASCE Geotechnical Practice of Disposal of Solid Waste Materials. pp 327-347.

Morsy, M.M. 1994. Effective stress modeling of creep behaviour of clay. Ph.D. thesis, University of Alberta, Edmonton, Alberta, Canada.

Morsy, M.M., Chan, D.H., and Morgenstern, N.R. 1994. An effective stress model for creep of clay. Submitted to the Canadian Geotechnical Journal.

Murayama,S., and Shibata, T. 1961. Rheological properties of clays. Proceedings, 5th International Conference in Soil Mechanics and Foundation Engineering, Paris, France, July 17-22, 1961. Vol. 1 pp.269-273.

Tevenas, F., Leroueil, S., and Roy, M. 1978. Creep behaviour of an undisturbed lightly overconsolidated clay. Canadian Geotechnical Journal, **15**: 402-423.

Singh,A., and Mitchell,J.K. 1968.Generalized stress-strain-time function for soil. ASCE Journal of Soil Mechanics and Foundation Engineering, **94** (SM1): pp. 21-46.

Watts, B.D. 1980. Lateral creep deformation in the foundation of a high dam. M.Sc. thesis, University of Alberta, Edmonton, Alberta, Canada.

CHAPTER 6

CREEP EFFECTS BENEATH EMBANKMENT LOADING[1]

6.1 INTRODUCTION:

It has been recognized for decades that soft soils exhibit a property of continuing settlement under nominally constant effective stress (Buisman 1936). This phenomenon is commonly known as secondary consolidation and it is actually a special case of creep. Numerous studies have been conducted in the area of creep to provide a better understanding of the creep behaviour of soil and to determine the major factors affecting creep. In spite of this effort, creep generally remains a secondary issue in the long term design of geotechnical projects.

The problem of creep has often been treated as a theoretical exercise by formulating rheological models (Murayama and Shibata 1958; Schiffman 1959; Christensen and Wu 1964; and Abdel-Hady and Herrin 1969). Alternative studies have been undertaken in the laboratory by performing creep consolidation or triaxial tests and developing a phenomenological relationship that describes creep behaviour (Singh and Mitchell 1968). There are only a few cases where researchers have tried to study the problem of creep in the field. Wu et al. (1969) analyzed numerically the time-dependent ground movement of an excavation near Cleveland. The calculations were made assuming the creep behaviour of soil to be non-linear with time. They compared the measured movements with the calculated values and found a discrepancy between the measured and the calculated creep rate. It was concluded that this excavation was far from ideal as a case history to check creep predictions. In 1990, Borja et al. investigated the time-dependent deformation behaviour of the I-95 embankment near Boston. They showed, based on the comparison

---

[1] A version of this chapter has been submitted for publication to the Canadian Geotechnical Journal: Morsy, M.M., Morgenstern, N.R., Chan, D.H. 1994. Creep effects beneath embankment loading.

between the calculated and the measured settlements and lateral displacements, that creep was present and the results of the analysis underscored the creep importance on the deformation and pore pressure response of the I-95 embankment foundation. It appears from these two studies that investigations have been limited in comparing field measurements and calculated values without exploring the role of creep in the time-dependent behaviour of soil and the sensitivity of the creep behaviour with respect to the creep parameters used in the analysis. Notwithstanding many years of research, there is still considerable uncertainty regarding the role of creep in practice, beyond the simple one-dimensional application of the secondary consolidation theories.

To be of practical value research in the area of creep should provide the engineer with a simple creep model for the numerical analysis of the problems in the field. This model should be well understood in terms of its theoretical basis and the material parameters required to describe creep behaviour should be determinable from traditional laboratory tests.

As part of a research program on the time-dependent behaviour of soft clays under embankments, Morsy et al. (1994a) adopted an effective stress model to study the problem of creep in the field. The model employs the classical plasticity theory and the phenomenological creep rate relationships that are well established in geotechnical engineering. The material parameters required for the analysis are readily obtainable from traditional laboratory tests.

As the analysis is performed in terms of effective stresses, it is necessary to determine the pore pressures in the soil at each stage of the analysis. In order to avoid the complexity of accurate prediction of the pore pressures, an approach proposed by De Alencar et al. (1992) is used to prescribe the pore pressure in the analysis based on field measurements. In this approach the pore pressures are interpolated at each integration point in the finite element mesh based on field measurements at each stage of the analysis.

In order to test the capability of the model, Morsy et al. (1994b) incorporated the model into a finite element code PISA™, to analyze the time-dependent deformation of the clay foundation of Tar Island Dyke (TID), station 56+00, Alberta, Canada (see Figure(1)). This case history represents a unique opportunity to study numerically the influence of creep on the time-dependent behaviour of soft clay in terms of effective stresses. The satisfactory agreement between the calculated and the measured vertical and horizontal

displacements and shear strains validates the capability of the model in simulating complex boundary conditions in a practical geotechnical problem. The case history also emphasizes the need to include creep effects to account for all the observed deformations.

The main objective of this paper is to highlight the effect of creep on the time-dependent stress-strain behaviour of the dyke. In Morsy et al. (1994b), a time-dependent analysis of TID was performed based on the average value of the model parameters, which were obtained from laboratory tests. In this paper a sensitivity analysis is carried out to investigate the effect of the creep parameters on the calculated time-dependent deformation. The purpose of this sensitivity analysis is to provide a better understanding of the role of these creep parameters in the numerical modelling of creep in soft clay.

To emphasize the importance of the inclusion of the creep effects in the analysis, a time-independent effective stress analysis of TID (excluding the creep effect) was also performed. The calculated shear strains in the time-dependent and independent cases and the field measurements are plotted with time to show the importance of including the creep effect in the analysis and how excluding this effect could lead to underestimating the calculated time-dependent shear strain.

Based on the results of the two analyses, a comparison between the stress states in the dyke foundation in the two cases is presented to illustrate the effect of creep on the stress state in the soil. The comparison illustrates the effect of stress relaxation in the field. The results presented here show the value of the consideration of creep in the design of such long term projects where the soil is subjected to externally sustained load for a long period of time. They also add more information to our limited experience in dealing with the phenomena of creep in the field.

6.2 TAR ISLAND DYKE (TID):

Tar Island Dyke is located on the west bank of the Athabasca river near Fort McMurray, Alberta. The purpose of the dyke is to retain the tailings produced by Suncor. The dyke consists of a compacted downstream zone constructed from hydraulic fill and an uncompacted upstream zone which retains the pond as shown in Figure (1). The TID rests on a soft clay layer underlain by a sand and gravel layer which rests over a limestone bedrock.

By the end of 1980, the dyke reached a height of 87 m. During 1984, the dyke crest was raised to a height of 92 m which led to the shearing of inclinometer S81-101C (berm 303 m ; these are access roads at different elevations) near the contact of the foundation clay and the underlying sand and gravel. In 1988, a remedial measures program was completed and the main construction activities involved the construction of a toe berm (see Figure (6.1)), excavation of the dyke crest, and the relocation of the dyke crest inside the pond to reduce the shear strain rate in the foundation and improve the stability of the dyke. Addiltional details have been presented in Morsy et al. (1994b).

6.3 SENSITIVITY ANALYSIS OF CREEP PARAMETERS:

In the proposed time-dependent effective stress model (Hsieh et al. 1990; and Morsy et al. 1994a), the creep component of the time-dependent strain tensor is represented by six input parameters. In this model the creep strain tensor is divided into distinct but interdependent volumetric and deviatoric components. The volumetric creep component is mainly controlled by the secondary compression coefficient C_α (Taylor (1948)). The secondary compression equation takes the form:

$$\dot{\varepsilon}_v = \frac{C_\alpha}{(1+e)t_v}, \qquad [6.1]$$

where $\dot{\varepsilon}_v$ is the volumetric creep strain rate; C_α is the secondary compression coefficient; e is the current void ratio; and t_v is the volumetric age relative to an initial reference time $(t_v)_i$.

The deviatoric creep component is mainly controlled by the Singh-Mitchell creep parameters A, $\overline{\alpha}$, and m (Singh and Mitchell (1968)). The Singh- Mitchell creep equation takes the form, respectively:

$$\dot{\varepsilon}_a = A\exp(\overline{\alpha}\overline{D})\left(\frac{(t_d)_i}{t_d}\right)^m, \qquad [6.2]$$

where $\dot{\varepsilon}_a$ is the axial strain rate in a triaxial creep test; $(t_d)_i$ is an initial reference time after loading at which creep is assumed to commence; t_d is the deviatoric age relative to $(t_d)_i$; A, $\overline{\alpha}$ and m are the Singh-Mitchell equation material parameters and $\overline{D}$ is the deviatoric stress level. Table (6.1) shows the mean value of the creep parameters of the clay layer which were used in the analysis of TID (Morsy et al. 1994b).

Since there is little experience in transforming these parameters into field behaviour a sensitivity analysis was carried out to provide a better understanding of the influence of these creep parameters on the time-dependent shear strain and shear strain rate in the dyke foundation. In Morsy et al. (1994b), it is concluded that the observed time-dependent deformation in the dyke foundation resulted mainly from the induced shear stresses in the foundation due to the sustained dyke load. Based on this conclusion, the sensitivity investigation is limited to the deviatoric Singh-Mitchell creep parameters A and $\overline{\alpha}$ and ignored the volumetric creep parameter C_α.

6.3.1 Singh-Mitchell creep parameter A:

The influence of the Singh-Mitchell creep parameter A on the shear strain and the shear strain rate were investigated. The parameter A represents the value of shear strain rate at unit time (reference time) and zero deviator stress level as shown in Figure(6.2). It is meaningful, however, in a sense that it reflects the soils composition, structure, and stress history. Two analyses were carried using two values for A, 0.0257 (mean value) and 0.028%/year. The results of the analyses are summarized in Figures (6.3) and (6.4) at two locations, the toe and berm 291 m.

Beneath the toe, see Figure(6.3), the increase of the A value results in an increase in the shear strains by an average of 15% before the construction of the toe berm. While after the construction of the toe berm the increase in shear strain is 5% on average. The increase of the A value also results in an increase in the shear strain rate from 0.18%/year to 0.22%/year over the time period from December 1979 to December 1982. From December 1982 to June 1988 the rate raises from 0.04%/year to 0.05%/year. After construction of the toe berm, the shear strain rate increases from 0.105%/year to 0.13%/year.

Beneath berm 291 m, see Figure(6.4), due to the increase of the A value the shear strain values increase by 5% on average before December 1981. While after December 1981, the increase in shear strain is 15% on average. In terms of shear strain rate, before the construction of the toe berm, the rate raises from 0.15%/year to 0.17%/year. After the construction of the toe berm, the shear strain rate is the same in the two cases equal to 0.05%/year.

The results of this sensitivity analysis shows that a value of A equal to 0.028%/year provides a better prediction of the shear strain and shear strain rate in comparison with the measured values. The increase of the A value by 10% results in a noticeable increase in the predicted shear strain values but it has only a small effect on the shear strain rate.

6.3.2 Singh-Mitchell creep parameter $\overline{\alpha}$:

The effect of the Singh-Mitchell creep parameter $\overline{\alpha}$ on the shear strain and the shear strain rate was investigated at two different locations, the toe and berm 291 m. Three values of $\overline{\alpha}$ were used in the analysis, 2.0,2.47 (mean value), and 3.0. The parameter $\overline{\alpha}$ (see Figure (6.2)) controls the effect of stress intensity value on the creep rate. The results of the analysis are plotted in Figures (6.5) and (6.6). The values calculated based on $\overline{\alpha}$ = 2.47 are used as reference in the discussion below.

Beneath the toe, see Figure(6.5), in the case of $\overline{\alpha}$ = 2.0 the shear strains were reduced by an average of 30% in comparison with an $\overline{\alpha}$ value of 2.47. While in the case of $\overline{\alpha}$ = 3.0 the shear strain values increase by 15% on average. Table (6.2) summarizes the effect of $\overline{\alpha}$ on the shear strain rate in the toe region. From the table, it is seen that the reduction of $\overline{\alpha}$ to 2.0 has a greater influence on the shear strain rate than in the case of $\overline{\alpha}$ equal to 3.0.

Beneath berm 291 m, see Figure (6.6), both the reduction and the increase of $\overline{\alpha}$ causes a change of 15% on average in the shear strains. Table (6.3) summarizes the effect of the $\overline{\alpha}$ value on the shear strain rate. From the table , the change of the $\overline{\alpha}$ value has a slight effect on the shear strain rate.

The result of the sensitivity analysis of $\overline{\alpha}$ shows that the influence of changing the creep parameter $\overline{\alpha}$ on the shear strain and the shear strain rate is affected by the location with respect to the dyke center. This effect is higher at the toe and diminishes as one moves toward the dyke center.

6.4 CREEP EFFECT ON THE TIME-DEPENDENT SHEAR STRAIN:

Morsy et al. (1994b) summarized the construction of the 92 m Tar Island dyke which has taken place over twenty five years. The dyke was constructed over a fourteen meter thick clay layer (see Figure (6.1)). The loading of the dyke and the variation of the pond

level with time induced high excess pore pressures in the clay foundation. This excess pore pressure dissipated with time contributing to time-dependent deformations.

Piezometer measurements downstream of the 291 m berm (after 1978) showed that pore pressure dissipation was completed by 1978 where there was no more excess pore pressure. This indicates that the time-dependent deformation in the clay foundation is mainly due to creep after 1978.

Nevertheless it is of value to address the question of whether the dissipation of the pore pressure upstream of berm 291 m contribute to the time-dependent deformation taking place downstream of berm 291 m.

To address this question, a time-dependent analysis excluding the creep effect was carried out for the TID. The results are compared to the time-dependent analysis including the creep effect disscussed previously.

Over the time period between 1979 and 1993 the only construction activity was the raising of the dyke crest from elevation 325 m to 330 m, which would not create additional excess pore pressure over the entire domain of the clay foundation. In 1987, a toe berm (see Figure (6.1)) was constructed to reduce the shear strain rate in the clay foundation and to improve the dyke stability. The construction of the toe berm created local excess pore pressures in the area beneath the old toe.

Figure (6.7) compares the variation of the shear strain with time according to the creep dependent and creep independent analyses for the clay layer beneath the toe. The plot shows that before the construction of the remedial measures, the time-dependent shear strain in the clay layer is mainly due to the creep mechanism. In 1987, the construction of the toe berm created excess pore pressure in the old toe area. The dissipation of the excess pore pressure results in time-dependent deformation which accounts for thirty percent of the total time-dependent shear strain resulted from both the dissipation of excess pore pressure and creep.

Figure (6.8) shows the variation of the shear strain with time in the clay layer beneath berm 291 m. The comparison between the two cases shows that the dissipation of the excess pore pressure upstream berm of 291 m accounts for sixty percent of the total time-

time-dependent shear strain while the remaining forty percent results from the creep process due to the external sustained load.

6.5 CREEP EFFECT ON THE STRESS STATE IN THE CLAY LAYER:

Creep and stress relaxation are two processes often treated as two separate phenomena in which either the applied load or the state of deformation is held fixed, and the time variation of the other quantities are measured. Given the existence of a unique stress-strain-time relation for cohesive soil [e.g. Murayama and Shibata (1961); Akai et al. (1975); and Mitchell (1993)], it may be shown that creep and stress relaxation can be unified as one process.

In this section, the influence of the creep on the stress state in the foundation clay of the TID is investigated. For this purpose, a creep independent analysis was carried out to determine the stress state in the clay foundation as a result of the construction of the Dyke in the absence of creep.

Maximum shear stress contours, before the construction of the toe berm (1987), are plotted in Figures (6.9) and (6.10) for the creep independent and dependent analysis of the TID. Comparing the two plots, it is evident that the inclusion of creep in the numerical model not only results in time-dependent deformation in the clay but also results in a different stress state in the clay compared to the creep independent case. Figure(6.10) shows that the creep deformation in the clay layer causes simultaneously a relaxation and migration of the maximum shear stress within the clay layer. The relaxation process takes place in the central region of the clay layer resulting in a reduction in the maximum shear stresses. The migration process causes a redistribution and concentration of the shear stresses at the interfaces between the clay layer and the dyke and the lower sand and gravel layer. The final result of this process is a more isotropic stress state in the middle region of the clay layer.

To illustrate the results more clearly, two nodal points were chosen in the middle region of the clay layer at the toe and berm 291 m. The stress state at the two locations are plotted in figures (6.11) to (6.12) for the creep and the no-creep case. Based on the plots, it is obvious that the creep deformation in the clay layer causes a relaxation in the shear stresses as well as a rotation of the principal stresses.

The creep effect on stress state in the dyke foundation is also illustrated in terms of the mean and deviator stresses paths at three locations, the toe, berm 251 m, and berm 303 m. From Figures (6.13) to (6.15), it is evident that the creeping of the clay layer beneath the dyke has shifted the stress state in the clay layer away from the critical state line. This creates additional reserve resistance within the clay layer but reduces the reserve resistance at the interface with the stronger materials.

6.6 SUMMARY AND CONCLUSIONS:

In this paper the factors affecting the creep behaviour in the field have been studied based on the analysis of a case history of the Tar Island Dyke. First, a sensitivity analysis has been undertaken for the creep parameters of the model, which shows the following: a) the effect of changing the deviatoric Singh-Mitchell creep parameters A and $\overline{\alpha}$ on the shear strain and shear strain rate is higher at the toe of the dyke and the effect diminishes as one moves toward the center of the dyke; and b) the creep process is not controlled by one specific parameter but it is a combination of all the creep parameters in the model .

A comparison between the creep independent and creep dependent analyses shows clearly that the time-dependent deformation in the foundation of the dyke is due to both excess pore pressure dissipation and the creep response associated with the sustained dyke load. The contribution of each process varies depending on the location with respect to the center of the dyke. From the case history, it appears that the creep mechanism controlled the time-dependent deformation in the toe area. This domination is shifted to pore pressure dissipation effects as one moves toward the center of the dyke. Stress relaxation phenomena with associated stress redistribution have also been revealed in the dyke foundation.

Table (6.1) Creep parameters of the clay layer

Parameter	Symbol	Value
Secondary compression coefficient	C_α	0.032
Singh-Mitchell creep parameter	A	0.0257%/year
Singh-Mitchell creep parameter	$\overline{\alpha}$	2.47
Singh-Mitchell creep parameter	m	1.12

Table (6.2) Shear strain rate for different values of $\bar{\alpha}$ beneath the toe.

Time Period	$\bar{\alpha}$ = 2.0	$\bar{\alpha}$ = 2.47	$\bar{\alpha}$ = 3.0
Dec/79 to Dec/82	0.04 %/year	0.18%/year	0.22%/year
Dec/82 to June/88	0.04%/year	0.04%/year	0.096%/year
June/88 to Dec/91	0.025%/year	0.105%/year	0.118%/year

Table (6.3) Shear strain rate for different values of $\bar{\alpha}$ beneath berm 291.

Time Period	$\bar{\alpha}$ = 2.0	$\bar{\alpha}$ = 2.47	$\bar{\alpha}$ = 3.0
Dec/79 to Dec/87	0.13%/year	0.15%/year	0.17%/year
Dec/87 to Dec/91	0.04%/year	0.05%/year	0.058%/year

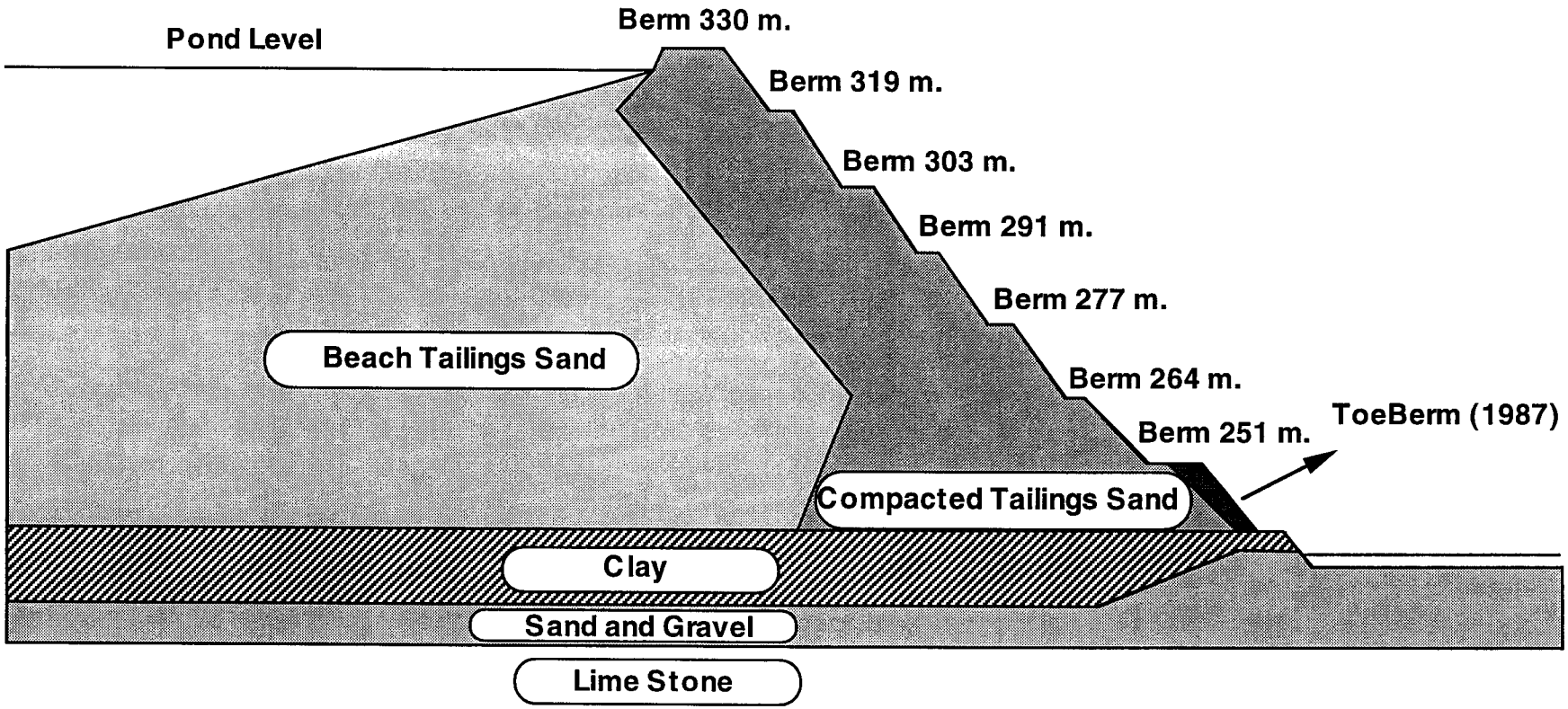

Figure (6.1) Typical section through Tar island dyke, station 56+00.

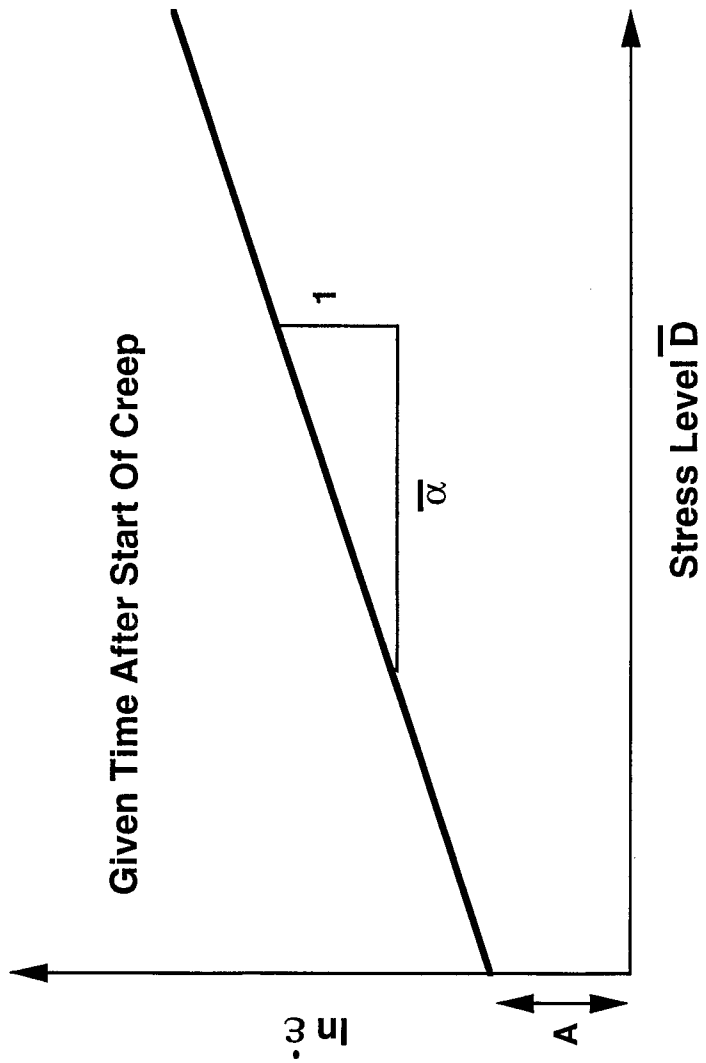

Figure (6.2) Singh Mitchel creep parameters A and $\bar{\alpha}$

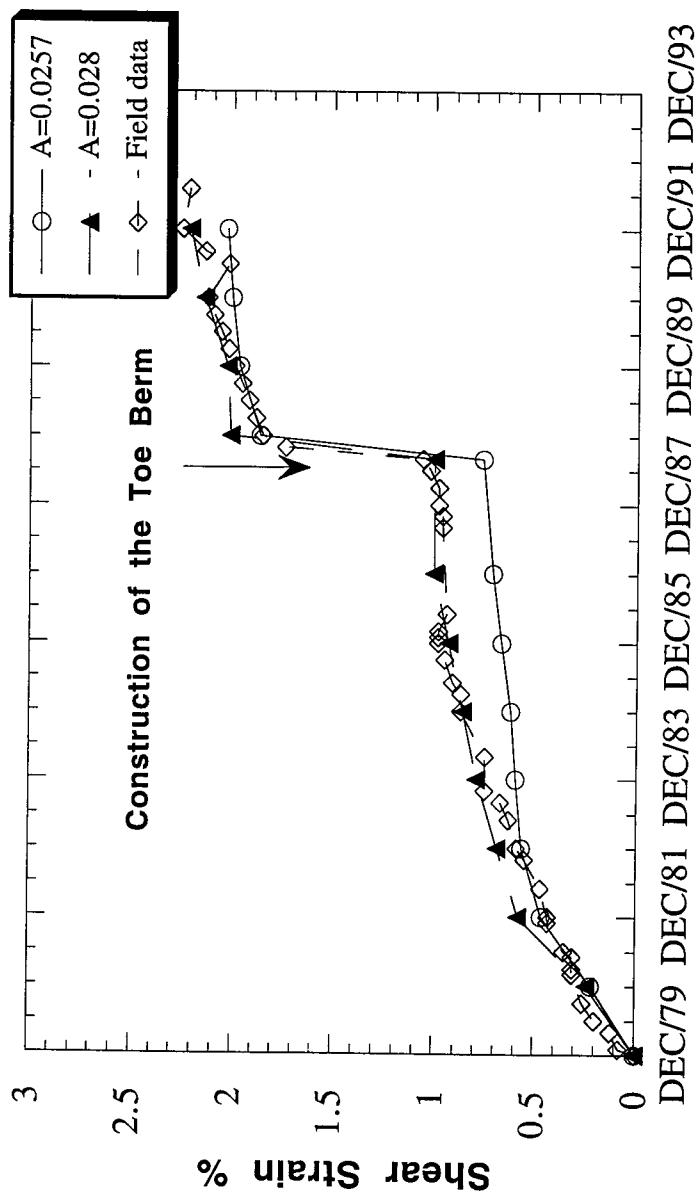

Figure (6.3) Shear strain vs. time at toe
for different values of Singh-Mitchell parameter A
(SI79-108,SI87-108A,Elevation 235.87)

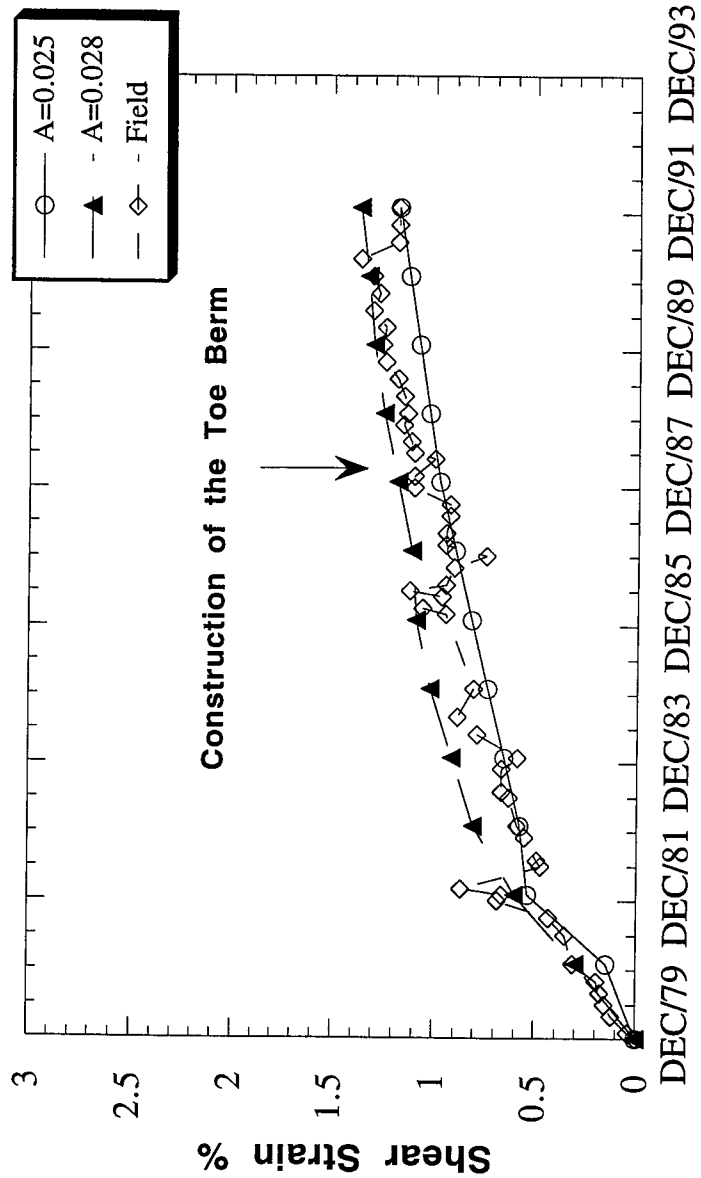

Figure (6.4) Shear strain vs. time at berm 291
for different values of Singh-Mitchell parameter A
(SI79-109,Elevation 235.7)

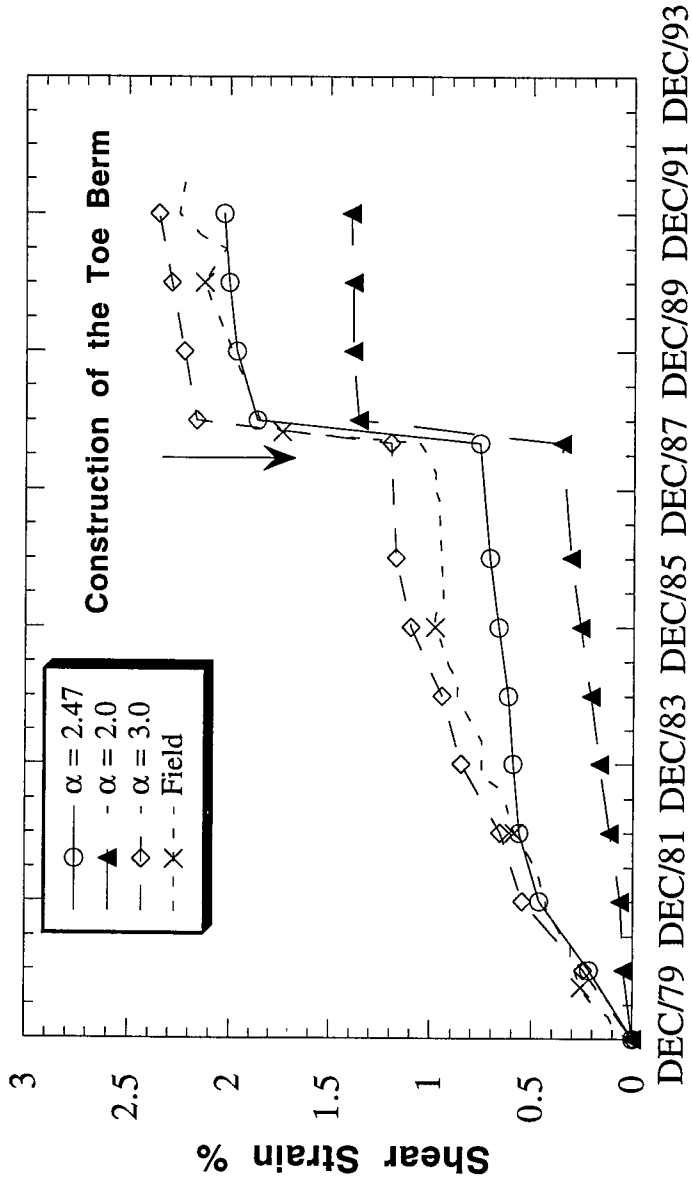

Figure (6.5) Shear strain vs. time at toe
for different values of Singh-Mitchell parameter α
(SI79-108,SI87-108A,Elevation 235.87)

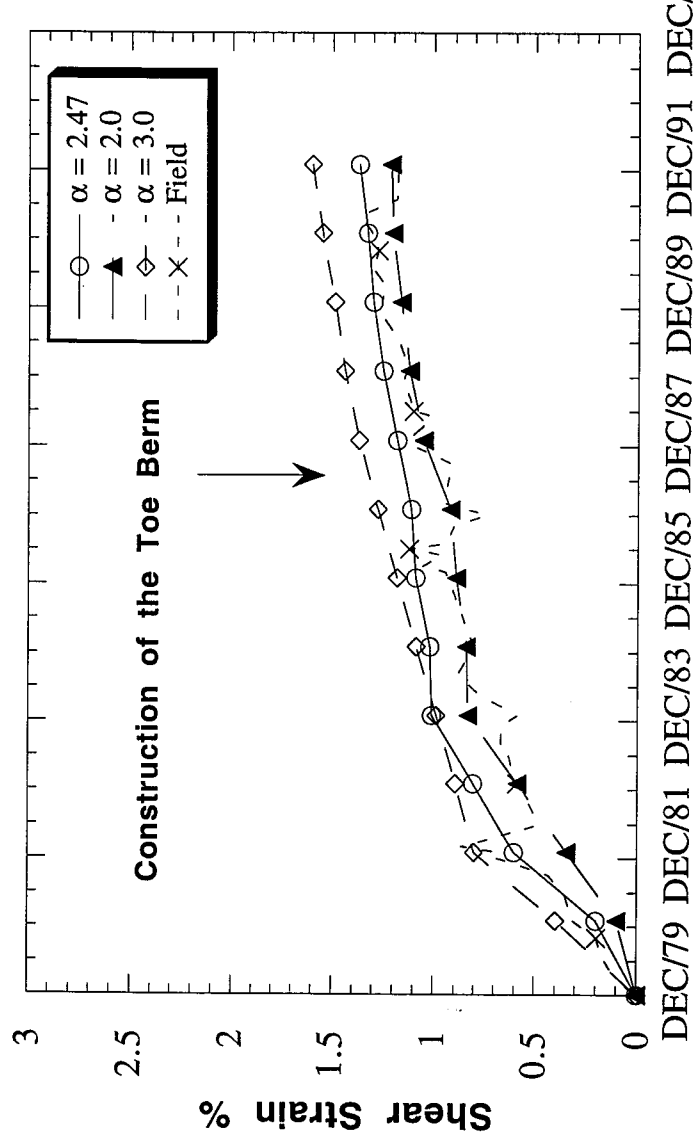

Figure (6.6) Shear strain vs. time at berm 291
for different values of Singh-Mitchell parameter α
(SI79-109,Elevation 235.7)

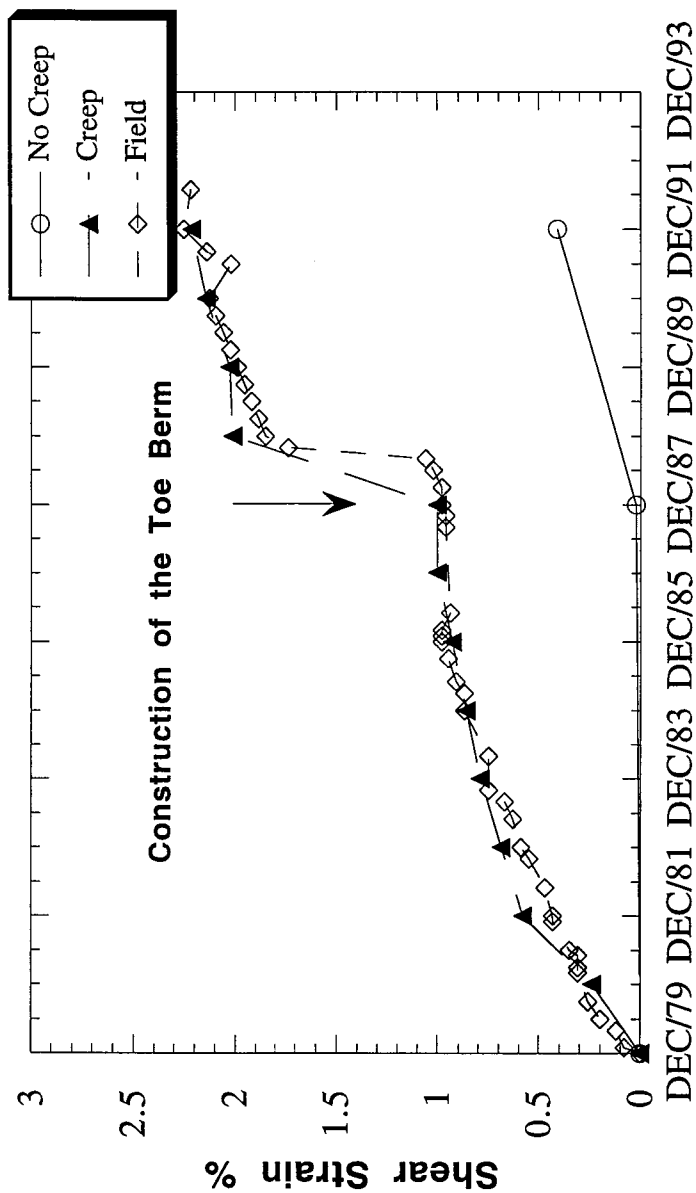

Figure (6.7) The effect of creep on the shear strain vs. time at toe (SI79-108,SI87-108A,Elevation 235.87)

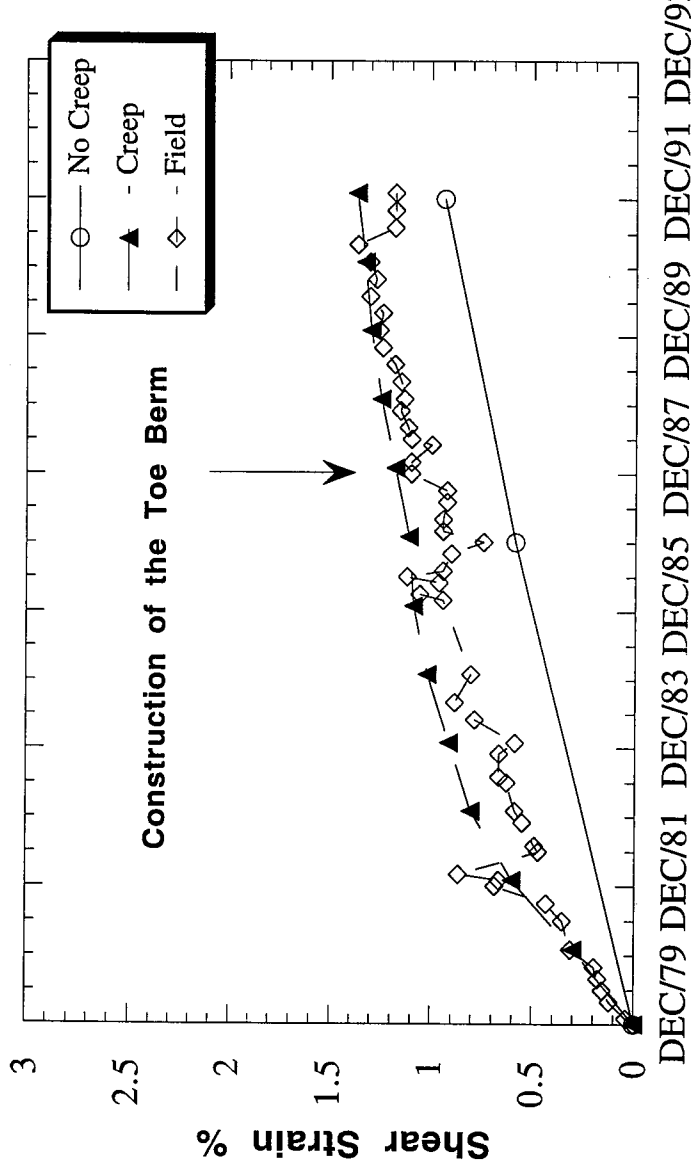

Figure (6.8) The effect of creep on the shear strain vs. time at berm 291 (SI79-109,Elevation 235.7)

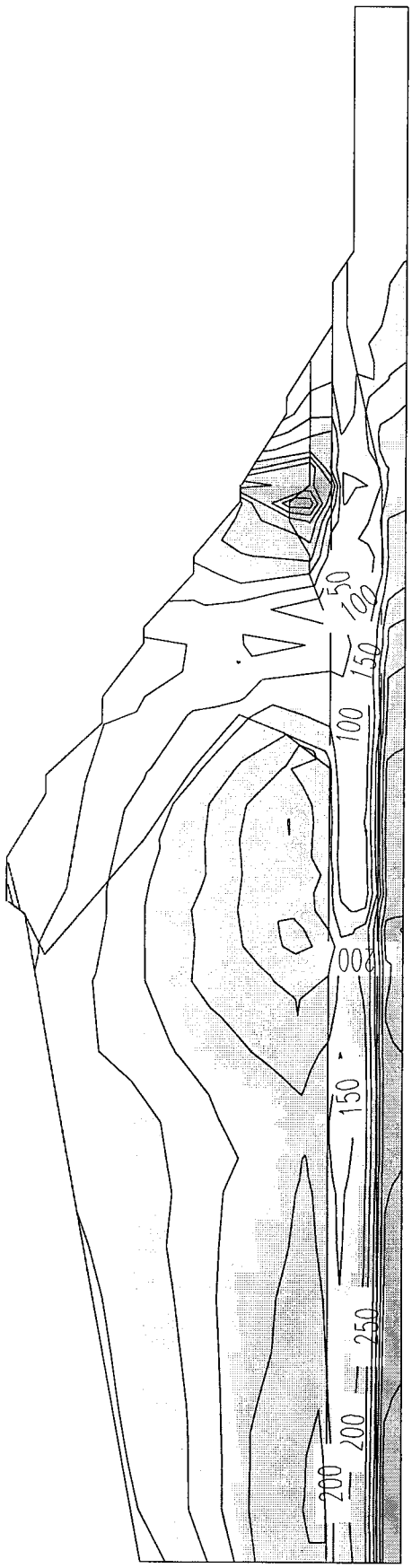

Figure (6.9) Maximum shear stress contours (Creep independent analysis) .

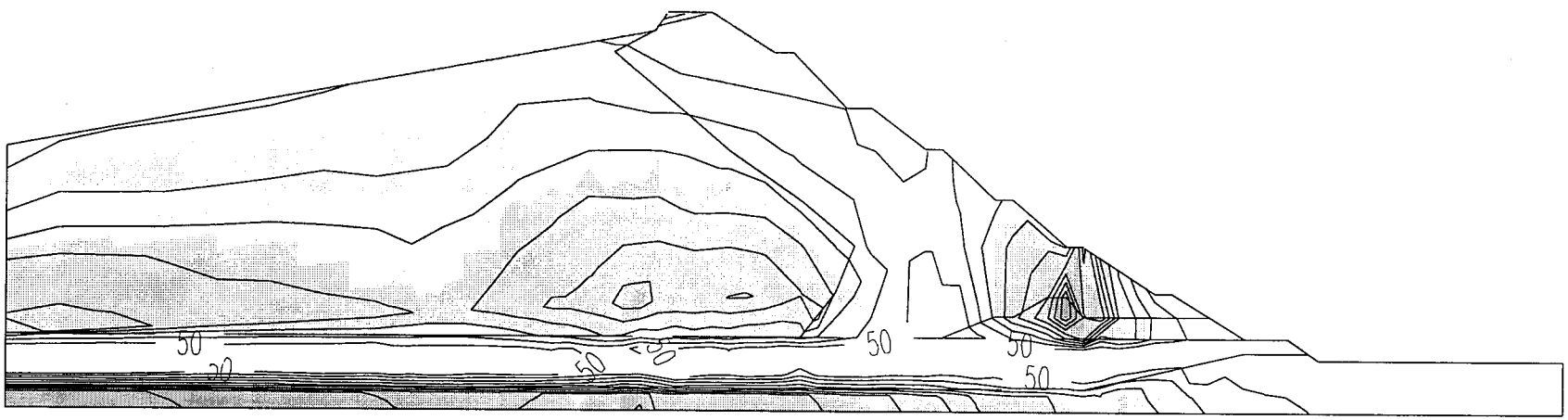

Figure (6.10) Maximum shear stress contours (Creep dependent analysis) .

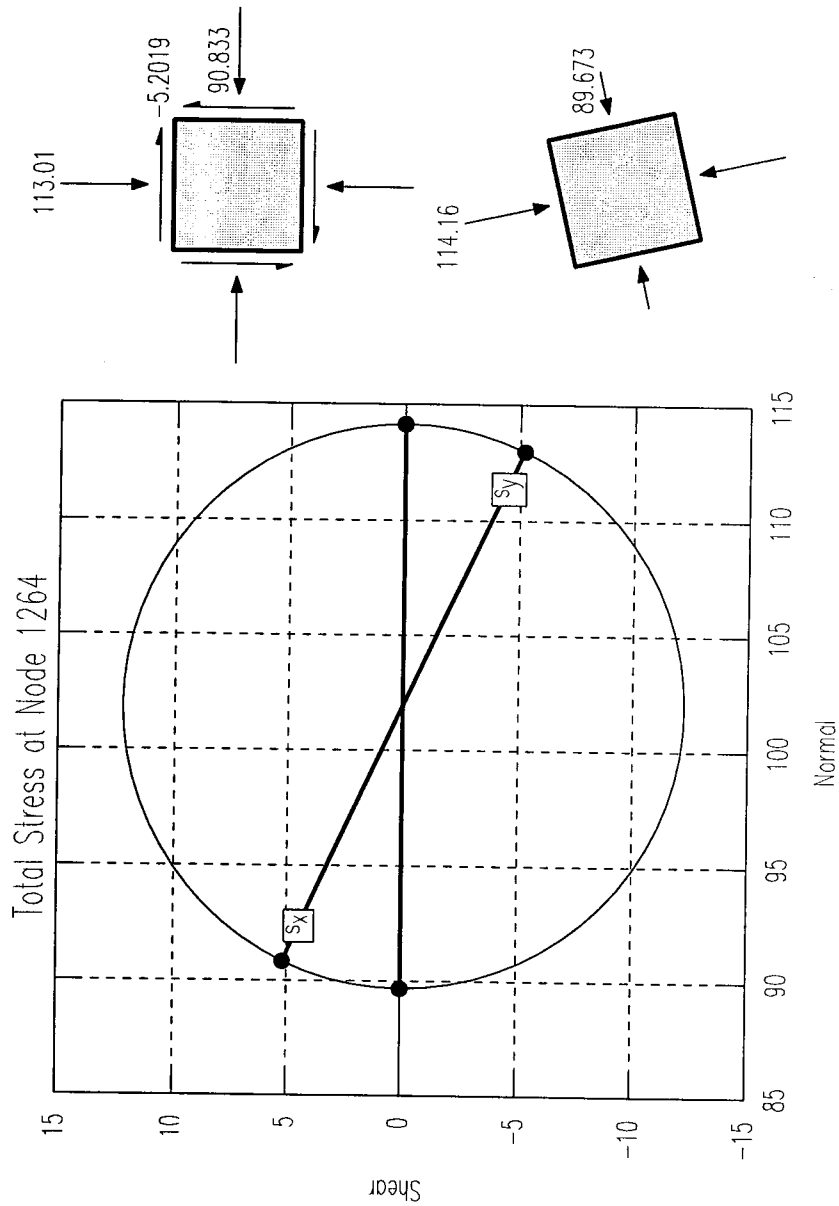

Figure (6.11a) Mohr circle and principal stresses direction for node 1264, toe (Creep independent analysis) .

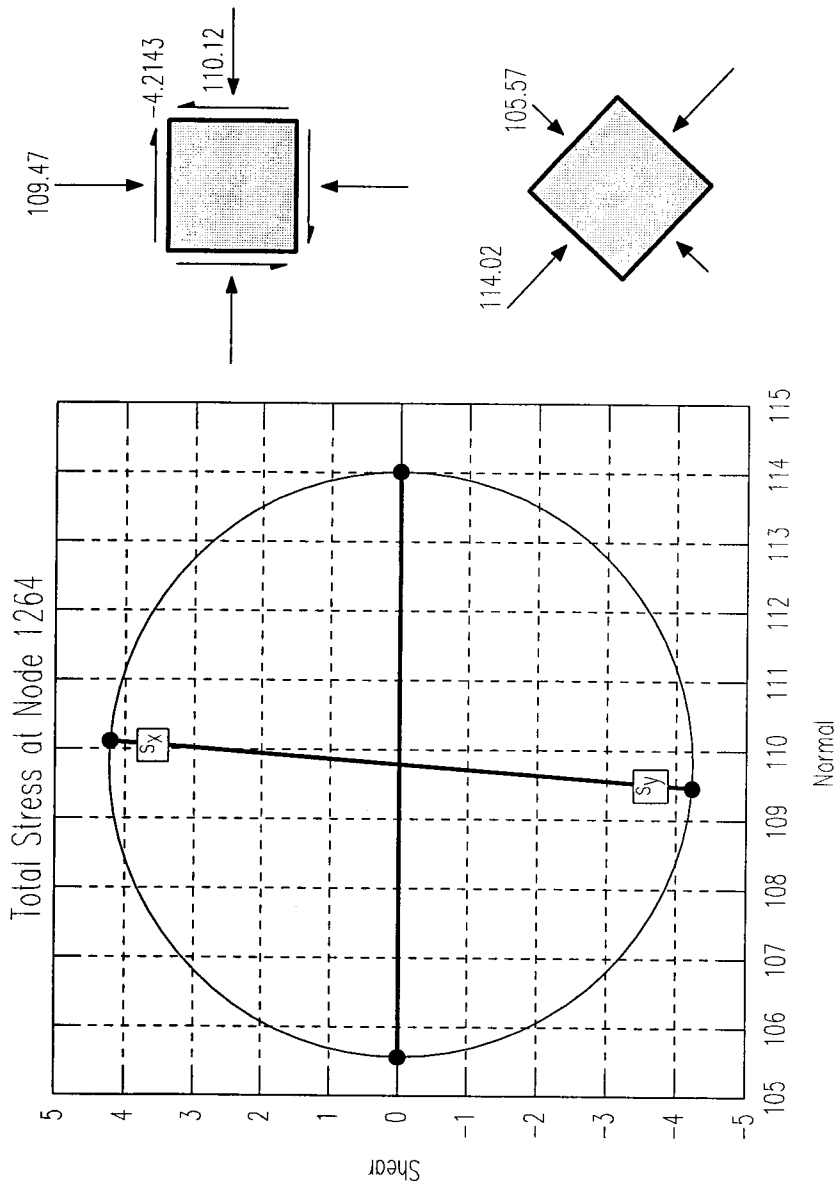

Figure (6.11b) Mohr circle and principal stresses direction for node 1264, toe (Creep dependent analysis) .

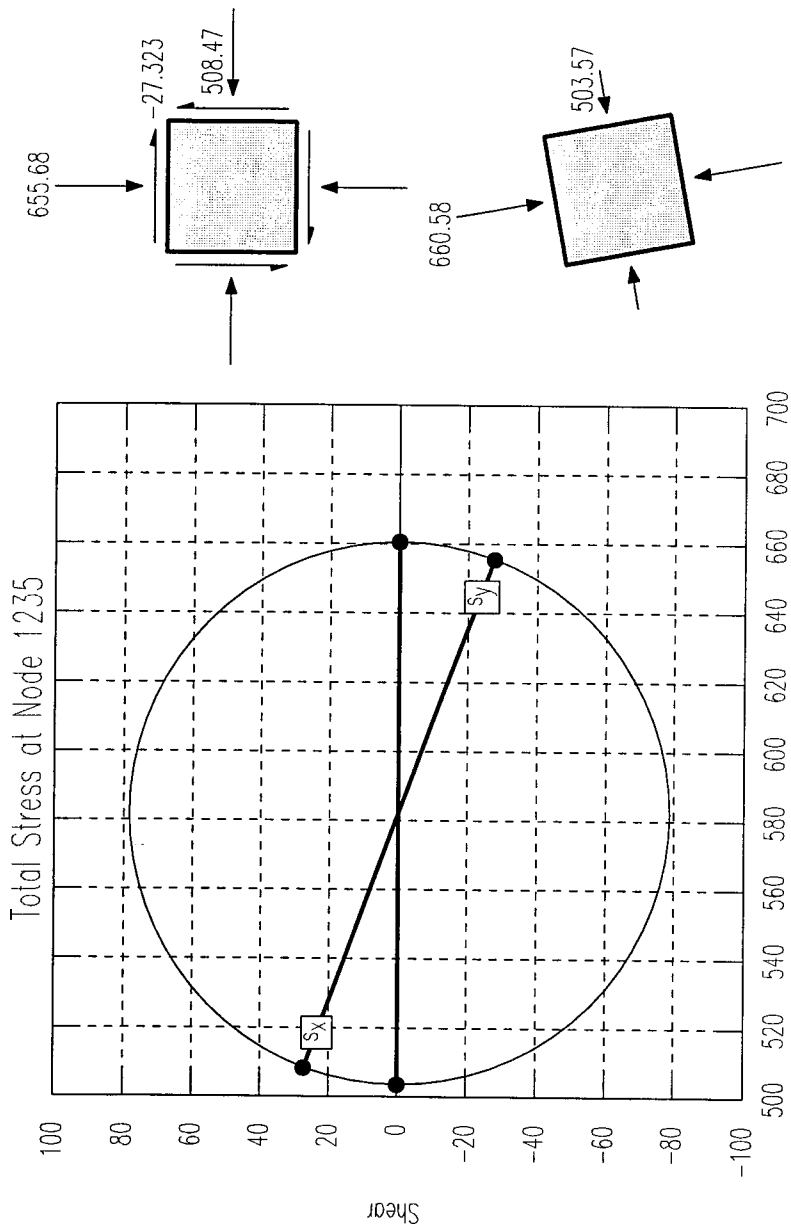

Figure (6.12a) Mohr circle and principal stresses direction for Node 1235, berm 291 m. (Creep independent analysis) .

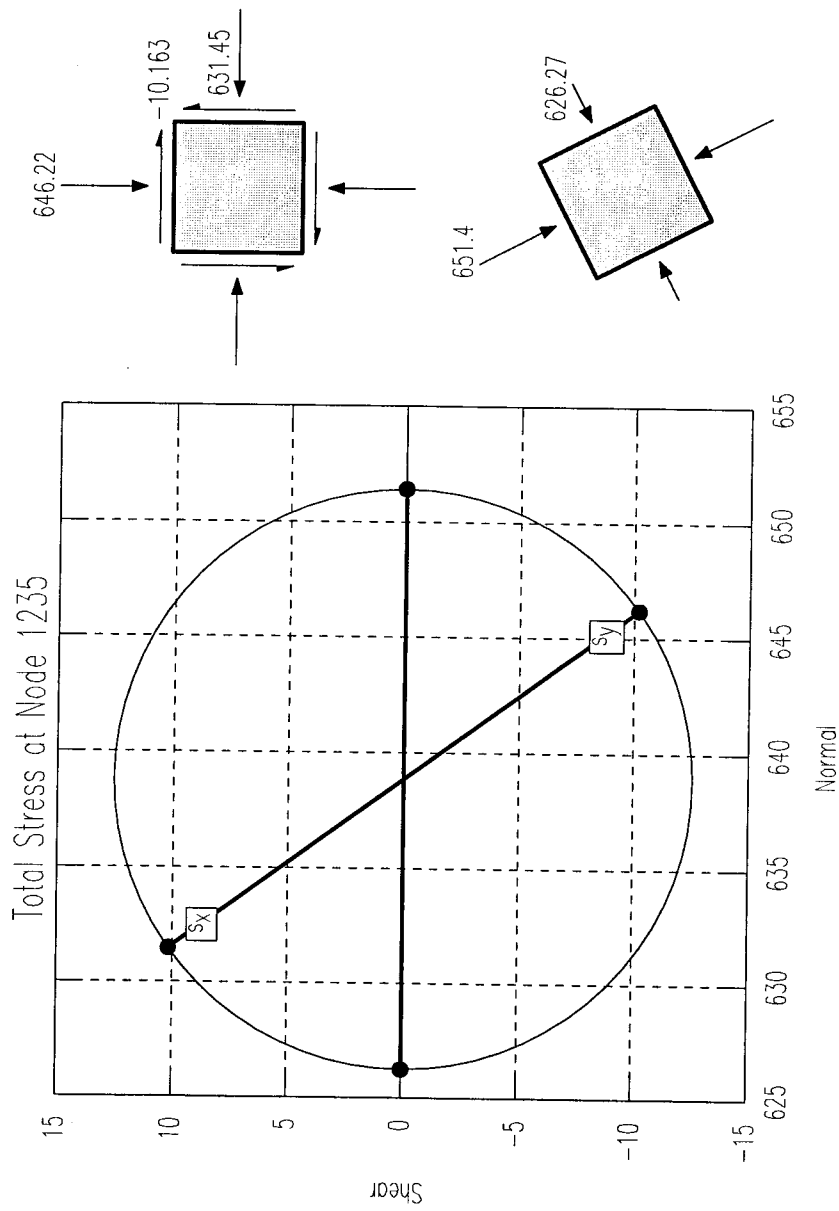

Figure (6.12b) Mohr circle and principal stresses direction for node 1235, berm 291 m (Creep dependent analysis) .

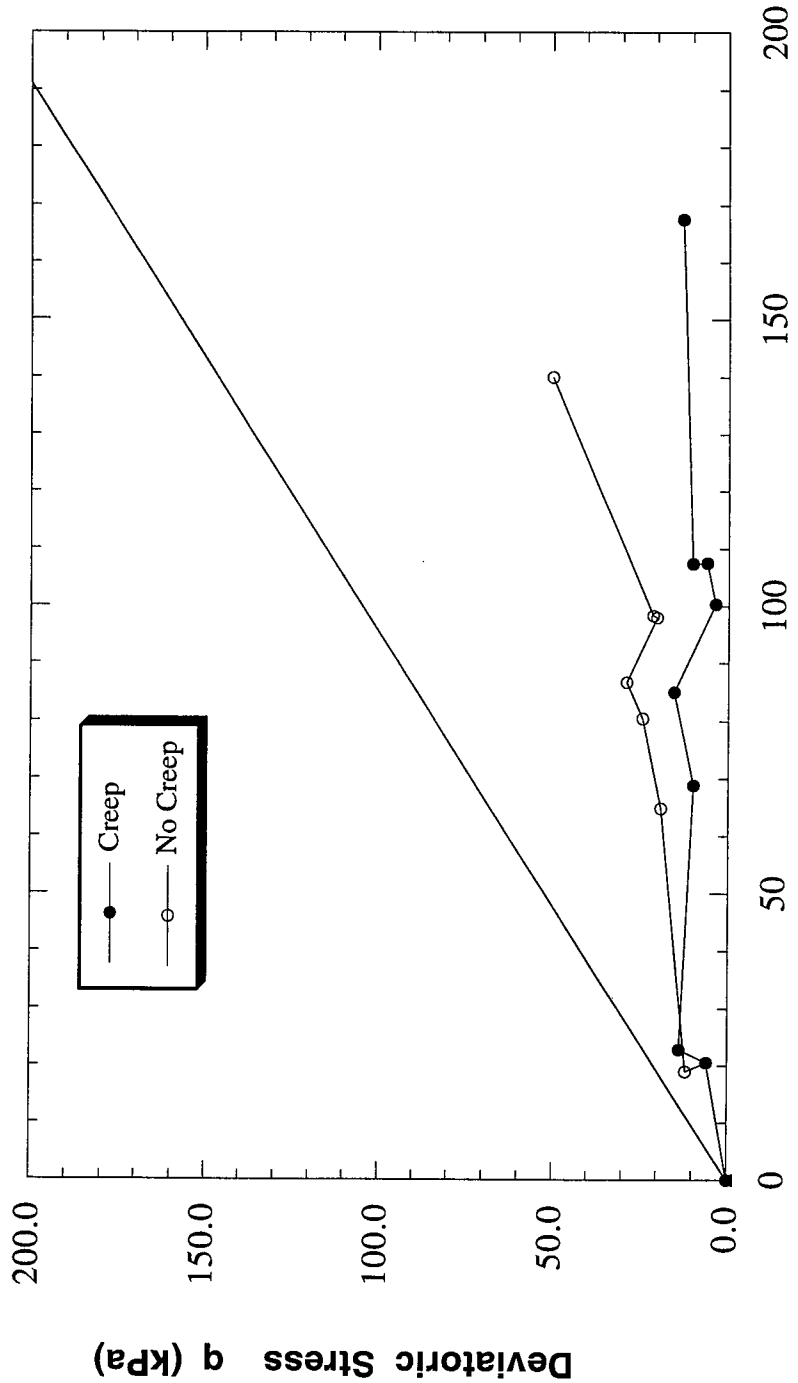

Figure (6.13) The P-q stress path at the toe region.

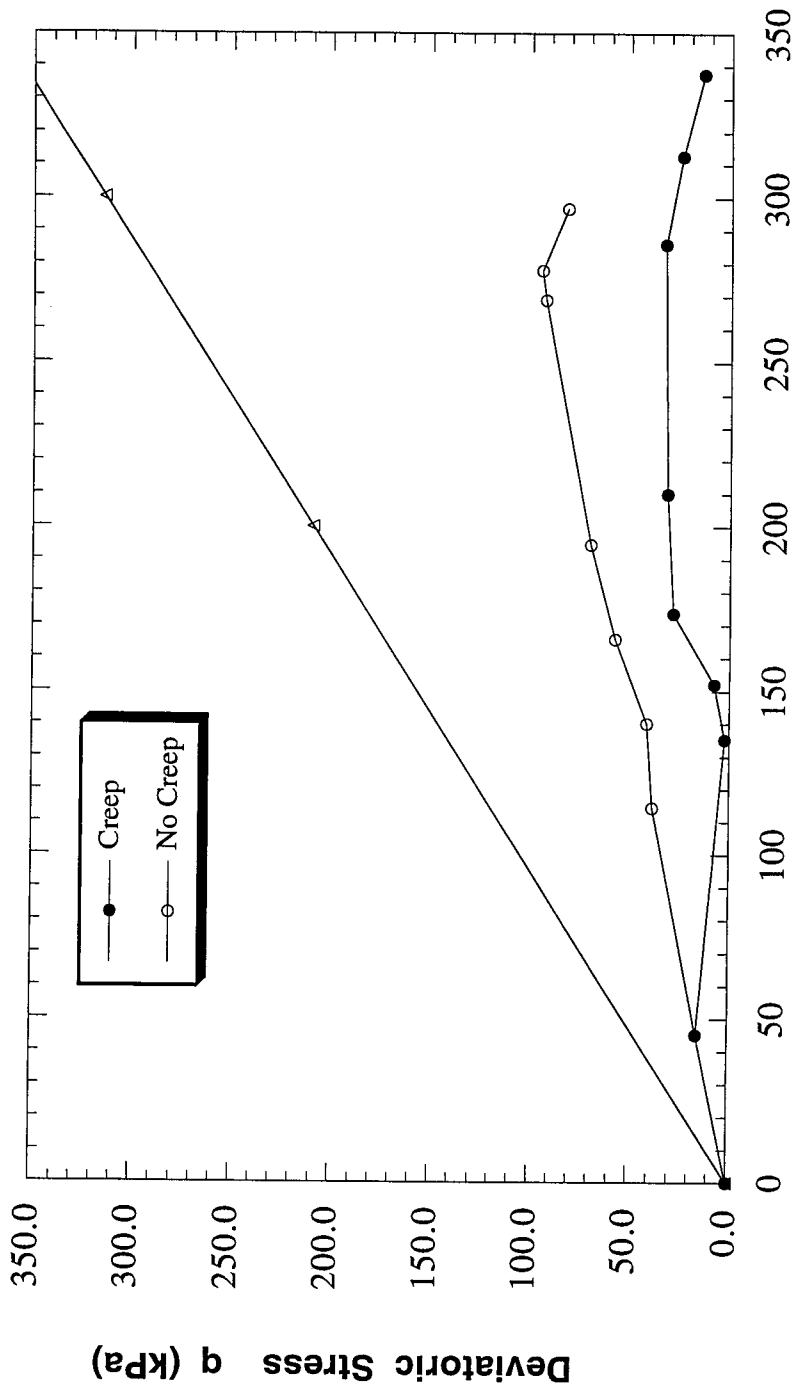

Figure (6.14) The P-q stress path at berm 251 m. region.

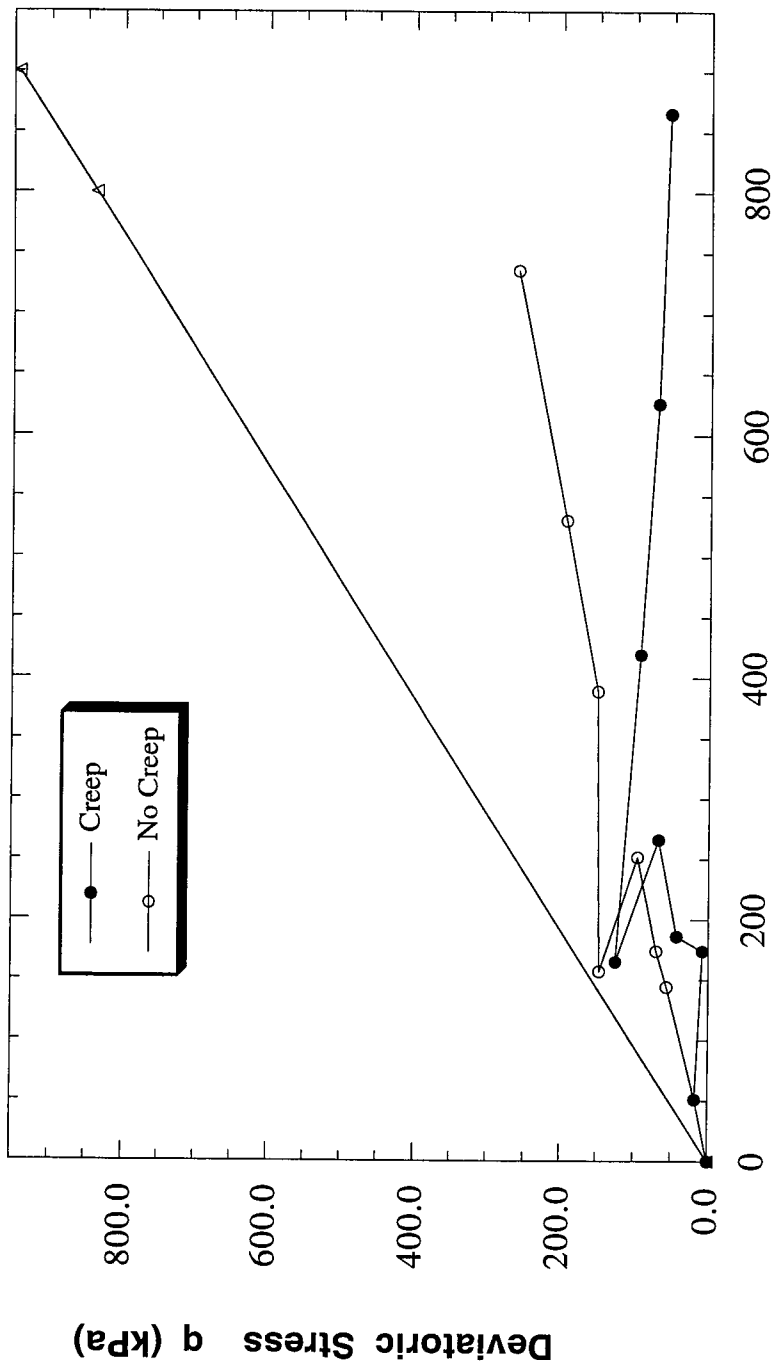

Figure (6.15) The P-q stress path at berm 303 m. region.

References:

Abdel Hadi, O.N., and Herrin, M. 1966. Characteristics of soil-asphalt as a rate process. ASCE Journal of the Highway Division, **92**(HW1): 49-69.

Akai,K., Adachi, T., and Ando, N. 1975. Existance of a unique stress-strain-time relation of clays. Soil and Foundation, **15** (1):1-16.

Borja, R.I., Hsieh, H.S., and Kavazanjian, E. Jr. 1990. Double-yield-surface model. II: Implementation and verification. ASCE Journal of the Geotechnical Engineering Division, **116**(GT9):1402-1421.

Buisman, K. 1936. Results of long duration settlement tests. Proceedings, 1st International Conference in Soil Mechanics and Foundation Engineering, Cambridge, U.S.A.,
June 22-26, 1936. Vol. 1. pp. 103-108.

Chan, D.H. and Morgenstern, N.R. 1992. User manual of program PISA. University of Alberta, Edmonton, Alberta, Canada.

Christensen, R.W., and Wu, T.H. 1964. Analysis of clay deformation as a rate process. ASCE Journal of Soil Mechanics and Foundation Engineering Division, **90**(SM6): 125-157.

De Alencar, J.A., Chan, D.H. and Morgenstern, N.R. 1992. Incorporation of measured pore pressure in finite element analysis. Proceeding of 45th Canadian Geotechnical Conference, Toronto, Ontario, 26-28 October,1992. pp. 62-1 - 62-10.

Hsieh, H.S., Kavazanjian, E. Jr., and Borja, R.I. 1990. Double-yield surface model.I:Theory. ASCE Journal of the Geotechnical Engineering Division, **116**(GT9): 1381-1401.

Mitchell, J.K. 1993. Fundamentals of soil behaviour. Second edition, John Wiley and Sons Inc., New York.

Morsy, M.M., Chan, D.H., and Morgenstern, N.R. 1994a. An effective stress model for creep of clay. Submitted to the Canadian Geotechnical Journal.

Morsy, M.M., Morgenstern, N.R. and Chan, D.H. 1994b. Simulation of creep deformation in the foundation of Tar Island Dyke. Submitted to the Canadian Geotechnical Journal.

Murayama, S., and Shibata, T. 1958. On the rheological characters of clay, part 1. Disaster Preventation Research Institute, Koyoto University. Bulletin **26**.

Murayama, S., and Shibata, T. 1961. Rheological properties of clays. Proceedings, 5th International Conference in Soil Mechanics and Foundation Engineering, Paris, France, July 17-22, 1961. Vol. 1 pp. 269-273.

Schiffman, R.L. 1959. The use of visco-elastic stress-strain laws in soil testing. ASTM Special Technical Publication No. 254. pp. 131-155.

Singh, A., and Mitchell, J.K. 1968. Generalized stress-strain-time function for soil. ASCE Journal of Soil Mechanics and Foundation Engineering Division, **94**(SM1): 21-46.

Taylor, D.W. 1948. Fundamentals of soil mechanics. John Wiley and Sons Inc. New York.

Wu, T.H., El Rafai, A.N., and Hsu, J.R. 1978. Creep deformation of clays. ASCE Journal of Geotechnical Engineering Division, **104** (GT1): 61-76.

CHAPTER 7

SUMMARY AND CONCLUSIONS

7.1 INTRODUCTION:

The mechanism of creep behaviour in cohesive soil has been known for decades, but there has been limited field evidence to reveal its magnitude. Several phenomenological relationships and rheological models to model creep in one dimension have been presented in the past. The difficulties associated with obtaining a numerical tool to analyze the creep problem in the field and the associated high cost of the finite element analysis to conduct such studies have deterred the practicing geotechnical engineer from considering creep behaviour in practice. The finite element analysis is a technique which demands patience, skill and experience. Many practicing geotechnical engineers have limited knowledge of finite element modelling and unfortunately this leads to too great emphasis on results than what is involved in getting the results.

7.2 SUMMARY AND CONCLUSIONS:

The applicability of a numerical model to perform quantitative analysis and calculations of the effect of the creep mechanism on the time-dependent behaviour in real geotechnical engineering structure has been demonstrated.

The adopted numerical model (double yield surface model) was originally developed by Hsieh (1987) to simulate the time dependent behaviour (creep) of cohesive soil in three dimensional stress conditions. The model uses two well known phenomenological relations (Taylor 1948; and Singh and Mitchell 1968) to evaluate creep deformation. In the present study the model is extended to include the observed pore pressure in order to model creep deformations in terms of effective stresses. An interpolation technique, developed by De Alencar (1988) is used to interpolate the pore

pressure within the soil domain based on the field measurements. The model is implemented in a finite element numerical scheme to provide a practical tool for numerical simulation of the time dependent behaviour (creep) of field problems with complex boundary conditions.

To test the proposed scheme, a set of drained creep triaxial tests for the Tar Island Dyke (TID) clay are numerically simulated. The results of the analysis show an excellent agreement between the calculated and the measured values and it also shows the importance of the the inclusion of creep deformation in the adopted model.

The next step is obviously to verify the validity of the proposed numerical scheme in terms of large-scale field test simulations. The field case chosen for the analysis is Tar Island Dyke. The lateral deformations and pore pressures have been measured over twenty five years of construction and operation. Based on the nature of the lateral deformation and piezometer readings in the clay foundation, it is postulated that the movements were a result of creep under drained conditions. The numerical scheme used in the finite element analysis of the Tar Island Dyke is presented in chapter 3. The validity of the scheme is emphasized by the satisfactory agreement between the measured and the calculated vertical and horizontal deformations and shear strains. The analysis also shows the importance of the inclusion of creep in the scheme for the analysis of this type of problem.

In chapter 6 the study focuses on the creep component in the analysis of the TID to provide a better understanding of the problem of creep in the field and the major factors that influence this behaviour. Sensitivity analyses are carried out to study the influence of the model creep parameters on the creep behaviour of the dyke foundation. The analyses show that the creep process is not controlled by one specific parameter but it is the combined effect of all the creep parameters. A creep independent analysis is also carried out to illustrate the influence of creep on the strain and stress state in the dyke foundation. In the case of the strain state in the dyke foundation, the time dependent deformation at the dyke toe is mainly controlled by the creep mechanism and this domination shifts to the process of pore pressure dissipation at the center of the dyke as one moves toward the dyke center. For the stresses in the clay, creep causes a process of redistribution of the stresses in terms of stress relaxation in the middle region of the clay layer and stress concentration at the upper interface between the clay layer and the dyke and the lower interface between the dyke and the sand and gravel layer. The analyses

show that the creep process reduces the stress state in the clay layer by shifting the stress state away from the critical state line.

As a final conclusion of the study, the numerical scheme proposed in the study provides a simple and powerful tool for the analysis and design of this class of problem adopting the history matching approach. The characteristics of the approach are:

a) the material parameters required to model the time-dependent behaviour of soils are obtainable from traditional laboratory tests;

b) when pore pressure measurements are available, the scheme will help the geotechnical engineers to avoid the problem of accurate prediction of the change of the pore pressure regime in the soil domain, at any step of construction, as a function of time due to external loads, dissipation of pore pressure, and change in the ground water elevation.

7.3 RECOMMENDATIONS FOR FUTURE WORKS:

On the constitutive model:

1) For most clays, the slope e (void ratio)-ln P (mean stress) curve in virgin compression, denoted by the parameter λ, is in reality a function of effective stress and void ratio, λ is however, assumed constant in the study and in general practice for normally consolidated clays with low to medium sensitivity. For highly sensitive clays, which are more susceptible to structural breakdown, a bilinear or multi-linear e-ln P relationship could be adopted to better represent real soil properties.

2) The C_α value, coefficient of secondary compression, can be replaced by a C_α^* value, the apparent coefficient of secondary compression. The C_α^* should be determined according to the procedures proposed by Fuleiham and Ladd (1976) to account for the effect of the deviatoric stress level.

3) A more detailed study is required to reveal the effect of the two factors, the accuracy and the type of creep laboratory tests, on the determined values of the creep parameters of the model. How do these two factors affect the prediction of the creep behaviour of cohesive soil?

4) Material anisotropy and overconsolidation have been discussed briefly by Sekiguchi and Ohta (1977) and Pender (1977), respectively. They have shown that these factors not only influence the size of the yield surface but also its shape. Inclusion of these factors would provide a better interpretation of preconsolidation effects for states other than isotropic or K_o-conditions.

For the finite element program:

1) An explicit scheme has been used in the time marching to determine the strain over a specified time step. For the stability of the analysis, a large number of small time steps were used in the time dependent analyses. It is however preferred to implement an implicit scheme in the finite element code to overcome the unstability of the analysis.

2) Sporadic numerical instabilities were encountered while using PISA^{TM} for the effective stress analysis. The nature of this instability is unclear. It is however suspected that the magnitudes of deviatoric and volumetric age (t_d and t_v) may sometimes become unreasonably large, resulting in the instability. A more robust algorithm in coding this constitutive model into the finite element program is recommended to overcome the instability.

Finally, although this work shows promising results in further understanding of the creep mechanism in the field as well as providing a simple numerical tool for the practical analysis and design of field problems, more case histories need to be analyzed to obtain more comprehensive knowledge.

References:

De Alencar, J.A. 1988. Deformation of dams on sheared foundations. Ph.D. thesis, University of Alberta, Edmonton, Alberta, Canada.

Fuleihan, N.F., and Ladd, C.C. 1976. Design and performance of Atchafalay flood control levees. Research repoet R76-24, Department of Civil Engineering M.I.T.

Hsieh, H.S. 1987. A non-associative cam-clay plasticity model for the stress-strain-time behaviour of soft clays. Ph.D. thesis, Stanford University, California, U.S.A..

Pender, M.J. 1977. A unified model for soil-stress-strain behaviour. Proceedings of specialty session 9, 9th International Conference of Soil Mechanics and Foundation Engineering, Tokyo, Japan, 1977. pp. 213-222.

Sekiguchi, H., and Ohta, H. 1977. Induced anistropy and time depending in clays. Proceedings of specialty session 9, 9th International Conference of Soil Mechanics and Foundation Engineering, Tokyo, Japan, 1977. pp. 239-244.

Singh, A., and Mitchell, J.K. 1968. Generalized stress-strain-time function for soil. ASCE Journal of Soil Mechanics and Foundation Engineering Division, **94**(SM1): 21-46.

Taylor, D.W. 1942. Research on consolidation of clays. Report Serial No. 82, Department of Civil Engineering, MIT, Cambridge, Massachusetts.

Watts, B.D. 1980. Lateral creep deformations in the foundation of a high dam. M.Sc. thesis, University of Alberta, Edmonton, Alberta, Canada.

Appendix A :

PORE PRESSURE INTERPOLATION SCHEME FOR FINITE ELEMENT ANALYSIS:

The numerical scheme proposed in chapter 3 requires the incorporation of pore pressure into the finite element analysis based on field measurements. Pore pressure is often measured at a limited number of locations. In the finite element analysis, it is required to determine the magnitude of the pore pressure in every element within the domain of interest. Therefore an interpolation scheme is required to calculate pore pressure in every element. An interpolation scheme proposed by De Alancar et al. (1992) is presented in this appendix. The scheme has the following steps:

1) An initial pore pressure distribution is assumed for the entire domain. In the case of a finite element analysis, this means that an initial set of values are assigned at each integration point of the mesh. The initial pore pressure distribution may be specified by the user based on the knowledge of the water table.

2) Based on the pore pressure distribution, the pore pressure at the piezometers locations are calculated using a weighting scheme. Since the piezometer positions rarely coincide with the position of an integration point in a finite element scheme, an interpolation is required. The pore pressure at the piezometer locations x^*_i can be calculated from the existing pore pressure at locations x_i as:

[A.1] $$u^*_i = \sum_{j=1}^{m} \lambda_{ij}\, u_j,$$

where

u^*_i is the pore pressure at the piezometer locations x^*_i, the * quantity refers to the piezometer locations;

u_j is the pore pressure at the piezometer locations x_j which, at this time correspond to the integration point;

λ_{ij} is the interpolation coefficient between points x^*_i and x_j, and;

m is the number of points in the interpolation.

The interpolation coefficient λ_{ij} is defined as:

[A.2a] $$\lambda_{ij} = \frac{W_{ij}}{\sum_{k=1}^{m} W_{ik}},$$

and

[A.2b] $$\sum_{j=1}^{m} \lambda_{ij} = 1,$$

where W_{ik} is a weight function given by:

[A.3] $$Wij = \exp (d_{ij})^n,$$

where

d_{ij} is the distance between points i and j;

n is an exponent, values of 1 to 4 are used in this study.

3) The errors between the calculated and the observed pore pressure at the piezometers locations are determined and compared with a specified tolerance.

4) If the errors at the piezometer locations are larger than the specified tolerance, a correction factor F^* is calculated:

[A.4] $$^tF^*_i = \frac{U^*_i}{t_{u^*_i}},$$

where

$^tF^*_i$ is the correction factor at piezometer i at iteration t;

U^*_i is the measured pore pressure at piezometer i;

$t_{u^*_i}$ is the interpolated value at location of piezometer i based on the interpolated pore pressure distribution at iteration t.

The correction is not applied at the piezomter locations. It is applied at the finite element integration points. The adjustment at the integration points is carried out using the same expression given by equation (A.1) as:

[A.5] $$ {}^{t+1}F_i = \sum_{j=1}^{m} {}^{t}F^*_j, $$

[A.6] $$ {}^{t+1}u_i = {}^{t}u_i \, {}^{t+1}F_i, $$

where

${}^{t+1}F_i$ is the correction factor at integration point i at iteration t+1,

${}^{t+1}u_i$ is the pore pressure at integration point i at iteration t+1,

λ_{ij} is given by Equation (A.2a).

The error for all piezometer locations is defined as:

[A.7] $$ E = \sqrt{\frac{\sum_{j=1}^{N} [{}^{t+1}F^*_j - {}^{t}F^*_j]^2}{\sum_{j=1}^{N} [{}^{t}F^*_j]^2}}, $$

where

E is the error;

N is the total number of piezometers.

5) Steps 2, 3, and 4 are repeated until the errors in the calculated pore pressure are sufficiently small.

Appendix B :

In this appendix, the derivation of the elasto-plastic stress strain matrix $[\bar{C}]$ and the time dependent stress relaxation term $\{\dot{\sigma}^t\}$ based on the stress state of the soil element with respect to the double-yield surface are given in details.

Case A: Fully plastic process on the F and G surfaces:

The total strain-rate tensor $\{\dot{\varepsilon}\}$ is decomposed in the following manner :

[B1] $$\{\dot{\varepsilon}\} = \{\dot{\varepsilon}^e\} + \{\dot{\varepsilon}_F^P\} + \{\dot{\varepsilon}_G^P\} + \{\dot{\varepsilon}^t\},$$

where $\{\dot{\varepsilon}^e\}$ is the elastic strain increment, $\{\dot{\varepsilon}_F^P\}$ and $\{\dot{\varepsilon}_G^P\}$ are the plastic strain increment induced by the Modified Cam-clay yield surface F and the horizontal yield surface G, respectively. While the $\{\dot{\varepsilon}^t\}$ denotes the creep strain rate (Equation (3.10)). $\{\dot{\varepsilon}^e\}$ can be expressed as following,

[B2] $$\{\dot{\varepsilon}^e\} = [C^e]^{-1}\{\dot{\sigma}\},$$

where $\mathbf{C^e}$ is the elastic stress-strain matrix.

Applying the associative flow rule on both yield surfaces F and G:

[B3] $$\{\dot{\varepsilon}_F^P\} = \phi\{\frac{\partial F}{\partial \sigma}\},$$

and obtaining the volumetric part

[B4] $$\dot{\varepsilon}_v^P = \phi\frac{\partial F}{\partial P},$$

and

[B5] $$\{\dot{\varepsilon}_G^P\} = \theta\{\frac{\partial G}{\partial \sigma}\},$$

and obtaining the deviatore strain

[B6] $$\dot{\gamma}^P = \theta\sqrt{\frac{2}{3}}\left\|\frac{\partial G}{\partial \sigma}\right\|,$$

where ϕ and θ are the proportionality factors whose values are to be determined. Equation [B1] can now be written as :

[B7] $$\{\dot{\varepsilon}\} = [C^e]^{-1}\{\dot{\sigma}\} + \phi\{\frac{\partial F}{\partial \sigma}\} + \theta\{\frac{\partial G}{\partial \sigma}\} + \{\dot{\varepsilon}^t\},$$

or

[B8] $$\{\dot{\sigma}\} = [C^e](\{\dot{\varepsilon}\} - \phi\{\frac{\partial F}{\partial \sigma}\} - \theta\{\frac{\partial G}{\partial \sigma}\} - \{\dot{\varepsilon}^t\}).$$

Invoking the consistency requirement on both yield surface the time derevative of F and G become :

[B9] $$\dot{F} = \{\frac{\partial F}{\partial \sigma}\}^T\{\dot{\sigma}\} + \frac{\partial F}{\partial P_c}\dot{P}_c = 0,$$

[B10] $$\dot{G} = \{\frac{\partial G}{\partial \sigma}\}^T\{\dot{\sigma}\} + \frac{\partial G}{\partial q_c}\dot{q}_c = 0,$$

where the time derivative $\dot{P}_c$ and $\dot{q}_c$ are:

[B11] $$\dot{P}_c = \frac{\partial P_c}{\partial \varepsilon_v^P}\dot{\varepsilon}_v^P + \frac{\partial P_c}{\partial t_v},$$

$$\dot{P}_c = \phi\frac{\partial F}{\partial \varepsilon_v^P}\frac{\partial F}{\partial P} + \frac{\partial P_c}{\partial t_v},$$

[B12] $$\dot{q}_c = \frac{\partial q_c}{\partial \gamma^p}\dot{\gamma}^p + \frac{\partial q_c}{\partial P_c}\dot{P}_c + \frac{\partial q_c}{\partial t_d},$$

$$\dot{q}_c = \theta\frac{\partial q_c}{\partial \gamma^p}\sqrt{\frac{2}{3}}\left\|\frac{\partial G}{\partial \sigma}\right\| + \phi\frac{\partial q_c}{\partial P_c}\frac{\partial P_c}{\partial \varepsilon_v^P}\frac{\partial F}{\partial P} + \frac{\partial q_c}{\partial P_c}\frac{\partial P_c}{\partial t_v} + \frac{\partial q_c}{\partial t_d}.$$

Subsituting equations [B8],[B11], and [B12] into equations [B9] and [B10] results in the following simultaneous equation of ϕ and θ in the matrix form,

[B13] $$\begin{bmatrix}\alpha_{11} & \alpha_{12}\\ \alpha_{21} & \alpha_{22}\end{bmatrix}\begin{Bmatrix}\phi\\ \theta\end{Bmatrix} = \begin{Bmatrix}b_1\\ b_2\end{Bmatrix},$$

where

[B14.1] $$\alpha_{11} = \{\frac{\partial F}{\partial \sigma}\}^T [C^e] \{\frac{\partial F}{\partial \sigma}\} - \frac{\partial F}{\partial P_c} \frac{\partial P_c}{\partial \varepsilon_v^P} \frac{\partial F}{\partial P};$$

[B14.2] $$\alpha_{12} = \{\frac{\partial F}{\partial \sigma}\}^T [C^e] \{\frac{\partial G}{\partial \sigma}\};$$

[B14.3] $$\alpha_{21} = \{\frac{\partial G}{\partial \sigma}\}^T [C^e] \{\frac{\partial F}{\partial \sigma}\} - \frac{\partial G}{\partial q_c} \frac{\partial q_c}{\partial P_c} \frac{\partial P_c}{\partial \varepsilon_v^P} \frac{\partial F}{\partial P};$$

[B14.4] $$\alpha_{22} = \{\frac{\partial G}{\partial \sigma}\}^T [C^e] \{\frac{\partial G}{\partial \sigma}\} - \frac{\partial G}{\partial q_c} \frac{\partial q_c}{\partial \gamma^P} \sqrt{\frac{2}{3}} \left\| \frac{\partial G}{\partial \sigma} \right\|;$$

[B14.5] $$b_1 = \{\frac{\partial F}{\partial \sigma}\}^T [C^e] (\{\dot{\varepsilon}\} - \{\dot{\varepsilon}^t\}) + \frac{\partial F}{\partial P_c} \frac{\partial P_c}{\partial t_v};$$

[B14.6] $$b_2 = \{\frac{\partial G}{\partial \sigma}\}^T [C^e] (\{\dot{\varepsilon}\} - \{\dot{\varepsilon}^t\}) + \frac{\partial G}{\partial q_c} (\frac{\partial q_c}{\partial P_c} \frac{\partial P_c}{\partial t_v} + \frac{\partial q_c}{\partial t_d}).$$

Solving [B13] for ϕ and θ gives,

[B15.1] $$\begin{Bmatrix} \phi \\ \theta \end{Bmatrix} = D^{-1} \begin{bmatrix} \alpha_{22} & -\alpha_{12} \\ -\alpha_{21} & -\alpha_{11} \end{bmatrix} \begin{Bmatrix} b_1 \\ b_2 \end{Bmatrix},$$

[B15.2] $$\begin{Bmatrix} \phi \\ \theta \end{Bmatrix} = \begin{bmatrix} \alpha'_{11} & \alpha'_{12} \\ \alpha'_{21} & \alpha'_{22} \end{bmatrix} \begin{Bmatrix} b_1 \\ b_2 \end{Bmatrix},$$

where $D = \alpha_{11}\alpha_{22} - \alpha_{12}\alpha_{21} \neq 0$.

Having obtained the values of ϕ and θ, equation [B8] simplifies to :

[B16] $$\{\dot{\sigma}\} = [\bar{C}]\{\dot{\varepsilon}\} - \{\dot{\sigma}^t\},$$

[B17] $$[\bar{C}] = [C^e] - \alpha'_{11}[C^e]\{\frac{\partial F}{\partial \sigma}\}\{\frac{\partial F}{\partial \sigma}\}^T[C^e] - \alpha'_{12}[C^e]\{\frac{\partial F}{\partial \sigma}\}\{\frac{\partial G}{\partial \sigma}\}^T[C^e]$$

$$-\alpha'_{21}[C^e]\{\frac{\partial G}{\partial \sigma}\}\{\frac{\partial F}{\partial \sigma}\}^T[C^e] - \alpha'_{22}[C^e]\{\frac{\partial G}{\partial \sigma}\}\{\frac{\partial G}{\partial \sigma}\}^T[C^e],$$

and the stress relaxation rate is given by :

[B18] $$\{\dot{\sigma}^t\} = [\bar{C}]\{\dot{\varepsilon}^t\} + \alpha'_{11}[C^e]\{\frac{\partial F}{\partial \sigma}\}\frac{\partial F}{\partial P_c}\frac{\partial P_c}{\partial t_v} + \alpha'_{12}[C^e]\{\frac{\partial F}{\partial \sigma}\}\frac{\partial G}{\partial q_c}(\frac{\partial q_c}{\partial P_c}$$

$$\frac{\partial P_c}{\partial t_v} + \frac{\partial q_c}{\partial t_d}) + \alpha'_{21}[C^e]\{\frac{\partial G}{\partial \sigma}\}\frac{\partial F}{\partial P_c}\frac{\partial P_c}{\partial t_v} + \alpha'_{22}[C^e]\{\frac{\partial G}{\partial \sigma}\}\frac{\partial G}{\partial q_c}$$

$$(\frac{\partial q_c}{\partial P_c}\frac{\partial P_c}{\partial t_v} + \frac{\partial q_c}{\partial t_d}).$$

Case B: Semiplastic process on the F yield surface:

In the event that only F yield surface is involved in the deformation process, equation [B15.2] is reduced to :

[B19] $$\phi = \alpha_{11}^{-1} b_1.$$

The resulting elasto-plastic stress-strain matrix is :

[B20] $$[\bar{C}] = [C^e] - \alpha_{11}^{-1}([C^e]\{\frac{\partial F}{\partial \sigma}\}\{\frac{\partial F}{\partial \sigma}\}^T[C^e]).$$

While the stress-relaxation rate term simplifies to :

[B21] $$\{\dot{\sigma}^t\} = [\bar{C}]\{\dot{\varepsilon}^t\} + \alpha_{11}^{-1}(\frac{\partial F}{\partial P_c}\frac{P_c}{t_v}\frac{C_\alpha}{C_c - C_r})[C^e]\{\frac{\partial F}{\partial \sigma}\}.$$

Case C: Semiplastic process on the G yield surface:

In the event that only G yield surface is involved in the deformation process, equation [B15.2] is reduced to:

[B22] $$\theta = \alpha_{22}^{-1} b_2.$$

The resulting elasto-plastic stress-strain matrix is :

$$[B23] \qquad [\bar{C}] = [C^e] - \alpha_{221}^{-1}([C^e]\{\frac{\partial G}{\partial \sigma}\}\{\frac{\partial G}{\partial \sigma}\}^T[C^e]).$$

While the stress-relaxation rate term simplifies to

$$[B24] \qquad \{\dot{\sigma}^t\} = [\bar{C}]\{\dot{\varepsilon}^t\} + \alpha_{22}^{-1}(\frac{\partial G}{\partial q_c}\frac{\partial q_c}{\partial P_c}\frac{\partial P_c}{\partial t_v} + \frac{\partial G}{\partial q_c}\frac{\partial q_c}{\partial t_d})[C^e]\{\frac{\partial G}{\partial \sigma}\}.$$

Case D: Elastic process:

In the event that the soil element stress state is within the elastic domain of the double yield surface :

$$[B25] \qquad [\bar{C}] = [C^e] = \begin{bmatrix} C_1 & C_2 & C_2 & 0 & 0 & 0 \\ C_2 & C_1 & C_2 & 0 & 0 & 0 \\ C_2 & C_2 & C_1 & 0 & 0 & 0 \\ 0 & 0 & 0 & \mu^e & 0 & 0 \\ 0 & 0 & 0 & 0 & \mu^e & 0 \\ 0 & 0 & 0 & 0 & 0 & \mu^e \end{bmatrix},$$

where

$$C_1 = K^e + \frac{4}{3}\mu^e \qquad \text{and} \qquad C_2 = K^e - \frac{2}{3}\mu^e.$$

While the stress-relaxation term is equal to :

$$[B26] \qquad \{\dot{\sigma}^t\} = [C^e]\{\dot{\varepsilon}^t\}.$$

Evaluation of the derivatives:

The derivatives of F are as follows:

$$[B27] \qquad \frac{\partial F}{\partial P} = 2P - P_c;$$

[B28] $$\frac{\partial F}{\partial q} = \frac{2q}{M^2};$$

[B29] $$\frac{\partial F}{\partial P_c} = -P;$$

[B30] $$\{\frac{\partial F}{\partial \sigma}\} = \frac{\partial F}{\partial P}\{\frac{\partial P}{\partial \sigma}\} + \frac{\partial F}{\partial q}\{\frac{\partial q}{\partial \sigma}\};$$

[B31] $$\{\frac{\partial P}{\partial \sigma}\} = \frac{1}{3}\{m\};$$

[B32] $$\{\frac{\partial q}{\partial \sigma}\} = \frac{3}{2q}(\{\sigma\} - \frac{1}{3}P\{m\}).$$

where
$\{m\}^T$ is the identity matrix = <1, 1, 0, 1, 0, 0>.

The derivative of G are as follows:

[B33] $$\frac{\partial G}{\partial P} = 0;$$

[B34] $$\frac{\partial G}{\partial q} = 1;$$

[B35] $$\frac{\partial G}{\partial q_c} = -1;$$

[B36] $$\{\frac{\partial G}{\partial \sigma}\} = \frac{\partial G}{\partial P}\{\frac{\partial P}{\partial \sigma}\} + \frac{\partial G}{\partial q}\{\frac{\partial q}{\partial \sigma}\}.$$

Equations [B30] and [B36] define the normals at any point on the F and G surfaces, respectively.

Appendix C:

In this appendix, the authors show the approximate evaluation of the hyperbolic stress-strain parameters in the absence of consolidation undrained triaxial test data for the TIC.

Hyperbolic stress-strain parameter a:

The shear elastic modulus is defined by:

[C1] $$\mu^e = \frac{1}{2}\frac{3K^e - 6K^e\nu}{1+\nu},$$

where ν is the poisson ratio.

The Bulk modulus K^e is defined by:

[C2] $$K^e = \frac{(1+e)P}{\kappa},$$

where e and P are the current void ratio and mean stress.

[C3] $$e = e_a - \lambda \ln P$$

For $P=P_c= 650$ KPa,
where P_c is the preconsolidation pressure of TIC from the oedometer test (Watts 1980).

Subsituting in equation [C3] $e_a = 0.898$, $C_c = 0.10665$.

The current void ratio $e = 0.5909$.

Assuming $\nu = 0.2$,
the bulk modulus K^e = 79,773.0 KPa,
from equation [C1] the shear modulus μ^e = 59,830 KPa,
from equation (3.6),

[C4] $$a = \frac{P_c R_f}{3\mu^e},$$

based on $R_f = 0.89$ (Watts 1980),
the hyperbolic stress-strain parameter $a = 0.0032$.

Hyperbolic stress-strain parameter b:

The hyperbolic stress-strain parameter b is determined using the following equation proposed by Borja et al. (1985):

[C5] $$\frac{b}{R_f} = \frac{2^{(1-\frac{C_r}{C_c})}}{M},$$

for $R_f = 0.89$,
the hyperbolic stress-strain parameter $b = 1.398$.

Appendix D :

In this appendix, the authors show the approximate evaluation of the hyperbolic stress-strain parameters in the absence of consolidation undrained triaxial test data for the TIC.

Hyperbolic stress-strain parameter a:

The shear elastic modulus is defined by:

[D1] $$\mu^e = \frac{1}{2}\frac{3K^e - 6K^e\nu}{1+\nu},$$

where ν is the poisson ratio.

The Bulk modulus K^e is defined by:

[D2] $$K^e = \frac{(1+e)P}{\kappa},$$

where e and P are the current void ratio and mean stress.

[D3] $$e = e_a - \lambda \ln P$$

For $P=P_c= 650$ KPa,
where P_c is the preconsolidation pressure of TIC from the oedometer test (Watts 1980).

Subsituting in equation [D3] $e_a = 0.852$, $C_c = 0.28$.

The current void ratio $e = 0.06438$.

Assuming $\nu = 0.2$,
the bulk modulus $K^e = 53{,}101.43$ KPa,
from equation [D1] the shear modulus $\mu^e = 39{,}826.07$ KPa.

The hyperbolic stress-strain parameter a is calculated using the following equation:

[D4] $$a = \frac{P_c R_f}{3\mu^e},$$

based on $R_f = 0.89$ (Watts 1980),
the hyperbolic stress-strain parameter $a = 0.0048$.

Hyperbolic stress-strain parameter b:

The hyperbolic stress-strain parameter b is determined using the following equation proposed by Borja et al. (1985):

[D5] $$\frac{b}{R_f} = \frac{2^{(1-\frac{C_r}{C_c})}}{M},$$

for $R_f = 0.89$,
the hyperbolic stress-strain parameter $b = 1.57$.